2009

Hierarchical complexity in metal-organic materials: From layers to polyhedra to supermolecular building blocks

John Jackson Perry
University of South Florida

Hierarchical Complexity in Metal-Organic Materials:

From Layers to Polyhedra to Supermolecular Building Blocks

by

John Jackson Perry IV

A dissertation submitted in partial fulfillment
of the requirements for the degree of
Doctor of Philosophy
Department of Chemistry
College of Arts and Sciences
University of South Florida

Major Professor: Michael J. Zaworotko, Ph.D.
Mohamed Eddaoudi, Ph.D.
Brian Space, Ph.D.
Stephen J. Loeb, Ph.D.

Date of Approval:
November 7, 2009

Keywords: crystal engineering, coordination polymer, MOF, topology, crystal chemistry, supramolecular chemistry

Dedication

To my family for their enthusiasm, support and encouragement…

…and to Miranda for everything

Acknowledgments

First and foremost, I would like to take this opportunity to express my sincerest and immense appreciation towards my Ph.D. advisor Dr. Michael J. Zaworotko for his guidance and support throughout my doctoral research. I am eternally grateful for his allowing me to join his research group and providing me with the opportunity to pursue my studies in this fascinating and stimulating field of research.

Additionally, many thanks and accolades are due to the remaining members of my dissertation examination committee—Dr. Mohamed Eddaoudi, Dr. Brian Space, and Dr. Stephen J. Loeb—for their guidance and helpful suggestions pertaining to the work presented herein. I would especially like to thank Dr. Gregory McColm for graciously agreeing to act as chairperson for the examination committee and taking the time to review the dissertation in its entirety.

I would be remiss not to thank the numerous students and post-doctoral fellows both past and present in the research groups of Dr. Zaworotko and Dr. Eddaoudi (Especially my closest companions; Miranda Cheney, Greg McManus, Zhenqiang Wang, and Jason Perman, without whom this would not have been possible) as well as all members of SMMARTT, for all of their support and stimulating scientific collaboration. Finally, I would especially like to acknowledge and thank Dr. Randy Larsen for his countless hours of discussion, mentoring, and guidance through the years.

Table of Contents

List of Tables

List of Figures

Hierarchical Complexity in Metal-Organic Materials: From Layers to Polyhedra to Supermolecular Building Blocks

John J. Perry IV

ABSTRACT

The design and synthesis of novel functional materials with fine-tunable physical and chemical properties has been an aspiration of materials scientists since at least Feynman's famous speech "*There's Plenty of Room at the Bottom*" which has fittingly been credited with ushering in the nanotechnology era. Crystal engineering, as the solid-state manifestation of supramolecular chemistry, is well positioned to make substantial contributions to this worthwhile endeavor. Within the realm of crystal engineering resides the subdiscipline of metal-organic materials (MOMs) which pertains most simplistically to the coordination bond and includes such objects as coordination polymers, metal-organic frameworks (MOFs), and discrete architectures, each of which share the common aspect that they are *designed* to be modular in nature. While metal-organic materials have been studied for quite some time, only recently have they enjoyed an explosion in significance and popularity, with much of this increased attention being attributed to two realizations; that this inherent modularity ultimately results in an almost overwhelming degree of diversity and subsequently, that this diversity can give rise to effective control of the properties of functional materials. At long last the goal of attaining fine-tunablity may be within our grasp.

In addition to high levels of diversity, MOMs are also characterized by a broad range of complexity, both in their overall structures and in the nature of their constituents. From the simplest molecular polygons to extended 3-periodic frameworks of unprecedented topologies, MOMs have the capacity to adopt an array of structural complexities. Moreover, there has been a recent trend of increasing complexity of the very building blocks that construct the framework. It is the aim of the research presented in this dissertation to survey these two principle aspects of MOMs, diversity and complexity, by focusing upon the use of polycarboxylates and first row transition metals to synthesize several series of closely related materials imbued with varied levels of complexity. Through the use of single crystal X-ray diffraction and the charcterization of the materials' properties, the structure-function relationship has been probed. Finally, novel design strategies incorporating supermolecular building blocks for the creation of a new generation of MOMs has been addressed.

Chapter 1

Introduction

1.1 Preamble

"…What could we do with layered structures with just the right layers? What would the properties of materials be if we could really arrange the atoms the way we want them? They would be very interesting to investigate theoretically. I can't see exactly what would happen, but I can hardly doubt that when we have some control of the arrangement of things on a small scale we will get an enormously greater range of possible properties that substances can have, and of different things that we can do."

Richard P. Feynman[1]

December 29th, 1959 Caltech

The modern synthetic chemist aspires to fathom the underlying principles, the governing dynamics of the natural world, precisely so that they may be able to intelligently design and subsequently synthesize novel materials incorporated with specific desired properties. The dream and long-term objective of these chemists and scientists of other related disciplines, is to wrest control over the dominion of matter, so that they might reshape and remold it with an eye toward dictating what the exact properties of those materials will be. It is believed that once we have gained sufficient ability to determine, on the atomic level, the structure of matter we will concomitantly inherent the ability to influence the properties of materials and in turn vastly expand those things we can achieve.

1.1.1 Crystals and Crystallochemistry

"The thin snow now driving from the north and lodging on my coat consists of those beautiful star crystals,…How full of the creative genius is the air in which these are generated! I should hardly admire more if the real stars fell and lodged on my coat…The same law that shapes the earth-star shapes the snow-star. As surely as the petals of a flower are fixed, each of these countless snow-stars comes whirling to earth, pronouncing thus, with emphasis, the number six. Order, κόσμος (cosmos).

Henry David Thoreau[4]

The inherent symmetry and immense beauty that crystals exhibit has probably contributed to their being compelling objections of interest and desire since they were first discovered as naturally occurring gem stones or when man first took a closer look at snowflakes (Fig. 1.1).[5, 6] Modern western science traditionally establishes the advent of scientific inquiry regarding crystals to be the works of Johannes Kepler (December 27th, 1571 – November 15th, 1630) or more specifically his treatise *A New Year's Gift, or On the six-cornered Snowflake.*[7] However, it is clear that going back at least to the second century B.C. that the ancient Chinese were already well aware of the six-sidedness of these crystals.[7]

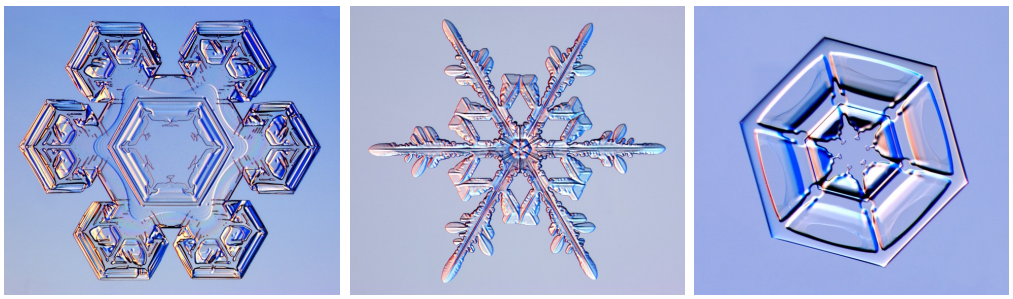

Figure 1.1 Photographs of snow crystals.

Crystals, or a crystalline solid, is a material whose constituents— in the form of atoms, molecules, or ions—are arranged in an orderly periodic array which extends in three spatial directions. The term crystal is derived from the ancient Greek κρυσταλλος (*krustallos*) which literally meant ice or clear-ice. This stemmed from the fact that they believed crystals (namely rock crystal or quartz) to be a form of hardened water. In fact they used this term to convey meaning for anything that congealed by freezing, not simply for the chemical structure we know of today as water. The majority of matter in the natural world adopts a crystalline form upon solidifying. The study of crystals and their internal structures was greatly aided by the discovery of X-rays, a form of electromagnetic radiation with extremely small wavelength, by W.C. Röntgen in 1895. While predominately used in the medical sciences for imaging inside the human body, X-rays have also been critical to the analysis of crystal structures. The modern science of crystals, or crystallography[8] was essentially established not long after the discovery of this new form of electromagnetic radiation, when in 1912 Max von Laue (1879-1960) suggested to Walter Friedrich and Paul Knipping, a research assistant and a doctoral candidate at the University of Münich respectively, that they attempt to pass X-rays through a crystal of copper sulfate and collect the pattern of spots that occur on a photographic plate. This was successful, and from a separate diffraction experiment involving zinc blende, von Laue was able to demonstrate that the observed pattern of spots could only be caused by the diffraction of very short waves by a regular arrangement of atoms or molecules in the crystal. Not long thereafter the Braggs, William H. Bragg and his son William Lawrence Bragg, extended this diffraction method to

analyze the arrangement of atoms in common crystalline materials.[9, 10] Since that time crystallography has steadily grown and flourished in its capacity to address the underlying atomic structure of crystalline materials. Over time better X-ray sources were created resulting in better diffraction of X-rays, but the basic photographic plate remained largely unchanged. Still the field made countless improvements and grand discoveries; the structure of some large proteins and the double helix nature of DNA being just a few. With the invention of the computer and the CCD detector however, the field has exploded and progressed to such a degree that X-ray diffraction data acquisition and structure solution for small organic molecules is rather routine. In fact the larger companies which supply X-ray diffractometers and structure solution software already sell fully automatic, black-box lab bench X-ray diffractometers which can collect and analyze a sample entirely on its own. While this has not been perfected, and may never be for more convoluted crystal structures, the progress from just 50 years ago is astounding.

Generally the importance of the crystalline nature of some materials lies in the very fact that they are crystals; that they are construct of a periodic array of their own constituents instills unto them the capacity to diffract X-rays. This ability to cause the diffraction of X-rays then gives rise to the happy happenstance that we can utilize such an observable (and recordable) phenomenon to discern the structure of that material on the molecular level. With crystallography, we are able to view the structure of crystals down to atomic resolution, so that understanding the structure-property relationship in materials is greatly facilitated.

1.1.2 Solid State Chemistry

As the name suggests, solid state chemistry is the study of matter which exists in the solid state under some set of conditions (temperature, pressure) in which the observations are conducted. More pointedly, solid state chemistry comprises the synthesis, structural determination, characterization, and investigation of the ensuing properties of both crystalline and amorphous materials. Traditionally, solid state chemistry has been very closely aligned with crystalline materials and crystallography, mainly due to the aspect that crystalline substances are often amenable to solid-state structure elucidation at a precision level suitable for evaluating structure-property relationships. Additionally, there are many properties of crystalline solids that arise solely due to the fact they exist as crystals, and indeed the extent to which some of these phenomena are observed (or are absent) can depend critically on the quality of the crystal in question. It is not impractical, however, to also address the solid state chemistry of amorphous materials, which with no long range order can be somewhat more complicated when attempting to decipher exact structural features. What makes solid state chemistry so attractive and essential is the obvious realization that the vast majority of materials with practical importance in our current technological society are solids at ambient conditions. This includes both amorphous (plastics, polymers, glasses, etc.) and crystalline examples of matter which have been harnessed by mankind to fashion devices with useful applications; superconductors, insulators, catalysts, magnets, optics, lasers, and ion conductors (batteries and fuel cells) are just a small sampling of the types of valuable technologies that have been developed with the aid of solid state chemistry.

1.1.3 Nanoscience

Just as the vast majority of the research that will be presented in this dissertation can be classified as belonging to the investigation of solid state crystalline materials, so too can it aptly be described as a foray into the broad field of nanoscience. Nanoscience pertains to the investigation of materials within a limited size scale, and the unique (and sometimes peculiar) phenomena and properties associated with those limitations. Nanoscience or nanotechnology[11] entails materials that are within the scale range of between one and one hundred nanometers, where a nanometer (nm) is one billionth of a meter (10^{-9}). A common analogy to the size comparison between a nanometer and that of a meter is the size of a marble to that of the Earth. Nanoscience in general has been an extremely popular and fast-growing field the last half of the 20^{th} century, mainly due to the fact that it represents the convergence of the major branches of the natural sciences; physics, chemistry, and biology. While the largest impetus for the development of nanoscience and nanotechnology has been the goal of miniaturization, perhaps more intriguing are the additional applications which hold the potential to revolutionize practically every aspect of our daily lives from medicine to electronics to energy production.

1.2 Supramolecular Chemistry

" Supramolecular chemistry is a highly interdisciplinary field of science covering the chemical, physical, and biological features of the chemical species of greater complexity than molecules themselves…It's roots extend into organic chemistry and the synthetic procedures for molecular construction, into coordination chemistry and the metal ion-ligand complexes, into physical chemistry and the experimental and theoretical studies of interactions, into biochemistry and the biological processes that all start with substrate binding and recognition, into materials science and the mechanical properties of solids. A major feature is the range of perspectives offered by the cross-fertilization of supramolecular chemical research due to its location at the intersection of chemistry, biology, and physics."

Jean-Marie Lehn[12]

1.2.1 History and Nature

Supramolecular chemistry[13-15], or as defined by Lehn[12] as chemistry beyond the molecule, is the study of weak noncovalent interactions which arise between two or more separate molecular entities. The foundation of supramolecular chemistry lies squarely in the synthetic chemist's desire to achieve the level of complexity and functionality displayed by nature itself. Foremost, supramolecular chemistry in the context of both nature and the laboratory deals with the concept of molecular recognition. Molecular recognition is responsible for the existence of all complex chemical systems, not least of which is life itself. The manner in which two complimentary strands of DNA intertwine to form its characteristic double helix is a classic (and beautiful!) example. The way higher order (tertiary) structures of proteins can consistently and spontaneously regenerate from their primary structures is another. While this supramolecular chemistry developed by nature has existed for millennia, our ability to mimic nature and construct

interesting supramolecular systems of our own is relatively infantile. It has only been since perhaps the turn of the last century that we have even thought of matter on terms that could be considered reconcilable with supramolecular chemistry. The works of Ehrlich[16] (receptors and binding) and Fischer[17] (lock and key molecular recognition) were seminal to the development of the this field.

1.2.2 Noncovalent Interactions

In dealing with the chemistry of molecules, the nature of the chemical bond is paramount. Seventy years ago, in his seminal and still influential masterpiece, Pauling[18] put forth the collective ideas of the time regarding what exactly a chemical bond might be as well as to delineate their importance in governing the observed properties of molecules. It is of the utmost importance that the synthetic chemist has some grasp of the nature of these interactions, if one wishes to manipulate them for the sake of molecular synthesis. Simply put, molecular synthesis is the breaking of these bonds followed by controlled rearrangement of atoms concluded only by the reformation of new, strong interactions that define the molecules. Analogous to the manipulation of covalent intramolecular bonds in the endeavor of molecular synthesis, is the need to understand and manipulate the noncovalent intermolecular interactions (supramolecular synthesis) responsible for the association of molecules in supramolecular assemblies. While Pauling classified three categories of chemical interaction which he grouped into three bond types (electrostatic, covalent, and metallic) and focused heavily on covalent intramolecular bonds, he also addressed the idea of a hydrogen bond, which inspired much of the

groundbreaking chemical research that would lay the foundation for the development of the field of supramolecular chemistry.

The hydrogen bond is easily the most important of all the noncovalent interactions found in supramolecular assemblies as it provides a robust and perhaps more importantly directional interaction that can be harnessed for the rational synthesis of complex supramolecular architectures. It is however, only one of many different interactions to be classified as noncovalent (Table 1.1). Generally, noncovalent interactions run the gamut from being attractive to being repulsive in nature, and can range in strength from extremely weak to rivaling a weaker covalent bond. While any one noncovalent interaction may be rather weak, the key to supramolecular chemistry lies in the principle that it is extremely rare to observe a single interaction in a species. Rather the formation of a supramolecular entity is the result of the concerted interplay of many noncovalent interactions simultaneously.

Table 1.1 Common noncovalent interactions.

Interaction Type	Energy (kJ/mol)	Examples
Ion – Ion	100 - 350	$Na^+ Cl^-$; complex ions; organic ions
Ion – Dipole coordinate covalent bond M – L (M = transition metal; L = Lewis base)	50 - 200	Coordination complex; coordination polymer; Crown ethers binding metal cations
Dipole – Dipole	5 – 50	Solid – state organic carbonyls
Hydrogen Bond D-H···A	4 – 120	DNA double helix; Secondary/Tertiary protein structures
π – π Stacking face-to-face and CH··· π	0 – 50	Graphite; DNA double helix; Benzene herringbone pattern
van der Waals - London dispersion - exchange-repulsion	< 5	Noble gases; Inclusion compounds

1.2.3 Supramolecular Isomerism

A phenomenon of molecular chemistry that is closely paralleled in supramolecular chemistry is the concept of isomerism. In molecular species the ability of a compound (or element in the case of allotropes; diamond, graphite, fullerenes, and carbon nanotubes) to exist in multiple forms is a commonly identified occurrence. On the molecular level, structural isomerism (sometimes referred to as constitutional isomerism) is the existence of more than one compound with the same molecular formula. In the context of supramolecular assemblies, and in particular polymeric network structures (e.g. metal-organic materials), the concept of supramolecular isomerism is extremely salient. Zaworotko has defined supramolecular isomerism as the existence of more than

one type of superstructure for the same molecular components or building blocks.[19, 20] That is to say, two or more architectures constructed from identical metal ions and ligands, but arranged in unique manners (Fig. 1.2).

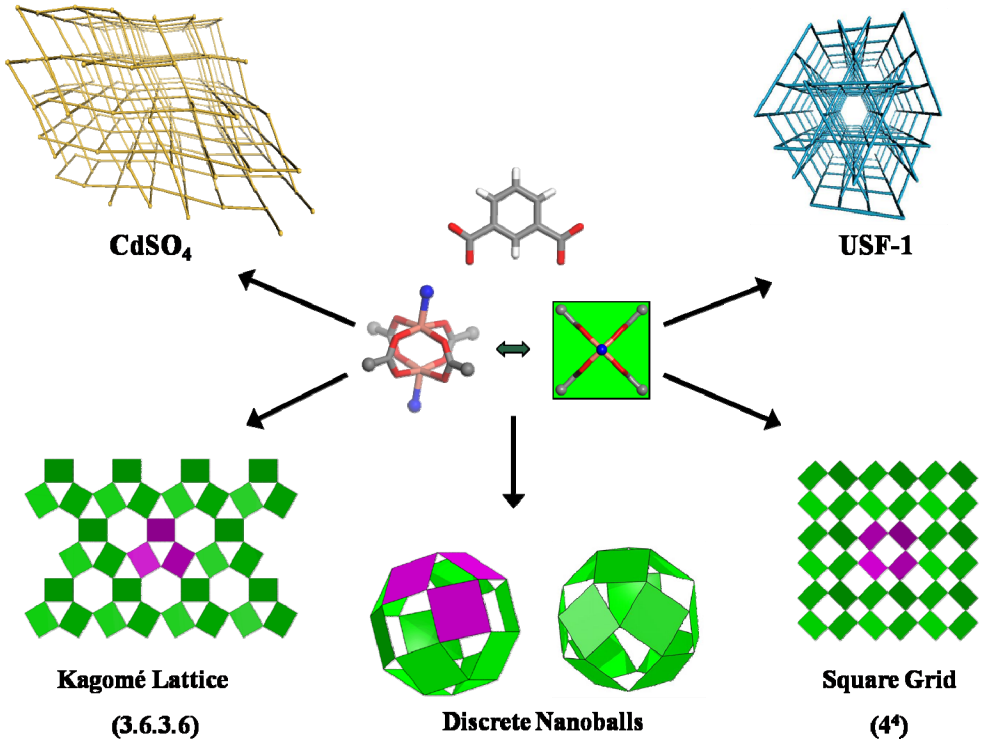

Figure 1.2 Schematic illustrating the concept of supramolecular isomerism. Several distinct supramolecular architectures are possible from the same molecular components.

In observing the possibility of isomerism at the supramolecular level, and interpreting it in relation to isomerism at the molecular level, Zaworotko also identified several forms of supramolecular isomerism; when the same components lead to distinct architectures for the superstructure (structural), when the use of flexible ligands results in networks that can be considered topological equivalent while the ligands adopt unique orientations (conformational), when the superstructure has the ability to exist in

interpenetrated (interwoven) or non-interpenetrated forms, or interpenetrated to varying degrees and types of interpenetration (catenane), or finally when two superstructures composed of the same components are constructed into enantiomorphic frameworks which are chiral (optical). Supramolecular isomerism represents both a blessing and a curse from the vantage point of controlling supramolecular structures. With an assortment of possible structures for the same building blocks, it may be difficult to elicit the overriding factors that dictate final structure, hampering our ability to control, on the supramolecular level, the architectures of the materials we make. Conversely, the susceptibility of these assemblies to the phenomenon of supramolecular isomerism will inherently lend itself to a dramatic amplification of the diversity in what may be possible for us to synthesize.

1.3 Crystal Engineering

"…crystal engineering, which is defined as the understanding of intermolecular interactions in the context of crystal packing and in the utilisation [sic] of such understanding in the design of new solids with desired physical and chemical properties…The almost perfect alignment of molecules in an organic crystal results usually in highly predictable physical and chemical properties which in turn justify efforts at crystal engineering."

Gautam R. Desiraju[21]

1.3.1 History and Scope

Crystal engineering[21-24] is the rational understanding of the influence noncovalent interactions have on the crystal packing of molecules in the crystalline state, and the attempt to parlay that understanding into a high level of control over the solid-state

structure of materials. If we are to realize Feynman's dream of being able to exquisitely control the arrangement of atoms (or molecules) at the most precise of levels then we must have a comprehensive understanding of all the factors which influence the materials' structure. It is only when we have complete control over the structure of matter, that we will be fully able to dictate the properties of those materials. As it is described here, it is clear that crystal engineering can be viewed as simply the solid-state manifestation of supramolecular chemistry and that many of the principles remain the same.

The term crystal engineering was first used by Pepinsky[25] in terms of crystallography, but perhaps the first use of the term in a manner that is on par with its use today was by Schmidt, who used crystal engineering in relation to topochemical reactions. In the 1970's, Schmidt[22] was studying the photochemical dimerization of olefins (such as cinnamic acids), and came to the realization that the nature of the crystal structure, in terms of crystal packing, was essential to the materials ability to react in the solid state. Whether a molecule was imbued with the functionality necessary for the reaction to take place is not the only criteria for the reaction to proceed in the solid state; of equal importance is *how* the molecules are arranged with respect to one another in the crystal. In light of this understanding, Schmidt proposed a new way of thinking about the crystal in which he aimed to be able to control the arrangement of molecules in the crystal structure so as to control their supramolecular reactivity and termed this endeavor crystal engineering.

In the later part of the 20th century Desiraju[21, 26-42] and Etter[43-52] were largely responsible for extending the field of crystal engineering. Desiraju extensively studied the presence and influence of weaker noncovalent interactions, such as CH•••π and CH•••X interactions, in the crystal structures of small organic molecules. Etter was largely responsible for investigating the weaker noncovalent interactions observed in the crystallization of two or more different molecules into a single crystal and laid the foundations for the growing field of cocrystallization, before her untimely death.

1.3.2 Cambridge Structural Database

In parallel with the increasingly more powerful X-ray diffraction detectors and computer software used to process diffraction data and subsequently solve crystal structures has been the advent of another tool which has quickly become indispensible to the modern crystal engineer. The early adoption of databases designed to store, and more importantly, easily retrieve the crystallographic data of a large number of crystal structures has been paramount to the success and rapid growth of this fledgling field. These databases provide the capability for the crystal engineer to survey a large segment of the known crystal structure population in a relatively short amount of time where ultimately they can contribute to the ability of recognizing patterns and discerning trends. The ability to recognize and then be able to exploit these patterns in the design of new crystal structures is essential to the goals and *modus operandi* of crystal engineering.

Today there are several unique databases which are maintained and updated periodically with newly published crystal structures. The Inorganic Crystal Structure

Database (ICSD)[53] is composed of nearly 120,000 purely inorganic structures which have been peer-reviewed, including over 1,400 crystal structures of the elements. The Protein Data Bank (PDB)[54] is a world-wide consortium of published 3D crystal structures of proteins and includes polypeptides and polysaccharides composed of at least 24 residues. The Nucleic Acid Database (NDB)[55] is a repository of 3D structural information pertaining to nucleic acids. There are even databases devoted to structures which have been elucidated solely from powder diffraction data, such as the one maintained by the International Centre for Diffraction Data (ICDD).[56] However, the standard bearer for the field of crystal engineering is easily the CSD.

The Cambridge Structural Database (CSD)[57] is the world's preeminent repository for small molecules (i.e. excluding large biomolecules) containing organic carbon atoms. This would include the types of molecules which fall into the classifications of small organic molecules, coordination compounds (metal-organic materials), and organometallic compounds. Additionally, the structures contained in the CSD were determined from a variety of methods including single crystal X-ray diffraction, powder X-ray diffraction, and neutron scattering. The CSD also retains other pertinent data related to the crystal structure (atomic coordinates, angles, bond distances, etc.) such as chemical information, crystallographic information (spacegroup, X-ray experimental conditions, R-factor), and even bibliographic information detailing where the crystal structure was originally published, all which can be useful to the crystal engineer.

To date the CSD contains nearly half a million crystal structures and is fully retrospective to 1923. Furthermore, in confluence with the adoption of X-ray

crystallography for routine structural analysis and identification in the chemical sciences, the CSD has enjoyed exponential growth rates over the last four decades (Figure 1.3).[58] From the graph we can see clearly that the average number of crystal structures published has increased drastically over the years; the 1970's (~ 2,400), the 1980's (~ 6,300), the 1990's (~ 13,400), the 2000's (~ 28,400). What cannot be easily established however, from this graph is the nature of the materials whose crystal structures were determined.

A closer examination reveals that while the majority of the crystal structures added to the CSD in the 1970's and 1980's were small organic molecules, recently there has been a trend of predominately "inorganic" MOMs and organometallics. Out of the

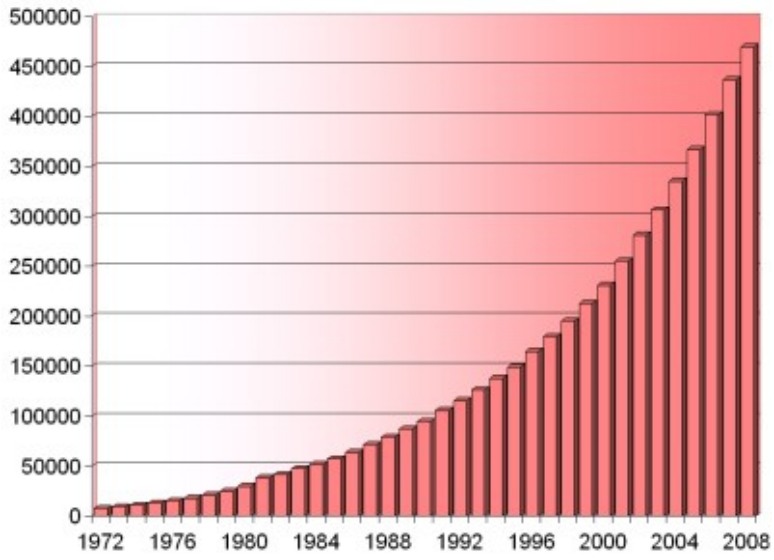

Figure 1.3 Exponential growth of the Cambridge Structural Database since 1970.

494,228 structures deposited in the CSD, only just over 200,000 (~ 42 %) are considered purely organic. This dominance of the CSD by inorganic compounds, while a relatively

recent event, is also exposed by the fact that the peer-reviewed journal with the highest number of structures contributed to the CSD is *Inorganic Chemistry*. The wide utilization of the CSD by those working with crystal structures has also been facilitated by the adoption of a standardized data format, the Crystallographic Information File or CIF[59], which is designed to be both computer and human readable and easily transferred electronically between individuals. The CIF format is supported by the International Union for Crystallography (IUCr)[60], and is the standard data file used by the majority of peer-reviewed journals which publish crystal structures.[61]

1.3.3 Crystal Engineering vs. Crystal Structure Prediction

Briefly, I believe it is important to clarify the seemingly mundane albeit critical difference between the conceptual ideas of crystal engineering (i.e. the design of crystalline solids) and that of crystal structure prediction[19, 62-70]. Crystal structure prediction is the more precise exercise of the two, and entails the *ab initio* determination of the precise crystallographic data (including space group, cell parameters, etc.) and exact packing details to be observed in a particular crystal structure. To achieve this there must be a high level of understanding regarding the molecular recognition features of small molecule compounds and in turn an understanding of how these molecular recognition events will influence crystallographic symmetry operations (leading to space group determination). While great strides have been made in the area of crystal structure prediction, in general we are still unable to fully achieve this endeavor. Currently, much work centers on the concept of analyzing a molecule and attempting to optimize how it close packs. This involves computer simulations and energy minimization, and can be

very useful in some simple instances. However, when dealing with flexible of relatively convoluted molecules these methods often fail.

Crystal engineering on the other hand, is concerned with the supramolecular synthesis of solid-state structures. It aims to achieve reliable control over network structures and network prediction. The endeavor of crystal engineering is to generate a design and then implement that design, for the (supramolecular) synthesis of novel materials, and to do so with high fidelity. There has been some consternation among researchers over the use of the term crystal engineering, as some feel that what it defines does not truly represent engineering in the fullest meaning of the word. However, these individuals are applying their own interpretation of what some definition should mean to a concept that has already clearly been defined. To then decry that the subject matter does not hold up to what your expectations of it are, while it clearly accomplishes the goals delineated by its originators is, I believe, somewhat fatuous.

1.4 Metal-Organic Materials

"…'Tis but thy name that is my enemy. Thou art thyself, though not a Montague. What's Montague? It is nor hand, nor foot, nor arm, nor face. O, be some other name belonging to a man. What's in a name? That which we call a rose by any other word would smell as sweet…"

William Shakespeare, Romeo and Juliet, (Act II, Scene ii)[71]

Metal-organic materials, or MOMs (Fig. 1.4), is an idiom adopted to represent a very broad and encompassing class of materials comprised of metal moieties and organic

molecules which act as ligands. The name was chosen to be as general as possible, specifically because it is meant to include a rather large population of known and as of yet unknown compounds under a single definition. In these materials, the organic molecule is connected to the metal ion *via* coordinate covalent bonds, and thus MOMs are squarely within the realm of coordination chemistry. MOMs are exemplified by a diverse collection of compounds that can be either discrete or polymeric in nature. Currently, there is some consternation among active researchers in the field (and some outside observers) over the nomenclature used to describe the structures being investigated. In the case of polymeric or periodic structures, names such as coordination polymers (CPs), metal-organic frameworks (MOFs), porous coordination polymers (PCPs), and hybrid inorganic-organic materials have all been used to describe compounds which are essentially identical. When discussing discrete structures, such names as metal-organic polyhedra (polygons), molecular capsules, nanoballs, and molecular polyhedra (polygons) among several others have been used. The utilization of so many different terms to describe compounds that are so closely related has, at times, introduced confusion and ambiguity into the research field.

1.4.1 History and Relevance

Whereas compounds which could accurately be described as belonging to metal-organic materials have existed for several decades[72-85] going back to Alfred Werner (1866-1919) and the establishment of coordination chemistry, it has only been since the early 1990's that MOMs have garnered broad attention from the scientific community.

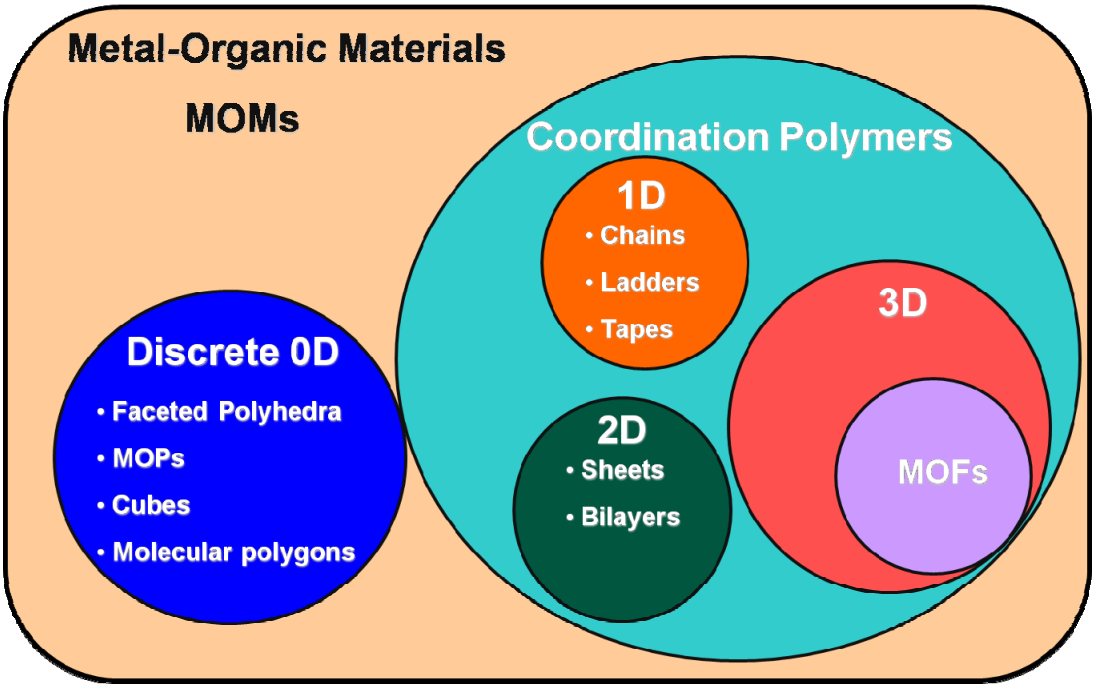

Figure 1.4 The universe of metal-organic materials.

This renewed and increased interest may be due to several factors, chief among which would be that they are prototypal for a diverse range of materials that are amenable to the design strategies of crystal engineering. Additionally, MOMs are inherently modular in nature, they can be synthesized in "one-pot reactions" through self-assembly making them facile to prepare, and quite often they are very aesthetically pleasing adding to their interest. Typically, MOMs are crystalline compounds, making the analysis of structure-property relationships feasible for these materials. It is the very fact that MOMs represent a diverse class of crystalline compounds that are capable of being crystal engineered to fine-tune their structural features and in turn investigate the effect on observed properties that make MOMs such attractive targets for materials chemists.

In the early 1990's the resurgence of metal-organic materials (coordination polymers) was made possible by the influential works of R. Robson[86-98], M. Fujita[99-104], and S. Kitagawa[105-113] among others[114-126]. These researchers utilized the so-called "node and spacer" approach to generate coordination polymers *via* the coordination of linear ditopic organic molecules to transition metal cations. The materials that they produced could be discrete (0-periodic molecular cages), 1-periodic (chains, ladders, etc.), 2-periodic (layers or bilayers), or 3-periodic (i.e. diamondoid, Prussian blue, etc.) networks. One common thread among the work of these researchers was that they all utilized single transition metal ions as the nodes and multi-topic pyridyl type ligands in the construction of their frameworks. They judiciously selected transition metals that adopted square planar, tetrahedral or octahedral coordination geometries and paired them with linear bridging ligands to generate the extended structure. Early on it was apparent that these materials were to have interesting properties that could be exploited for numerous potential applications, especially such properties as magnetism and porosity. It was a direct goal of these early researchers to develop materials with the capacity to enclathrate small organic molecules, whether for chemical sensing, separations (size and shape exclusion), or storage applications. However, a particularly daunting drawback to these early MOMs was the observation that generally speaking, materials constructed from single transition metal ions and bridging multi-topic pyridyl-type ligands were insufficiently stable to the removal of solvent and guest molecules *in vacuo*, sometimes resulting in the collapse of the overall structure. This reality hampered the progress of

these materials' potential applications and directly contributed to the development of a new strategy for the fabrication of metal-organic materials.

A second generation of MOMs[19, 63, 127-140] was ushered in upon the adoption of multiple metal clusters as the nodes of frameworks by Yaghi and co-workers. These multiple metal clusters were still predominately based on transition metals, but now involved ligands (i.e. carboxylic acids) capable of bridging the metal ions together into stable complexes. In fact, these new nodes were based on well known discrete metal-organic complexes (i.e. copper acetate, Basic zinc acetate, etc.) where the original monocarboxylic acid is replaced with a ligand containing multiple carboxylic acids and capable of bridging the separate nodes. With the use of multiple metal clusters, the robustness of the structures was enhanced ultimately resulting in materials that were capable of being evacuated *in vacuo* which in turn contributed to their ability to be successfully probed for potential application. The realization that discrete and extended crystalline compounds were now obtainable, both as designer materials and robust in nature led directly to an explosion is research activity and a bevy of research groups interested in the various applications of these materials. As a powerful visual illustration of this rapid growth, Figures 1.5 depicts the number of results obtained when the query "coordination polymers" and "metal-organic frameworks" was entered and searched in the ISI Web of Science database.[141]

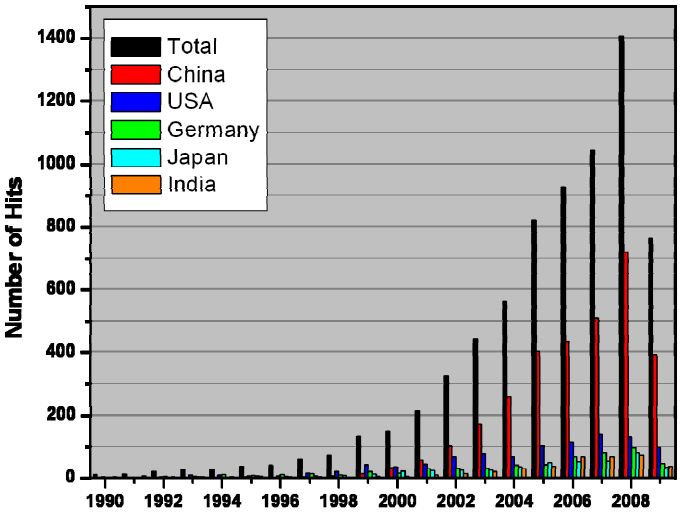

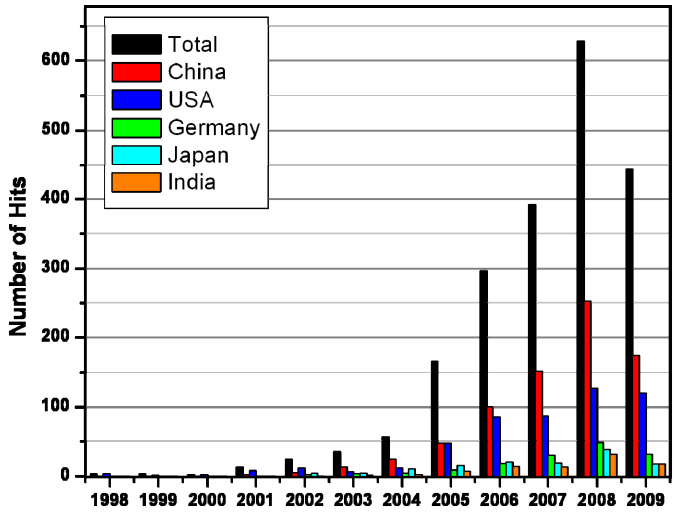

Figure 1.5 Number of results for the search query "coordination polymers" (**top**) and "metal-organic frameworks" (**bottom**) from ISI's Web of Science database, broken down by country.

1.4.2 Design Principles

Perhaps the most imperative aspect of metal-organic materials is the perception that they can be designed from first principles. While absolute control over the *exact crystal structure* may remain elusive, we do currently possess the ability to direct the

general structural motif of a great many MOMs of interest. Thus, it is often possible to dictate the structural details (topology, cavity size, pore shape, pore dimensions, etc.) of a particular material, by taking advantage of the modular nature of these materials. Once a blueprint has been established for the generation of a particular framework structure (topology), it is often possible to then amend the reaction conditions so as to incorporate new, different components (metal ions; organic ligands) that result in the same framework structure, albeit with augmented dimensions or functionality.

As the field of metal-organic materials progressed, several reliable methods of designing these materials emerged. The most obvious, unifying theme which connects these separate design strategies is the fact that they are all geometrical in nature. As we shall unveil in the following sections, each strategy involves the interpretation of the frameworks as being constructed from smaller geometrical shapes. The generation of new materials then becomes an exercise in isolating chemical moieties that can adopt particular geometrical shapes and determining how best to combine these structures into the overall frameworks.

1.4.2.1 Node and Spacer Approach

The foundations for all that would follow, in regards to designing metal-organic materials, lie with the seminal works of A. F. Wells[142-149], who introduced a simple and practical interpretation of periodic inorganic crystal structures. In Wells' interpretation, individual metal ions were treated as nodes which were connected *via* linear spacers that represented bonding. An essential caveat of this "node and spacer" (Fig. 1.6) approach to

the interpretation of inorganic crystal structures is that the resultant network topology is contingent on the geometry and coordination environment of the nodes alone, while the spacer unit is simply a linear bridge between adjacent nodes. Therefore, if one wished to target a diamondoid topology, it would be prudent to adopt a node that conforms to a tetrahedral geometry. Similarly, if one sought a square grid structure, then they should adopt a square planar node.

Wells' node and spacer approach can immediately be used in the design and interpretation of metal-organic materials. As with purely inorganic compounds, the metal moiety of the MOM is treated as the node, while in lieu of the bond the organic moiety (ligand) is regarded as the spacer. By utilizing transition metals with easily controllable coordination geometries and rigid rod-like bridging ligands (i.e. 4,4′-dipyridyl), it became feasible to design and fashion a host of materials with unique topologies. This method demonstrated for the first time the effectiveness of breaking an extended periodic structure down into unique nodes and determining how those nodes are connected, for the design of novel materials. Previous to this point, the node and spacer approach was merely a method of interpreting a structure which had already existed, but now the same principles could be applied to the construction of new motifs. The adoption of the "node and spacer approach" leads directly to the reemergence of coordination polymers, now as compelling targets for crystal engineers.

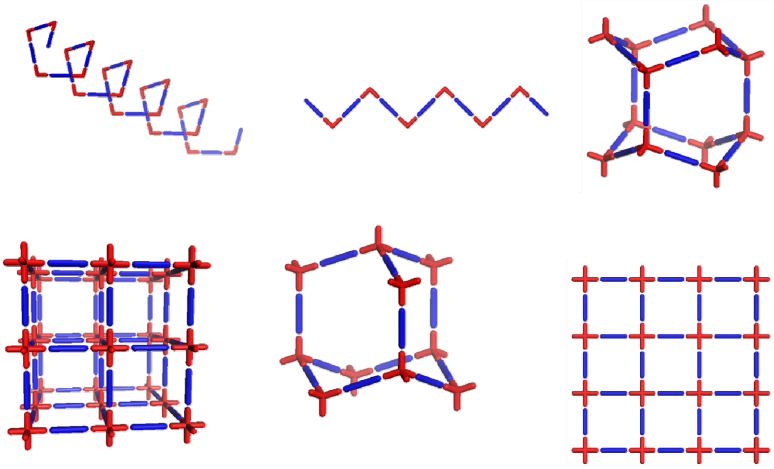

Figure 1.6 The node and spacer approach to metal-organic materials. Nodes of various coordination geometries (red) can be combined with linear spacers (blue) to generate a range of topologically distinct networks. **Top:** *Left & Center* Angular 2-connected nodes can lead to 1-periodic helices and chains. *Right* Hexagonal diamond (Lonsdalite) constructed from tetrahedral nodes. **Bottom:** *Left* Octahedral nodes generate Prussian Blue analogues. *Center* Cubic diamond constructed from tetrahedral nodes. *Right* 2-periodic square grid layers can be accommodated by adopting square planar nodes.

1.4.2.2. Secondary Building Units

Whereas the first incarnation of the "node and spacer" approach toward the design and synthesis of metal-organic materials dealt almost exclusively with single transition metal ions as the so-called nodes, another design strategy emerged not long thereafter which focused upon the utilization of relatively larger scale, multiple metal clusters as the structural building unit in both discrete and extended MOMs. In this design strategy, known discrete complexes composed of multiple metal centers bridged by appropriate ligands (typically carboxylates) were identified and classified based upon their geometrical characteristics. In this method, the terminating monocarboxylates which hold the metal clusters together are seen as possible points of extension, where two or more of these clusters could possibly be linked if bridged by the appropriate polycarboxylate.

Essentially, this design strategy allows the crystal engineer to scour the literature for examples of known molecular complexes that adopt particular geometrical patterns and then contemplate connecting these geometrical shapes together into networks by replacing the original monocarboxylates with a suitable polycarboxylate. Yaghi and co-workers were the first to describe this new strategy and named the new clusters secondary building units (SBUs)[150-153] (Fig. 1.7) borrowing the term from the study of zeolites[154-156].

The implementation of the SBU design strategy has been important to the maturation of the field for several reasons. The most apparent contrast with the node and spacer approach is one of scale. While the node and spacer method does not explicitly demand single metal ions (and we shall see that tenets of this methodology are still responsible for the interpretation of structures composed of SBUs, as the SBU is simply treated as the node), in practice those who adopted the node and spacer approach early on in the development of MOMs typically utilized single metal ion nodes in their frameworks. With the inclusion of multiple metal clusters as the nodes upon which the frameworks are based, it was necessarily going to result in nodes which are relatively larger in size than their single metal ion counterparts. In the case of a single transition metal ion, the size of the node is only the atomic radius of the metal in question, whereas in the situation of a multiple metal cluster bridged by multiple carboxylates the size of the node can easily approach one or more nanometers (tens of ångströms). When incorporating multiple metal nodes which are inherently larger, it follows that the scale of the framework itself (dimensions of channels, volume of cavities, etc.) will also be augmented.

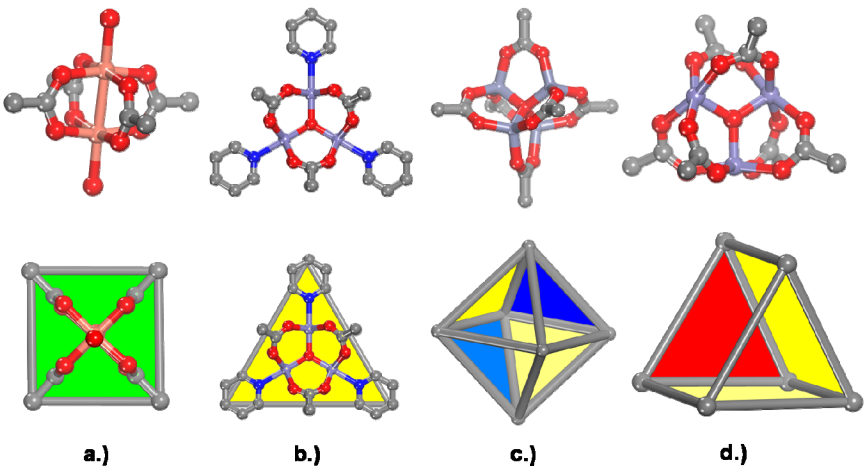

Figure 1.7 Examples of commonly observed Secondary Building Units (SBUs) used in metal-organic materials. a.) Cupric acetate exists as a dimetal tetracarboxylate square paddlewheel cluster with formula $[M_2(O_2CR)_4L_2]$ (M = transition metal, L = axial ligand) which can be viewed as a square. Basic Chromium(III) acetate, a μ_3-oxo trimetallic hexacarboxylate with molecular formula $[M_3O(O_2CR)_6]$ can be interpreted as either a triangle (b) or as a triangular prism (d). Basic Zinc acetate, which can be interpreted as a octahedron is a μ_4-oxo tetrametallic hexacarboxylate cluster with molecular formula $[M_4O(O_2CR)_6]$.

In addition to the necessary increase in scale, the implementation of SBUs can also contribute to an increase in the robustness of a framework. One common observation made about the use of SBUs in lieu of single metal ions was the relative increase in thermal stability. When Yaghi and co-workers began to investigate the use of SBUs in the generation of MOMs, they also discovered that the use of these rigid building blocks could often preclude framework collapse, increasing the likelihood that a framework could be made to undergo loss of guest and solvent molecules *in vacuo*, which in turn increases the probability that the materials could be activated (as-synthesized occupants evacuated from within the framework cavities) due to the enhanced rigidity demonstrated by these MOMs.

Finally, in some instances, the use of secondary building units can have the added benefit of superior structural control. In many instances, the geometry of a particular SBU can be either extremely hard to isolate with a single metal ion because it prefers a small number of other more common coordination geometries, or virtually impossible to achieve as is the case for SBUs that adopt higher coordination numbers. By adopting SBUs the crystal engineer is able to achieve some geometries that entail high coordination numbers as well as unique geometries that are just not feasible in the case of single transition metals. This provides SBUs with a distinct advantage in that they can sometimes lead to framework structures that would previously be unattainable. Perhaps more importantly however, the method of secondary building units not only makes additional types of structures possible, it also demonstrates how to obtain those structures in a rational manner.

1.4.2.3 Molecular Paneling

Another design strategy, especially for the generation of 0-periodic discrete architectures, is based upon metal-directed self-assembly of so-called molecular panels. This design strategy is related to that of SBUs, in that it aims to rationally control the network structure which is obtained by taking advantage of the built in coordination geometry of the metal atoms. But whereas the principles of the secondary building unit strategy teach us to isolate known multiple metal clusters of specific geometry and then determine the most reliable methods of linking those structures together using *linear* connectors, the

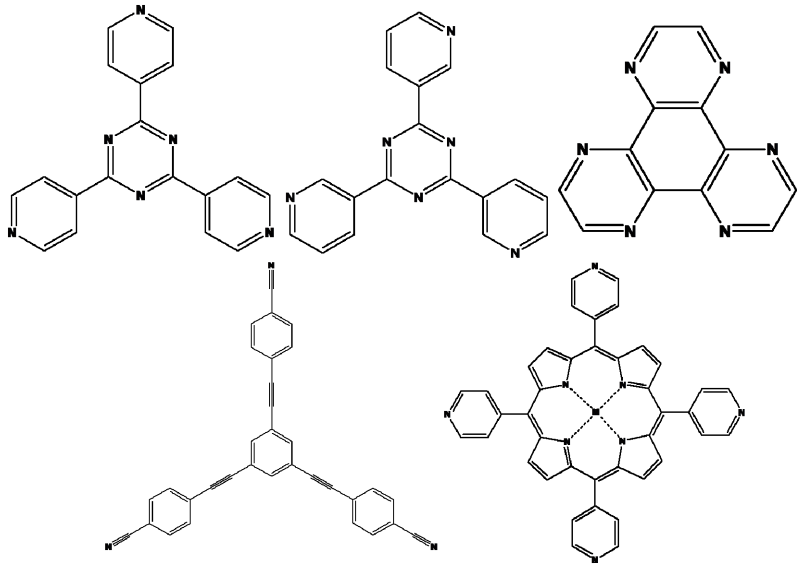

Figure 1.8 Common molecular panels.

design strategy of molecular paneling[104, 157-164] involves single transition metal ions (with predictable or controllable coordination geometry) as bridges by *planar* exo-multidentate organic molecules (i.e. molecular panels, Fig. 1.8).

Typically the metal ions are chosen to be as reliable and facile to prepare as possible, removing much doubt over the possible outcome of the reaction. In many cases the Pd(II) ion, with its ubiquitous square planar geometry, is adopted in the *cis*-protected form, which thereby guarantees a nearly perfect 90° orientation for the coordination of the molecular panels. The angle here is important because it represents a "turn" with respect to the orientation of subsequent molecular panels within a series. This "turn" is what is required to generate a convex hull seen in discrete molecular structures (Fig. 1.9). One salient feature to point out regarding molecular paneling is the realization that when linking planar multidentate ligands *via* coordination to metal ions (vertex-sharing as

opposed to edge-sharing) the structure will inherently be divided into regions of open windows and closed faces (the molecular panels themselves) so that any discrete structure fabricated based upon this strategy will have small openings possibly permitting access to the hollow interior of the structure.

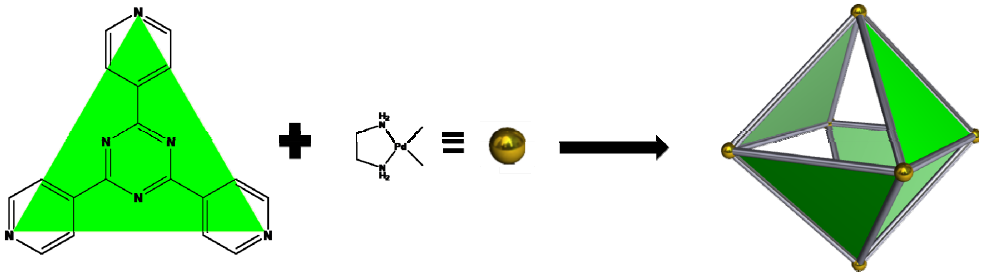

Figure 1.9 Schematic depicting the design principle of molecular paneling. Here a particular molecular panel in the shape of a triangle (2,4,6-tris(4-pyridyl)-1,3,5-triazine) is combined with the approprtiate metal moiety to generate octahedral M_6L_4 cages. To generate this descrete strucutre, a "turn" of ~90° is needed and so the use of *cis*-protected Pd(II) is a judicous choice.

1.4.3 Topological Analysis

Metal-organic materials represent an extremely diverse collection of possible compounds with an equally diverse assortment of potential structures. Additionally, as was seen in the previous section, they can be designed using any one of a number of strategies based principally upon geometrical concepts. Regardless of the design strategy employed, the underlying structure of the resultant MOM could span a truly immense range of possibilities, from simple 1-periodic chains to 3-periodic extended frameworks so complicated that they can only be deconstructed with the aid of computers and powerful graphic software. Therefore, some systematic method of analyzing the structures obtained will be needed so that we may be able to catalogue our results. And

just as we have seen that there is more than one way to design a MOM, we will find that there are indeed multiple methods of analyzing the structures that are produced. However what they all do hold in common is that are all, to some extent, based on the ideas of mathematical topology. Loosely this means that we are concerned merely with the connectivity of the nodes (in a topological sense, not necessarily a chemical one), and are *not* interested in the geometrical aspects of the framework (i.e. lengths, angles, etc.).

1.4.3.1 Wells' Notation

Perhaps the simplest method of analyzing metal-organic materials topologically is a system that was first described by A.F. Wells.[142-148] Wells, who had already deconstructed crystal structures into nodes and spacers which are then connected into a network (or net), found it rather easy to describe these structures from a topological standpoint. In particular, Wells looked to identify polygons that were generated by the linking of the nodes and spacers. He then introduced terminology to represent both the types of polygons and their numbers, which were incident to each node or vertex. By type of polygon he simply meant the number of sides (n-gon) and did not restrict them to be *regular* (same length edges, identical angles). In Wells' notation[149] we write (n, p) where n is the number of sides in the n-gon and p is the number of these n-gons intersecting at the same node. The three *regular* plane nets, shown in Figure 1.10, are a nice place to start in understanding Wells' notation.

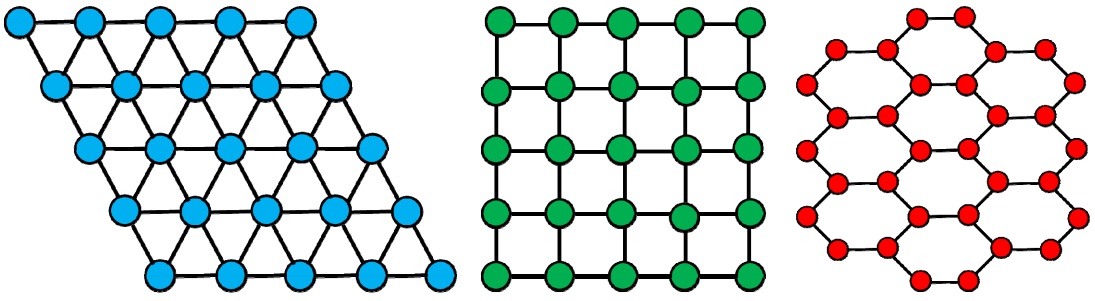

Figure 1.10 Schematic depicting the only three *regular* plane nets; (3,6) triangle tiling, (4,4) square grid, and (6,3) honeycomb.

If we evaluate the effectiveness of an analysis method by its ability to distinguish between two closely related albeit unique nets, the notation created by Wells is rather straightforward and works perfectly well for simple structures, especially those that are constructed from only a single type of node (uninodal).[165] It should be mentioned that Wells' methodology does not explicitly require the net to be uninodal, and in fact the notation is equipped to deal with binodal[166, 167] nets quite easily using either the form $(^{m}_{n}, p)$ or $(n, ^{p}_{q})$, but if we then extend the scenario to three or more unique vertices the notation becomes very convoluted. When we begin to delve into nets that are a bit more complex than the plane nets the method can quickly become entirely ineffective. It turns out that there are often many examples of topologically unique nets that can obey the same simple (n, p) notation, making another method of topological analysis, capable of discerning between these nets necessary.

1.4.3.2 Schläfli symbols

Another method of topological analysis used for crystal structures in general (and MOMs in particular) is the idea of *Schläfli symbols*. To explain how these symbols are derived, we will first need to be acquainted with some basic terminology borrowed from mathematical graph theory.[168, 169] The first convention that should be stressed is the use of the term *n*-periodic in lieu of the somewhat more common, but nonetheless incorrect *n*-dimensional. Individuals often use the terms 1-dimensional (1D), 2-dimensional (2D), or 3-dimensional (3D) to describe the number of directions a structure or network repeats. However this usage is incorrect for at least two reasons; in dealing with real world objects such as molecules and atoms it is obvious that the materials we are describing are in fact all 3D, but more precisely (and mathematically) it is incorrect because the word *n*-dimensional defines another meaning altogether. In the world of graph theory *n*-dimensional implies that the graph has an embedding (can be drawn) in three dimensional space. As it happens, *all* graphs are capable of being embedded in three dimensions and are therefore 3-dimensional. Better is the use of the term *n*-periodic in trying to describe the number of independent directions in which a particular net has translational symmetry.

A graph is a set of *vertices* (nodes) labeled *i, j, ...* and *edges* (spacer) which are simply line segments joining exactly two vertices (*i*, *j*). It is possible to have more than one edge defined between the same two vertices, as well as the case where there is a special type of edge between the same vertex (*i,i*) called a loop, but when a graph contains only one edge between any two vertices and no loops we call it a *simple* graph.

Next we can talk of a *path* or chain as a sequence of vertices ($x_1, x_2, \ldots, x_n$) linked by edges (x_1, x_2), (x_2, x_3), …, (x_{n-1}, x_n). A *circuit*, sometimes referred to as a cycle, is a closed path where the first and last vertices of the chain are identical, while a *ring* is a special circuit in which there are no shortcuts (Fig. 1.11). Finally, a graph is said to be *connected* if there exists at least one path between any two vertices. In crystal chemistry, and for the purposes of this dissertation, the term *net* shall indicate a periodic connected simple graph.[168]

When deconstructing a crystal structure we can assign individual atoms as vertices and the bonds between them as edges. In more complicated circumstances we may wish to define a cluster of atoms as a single node and some other abstract notion as the edge linking the vertices together. Once the vertices and edges have been well defined, it is then possible to assign to each *unique* (unrelated by symmetry) vertex a so-called Schläfli symbol. To achieve this we analyze the net for the presence of the *shortest cycles* as opposed to the *n*-gons identified for the Wells' notation. Since we are discussing cycles, we are limiting ourselves to closed paths that begin and end with the vertex in question. For a vertex that is connected to *n* other edges (*n*-connected in the parlance of chemistry, but not mathematics!) there will be $n(n-1)/2$ different angles formed by the incident edges. It is precisely these angles where a possible cycle will be located and thus this is also the number of cycles one can expect for each *n*-connected vertex.

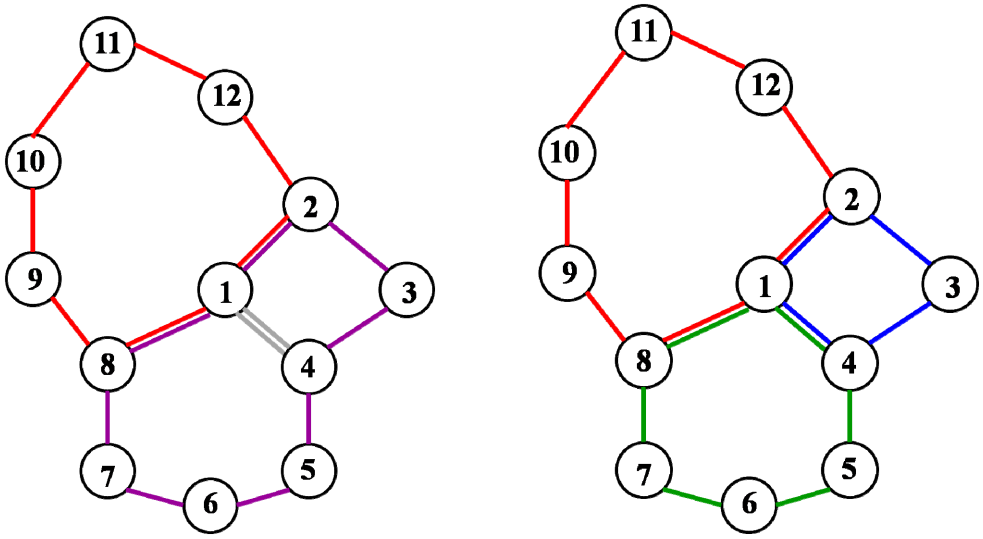

Figure 1.11 Schematic illustrating the concepts of cycles, rings, and short-cuts. **Left:** Both the red (1, 2, 12, 11, 10, 9, 8, 1) and purple (1, 2, 3, 4, 5, 6, 7, 8, 1) paths represent cycles. **Right:** The red cycle is also a ring, but the purple cycle has a **short-cut** (1,4) (grey in the left figure). However it can be broken down into two new cycles which are themselves rings (blue and green cycles).

In a 3-periodic connected graph there can be infinite number of cycles for a given vertex, and it is for this reason that we identify only the shortest such cycles for a given angle and ignore the remainder. This Schläfli symbol[170], sometimes referred to as a point symbol, takes the form $A^a.B^b.C^c.[...].N^n$ and is composed of the numbers $A< B< C,$ $...,<N$ which represent the length of the shortest cycle and superscripts *a, b, c, ..., n* which signify the number of each those cycles. Here $a + b + c + \ldots + m = n(n\text{-}1)/2$. Thus the 2-periodic regular plane tilings[171, 172] which were described previously by Wells' notation as (3,6), (4,4), and (6,3) can now be defined using Schläfli symbols as 3^6, 4^4, and 6^3 respectively. For another example we look back at Figure 1.11 above. In this simplified cartoon, the vertex labeled **1** has three adjacent *neighbors* and is therefore considered 3-connected. We would then expect a total of three angles and subsequently

three cycles to be generated from the corresponding edges, and indeed we do observe these three cycles. In order of shortest cycle we observe one 4-gon, one 6-gon, and one 7-gon making the correct Schläfli symbol for this vertex $4^1.6^1.7^1$, where 1 + 1 + 1 = 3 = total number of shortest cycles for the vertex. Typically we omit a superscript of one, thus making the symbol 4.6.7 for vertex **1.** The Schläfli symbol represents a marked improvement over that of Wells' notation, since it is equipped to deal with the common occurrence of more than one type of cycle (*n*-gon) meeting at a vertex. It is however, not without some drawbacks. There still exist some nets, which while they contain the same types and numbers of shortest cycles, remain topologically distinct. In these situations, Schläfli symbols fail to distinguish between the two nets.

1.4.3.3 Vertex symbols

A topological method closely related to Schläfli symbols, but which has been modified to better distinguish between nets that might have the same types and numbers of shortest cycles for a given vertex (and hence the same Schläfli symbol) is one that is based upon identifying the *shortest rings* occurring in the structure. This method, based solely upon the use of shortest rings, results in what is called a vertex symbol for each unique vertex. Vertex symbols are currently the favored method of topological analysis for metal-organic materials. In this notation, we write $A_a \bullet B_b \bullet C_c \bullet [...] \bullet N_n$ where *A, B, C, ..., N* represent the length of the shortest rings and *a, b, c, ..., n* represent the total number of those sized rings for that vertex. It is important to point out that the total number of coefficients (large numbers spaced by bullets) is always equal to the number of angles for an *n*-connected vertex so that for a 3-connected vertex the symbol would

resemble $A_a \bullet B_b \bullet C_c$ while for a 4-connected vertex we would expect $A_a \bullet B_b \bullet C_c\ D_d \bullet E_e \bullet F_f$. This notation is equally valid for higher coordination numbers but is somewhat less frequently used. In the case of 5-connected or 6-connected vertices we would have a symbol with 10 or 15 elements respectively, whereas with a 12-connected vertex (which is by no means unheard of) the vertex symbol would have 66 elements, much too many to be of any practical use to write out by hand.

There are also examples of topologically independent nets which are represented by identical vertex symbols for each of their unique vertices, but this is decidedly less common than that of the Schläfli symbol. In these circumstances we can go to another common method of topological analysis to distinguish between two closely related nets. For each unique vertex in a net we can determine its coordination sequence (CS) and topological density (TD_{10}). The coordination sequence of a vertex is simply a sequence or listing of the k^{th} topological neighbors $\{n_1, n_2, n_3, \ldots, n_k\}$ of a particular vertex. The k^{th} neighbor of a vertex is any other vertex where the shortest path between the two vertices is of length k (Fig. 1.12).

The topological density is simply the sum of the first k neighbors of a particular vertex, and while there is no set rule, we typically look at the first ten neighbors to sufficiently distinguish two vertices. A nice example showing how coordination sequences and topological density can help resolve the differences in two closely related nets is the case of diamond and Lonsdaleite. Lonsdaleite is the hexagonal form of diamond[173], which has only been observed naturally in meteorites that have fallen to earth.

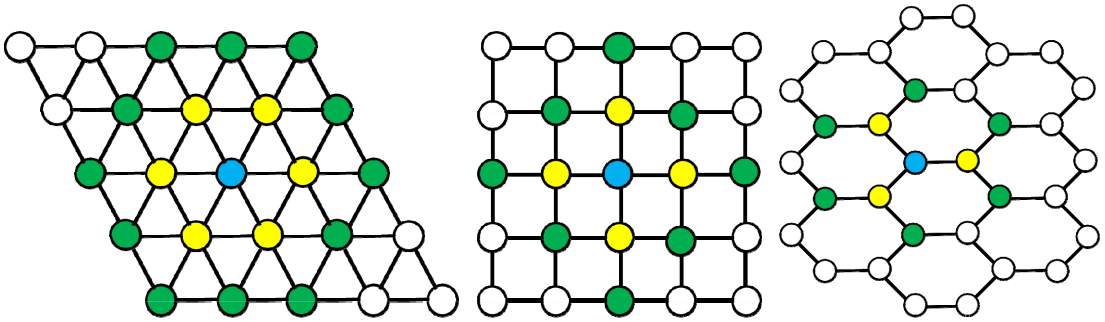

Figure 1.12 Schematic illustrating the concept of k^{th}-topological neighbors. The central vertex (blue) is directly adjacent to its first (nearest) neighbors (colored yellow) which have a shortest path length of 1 unit i.e. $k = 1$. The second neighbors (colored green) to the central vertex are those who have a shortest path length of exactly $k = 2$, and are themselves the first neighbors to a first neighbor of the central vertex. We note that the topological density decreases from left to right: $TD_2 = 18$, 12, and 9 respectively.

The high temperatures and pressures involved in a meteorite's descent from the heavens causes graphite in the meteor to transform into diamond, albeit retaining the graphite's hexagonal crystal lattice. Both diamond (cubic diamond) and Lonsdaleite (hexagonal diamond) have the vertex symbol $6_2•6_2•6_2•6_2•6_2•6_2$ for their one unique vertex. However, as illustrated in Table 1.2, their coordination sequences (CS) and topological densities (TD_{10}) are distinct. Unfortunately, there is no guarantee that two unique nets will not have identical coordination sequences, merely the fact that if their coordination sequence *is* different it must imply the two nets are indeed themselves different. A prominent example of two different nets which have the same CS would be the nets which underlie the structures of the two zeolites **RHO** and **LTA**.

Table 1.2 Comparison of the coordination sequence (CS) and topological density (TD_{10}) for diamond and Lonsdaleite nets.

k	1	2	3	4	5	6	7	8	9	10	TD_{10}
diamond	4	12	24	42	64	92	124	162	204	252	981
lonsdaleite	4	12	25	44	67	96	130	170	214	264	1027
Difference	0	0	1	2	3	4	6	8	10	12	46

1.4.3.4 RCSR and net enumeration

More recently, a universal system of nomenclature with which to identify and classify nets has been proposed and widely adopted. In this system each unique net is provided with an independent three letter symbol which is always presented in bold font and is modeled after the symbol names given to the various zeolite topologies. While the zeolite symbols were comprised of three capital letters in bold, the Reticular Chemistry Structure Resource (RCSR)[174] symbols are always comprised of lower case letters. In fact all but two of the zeolite codes have been adopted in the RCSR system, where capitalization is replaced with the identical albeit lowercase letters. In addition to the standard three lowercase bold letters, there is also the possibility of a net requiring an extension to its RCSR symbol name. These extensions allow closely related, but still topologically different nets to be given a name showing their relation. Some common extensions that can be amended to an RCSR symbol are; **–a** for an augmented net where the vertices of the original net are replaced with a cluster of vertices the shape of the original coordination figure of the vertex, **–b** for the binary (binodal) version of a net that was originally uninodal, **–c** for when a net undergoes catenation (interpenetration), **–d** for the dual of a particular net (when a net is self-dual the original nets symbol and the one

extended with a **–d** are both correct), and **–e** which is used to signify the so called edge net obtained by replacing each edge with a new vertex and then linking the new vertices to form a net. Along with the universal symbols which can be used to "name" a particular topological net, a searchable database has been developed that can be used to investigate nets and their relationships to one another. The RCSR Database[175] currently has over 1600 identified nets and includes such information as the space group (i.e. symmetry), unit cell parameters, vertices locations, and the natural tiling for the net, as well as exportable files which can be used to investigate the tiling in ***3dt***, a superb graphical program developed by Olaf Delgado-Friedrichs.[176]

1.4.4 Properties and Applications of Metal-Organic Materials

Metal-organic materials are clearly an intriguing class of compounds that very often represent entirely new forms of matter. They can be intelligently designed based upon first principles to include specific molecular components and to adopt particular topologies or superstructures, typically with high fidelity. Metal-organic materials are usually crystalline in nature, and are therefore amenable to precise structure solution. Additionally, MOMs can often be imbued with extraordinary levels of intrinsic symmetry and stunning beauty. All of these features make metal-organic materials attractive targets for solid state chemists, but even taken together they still fail to adequately explain the explosive growth the field has witnessed in the past two decades (Figs. 1.5 and 1.6). Perhaps the most significant aspect of metal-organic materials remaining, and the apparent motivation for this observed escalation in scientific interest, pertains to these materials physical and chemical properties.

The properties of metal-organic materials, and the ensuing potential applications, are both numerous and varied. It is the very nature of these hybrid materials, being composed of both metal ions and organic molecules, which make their observable properties so potentially diverse. Both the metal and the organic moiety can separately contribute to the materials observed properties, or in special circumstance, they can combine to result in the desired effect. On top of the fact that they contain metals, with all of the intriguing prospects that arise upon introducing those metals' properties into the final material, many MOMs are also extended frameworks with cavities whose shapes and dimensions can be tailored by the crystal engineer. Indeed, many MOMs, especially those constructed using SBUs, have been demonstrated to be permanently porous[153, 177-184], indicating that they are amenable to the removal of guest and or solvent molecules from within their cavities. With the ability to generate customized cavities and channels within a crystalline material with an extended framework structure, the crystal engineer can now contemplate the prospect of encapsulating new molecules in these chambers. Both the presence of metal ions, and to a lesser extent the incorporation of specific functional organic ligands, and the existence of made to order cavities provide for the majority of the properties sought after in MOMs.

Perhaps the single most sought after property of metal-organic materials is the sorption of gases[153, 179, 180, 185, 186] in general and that of molecular hydrogen gas[184, 185, 187-198] in particular. The storage of molecular hydrogen holds great potential for its use as a clean renewable energy source as a direct fuel or for its use in fuel cells. The U.S. Department of Energy (DOE) has established several guidelines such as sufficient weight

percent (2010: 2 kWh/kg, 6 wt %; 2015: 3 kWh/kg 9 wt %), percent volume (2010: 1.5 kWh/L; 2015: 3 kWh/L), and cost (2010: $4/kWh; 2015: $2/kWh) as well as other factors such as rate of refueling/release of H_2 and appropriate levels of safety in an attempt to direct research efforts in the area of hydrogen storage.[199] In terms of money (grants, centers of excellence, etc.), time, and effort (i.e. the number of different research groups tackling the same challenge simultaneously), hydrogen storage is by far the most invested potential application concerning metal-organic materials, and justly so, because if any material, be it a MOM or otherwise, should be demonstrated to sufficiently and efficiently demonstrate the outlined goals prescribed by the DOE it will truly revolutionize the world.

In terms of the presence of metal ions, perhaps the most obvious property which might be instilled into a MOM would be molecular magnetism.[108, 200-209] By introducing metal ions which are magnetically active, it should be possible under the correct conditions to synthesize materials that are themselves magnetically active, potentially leading to solid state magnets with fine-tunable magnetic responses. It is not sufficient however to merely include the so-called magnetic moment carriers, be they paramagnetic metal ions or open-shelled organic molecules which will act as ligands. Magnetism, as a cooperative phenomenon, requires an exchange between these magnetic moments, thus magnetism requires the moment carriers to be brought within proximity to one another, a feat which can be often be achieved in metal-organic materials.[200] To date the majority of magnetic MOMs have been synthesized utilizing paramagnetic first-row transition metals such as V, Cr, Co, Mn, Fe, Ni, and Cu. Additionally, it may also be possible to introduce

magnetic centers as the guests that occupy the open cavities of a MOM while the framework itself is essentially non-magnetic. Another interesting potential application concerning the magnetic properties of a particular MOM would be the ability to fashion a sensor based upon fluctuations in magnetic response that might be induced by the presence of various guest molecules.

In addition to magnetism, metal ions can also impart into the framework centers of catalytic activity[210-221]. Interestingly, one of the very first applications proposed for the crystalline metal-organic materials was their use as heterogeneous catalysts[90], which was quickly demonstrated in the case of cyanosilyation of aldehydes.[100] More so than simply the presence of catalytically active open metal sites where the catalytic process might take place, MOMs also hold the capacity to be useful catalysts through several other methods. First, the catalytic site might be incorporated into the strut of the framework *via* a metalloligand. It is also possible to encapsulate into the open cavities of extended MOMs either molecular species or larger clusters which act as the catalytic sites, as was eloquently demonstrated by Eddaoudi and co-workers[222] when they encapsulated a metalloporphyrin into the large cavity generated in one of their Zeolite-like Metal-organic frameworks (ZMOFs). Finally, in a small number of cases[213, 215, 223] porous MOMs have also been shown to act as catalysts without the aid of metal centers. Rosseinsky and co-workers[223] have demonstrated a situation in which an amino acid can be judiciously situated in a MOM such that it's carboxylic acid can remain uncoordinated and be selectively protonated with the use of HCl. This carboxylic acid is then able to act as a Brønsted acidic catalyst. The idea to take advantage of MOMs as new heterogeneous

catalysts was a lucid extension of the relationship they hold with zeolites, another class of solid state porous materials. Early on it was apparent that MOMs were analogous to the structures of zeolites, so that it was only reasonable to speculate that one of zeolites' most prolific characteristics and applications, namely catalysis, might also be an enticing prospect for metal-organic materials.

Another example of a property seen in MOMs which can be related to the presence of particular metals, at least in some instances, is the phenomena pertaining to several forms of emissivity (fluorescence, phosphorescence, and scintillation), broadly entitled as luminescence.[131, 133, 224-233] In addition to metal-based emission however, there is also the possibility of the luminescence originating from ligand-localized emission, metal-to-ligand charge transfer (MLCT), ligand-to-metal charge transfer (LMCT), or emission from guest molecules adsorbed into the cavities of extended MOMs. Luminescence properties in metal-organic materials are interesting both as an avenue of basic science directed towards understanding MOMs in general as well as the latent application of monitoring the modulation of observable luminescence phenomena in relationship to the uptake or release of specific guest molecules, i.e. sensing *via* luminescence.

As opposed to the influence of the metal component in the determination of the observed physical properties of metal-organic materials, the nature of the organic spacer, both in its own functionality and in the way it dictates the dimensions and shape of the cavities and channels of extended MOMs, can also have a significant effect on observable properties. Indeed some properties can be achieved regardless and unmitigated by the

nature of the metal ion present. For example the principle of size or shape exclusion is currently an attractive target for the manufacture of MOMs with the ability to separate and purify small molecule organics (solvents and gases).[100, 110, 226, 234-238] Currently, one very active area of research related to size selectivity is the goal of CO_2 sequestration to slow (or start to reverse) the deleterious effects that this and other green house gases are having on the environment. These abilities may also lead to novel materials with the potential to be efficient decontaminates (i.e. water or soil remediation; nerve, chocking, or biological agent sequestration) which can be used to clean up hazards caused by mankind.

Non-linear optical behavior (NLO) is another phenomenon which can be seen in appropriately engineered metal-organic materials.[239-245] NLO pertains to the behavior of electromagnetic radiation (light) in the presence of material whose dielectric polarization responds nonlinearly to the electric field, otherwise called non-linear media. NLO properties cover a range of phenomena, but the most common involve the concepts of frequency mixing. Common forms of frequency mixing include Second Harmonic Generation (SHG, frequency doubling), in which the light's wavelength is reduced by half, Third Harmonic Generation (THG) where the wavelength is a third of the original, Sum Frequency Generation (SFG), where two light of two different frequencies are combined to form light with a frequency equal to the sum, Difference Frequency Generation (DFG), among many others.[241] A critical requirement for the observation of NLO properties in MOMs is that the material crystallizes into a noncentrosymmetric spacegroup. It also helps to insure that there are efficient electron donor and electron

acceptor moieties linked *via* a conjugated bridge, as well as adopting metal chromophores which will largely allow light to pass through the material without being adsorbed (i.e. high transmission rate), because what good is a noncentrosymmetric material with nice potential for NLO properties if it cannot efficiently transmit the light that is passed through the material.

Generically, metal-organic materials are becoming increasingly plausible as functional assets for useful applications within industrial settings.[127, 238, 246-251] Another intriguing challenge for the field of metal-organics rests with the desire to fabricate MOMs into thin films[252-257], as opposed to bulk crystalline powders, mainly due to the fact that before many of these materials can be fashioned into any type of practical device, they must first be rendered into functional thin film coatings which can interface with the electrical components. As more MOMs are designed and synthesized to exhibit specific physical and chemical properties, and as those properties are successfully translated from the bench-top to the marketplace, the impetus will only continue to grow. Undeniably we have only just begun a new golden age of metal-organic materials; increasingly our ability to impart explicit desirable properties into engineered crystalline mater is equally matched by our ability to subsequently fabricate useful devices.

Chapter 2

Two-Periodic Layered Structures

2.1 Introduction

In terms of their complexity 2-periodic metal-organic materials are inherently more intricate than that of a discrete 0-periodic polygon or a 1-periodic structure in the form a chain, ladder, or helix. By definition a 1-periodic structure propagates in only a single spatial direction. Topologically, the 1-perioidc structures are all reducible to chains, in which each node is 2-connected. Therefore the only variation afforded to these materials is based upon geometry; the angles and conformations of how the next building unit is oriented with respect the one before it is the only possible variable. However, in the case of the 2-periodic structures, while the variation in geometry is still a viable option, now several possible interconnections of nodes (i.e. the shapes they make in linking together) can also have a profound influence on the structure which is generated and in turn affect the properties of the material.

2.1.1 Clay Mimics

Commonly, 2-periodic architectures are referred to colloquially as layered or *lamellar* structures. This is because inevitably their topologies are described by planar

networks; the simple connected graphs which represent their connectivity can be embedded in $\mathbb{R}^2$. These materials closely resemble naturally occurring clay-like materials, which also exist as individual layers closely stacked one upon another to build up the bulk material. Graphite is another particularly relevant material which is an example of a layered structure.

The properties of 2-periodic layered materials can often mimic the action of clays. One notable property exhibited by clay-like compounds is their ability to expand; the ability for the layers to move apart for the intercalation of guests. This makes clays excellent natural filters capable of removing ions and small molecules from water sources as they pass through the clay material, ensuring their purification. We can thank clays and related materials for the part they play in filtering and purifying water as it seeps into the ground and is passed ultimately to the water aquifer. Many researchers working with 2-periodic structures early in their development looked to the classical properties of clays as good targets for applications which could be applied to these types of metal-organic materials.

2.1.2 Common Topologies

The simplest 2-periodic topologies are those which are constructed from only one type of node and one type of polygon. When the single type of polygon is also regular, the resultant *tiling* (covering) of the plane is also called a regular tiling. These can often be referred to as platonic tilings, in a manner analogous to the concept of platonic solids.

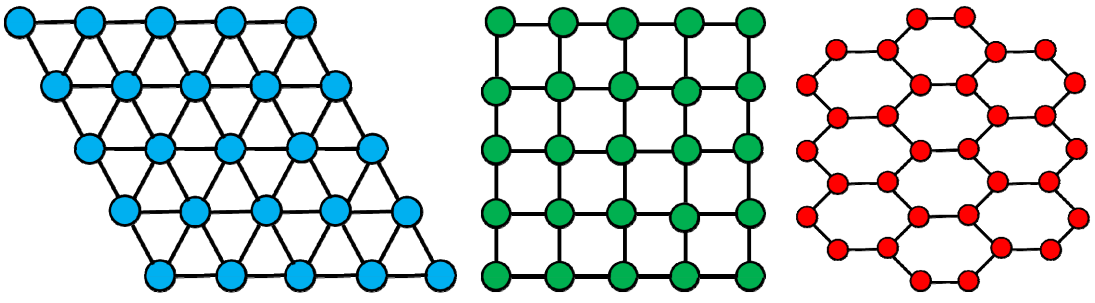

Figure 2.1 Schematic depicting the only three *regular* plane nets; (3,6) triangle tiling, (4,4) square grid, and (6,3) honeycomb.

There are exactly three regular tilings for a plane: the (3,6) triangular lattice composed of 6-connected nodes, the (4,4) square lattice composed of 4-connected nodes, and the (6,3) honeycomb lattice composed of 3-connected nodes (Fig. 2.1).

The next step up in complexity for 2-periodic topologies would be the situation in which there is still only a single type of node (vertex transitive), but now more than one type of convex polygon is formed at the intersection of vertices. This type of tiling is deemed to be semi-regular (Archimedean) and there are exactly eight of them (Fig 2.2).

2.2 Kagomé Lattices (3.6.3.6)

One of the more interesting 2-periodic topologies is that of the so-called Kagomé lattice. This lattice is constructed from a single type of 4-connected node so as to generate a net with (3.6.3.6) topology. This means that it contains both triangular (two) and hexagonal (two) polygons meeting at each node in an alternating fashion. The name of this lattice comes from the Japanese word for a common type of bamboo basket weaving (Fig. 2.3).

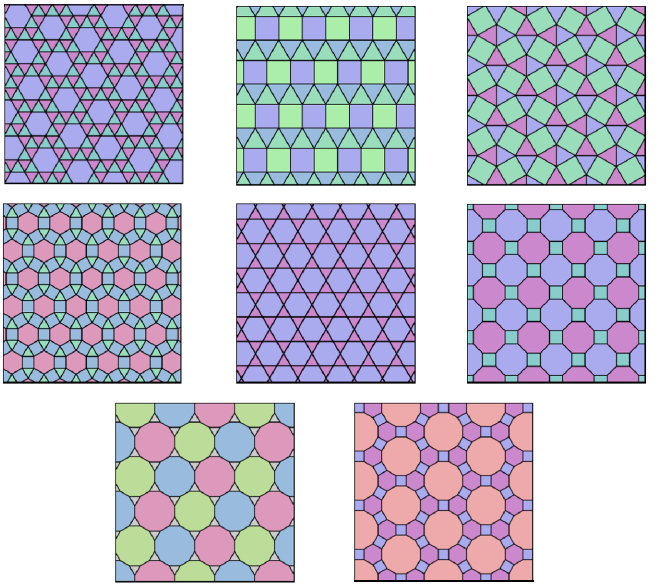

Figure 2.2 Semi-regular plane tilings. ***Top (left to right):*** (3^4.6), (3^3.4^2), (3^2.4.3.4). ***Middle (left to right):*** (3.4.6.4), (3.6.3.6), (4.8^2). ***Bottom (left to right):*** (3.12^2), (4.6.12).

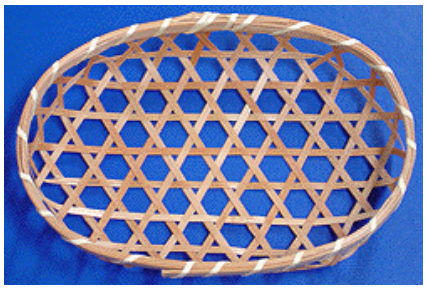

Figure 2.3 Basket weaving depicting a Kagomé lattice.

2.2.1 Spin Frustration and Magnetism

One of the principle reasons for so much interest in the Kagomé lattice is the concept of spin frustration and its implications for magnetism. Spin frustration occurs when a topology is situated in such a manner so that if spin moments are positioned at the vertices of the lattice they are unable to cancel each other out through opposite alignment.

As an example take a simple equilateral triangle (Fig 2.4). If you were to begin placing spin moments at the vertices so that they could only adopt one of two possible orientations (up or down), you could effectively balance out the charge of the first spin moment with that of the second. However when, you attempt to place the third spin moment, it becomes impossible to orient this spin so as to leave no net spin for the system. Thus spin frustration inherently leads to interesting magnetic properties. The Kagomé lattice[130, 258-273] is one such lattice which exhibits spin frustration, and so is a very important 2-periodic topology for metal-organic materials and solid state materials chemists in general.

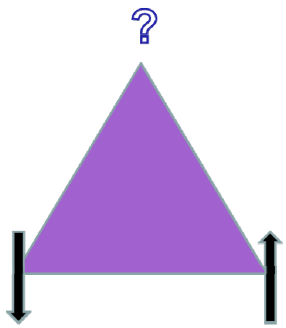

Figure 2.4 A cartoon illustrating the concept of spin frustration.

2.2.2 Structural Analysis

2.2.2.1 5-benzyloxy-1,3-bdc Kagomé Lattices

The first Kagomé lattice that I synthesized was achieved with a functionalized version of a 1,3-benzenedicarboxylic acid (1,3-bdc), in which the 5th position was substituted with a benzyl ether group **L1** (Fig. 2.5). In actuality, this ligand was

synthesized in an attempt to control the supramolecular isomerism observed by Zaworotko and co-workers[272] when working with 1,3-bdc and Cu^{2+}.

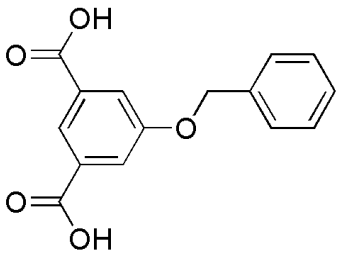

Figure 2.5 5-benzyloxy-1,3 benzenedicarboxylic acid, **L1.**

It was observed that when attempting the synthesis of metal-organic Kagomé lattices from these components *via* room temperature slow diffusion/layering reactions, that multiple compounds were often obtained. Careful analysis of the possible structures afforded by the combination of dimetal tetracarboxylate square paddlewheel SBUs through an angle of 120° (aptly provided by the use of the 1,3-bdc moiety) revealed that several of the structures could be distinguished by the location of where the 5th position of the 1,3-bdc ligand was located. In the case of the two 2-periodic isomers (square grids and Kagomé), the 5th position of the ligand was oriented into the characteristic cavity of the respective networks; the relatively small square cavity seen in the square grid compounds, and the somewhat larger, albeit still restrictive hexagonal cavity observed in the Kagomé structure. The ligand **L1,** was synthesized because it was believed to be too bulky for inclusion into either cavity and that steric hindrance might help prevent the formation of either of these topologies, leaving only 3-periodic structures or preferably, the 0-periodic nanoball. These assumptions were incorrect, and the hexagonal cavity of

the Kagomé lattice, or more aptly the hexagonal *channels* formed by the eclipsed stacking of subsequent Kagomé layers were more than adequate to accommodate these pendent arms (Fig 2.6).

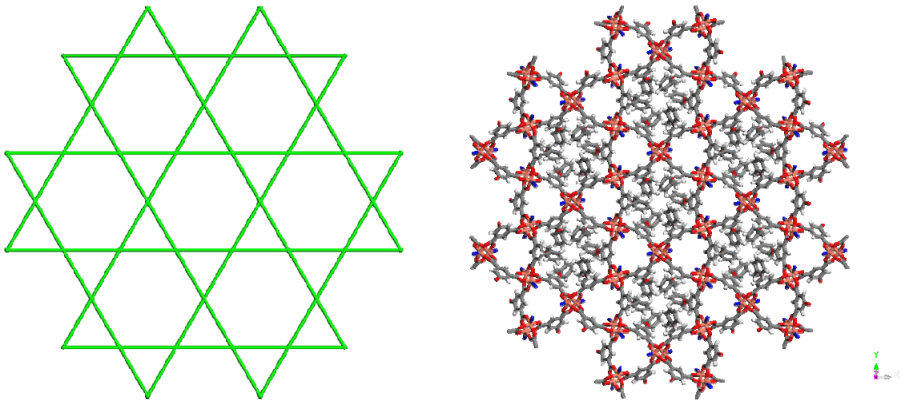

Figure 2.6 Cartoon illustrating the Kagomé lattice (***left***) and the metal-organic Kagomé lattice as seen in compounds **[1]** and **[2]** (***right***).

In compounds **[1]** and **[2],** the Cu^{2+} and Zn^{2+} analogues generate nearly identical structures dictated by the nature of the 5-benzyloxy ligands. Both structures crystallize in the trigonal space group P-3, with nearly identical cell parameters (Appendix C-1 and C-2). The 5-benzyloxy groups thread into the hexagonal channels alternating up or down around the hexagonal ring in the orientation they point. These benzyloxy groups thread deep into the center of the cavity, as every first and third layer each contributing 3 benzyloxy groups, interact through six concerted CH•••π interactions in a so-called *sextuplet phenyl embrace* (Fig. 2.7). The distance range observed for these CH•••π interactions were measured to be within the range of 5.186 Å to 5.194 Å as measured from the centroid of one phenyl ring to the centroid of an adjacent ring.

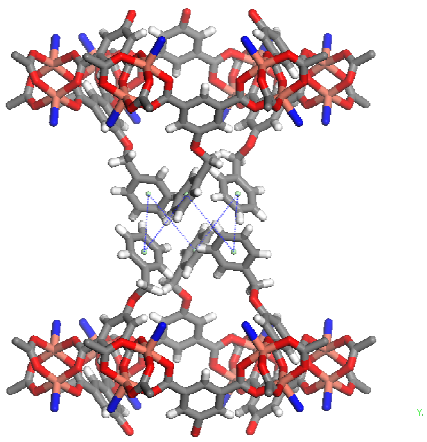

Figure 2.7 Illustration of Sextuplet Phenyl Embrace as seen in compound **[1].**

The distance of interlayer separation between adjacent layers in these structures was observed to be ~9.63 Å in the case of Cu^{2+} and ~9.53 Å in the case of Zn^{2+}, both corresponding to the length of the unit cell along the *c*-axis. Interestingly, the observed distance of interlayer separation for these two compounds is *shorter* than was observed in the case of the parent metal-organic Kagomé lattice first reported by Zaworotko et.al.[272] This is a strong indication that the existence of the sextuplet phenyl embrace has brought the layers closer together than would otherwise be observed, indicating that the repeating pattern of these strong supramolecular motifs has aided the stability of these compounds. The bowl shaped triangular windows, as measure from the closest point of contact at the base of the bowl was observed to be 6.172 Å (not accounting for van der Waal radii) along the sides of triangle drawn from the carbon atom of one 1,3-bdc ligand to an adjacent one. Within this triangular bowl shaped cavity resides disordered solvent, most likely MeOH. The diameter of the hexagonal cavity corresponds to the lengths of the *a*- and *b*-axes, ~18.40 Å in the Cu^{2+} version and 18.48 Å in that of the Zn^{2+}.

If the pyridine axial ligand is replaced with another pyridyl type base for the synthesis, other versions of the Kagomé lattice will be produced. The choice of the axial ligand (based upon its size) directly controls the length of the interlayer separation seen in these structures. In the case of the isoquinoline, a base with an extra benzene ring on the end, the separation is farthest at ~12 Å. If an axial ligand is chosen which is in between the size of pyridine and isoquinoline, as is the case for 4-methoxypyridine, the interlayer separation is also intermediate (~10.4 Å). The Kagomé skeleton however remains largely unchanged. What is affected however, in the case of the benzyloxy derivatives is the sextuplet phenyl embrace. For this supramolecular motif to occur, the phenyl rings must be within the correct proximity of each other. In the case of both the 4-methoxypyridine and the isoquinoline, the presence of these enlarged bases pushes the layers further apart due to steric hindrance and thus the phenyl rings do not come within the required distance for the interactions to take place. Therefore in these structures **[3-6]** (Appendix C-3 – C-6) the SPE does not occur. In the case of the 4-methoxypyridine base the interlayer separation is such that the benzyloxy groups cannot interact with any other free groups. In these structures the phenyl rings are free to twist in the hexagonal channel and are disordered slightly in the crystal structure.

In the case of the isoquinoline however the layers are pushed apart to such an extent that the benzyl ether groups are able to interact with the isoquinoline groups attached to adjacent layers through predominately face-to-face π-π stacking interactions (Fig. 2.8).

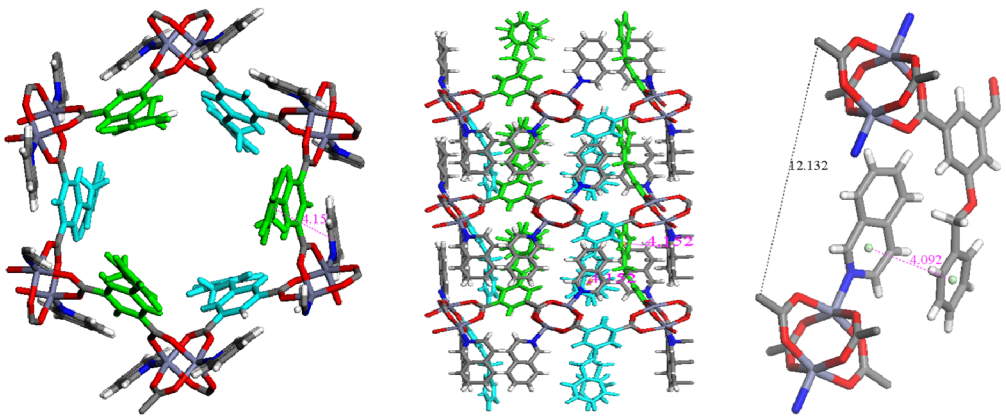

Figure 2.8 Illustration of the face-to-face π-π stacking interactions observed in compounds **[5]** and **[6].**

2.2.2.2 5-hexyloxy-1,3-bdc Kagomé Lattice

Another derivative of the Kagomé lattice which was synthesized was the 5-hexyloxy derivative. This structure was generated though the self assembly of Zn^{2+} ions together with 5-hexyloxy-1,3-benzenedicarboxylic acid, **L3** (Fig. 2.8).

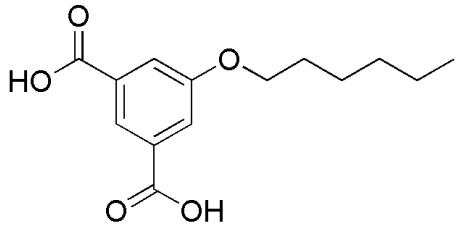

Figure 2.9 5-hexyloxy-1,3-benzenedicarboxcylic acid, **L3**.

$\{[Zn_2(5\text{-hexyloxy-1,3-benzenedicarboxylate}_2)(4\text{-picoline})_2]_3\}_n$, compound **[7]**, crystallized with nearly identical cell parameters as other Zn^{2+} versions of the Kagomé lattice; this compound crystallized in the Trigonal P-3 space group with unit cell dimensions of a = b = 18.9529(6) Å, c = 10.7825 (7) Å, V = 3354.3(3) $Å^3$, and Z = 3. As

with the other examples of Kagomé lattice, especially the Zn^{2+} versions which all adopt slightly larger unit cells when comparing the same 1,3-bdc and axial ligands due to a slightly larger SBU, this version of Kagomé contains the basic skeleton of the lattice in which hexagons and triangles meet at a common vertex. As was the case for the other Kagomé lattices, the dimensions of those cavities are based upon the dimensions of the unit cell; the shortest distance in the bowl shaped triangular cavity is measured from the bottom of the metallocalix-[3]-arene from carbon to carbon on opposite bdc groups. At the bottom of the bowl these all point towards each making this the bottleneck for the cavity and the dimension was measured to be 6.346 Å on each side of an equilateral triangle before taking into account van der Waals radii, which reduces the cavity further to ~4.0 Å, just big enough for small organic solvent molecules to occupy. Indeed, located within the triangular cavity but between layers are disordered *o*-dichlorobenzene molecules. Located with the larger hexagonal cavities are disorder alcohol solvent molecules. The hexagonal cavity dimensions correspond to the unit cell length in the *a*- and *b*-axes (where the cavity lies) and was measured to be 18.953 Å, form center of the Zn-Zn internuclear axis of one SBU to another. The interlayer separation (Fig. 2.9) for this compound again corresponds to the *c*-axis length and is therefore ~10.78 Å (it adopts this distance in good agreement with the length of the axial pillar as was seen in the benzyloxy Kagomé lattices). The large hexagonal channels are filled with the hexyloxy pendant chains threading up and down the channel in a manner analogous to the benzyl ether moieties. The presence of these alkyl chains greatly alters the chemical nature of

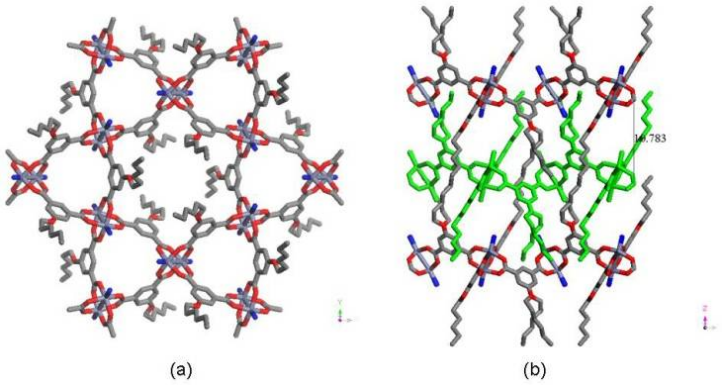

Figure 2.10 Stick representation of $\{[Zn_2(5\text{-hexyloxy-1,3-benzenedicarboxylate}_2)(4\text{-picoline})_2]_3\}_n$, compound **[7].** a.) a view down the *c*-axis illustrating the presence of the hexyloxy side chains protruding into the center of the hexagonal cavity. b.) A scheme dipicting the interlayer separation and packing of subsequent layers in compound **[7].**

these channels. It is of little surprise that the only good quality crystal for this ligand came from the use of 4-picoline, given the nature of the alkoxy pendant chains.

2.2.3 Experimental

2.2.3.1 Synthesis

All reagents, unless described otherwise, were purchased from either Sigma-Aldrich or Fischer Scientific and used as received without further purification. Bulk solvents such as methanol, ethanol, acetone, and dichloromethane were first distilled and stored over drying media (4Å molecular sieves) before their use.

5-Benzyloxy-1,3-benzenedicarboxylic acid, **L1** (Fig. 2.5), was synthesized from commercially available dimethyl-5-hydroxy-1,3-benzenedicarboxylate and benzyl bromide *via* established procedures for the arylation of phenols.[274, 275] In a typical reaction dimethyl-5-hydroxy-1,3-benzenedicarboxylate (5.00 g, 0.0238 mol) and

potassium carbonate (K_2CO_3, 9.88 g, 0.0715 mol, 3 equivalents) were weighed out separately and dried on a vacuum pump for approximately three hours. A 3-neck round bottom flask was sealed with rubber septa and the air purged with N_2 for 15 minutes prior to the start of the reaction. Upon drying the diester and K_2CO_3 were added to the 3-neck round bottom flask equipped with two rubber septa and a cold-water condenser situated in a hot oil bath held at 80 °C along with approximately 100 mL of dry acetone. The solution was allowed to reflux for 30 minutes before benzyl bromide (6.78 mL, 0.0571 mol, 1.5 equivalents) was added *via* syringe through a rubber septum. The reaction was allowed to reflux for approximately 12 hours before monitoring the extent of completion through TLC.

After the reaction was determined to be complete the solution was cooled to room temperature, filtered through Celite, and the acetone solvent removed by heating under vacuum (Rotavap) leaving behind a dark yellow oil which solidified upon cooling. This solid was dissolved in ~100 mL dichloromethane (DCM), transferred to a separatory funnel, washed three times with *D. I.* H_2O, and dried over anhydrous Na_2SO_4. The DCM solvent was removed *via* rotavap and the solid recrystallized from hot ethanol. The ester product crystals were collected *via* filtration and dried, upon which they were added to a NaOH solution (20% by volume, 3 equivalents to the ester) and allowed to stir with a magnetic stir bar on a hot plate until fully dissolved. The conversion from ester to carboxylate was monitored *via* TLC and upon completion was worked up with HCl (10 % by volume) added dropwise until the solution was acidic by pH paper. The precipitate was filtered, washed with *D.I.* H_2O, and allowed to dry at which time 4.102 g (63.31 %

yield) of white solid was obtained. The spectroscopic data for **L1** (Appendix A-1, B-1) were consistent with previously reported data for this compound.[276] All NMR spectra were analyzed using SpinWorks 3.1.[211]

^{1}H NMR (250 MHz, Acetone-d_6, δ): 5.3(s, 2H, -O-CH_2-), 7.4(m, 3 H, -ArH), 7.6(d, J = 7.4 Hz, 2H, -ArH), 7.9(d, J = 1.44 Hz, 2H, -ArH), 8.3(t, J = 1.4 Hz, 1H, -ArH), 11.2(br, 2H, -COOH); mp 263-266 ºC (lit. 163-166 ºC).

5-(2-Naphthylmethoxy)-1,3-benzenedicarboxylic acid, **L2** (Fig. 2.10), was synthesized form commercially available 2-(Bromomethyl)-naphthalene and dimethyl-5-hydroxy-1,3-benzenedicarboxylate *via* established procedures for the arylation of phenols.[274, 275] In a typical reaction dimethyl-5-hydroxy-1,3-benzenedicarboxylate (5.00 g, 0.0238 mol) and potassium carbonate (K_2CO_3, 9.88 g, 0.0715 mol, 3 equivalents) were weighed out separately and dried on a vacuum pump for approximately three hours. A 3-neck round bottom flask was sealed with rubber septa and the air purged with N_2 for 15 minutes prior to the start of the reaction. Upon drying, the diester and K_2CO_3 were added to the 3-neck round bottom flask along with approximately 100 mL of dry acetone. The flask was equipped with two rubber septa and a cold-water condenser and situated in a hot oil bath held at 80 °C. The solution was allowed to reflux for 30 minutes before 2-(Bromomethyl)-naphthalene (5.79 g, 0.0262 mol, 1.1 equivalents) was dissolved in approximately 20 mL of dry acetone and added to the reaction mixture. The reaction was allowed to reflux for approximately 12 hours before monitoring the extent of completion through TLC.

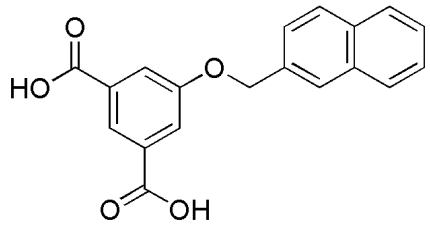

Figure 2.11 5-(2-naphthylmethoxy)-1,3-benzenedicarboxylic acid, **L2.**

When the reaction was determined to be complete the solution was cooled to room temperature, filtered through Celite, and the acetone solvent removed by heating under vacuum (Rotavap) leaving behind a dark yellow oil which solidified upon cooling. This solid was dissolved in ~100 mL dichloromethane (DCM), transferred to a separatory funnel, washed three times with *D. I.* H_2O, and dried over anhydrous Na_2SO_4. The DCM solvent was removed *via* rotavap and the solid recrystallized from hot ethanol. The ester product crystals were collected *via* filtration and dried, upon which they were added to a NaOH solution (20% by volume, 3 equivalents to the ester) and allowed to stir with a magnetic stir bar on a hot plate until fully dissolved. The conversion from ester to carboxylate was monitored *via* TLC and upon completion was worked up with HCl (10 % by volume) added dropwise until the solution was acidic by pH paper. The precipitate was filtered, washed with *D.I.* H_2O, and allowed to dry at which time 4.313 g (56.2 % yield) of white solid was obtained. The spectroscopic data for **L2** is given in Appendix A-2 and B-2. 5-(2-naphthylmethoxy)-1,3-benzenedicarboxylic acid was not observed to be present in SciFinder Scholar as either a product or a reactant.

^{1}H NMR (250 MHz, DMSO-d_6, δ): 5.4(s, 2H, -O-CH_2-), 7.6(m, 4 H, -ArH), 7.8(d, 2H, -ArH), 7.98(m, 3H, -ArH), 8.0(s, 1H, -ArH), 8.1(t, J = 1.3 Hz, 1H, -ArH), 13.3(br, 2H, -COOH); mp 254-260 °C

5-Hexyloxy-1,3-benzenedicarboxylic acid, **L3** (Fig. 2.8), was synthesized from commercially available dimethyl-5-hydroxy-1,3-benzenedicarboxylate and 1-iodohexane *via* established procedures for the alkylation of phenols.[277-279] In a typical reaction dimethyl-5-hydroxy-1,3-benzenedicarboxylate (5.00 g, 0.0238 mol) and potassium carbonate (K_2CO_3, 9.88 g, 0.0715 mol, 3 equivalents) were weighed out separately and dried on a vacuum pump for approximately three hours. A 3-neck round bottom flask was sealed with rubber septa and the air purged with N_2 for 15 minutes prior to the start of the reaction. Upon drying, the diester and K_2CO_3 along with approximately 100 mL of dry acetone were added to the 3-neck round bottom flask which was equipped with two rubber septa and a cold-water condenser situated in a hot oil bath held at 80 °C. The solution was allowed to reflux for 30 minutes before 1-iodohexane (10.5 mL, 0.0714 mol, 3 equivalents) was added *via* syringe through a rubber septum. The reaction was allowed to reflux for approximately 12 hours before monitoring the extent of completion through TLC.

When the reaction was determined to be complete the solution was cooled to room temperature, filtered through Celite, and the acetone solvent removed by heating under vacuum (Rotavap) leaving behind a dark yellow oil which solidified upon cooling. This solid was dissolved in ~100 mL dichloromethane (DCM), transferred to a separatory funnel, washed three times with *D. I.* H_2O, and dried over anhydrous Na_2SO_4. The DCM

solvent was removed *via* rotavap and the solid recrystallized from hot ethanol. The ester product crystals were collected *via* filtration and dried, upon which they were added to a NaOH solution (20% by volume, 3 equivalents to the ester) and allowed to stir with a magnetic stir bar on a hot plate until fully dissolved. The conversion from ester to carboxylate was monitored *via* TLC and upon completion was worked up with HCl (10 % by volume) added dropwise until the solution was acidic by pH paper. The precipitate was filtered, washed with *D.I.* H_2O, and allowed to dry at which time 3.428 g (54.09 % yield) of white solid was obtained. The spectroscopic data for **L3** (Appendix A-3, B-3) were consistent with previously reported data for this compound.[280]

^{1}H NMR (250 MHz, DMSO-d_6, δ): 0.9(t, J = 6.3 Hz, 3H, -CH_3), 1.2(m, 6 H, -CH_2-), 1.7(m, 2H, -CH_2-), 4.1(t, J = 6.4 Hz, 2H, -O-CH_2-), 7.6(s, 2H, -ArH), 8.1(t, J = 1.4 Hz, 1H, -ArH), 13.3(br, 2H, -COOH).; mp 233-236 ºC (lit. 240 ºC).

{[Cu_2(5-benzyloxy-1,3-benzenedicarboxylate)$_2$(pyridine)$_2$]$_3$}$_n$ [**1**]**,** was synthesized under ambient conditions *via* a slow diffusion/ layering method. In a typical synthesis, 5-benzyloxy-1,3-benzenedicarboxylic acid (**L1**) (84.1 mg, 0.310 mmol) is dissolved in 10 mL of methanol (MeOH) and combined with 2 mL of *o*-dichlorobenzene and pyridine (0.08 mL, 1.00 mmol, 3.2 equivalents). Layered on top of this mixture was a solution of $Cu(NO_3)_2 \cdot 2.5H_2O$ (69.7 mg, 0.299 mmol) dissolved in 7 mL MeOH, using a pure MeOH "blank" as a middle layer between the two solutions. The layered reaction was left undisturbed on the lab bench to allow for slow diffusion, and after two weeks green hexagonal plates suitable for single crystal X-ray diffraction were collected (96 mg, 77.77 % yield with respect to Cu).

{[Zn_2(5-benzyloxy-1,3-benzenedicarboxylate)$_2$(pyridine)$_2$]$_3$}$_n$ [**2**]**,** was synthesized under ambient conditions *via* a slow diffusion/ layering method. In a typical synthesis, 5-benzyloxy-1,3-benzenedicarboxylic acid (**L1**) (81.5 mg, 0.299 mmol) is dissolved in 10 mL of methanol (MeOH) and combined with 2 mL of *o*-dichlorobenzene and pyridine (0.08 mL, 1.00 mmol, 3.3 equivalents). Layered on top of this mixture was a solution of $Zn(NO_3)_2 \cdot 6H_2O$ (89.1 mg, 0.300 mmol) dissolved in 7 mL MeOH, using a pure MeOH "blank" as a middle layer between the two solutions. The layered reaction was left undisturbed on the lab bench to allow for slow diffusion, and after two weeks colorless hexagonal shaped rods suitable for single crystal X-ray diffraction were collected (107 mg, 86 % yield with respect to Zn).

{[Cu_2(5-benzyloxy-1,3-benzenedicarboxylate)$_2$(4-methoxypyridine)$_2$]$_3$}$_n$ [**3**]**,** was synthesized under ambient conditions *via* a slow diffusion/ layering method. In a typical synthesis, 5-benzyloxy-1,3-benzenedicarboxylic acid (**L1**) (83.2 mg, 0.306 mmol) is dissolved in 10 mL of methanol (MeOH) and combined with 2 mL of *o*-dichlorobenzene and 4-methoxypyridine (0.10 mL, 1.00 mmol, 3.3 equivalents). Layered on top of this mixture was a solution of $Cu(NO_3)_2 \cdot 2.5H_2O$ (69.7 mg, 0.299 mmol) dissolved in 7 mL MeOH, using a pure MeOH "blank" as a middle layer between the two solutions. The layered reaction was left undisturbed on the lab bench to allow for slow diffusion, and after two weeks green hexagonal plates suitable for single crystal X-ray diffraction were collected (65 mg, 43.2% yield with respect to Cu).

{[Zn_2(5-benzyloxy-1,3-benzenedicarboxylate)$_2$(4-methoxypyridine)$_2$]$_3$}$_n$ [**4**]**,** was synthesized under ambient conditions *via* a slow diffusion/ layering method. In a typical

synthesis, 5-benzyloxy-1,3-benzenedicarboxylic acid (**L1**) (80.2 mg, 0.295 mmol) is dissolved in 10 mL of methanol (MeOH) and combined with 2 mL of *o*-dichlorobenzene and 4-methoxypyridine (0.10 mL, 1.00 mmol, 3.4 equivalents). Layered on top of this mixture was a solution of $Zn(NO_3)_2 \cdot 6H_2O$ (90.1 mg, 0.303 mmol) dissolved in 7 mL MeOH, using a pure MeOH "blank" as a middle layer between the two solutions. The layered reaction was left undisturbed on the lab bench to allow for slow diffusion, and after two weeks colorless blocks suitable for single crystal X-ray diffraction were collected (115mg, 87.75 % yield with respect to Zn).

$\{[Cu_2(5\text{-benzyloxy-1,3-benzenedicarboxylate})_2(\text{isoquinoline})_2]_3\}_n$ [**5**]**,** was synthesized under ambient conditions *via* a slow diffusion/ layering method. In a typical synthesis, 5-benzyloxy-1,3-benzenedicarboxylic acid (**L1**) (88 mg, 0.323 mmol) is dissolved in 10 mL of methanol (MeOH) and combined with 2 mL of *o*-dichlorobenzene and isoquinoline (0.12 mL, 1.00 mmol, 3.1 equivalents). Layered on top of this mixture was a solution of $Cu(NO_3)_2 \cdot 2.5H_2O$ (67.8 mg, 0.292 mmol) dissolved in 7 mL MeOH, using a pure MeOH "blank" as a middle layer between the two solutions. The layered reaction was left undisturbed on the lab bench to allow for slow diffusion, and after two weeks green hexagonal plates suitable for single crystal X-ray diffraction were collected (76 mg, 82 % yield with respect to Cu).

$\{[Zn_2(5\text{-benzyloxy-1,3-benzenedicarboxylate})_2(\text{isoquinoline})_2]_3\}_n$ [**6**]**,** was synthesized under ambient conditions *via* a slow diffusion/ layering method. In a typical synthesis, 5-benzyloxy-1,3-benzenedicarboxylic acid (**L1**) (84.1 mg, 0.310 mmol) is dissolved in 10 mL of methanol (MeOH) and combined with 2 mL of *o*-dichlorobenzene

and isoquinoline (0.12 mL, 1.00 mmol, 3.2 equivalents). Layered on top of this mixture was a solution of $Zn(NO_3)_2 \cdot 6\ H_2O$ (69.7 mg, 0.299 mmol) dissolved in 7 mL MeOH, using a pure MeOH "blank" as a middle layer between the two solutions. The layered reaction was left undisturbed on the lab bench to allow for slow diffusion, and after two weeks green hexagonal plates suitable for single crystal X-ray diffraction were collected (90 mg, 65 % yield with respect to Zn).

$\{[Zn_2(5\text{-hexyloxy-1,3-benzenedicarboxylate})_2(4\text{-picoline})_2]_3\}_n$ [**7**]**,** was synthesized under ambient conditions *via* a slow diffusion/ layering method. In a typical synthesis, 5-hexyloxy-1,3-benzenedicarboxylic acid (**L3**) (81.3 mg, 0.305 mmol) is dissolved in 10 mL of methanol (MeOH) and combined with 2 mL of *o*-dichlorobenzene and 4-picoline (0.10 mL, 1.00 mmol, 3.3 equivalents). Layered on top of this mixture was a solution of $Zn(NO_3)_2 \cdot 6H_2O$ (90.1 mg, 0.303 mmol) dissolved in 7 mL MeOH, using a pure MeOH "blank" as a middle layer between the two solutions. The layered reaction was left undisturbed on the lab bench to allow for slow diffusion, and after two weeks colorless hexagonal shaped rods suitable for single crystal X-ray diffraction were collected (<10 mg, ~5 % yield with respect to Zn).

2.2.3.2 X-ray Crystallography

Single crystals suitable for X-ray crystallographic analysis for compounds **[1] – [7]** were selected following examination under a microscope. Intensity data were collected on a Bruker-AXS SMART APEX/CCD diffractometer using Mo k\α radiation (λ = 0.7107 Å).[281] The data were corrected for Lorentz and polarization effects and for

absorption using the SADABS program (SAINT).[282] The structures were solved using direct methods and refined by full-matrix least-squares on $|F|^2$ (SHELXTL).[283] Additional electron density, located in the void cavity space, assumed to be disordered solvent, was unable to be adequately refined was removed using the SQUEEZE/PLATON program.[284-286] Select crystallographic data is presented in tabular form in Appendix C-1 – C-7.

2.2.3.3 Powder X-ray Diffraction

Powder samples suitable for powder X-ray diffraction, FT-IR spectroscopy, and Thermal Gravimetric Analysis were obtained by removing a large amount of single crystals from the reaction scintillation vial by using a glass Pasteur pipette and depositing these crystal (along with mother liquor) in a small concave agar mortar. Excess solvent was removed *via* pipette, and surface solvent was removed by wicking action with a Kim-Wipe®. Upon wick drying, the crystals were transferred to a small piece of filter paper which was subsequently folded over and they were dried further and slightly crushed with gently pressure. The resulting dry powder (~30 mg) was then immediately applied to a PXRD sample puck prepared with a small amount of vacuum grease to fixate the powder sample, and the PXRD experiment performed without delay.

All of the Kagomé lattice compounds were analyzed for their bulk purity *via* PXRD, except for compound **[7]**. The synthesis of this compound, through slow/diffusion, layering methods, resulted in only a small amount of single crystals on the sides of the vials along with a large amount of powdery precipitate that settled along

the base of the vial. PXRD analysis of the powdery precipitate indicated that the material was amorphous. It was extremely difficult to isolate sufficient quantities of the material in a pure enough state to obtain a serviceable PXRD pattern.

2.2.3.4 FT-IR Spectroscopy

All compounds, including synthesized ligands, were characterized *via* infrared spectroscopy using a Nicolet Avatar 320 Fourier-Transform Infrared Spectrometer (FT-IR). Before each sample was analyzed, a background spectrum was obtained for purposes of zeroing out ambient noise in the form of the laboratory atmosphere. Each sample was measured in the range from 4000 cm^{-1} to 500 cm^{-1} wavenumbers (wavelength of 2500 nm to 20000 nm respectively) and scanned 64 times. Results were recorded in % transmittance and the spectrum analyzed using the EZ OMNIC© (V.5.1b, copyright 1992-199 Nicolet Instruments Corporation) computer software suite. A typical sample was a analyzed as a neat, dry solid (~10 mg) obtained *via* either vacuum filtration and air drying or gently drying with laboratory grade filter paper.

The FT-IR spectrum (Appendix B-1) for 5-benzyloxy-1,3-benzenedicarboxylic acid **L1,** illustrates the same broad featureless hump originating around 3300 cm^{-1} and bleeding into ~3000 cm^{-1} which is typical of carboxylic acids involved in hydrogen bonding, which is to be expected in solid state samples such how the ligand was analyzed. The spectrum as contains a sharp strong band at 1685.95 cm^{-1} indicative of the carbonyl stretch of an aromatic carboxylic acid. There also exists a moderately strong and

sharp band at 1030.20 cm^{-1} which I believe to be due to the presence of the ether functional group where the benzyl moiety attaches to the isophthalic ring.

The FT-IR spectrum (Appendix B-2) for 5-(2-naphthylmethoxy)-1,3-benzenedicarboxylic acid, **L2,** illustrates the same broad featureless hump originating around 3300 cm^{-1} and bleeding into ~3000 cm^{-1} which is typical of carboxylic acids involved in hydrogen bonding, and would be expected in solid state samples such how the ligand was analyzed. This spectrum also contains the moderate peak at around 1030 wavenumbers (1027.32 cm^{-1}) believed to be the ether group. The carbonyl stretch for this ligand was observed at 1688.84 cm^{-1} , within the range for aromatic carboxylic acids (1685- 1710 cm^{-1}).[287, 288]

2.2.3.5 Thermal Gravimetric Analysis

Thermal Gravimetric Analysis for compounds **[1] – [7]** was performed on a PerkinElmer STA 6000 Simultaneous Thermal Analyzer. Data acquisition and analysis was performed with the assistance of the Pyris Series suite of software. Roughly 10-20 mg of dry powder was placed in a sample crucible and heated a t a rate of 10 °C/min. form a temperature of 30 °C up to 700 °C under a N_2 atmosphere.

2.3 Square Lattice (4.4)

Another 2-periodic structure that is somewhat more common place is that of the (4,4) square grid lattice. This is the ubiquitous checkerboard pattern seen just about everywhere. The checkerboard orientation is only the most symmetric representation of

this topology; in fact a brickwall or herringbone pattern is also topologically a (4,4) net, but with a different geometry around the node.

2.3.1 Structural Analysis

Layering reactions utilizing 5-benzyloxy-1,3-bdc, **L1**, and the transition metals, Zn(II), Co(II), and Cd(II), with a terminal pyridyl axial base (pyridine; 4-picoline) afforded a series of closely related 2-periodic structures (compounds **[8] – [13]**, Appendix C-8 – C-13) which can be interpreted in two ways. In the first interpretation they can be simplified into (4,4) square grid networks, while in the second they more closely resemble the 4.8^2 *fes-like* topology (Fig 2.11).

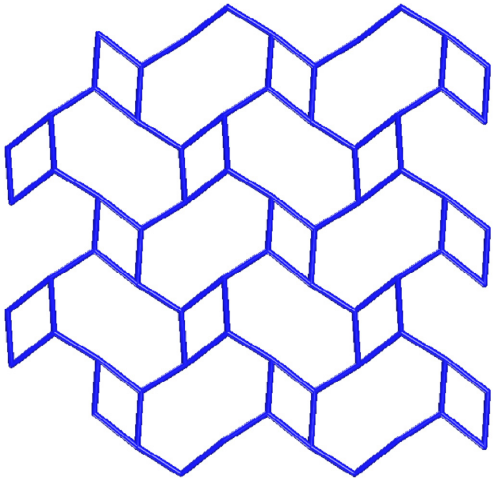

Figure 2.12 4.8^2 *fes*-like topology.

Each of these structures was obtained *via* self-assembly during a slow/diffusion reaction and subsequently remade *via* solvothermal reaction conditions. The use of solvothermal conditions generally increased the yield of the reaction, but made smaller

crystals. The diffraction quality of the crystals as made by the two processes were basically equivalent. In each of these structures, the 5-benzyloxy-1,3-bdc **L1** was reacted with one of Zn^{2+}, Co^{2+}, or Cd^{2+}. In contrast to the Kagomé lattice structures presented in the previous section, these materials are not sustained by the dimetal tetracarboxylate square paddlewheel SBU, but rather a different dimetal tetracarboxylate SBU (Fig 2.12) which has been seen for many different transition metals in the context of extended structures. This SBU can be interpreted as a square as well, although it is highly distorted when compared to that of the paddlewheel SBU.

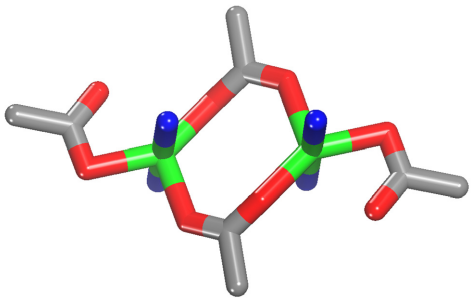

Figure 2.13 Dimetaltetracarboxylate secondary building unit observed in compounds **[8] – [13].**

Upon formation of this SBU with the selected bridging ligand, a series of 2-periodic sheets was observed. These sheet can be interpreted as (4,4) square grids if you simplify this SBU to a single 4-connected point at the center of the SBU. This simplification is a valid way of interpreting this structure. In a second interpretation, the carbon atoms of the four carboxylates are treated as the points of extension and connected into a geometrical figure (a rectangle) which represents the points of extension observed in the MOM. When this is done, these rectangles (or distorted squares) are then linked

through their vertices to generate a 2-periodic structure with a 4.8^2 *fes*-like topology. It is important to note that the 4.8^2 topology is also just the *sql-a* topology, which is when the vertex of a network is replaced with a vertex figure that has the same connectivity. Thus we simply replace the 4-connected single node with a 4-connected square (rectangle). The individual layers of these compounds stack on top of one another, but are slipped in an ABAB manner. The presence of the 5-benzyloxy groups, which thread through the rectangular cavity of the layers (Fig. 2.13), as well as the presence of the pyridine (or 4-picoline) groups, causes the layers to undergo interdigitation with one another (Fig 2.14). Upon this interdigitation, the phenyl rings from the ligand of one layer interact through edge-to-face CH•••π interactions (measured carbon-to-centroid; ranges 3.564 Å to 4.196 Å).

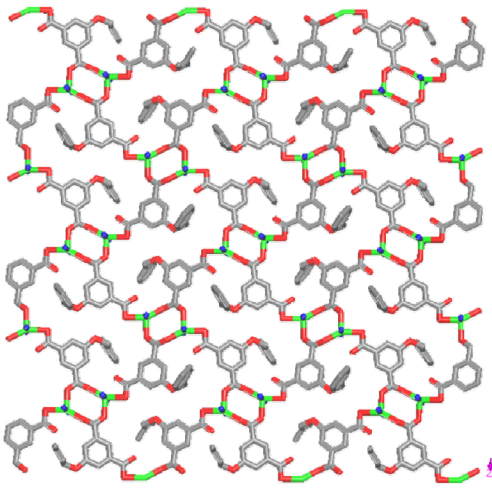

Figure 2.14 Illustration of individual layers of compounds **[8] – [13].**

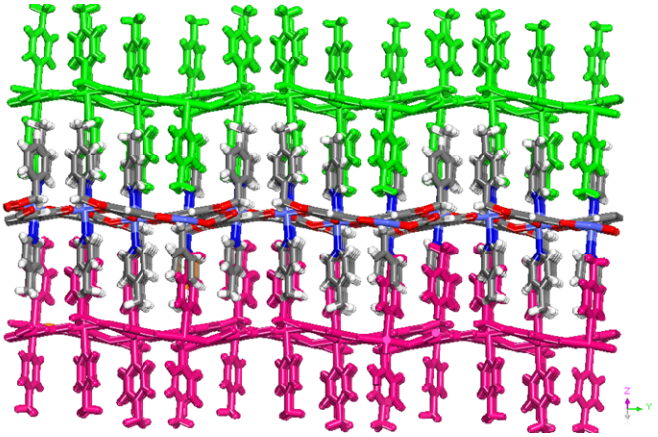

Figure 2.15 Interdigitation between layers as observed in compounds **[8] – [13].**

2.3.2 Experimental

2.3.2.1 Synthesis

All reagents, unless described otherwise, were purchased from either Sigma-Aldrich or Fischer Scientific and used as received without further purification. Methanol (MeOH) was first distilled and stored over drying media (4Å molecular sieves) before being used.

[Zn(5-benzyloxy-1,3-benzenedicarboxylate)(pyridine)$_2$]$_n$ [**8**], was initially synthesized *via* slow diffusion/layering under ambient conditions. In a typical reaction, 5-benzyloxy-1,3-benzenedicarboxylic acid (**L1**) (86.05 mg, 0.316 mmol) was dissolved in 10 mL MeOH while separately $Zn(NO_3)_2 \cdot 6H_2O$ (89.0 mg, 0.299 mmol) was dissolved in 7 mL MeOH. Pyridine was then added to the **L1**/MeOH solution (0.08 mL, 1.00 mmol) along with 2 mL of nitrobenzene. The methanolic solution of $Zn(NO_3)_2$ was subsequently layered over the methanolic solution containing the ligand, pyridine, and nitrobenzene

using a 5 mL “blank” MeOH middle layer. The reaction vessels were capped and left undisturbed to allow for slow diffusion. After several weeks, large colorless blocks of [**8**] were obtained (45 mg, 30.48% yield).

The synthesis of [**8**] was also attempted *via* a solvothermal process. In this reaction, equimolar quantities of $Zn(NO_3)_2$ and **L1** (0.300 mmol) were dissolved in 1 mL and 2 mL of N,N′-Dimethylformamide (DMF) respectively. Pyridine (0.08 mL, 1.00 mmol) was added to the **L1**/DMF solution along with 1 mL of ethanol. The two solutions were combined in a 20 mL scintillation vial, sealed with aluminum foil, capped and heated in a sand bath. The oven was ramped up from room temperature to 85 °C at a rate of 1.5 °C per minute, held constant for 12 hours and then cooled at a rate of 1.0 °C back to room temperature. Solvothermal reactions for [**8**] resulted in noticeably improved single crystal quality (colorless rhombohedral plates) as well as increased yield over that obtained *via* slow diffusion (100 mg, 67.5 % yield).

The cobaltous analog, $[Co(5\text{-benzyloxy-1,3-benzenedicarboxylate})(pyridine)_2]_n$ [**9**], was initially synthesized *via* slow diffusion/layering under ambient conditions. In a typical reaction, 5-benzyloxy-1,3-benzenedicarboxylic acid (**L1**) (82 mg, 0.301 mmol) was dissolved in 10 mL MeOH while separately $Co(NO_3)_2 \cdot 6H_2O$ (87.1 mg, 0.299 mmol) was dissolved in 7 mL MeOH. Pyridine was then added to the **L1**/MeOH solution (0.08 mL, 1.00 mmol) along with 2 mL of nitrobenzene. The methanolic solution of $Co(NO_3)_2$ was subsequently layered over the methanolic solution containing the ligand, pyridine, and nitrobenzene using a 5 mL “blank” MeOH middle layer. The reaction vessels were

capped and left undisturbed to allow for slow diffusion. After several weeks, large blocks light pink to red in color of [**9**] were obtained (33 mg, 22.65 % yield).

The synthesis of [**9**] was also attempted *via* a solvothermal process. In this reaction, equimolar quantities of $Co(NO_3)_2$ and **L1** (0.300 mmol) were dissolved in 1 mL and 2 mL of N,N′-Dimethylformamide (DMF) respectively. Pyridine (0.08 mL, 1.00 mmol) was added to the **L1**/DMF solution along with 1 mL of methanol. The two solutions were combined in a 20 mL scintillation vial, sealed with aluminum foil, capped and heated in a sand bath. The oven was ramped up from room temperature to 85 °C at a rate of 1.5 °C per minute, held constant for 12 hours and then cooled at a rate of 1.0 °C back to room temperature. Solvothermal reactions for [**9**] also resulted in marked improvement in single crystal quality (deep red rhombohedral plates) as well as enlarged yield with respect to that obtained *via* slow diffusion (120 mg, 82.35 % yield).

The cadmium analog, $[Cd(5\text{-benzyloxy-1,3-benzenedicarboxylate})(pyridine)_2]_n$ [**10**], was initially synthesized *via* slow diffusion/layering under ambient conditions. In a typical reaction, 5-benzyloxy-1,3-benzenedicarboxylic acid (**L1**) (86 mg, 0.316 mmol) was dissolved in 10 mL MeOH while separately $Cd(NO_3)_2 \cdot 6H_2O$ (91.6 mg, 0.296 mmol) was dissolved in 7 mL MeOH. Pyridine was then added to the **L1**/MeOH solution (0.08 mL, 1.00 mmol) along with 2 mL of nitrobenzene. The methanolic solution of $Cd(NO_3)_2$ was subsequently layered over the methanolic solution containing the ligand, pyridine, and nitrobenzene using a 5 mL "blank" MeOH middle layer. The reaction vessels were capped and left undisturbed to allow for slow diffusion. After several weeks, large colorless blocks of [**10**] were obtained (47 mg, 29.36 % yield).

The synthesis of [**10**] was also attempted *via* a solvothermal process. In this reaction, equimolar quantities of $Cd(NO_3)_2$ and **L1** (0.300 mmol) were dissolved in 1 mL and 2 mL of N,N′-Dimethylformamide (DMF) respectively. Pyridine (0.08 mL, 1.00 mmol) was added to the **L1**/DMF solution along with 1 mL of *o*-dichlorobenzene. The two solutions were combined in a 20 mL scintillation vial, sealed with aluminum foil, capped and heated in a sand bath. The oven was ramped up from room temperature to 85 °C at a rate of 1.5 °C per minute, held constant for 12 hours and then cooled at a rate of 1.0 °C back to room temperature. Solvothermal reactions for [**10**] also resulted in marked improvement in single crystal quality (colorless rhombohedral plates) as well as better yield with respect to that obtained *via* slow diffusion (120 mg, 82.35 % yield).

$[Zn(5\text{-benzyloxy-1,3-benzenedicarboxylate})(4\text{-picoline})_2]_n$ [**11**], was initially synthesized *via* slow diffusion/layering under ambient conditions. In a typical reaction, 5-benzyloxy-1,3-benzenedicarboxylic acid (**L1**) (88 mg, 0.323 mmol) was dissolved in 10 mL MeOH while separately $Zn(NO_3)_2 \cdot 6H_2O$ (93.0 mg, 0.313 mmol) was dissolved in 7 mL MeOH. 4-picoline was added to the **L1**/MeOH solution (0.10 mL, 1.00 mmol) along with 2 mL of nitrobenzene. The methanolic solution of $Zn(NO_3)_2$ was subsequently layered over the methanolic solution containing the ligand, 4-picoline, and nitrobenzene using a 5 mL "blank" MeOH middle layer. The reaction vessels were capped and left undisturbed to allow for slow diffusion. After several weeks, large colorless blocks of [**11**] were obtained (41 mg, 30.05% yield).

The synthesis of [**11**] was also attempted *via* a solvothermal process. In this reaction, equimolar quantities of $Zn(NO_3)_2$ and **L1** (0.300 mmol) were dissolved in 1 mL

and 2 mL of N,N′-Dimethylformamide (DMF) respectively. 4-picoline (0.10 mL, 1.00 mmol) was added to the **L1**/DMF solution along with 1 mL of ethanol. The two solutions were combined in a 20 mL scintillation vial, sealed with aluminum foil, capped and heated in a sand bath. The oven was ramped up from room temperature to 85 °C at a rate of 1.5 °C per minute, held constant for 12 hours and then cooled at a rate of 1.0 °C back to room temperature. Solvothermal reactions for [**11**] resulted in noticeably improved single crystal quality (colorless rhombohedral plates) as well as increased yield over that obtained *via* slow diffusion (105mg, 68.5 % yield).

[Co(5-benzyloxy-1,3-benzenedicarboxylate)(4-picoline)$_2$]$_n$ [**12**], was initially synthesized *via* slow diffusion/layering under ambient conditions. In a typical reaction, 5-benzyloxy-1,3-benzenedicarboxylic acid (**L1**) (86 mg, 0.316 mmol) was dissolved in 10 mL MeOH while separately $Co(NO_3)_2 \cdot 6H_2O$ (85.1 mg, 0.286 mmol) was dissolved in 7 mL MeOH. The **L1**/MeOH solution was combined with 4-picoline (0.10 mL, 1.00 mmol) and 2 mL of nitrobenzene. The $Co(NO_3)_2$ methanolic solution was subsequently layered over the methanolic solution containing 4-picoline, the ligand, and nitrobenzene using a 5 mL “blank” MeOH middle layer. The reaction vessel was capped and left undisturbed to facilitate slow diffusion. After several weeks, large blocks light pink to red in color of [**12**] were obtained (43 mg, 22.25 % yield).

The synthesis of [**12**] was also attempted *via* a solvothermal process. In this reaction, equimolar quantities of $Co(NO_3)_2$ and **L1** (0.300 mmol) were dissolved in 1 mL and 2 mL of N,N′-Dimethylformamide (DMF) respectively. 4-picoline (0.10 mL, 1.00 mmol) and 1 mL of methanol was added to the **L1**/DMF solution. The two solutions were

combined in a 20 mL scintillation vial, sealed with aluminum foil, capped and heated in a sand bath. The oven was ramped up from room temperature to 85 °C at a rate of 1.5 °C per minute, held constant for 12 hours and then cooled at a rate of 1.0 °C back to room temperature. Solvothermal reactions for [**12**] also resulted in marked improvement in single crystal quality (deep red rhombohedral plates) as well as enlarged yield with respect to that obtained *via* slow diffusion (120 mg, 82.35 % yield).

The cadmium analog, $[Cd(5\text{-benzyloxy-1,3-benzenedicarboxylate})(4\text{-picoline})_2]_n$ [**13**], was initially synthesized *via* slow diffusion/layering under ambient conditions. In a typical reaction, 5-benzyloxy-1,3-benzenedicarboxylic acid (**L1**) (86 mg, 0.316 mmol) was dissolved in 10 mL MeOH while separately $Cd(NO_3)_2 \cdot 6H_2O$ (93.6 mg, 0.306 mmol) was dissolved in 7 mL MeOH. 4-picoline was then added to the **L1**/MeOH solution (0.10 mL, 1.00 mmol) along with 2 mL of nitrobenzene. The methanolic solution of $Cd(NO_3)_2$ was subsequently layered over the methanolic solution containing the ligand, pyridine, and nitrobenzene using a 5 mL "blank" MeOH middle layer. The reaction vessels were capped and left undisturbed to allow for slow diffusion. After several weeks, large colorless blocks of [**13**] were obtained (49 mg, 29.6 % yield).

The synthesis of [**13**] was also attempted *via* a solvothermal process. In this reaction, equimolar quantities of $Cd(NO_3)_2$ and **L1** (0.300 mmol) were dissolved in 1 mL and 2 mL of N,N′-Dimethylformamide (DMF) respectively. 4-picoline (0.10 mL, 1.00 mmol) was added to the **L1**/DMF solution along with 1 mL of *o*-dichlorobenzene. The two solutions were combined in a 20 mL scintillation vial, sealed with aluminum foil, capped and heated in a sand bath. The oven was ramped up from room temperature to 85

°C at a rate of 1.5 °C per minute, held constant for 12 hours and then cooled at a rate of 1.0 °C back to room temperature. Solvothermal reactions for [**13**] also resulted in marked improvement in single crystal quality (colorless rhombohedral plates) as well as better yield with respect to that obtained *via* slow diffusion (128 mg, 84.35 % yield).

2.3.2.2 X-ray Crystallography

Single crystals of compounds **[8]-[10]** and **[13]** suitable for X-ray crystallographic analysis were selected following examination under a microscope. Intensity data were collected on a Bruker-AXS SMART APEX/CCD diffractometer using Cu k\α radiation (λ = 1.54178 Å).[281] The data were corrected for Lorentz and polarization effects and for absorption using the SADABS program (SAINT).[282] The structures were solved using direct methods and refined by full-matrix least-squares on $|F|^2$ (SHELXTL).[283] Select crystallographic data is presented in tabular form in Appendices C-8, C-9, C-10 and C-13.

Single crystals of compounds **[11]** and **[12]** suitable for X-ray crystallographic analysis were selected following examination under a microscope. Intensity data were collected on a Bruker-AXS SMART APEX/CCD diffractometer using Mo k\α radiation (λ = 0.7107 Å).[281] The data were corrected for Lorentz and polarization effects and for absorption using the SADABS program (SAINT).[282] The structures were solved using direct methods and refined by full-matrix least-squares on $|F|^2$ (SHELXTL).[283] Select crystallographic data is presented in tabular form in Appendices C-11 and C-12.

2.3.2.3 Powder X-ray Diffraction

Powder samples suitable for powder X-ray diffraction, FT-IR spectroscopy, and Thermal Gravimetric Analysis were obtained by removing a large amount of single crystals from the reaction scintillation vial by using a glass Pasteur pipette and depositing these crystal (along with mother liquor) in a small concave agar mortar. Excess solvent was removed *via* pipette, and surface solvent was removed by wicking action with a Kim-Wipe®. Upon wick drying, the crystals were transferred to a small piece of filter paper which was subsequently folded over and they were dried further and slightly crushed with gently pressure. The resulting dry powder (~30 mg) was then immediately applied to a PXRD sample puck prepared with a small amount of vacuum grease to fixate the powder sample, and the PXRD experiment performed without delay.

2.3.2.4 FT-IR Spectroscopy

All compounds, including synthesized ligands, were characterized *via* infrared spectroscopy using a Nicolet Avatar 320 Fourier-Transform Infrared Spectrometer (FT-IR). Before each sample was analyzed, a background spectrum was obtained for purposes of zeroing out ambient noise in the form of the laboratory atmosphere. Each sample was measured in the range from 4000 cm^{-1} to 500 cm^{-1} wavenumbers (wavelength of 2500 nm to 20000 nm respectively) and scanned 64 times. Results were recorded in % transmittance and the spectrum analyzed using the EZ OMNIC© (V.5.1b, copyright 1992-199 Nicolet Instruments Corporation) computer software suite. A typical sample was a

analyzed as a neat, dry solid (~10 mg) obtained *via* either vacuum filtration and air drying or gently drying with laboratory grade filter paper.

2.3.2.5 Thermal Gravimetric Analysis

Thermal Gravimetric Analysis for compounds **[8] – [13]** was performed on a PerkinElmer STA 6000 Simultaneous Thermal Analyzer. Data acquisition and analysis was performed with the assistance of the Pyris Series suite of software. Roughly 10-20 mg of dry powder was placed in a sample crucible and heated a t a rate of 10 °C/min. form a temperature of 30 °C up to 700 °C under a N_2 atmosphere.

2.4 Conclusion

In summary, this chapter has outlined several examples of novel, 2-periodic crystalline materials. These materials can be divided into two classifications based upon their topology; namely a platform of (4.8^2) *fes*-like structures as exemplified by the series of [M(5-benzyloxy-1,3-benzenedicarbocylate)(pyridine)$_2$]$_n$ (M = Zn^{2+}, Cd^{2+}, Co^{2+}) compounds, and a platform of (3.6.3.6) Kagomé lattice (*kgm*-like) structures exemplified by the series of compounds with formula unit {[M_2(5-benzyloxy-1,3-benzenedicarboxylate)$_2$(pyridine)$_2$]$_3$}$_n$ (M = Cu^{2+}, Zn^{2+}). These platforms, while only two examples, are indicative of the levels of complexity observed in metal-organic materials. That 2-periodic layered structures exhibit built in geometrical attributes (i.e. pore shape, pore dimensions, etc.) is a first rate indicator that they have inherent complexity not enjoyed by 1-perioic structures. Additionally, that individual layers in layered 2-periodic materials have the capacity to interact with adjacent layers adds to their interesting

supramolecular chemistry. Through the Kagomé platform of materials, the ability to control packing distances has been demonstrated in a systematic manner. Additionally, control over this packing distance can have related effects on other aspects of these materials supramolecular chemistry.

Chapter 3

Three-Periodic Frameworks from Pillaring Two-Periodic Layers

3.1 Introduction

Advancing from 2-periodic to 3-periodic metal-organic materials, it is to be expected that we shall, in general, observe increased complexity in those architectures which are available to us. Analogous to the extension from 1-periodic to 2-period structures, so too will the step up into 3-periodicity result in a higher degree of complexity. As was seen in the 2-periodic structures, where higher order lead to an increase in possibilities for what the node could accomplish, we observe the same trends in 3-periodic structures only now within more spatial directions. Geometries can still be distorted, and nodes can still be symmetrically unique, but the shear potential in the number of ways this can occur, in comparison to what can be observed in 2-periodic structures is truly staggering. This is one reason why, for practicality sake, we often limit our discussion of possible 3-periodic structures to only those that seem to be chemically feasible (i.e. uninodal, binodal, edge-transitive, networks).

3.1.1 3-Periodic Structures and Their Most Important Property

The most obvious trait of common 3-periodic when compared to that of their 2-periodic and 1-periodic counterparts is their ability to enclose space. More complicated 0-

periodic structures which adopt shapes reminiscent of polyhedra can also enclose space, making them, in my opinion more complicated than simple 2-periodic structures. These structures will be addressed in the next chapter. If a material has the capacity to enclose space, it also has the ability to entrap other smaller chemical entities. Naturally occurring zeolites, built from various cages sharing faces or bridged by rings, are prime example of this. Much of the interest in the materials arises from their ability to enclose objects within their framework. Metal-organic materials, primarily being modeled after zeolites, aim to harness this same ability; to enclose space and exhibit *porosity*.[177, 178, 183, 184]

3.1.2 Pillaring as a Design Strategy

While the majority of 3-periodic metal-organic materials are constructed by the direct self-assembly of judiciously selected building blocks predisposed towards generating such expansive structures (or even incapable of forming lower order structures), it is possible to obtain 3-periodic structures from components that are relatively less controllable. In some instances this is achieved by happenstance, where the components are combined and the conditions implemented such that 3-periodic structures arise serendipitously. Often, building blocks have the capacity to arrange in several different manners, adding to the latent diversity for these materials, but frequently to the detriment of the crystal engineer's control and predictability. In many instances, the answer is simply to conduct copious amounts of crystal engineering experiments, where one hopes to discern the principles controlling the formation of certain topologies with particular components. This however is not always a palatable solution, and so new design strategies which allow the crystal engineer access to 3-periodic topologies for

metal-organic materials constructed from relatively promiscuous components that might otherwise be difficult to control are exceedingly welcome.

One such possible design strategy is to isolate 2-periodic layered structures which are amenable to augmentation through the addition of an additional component. In this strategy, the SBU that comprises the metal-organic material must either have an open coordination site to accommodate the addition of a new ligand, or in its original state it should have labile axial groups that are easily replaced with stronger binding ditopic ligands. Based upon the use of the square paddlewheel SBU (Fig 3.1), there are at least three possible design strategies for the pillaring of two dimensional topologies into three dimensional frameworks; axial-to-axial, ligand-to-axial, and ligand-to-ligand (Fig. 3.2).

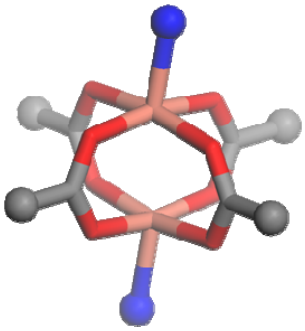

Figure 3.1 Illustration of the dimetal tetracarboxylate square paddlewheel SBU.

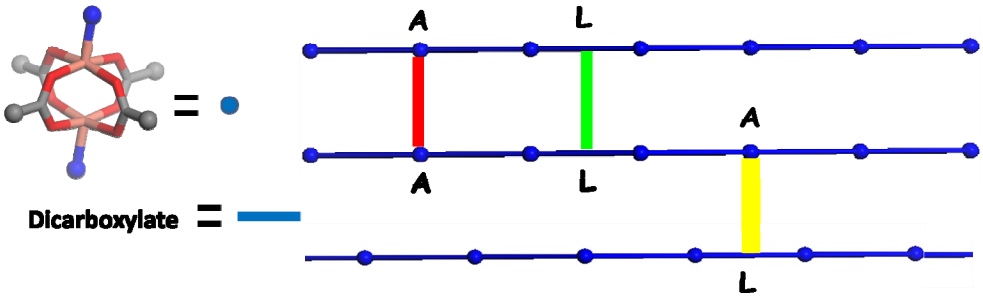

Figure 3.2 Cartoon illustrating the three possible pillaring design strategies; axial-to-axial, ligand-to-ligand, and ligand-to-axial

Each of the design strategies is based upon the location in the network where the pillaring will takes place. In the axial-to-axial strategy, the pillar is an additional chemical moiety, bifunctional in nature and capable of coordinating in the axial position of the SBU (blue atoms in Fig. 3.1). Using the axial-to-axial method, the individual layers should be layered directly above one another in an eclipsed fashion where the SBU's are collimated. The ligand-to-axial method, while not a pillar in the traditional sense, involves incorporating a judiciously designed organic ligand which is capable of forming the desired SBU (i.e. a dicarboxylate) and then contains another separate functional group, usually of a different type (i.e. pyridyl moiety) capable of coordinating in the axial position of another SBU. This method eliminates the requirement for the additional chemical constituent as the single organic ligand provides for both the bridging between SBUs in the 2D layers as well as the segment needed to pillar those layers into the 3-periodic framework. Adopting this motif will necessarily force subsequent layers to be slipped with respect to one another. The final method, ligand-to-ligand, involves an

appropriate organic ligand which can simultaneously link two SBUs into the desired 2-periodic topology while also connecting two different layers through an organic bridge.

3.2 Camphoric Acid Square Lattices with Dipyridyl Based Pillars

For the purposes of this chapter a single dicarboxylic acid, namely (1R, 3S)-(+)-1,2,2-trimethyl cyclopentane-1,3-dicarboxylic acid (camphoric acid, Fig. 3.3) was employed in combination with several first row transition metal cations (Zn^{2+}, Co^{2+}, and Ni^{2+}) and an assortment of roughly linear dipyridyl organic molecules (pillars) to investigate this diacid's ability to generate a series of closely related crystalline materials based upon the design principle of pillaring, which could subsequently be investigated further in relation to their physical and chemical properties and potential applications. This dicarboxylic acid is attractive for several reasons.

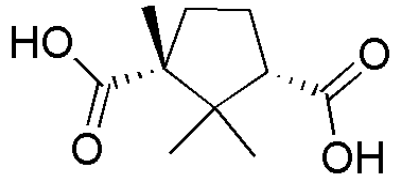

Figure 3.3 Chemical Sketch of (1R, 3S)-(+)-1,2,2-trimethylcyclopentane-1,3-dicarboxylic acid.

First and foremost in the synthesis of *practical* functional metal-organic materials is the general principal that the starting materials should be readily available (i.e. not too difficult to synthesize in high yield and high purity), cheap, and relatively non-toxic to either the user or the environment in general (even "useful" materials that kill the user or overtly poison of the environment will be subject to regulation or banishment). As a store

bought chemical which is also widely used in pharmaceuticals where humans can consume large amounts without harmful repercussions, camphoric acid satisfies each of these requirements. It may be argued that the first two points are somewhat flexible in that an appropriately useful material especially suited and capable of fulfilling some dire need of society will lead to improvements on both fronts. That is to say, if a particular object is the only one of its kind to achieve some necessary endeavor, then the ability to obtain the materials required to make that object will be of keen interest. In such cases, new ways of making difficult ligands might be explored as well as other means to bring down overall costs. One could say that if the need is vital enough and the material uniquely suited, then the rest is a matter of engineering and persistence. The last point, dealing with the toxicity of the material happens to be a little stickier, and the current political and social environment does not appear likely to become more lax anytime soon.

Camphoric acid[289-298] is also an intriguing ligand because it is chiral which in itself can sometimes lead to interesting physical properties exhibited in MOMs. If integrated into a robust porous framework, the presence of camphoric acids' two chiral centers may influence the observable properties of the MOM. Additionally, as will be seen in the section to follow, when camphoric acid is incorporated into layered sheets, the nature of the angle subtended between carboxylate groups and their relative orientation, together with the ligands relative size, combines to result in a unique and characteristic bow-tie motif. This bow-tie motif will prove to be more useful than simply a unique orientation, and as we shall see it affords the crystal engineer an increased level of structural control.

3.2.1 Camphoric Acid Square Lattices

The unique geometry of the individual layers (Fig 3.4) seen in a pillared camphoric structure belies the fact that this layer, at its roots is simply a (4,4) square grid topology. Just as the commonly observed brick wall pattern and a chess board (uncolored) are topologically equivalent, but with different local geometries, so too is this layer related to both of those patterns. However the bow-tie geometry of this material makes it interesting from the standpoint of controlling interpenetration and the generation of pores/channels.

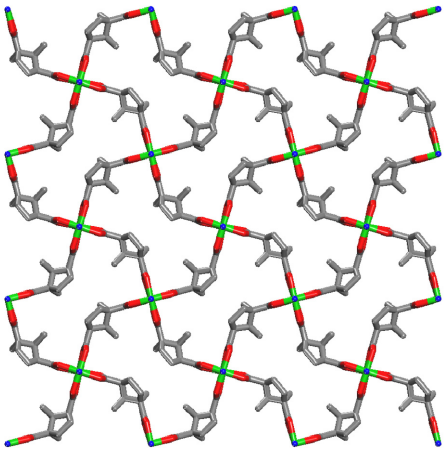

Figure 3.4 Illustration of a single layer from a pillared camphoric structure. Note the distorted bow-tie geomtey for this (4,4) square grid.

The length of the longest portion of the bowtie, as measured from carbon atoms on opposite camphorate ligands was observed to be 11.8 Å. At the closest approach, the width of the bow tie is only 4.099 Å in length, and when accounting for van der Waal radii this is reduced to ~1.7 Å. Careful observation shows that no material, except

perhaps H_2 molecules can pass through this "opening". All of the pillared camphoric acid structures have this layer as a repeating unit.

3.2.2 Dipyridyl Type Pillars

For the purpose of pillaring camphorate square grid layers into extended 3-periodic frameworks, it was decided that bifunctional organic molecules which contained pyridyl moieties (N-donor ligands) on either end would be employed. This is because of the relatively high probability of success that these molecules afford. One the one hand, 2-periodic layered structures composed of the camphoric diacid with several different transition metals, built from dimetal tetracarboxylate square paddlewheel SBUs, and generating a (4, 4) MOF-2 topology had already been known.[297] In these structures, the terminal axial ligand coordinating to the metal ions was typically either a mono- pyridyl type ligand (pyridine, picoline, methoxypyridine, etc.) or a solvent molecule. Additionally, the square paddlewheel SBU is renowned for its ability to be pillared with dipyridyl type linkages along its metal-metal axis. The preeminent dipyridyl type pillar is the one that lends its name to the category, 4,4′dipyridyl (also 4,4′-bipyridyl; bipy). This molecule is perfectly linear with respect to the orientation of how the two nitrogen atoms coordinate to metal ions, but the rings themselves do have the capacity to rotate freely around this same axis. Other pillars closely related to bipy modify the length between the two coordinating nitrogen atoms, introduce additional functionality into the rings, or achieve both simultaneously. The pillars selected for this study (Fig. 3.5) were chosen to cover a range of dimensions as well as to incorporate some diversity in functionality. All of the pillars were available for purchase form commercial sources and used as is, save

for N,N′-di(4-pyridyl)-1,4,5,8-naphthalenetetracarboxydiimide[299] (BIP-PY), which was synthesized by another researcher in the lab.

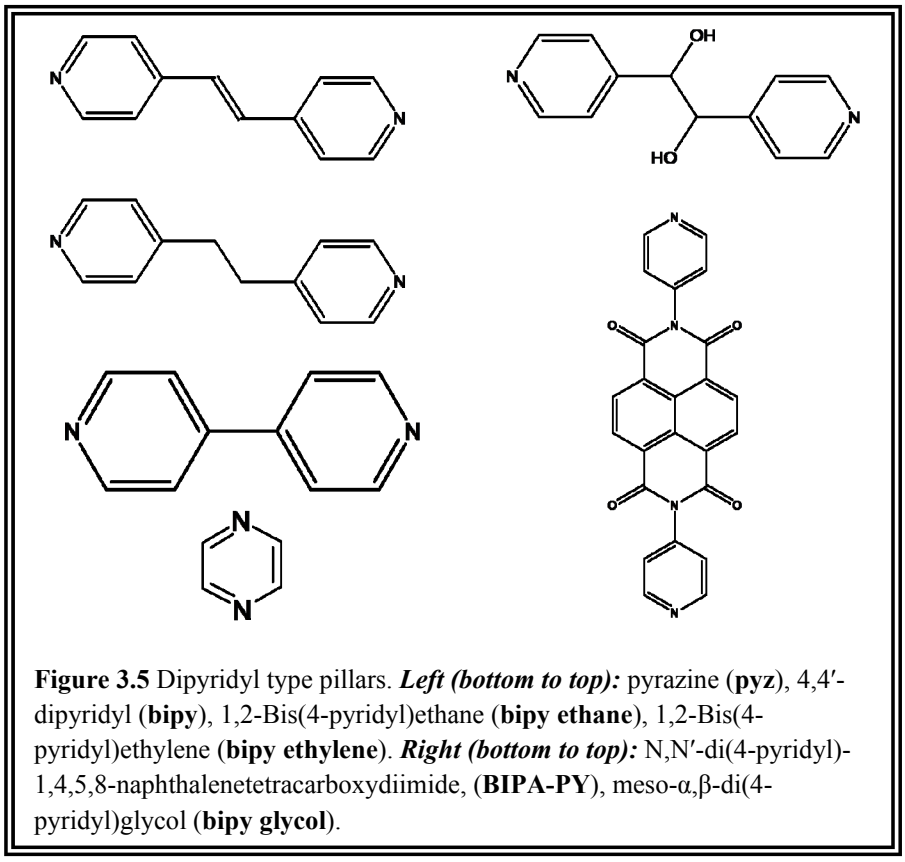

Figure 3.5 Dipyridyl type pillars. ***Left (bottom to top):*** pyrazine (**pyz**), 4,4′-dipyridyl (**bipy**), 1,2-Bis(4-pyridyl)ethane (**bipy ethane**), 1,2-Bis(4-pyridyl)ethylene (**bipy ethylene**). ***Right (bottom to top):*** N,N′-di(4-pyridyl)-1,4,5,8-naphthalenetetracarboxydiimide, (**BIPA-PY**), meso-α,β-di(4-pyridyl)glycol (**bipy glycol**).

3.2.3 Structural Analysis

3.2.3.1 Layer Arrangements

When an extended 3-periodic structure is said to be the result of pillaring other 2-periodic layers, it may sometimes be of benefit to retain some of the structural identifiers of the individual layers. If this were not the case, then the choice of the layer would not be of any consequence. If the goal is to preserve a particularly shaped pore and extend this into a channel, then control over how individual layers align through the pillaring

process will be needed. In the case of undistorted square grids and similar structures this alignment is of no importance; rather all alignments are equivalent. However, in some cases, as with camphoric acid, the individual layer is so oriented so as to produce very unique local geometry around the nodes. In these cases, how subsequent layers align could have very important consequences. As an example take an individual layer of the pillared camphoric structures. There are definitive directions in this distorted brick wall structure. When the layers begin to stack, two possibilities arise; either the layers stack perfectly eclipsed in an AAA fashion, or they stack in an anti-parallel ABAB fashion as depicted in Figure 3.6. If there was a desire to retain the unique geometry of the individual layer and extend this into a column running parallel to the pillar axis, it would be necessary to ensure that the anti-parallel packing does not occur. Specifically in the case of camphoric acid, it turns out that the alignment is not that important after all, as the tight bow-tie confirmation already precludes channel development.

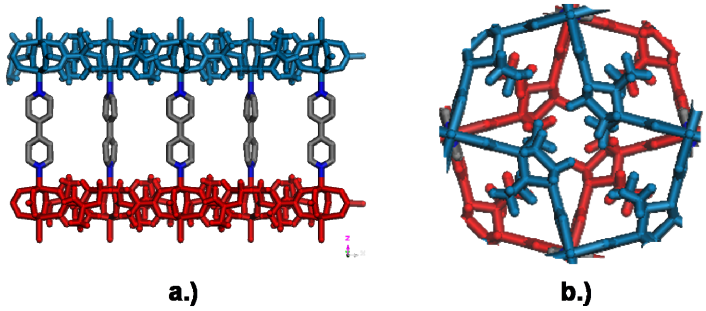

Figure 3.6 Cartoon illustrating the anti-parallel stacking of layers observed in compounds **[16] – [18].** The two layers (red and blue) are not equivalent. Notice the orientation of the bow-ties in the two layers in the figure to the right.

3.2.3.2 Lack of Entanglements in Camphoric Based Structures

The unique bow-tie geometry of the (4,4) square grid layer structure seen in the pillared camphoric structures has at least one important implication for the overall solid-state structure. Typically, MOF-2 type layers which are then pillared into extended 3-periodic frameworks, have the potential to undergo interpenetration. The nature of the topology and the dimension of the cavities, are often amenable to a second (or third, or more, etc.) network interweaving with the first. The concept of interpenetrating is sometimes seen as a negative aspect of some frameworks as it can take up space or block access to channels. It is also sometimes difficult to control whether a framework exists in an interpenetrated form or not. This often makes interpenetration the anathema of crystal engineers who aim to control every aspect of a materials synthesis.

In the case of the camphoric structures, the tight bow-tie arrangement of the individual layers precludes the possibility of interpenetrating though these sheets. This implies that a greater control over the possible assembly of these materials can be had by the synthetic chemist. It also means that when using this ligand in a pillaring motif, one needs not worry about the possibility of interpenetration occurring and thus, designed structures can be obtained with a higher degree of certainty.

3.2.3.3 Controllable Pore Size and Predictable Surface Areas

As the potential for interpenetration is of no concern, and the ligand has been judiciously selected so that it effectively precludes the possibility of any channels or columns existing along the direction of the pillar, we have generated a synthetic system

in which the individual layers are essentially sheets or walls with no holes for small molecules or gases to pass through. Additionally, these sheets are situated on struts (i.e. the pillar) which we control, both in terms of functionality and in terms of metrics. Therefore we have devised a reliably controllable system of a closed surface where we can practically dial in the distance between walls. This is typically not an easy feat. Thus the small channel formed perpendicular to the pillar axis, and regulated by the length and girth of the pillars we choose, is the only determining factor controlling the pore size for this material. This is truly an example of exquisite control of the structure of a material. By dialing in the length of the pillar, we also can predictably adjust the distance between the walls, and therefore control the expected surface area for this platform of materials.

3.2.4 Applications and Properties

3.2.4.1 Gas sorption

Once synthesized, the crystalline materials were treated through a number of protocols in an attempt to "activate" them prior to gas sorption measurements. By "activate", we mean to replace otherwise higher boiling solvent molecules and guests present in the crystal structure with relatively low boiling solvent molecules, in an attempt to facilitate the complete removal of all guest and solvent molecules upon vacuum evacuation. The presence of any higher boiling solvent molecules, such as N,N′-dimethylformamide which is present in the reaction solution, may mitigate the materials ability to uptake the sorbent gas being investigated. In a typical activation process the reaction solution in the vial containing the crystalline samples of aryloxy nanoballs was

removed *via* Pasture pipette and the crystals washed with neat reaction solvent, in this case DMF. The washing process is prescribed to remove any unreacted starting materials such as ligand or metal ions which may still be present in the mother liquor and possibly coat the sample crystals. The crystals were allowed to sit in the fresh DMF for approximately 15 minutes before the process was repeated, the DMF removed and replaced with a fresh aliquot. The sample was washed three times with fresh DMF. After the third washing, the DMF solvent was removed and a second, typically a low boiling solvent was introduced. Again the crystals were allowed to sit immersed in the new solvent, however now the sample was left undisturbed for ~12 hours. After ample time immersed in the exchange solvent, so chosen that is may diffuse into the material while any other solvent guest present will subsequently diffuse out of the material into the bulk exchange solvent, the process is repeated. Typically the samples were exchanged at least three times before the sorption experiments commenced.

Upon activation each of the synthesized pillared camphoric acid structure (compounds **[14] – [29]**) was investigated for its sorption abilities. With early success from the [Ni(camphorate)(**bipy**)$_{0.5}]_n$, compound **[17],** it looked promising that our strategy of designing a material with predictable and exquisitely controllable pore sizes and scalable surface areas would provide a unique series of materials with which to test the hypothesis that small pore sizes lead to increased isosteric heats of adsorption at low temperatures and pressures. Much of the evidence collated so far in the community seem to validate this assumption, however few systematic studies exist to definitively set the record straight; comparisons of materials that are somewhat closely related albeit still

different have had to suffice. The camphoric system was supposed to provide a truly systematic series of compounds that were intimately controllable down to their single pore/channel size and the functionality of their surfaces.

Unfortunately the vast majority of these structures never made it past the activation stage, failing to exhibit any significant levels of porosity, despite dogged attempts to activate them through myriad protocols. The quirky aspect is that the majority display high levels of thermal stability as demonstrated by TGA analysis. [Ni(camphorate)(**bipy**)$_{0.5}$]$_n$, compound **[17]**, was the first pillared camphorate structure studied in our lab to demonstrate high levels of porosity. Following an activation protocol as outlined above, using any number of solvents (acetone, $CHCl_3$, MeCN, MeOH, EtOH, and DCM, among others) this crystalline material was suitable evacuated upon exposure to a vacuum pump for ~14 hours, that the material demonstrated the ability to absorb a significant amount of N_2 gas when analyzed on the QuantumChrome Instruments NOVA 2000. Five point B.E.T. (Brunauer-Emmett-Teller)[300] calculations used for estimating the accessible surface area of a porous solid, predicted a surface area roughly 1450-1500 m^2/g after exchange with each of these solvents, with dichloromethane performing the best. Further analysis was conducted using a QuantumChrome Instruments Autosorb-1, on which isotherms for the sorption of molecular hydrogen (77K and 87K) (Fig. 3.7, green and black respectively) and nitrogen (77K) (Fig. 3.7, red) were collected. The collection of this data revealed an estimated surface area of 1450 m^2/g in good agreement with the observed value from the NOVA 2000 instrument. All isotherms were observed to be type I (Langmuir isotherms) which is indicative of microporous materials.

Hydrogen storage isotherms conducted at 77K showed a maximum uptake of 1.6 wt % H_2 at $P/P_0 = 1.0$ (with P_0 set at 760 torr). Use of the two different temperature isotherms facilitated calculation of the heats of adsorption (Q_{st}) for this material, which was observed to be ~5.8 kJ/mol at low loading dropping to a slightly lower value of ~5.3 kJ at 100% loading (Figure 3.8, red)

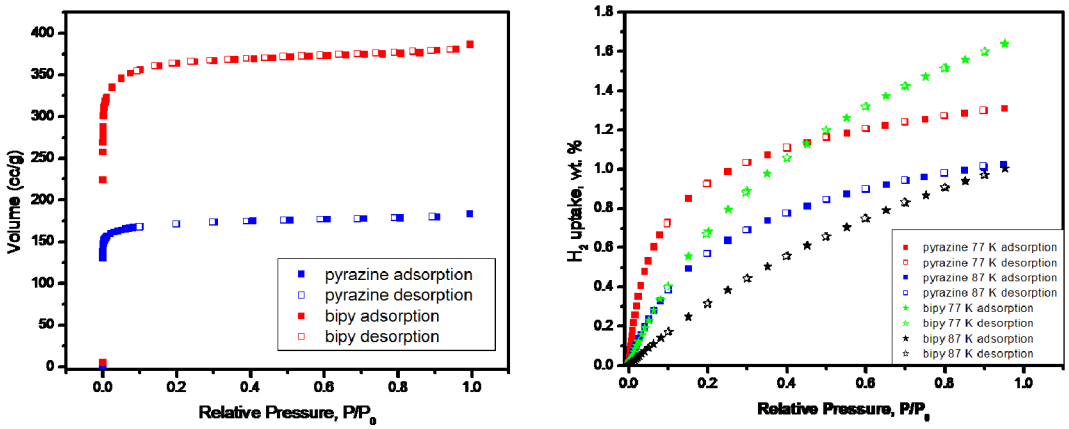

Figure 3.7 ***Left:*** N_2 Isotherm (77K) for compounds **[14]** (red) and **[17]** (blue)**.** H_2 isotherms (77K and 87K) for compounds **[14]** (red) and **[17]** (blue)**.**

Calculations (using a probe size of 1.8 Å) suggest that this material has a pore volume of 0.591 cc/g while the data from the Autosorb-1 experiments suggests a pore volume of 0.588 cc/g in very good agreement. A second structure, [Ni(camphorate)(**pyrazine**)$_{0.5}$]$_n$, compound **[14],** was also show to be highly porous, and fortuitously allowed us at least one compound to compare with. All of this material's isotherms and Heats of adsorption plot are given in the above figures for easy reference. As expected, with a smaller pore size (Fig 3.9) (4.6 Å x 4.2 Å for **pyrazine** versus 8.8 Å x 4.4 Å for **bipy**), the **pyrazine** compound demonstrated a markedly higher Q_{st} (~7.3

kJ/mol vs. ~5.8 kJ/mol). Here the calculated pore volume was 0.29 cc/g, while the value obtained from data collected on the Autosorb-1 indicated a pore volume of 0.28 cc/g. Additionally, a third sample, [Co(camphorate)(**pyrazine**)$_{0.5}$]$_n$, compound **[15]**, was also shown be porous with similar results to that of the camphorate analogue.

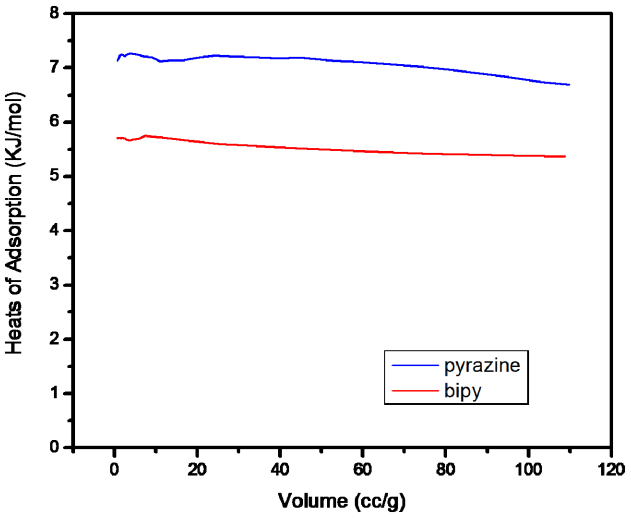

Figure 3.8 Plot of Isosteric Heats of Adsorption (kJ/mol) vs. volume (cc/g).

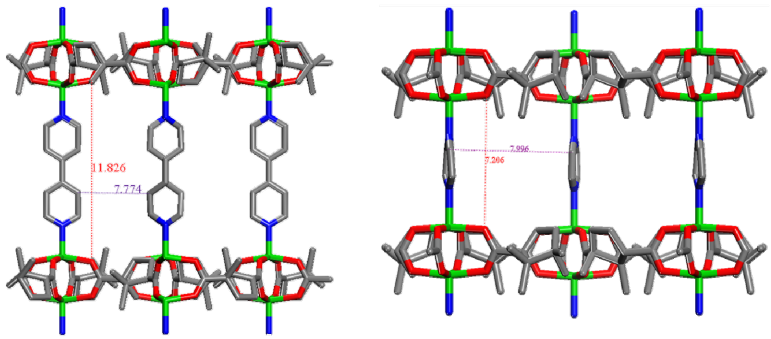

Figure 3.9 Illustration of the relative pore sizes in compounds **[17]** (*left*) and **[14]** (*right*).

3.2.4.2 Dichroism in Metal-Organic Materials

One very peculiar aspect of [Co(camphorate)(**bipy**)$_{0.5}$]$_n$, compound **[18],** was that upon completion of the solvothermal reaction there appeared to be crystal of two very different colors in the same vial (Fig 3.10). The existence of both deep red and deep blue square plate crystals in the reaction vial was not immediately a reason of concern (interest maybe), as many times in the synthesis of metal-organic materials there is a real possibility for the reaction to generate more than structure. Additionally, the different possible crystal structures often produce very distinct crystal morphologies and colors. Cobalt is also known to adopt both colors in various coordination environments, so it was not as if the colors were outlandish. Upon mounting a single crystal on the goniometer head of the single crystal X-ray diffraction instrument, and rotating the crystal to ensure the incidence of X-rays would be uniform, it was observed that crystals appeared to change color from red to blue, as the crystal swept through an angle of 90°. Further observation under a digital optical microscope equipped with a rudimentary light polarizer, revealed that indeed the color of the light transmitted by these crystals was dependent upon the polarization of the incident light. This variable transmittance of light by a crystal based upon the polarization of the light as it hits the crystal is a very common phenomenon in gem stones and other naturally occurring crystals in rock. The term for such a property is pleochroism (for many colors) or dichroism in the case when only two colors are observed. Pleochroism is an important aspect of geology because it can aid in the identification of trace substances in rock samples, based upon how polarized light behaves. Dichroism is seldom if ever mentioned in the case of metal-organic materials

however, and indeed a literature search for examples in MOMs was unsuccessful. Essentially, the existence of this optical phenomenon for these particular crystals indicates that they absorb light differently along unique directions in the crystal as light is transmitted through the sample. Further investigation of this phenomenon using specular reflectance with Dr. Ronald Musselman is ongoing, but at this time a detailed account for the observed selective adsorption of polarized light is lacking.

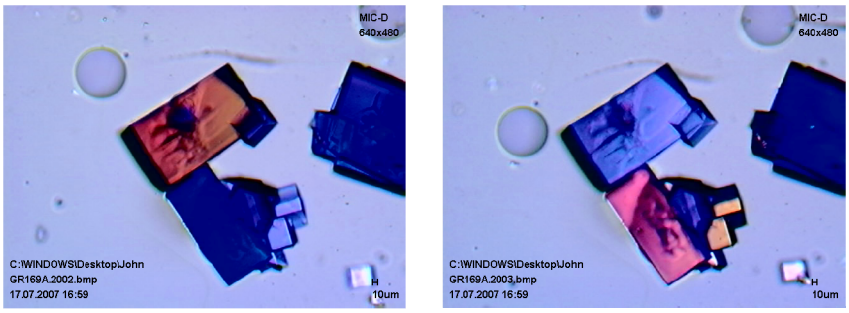

Figure 3.10 Digital photograph depicting the observed Dichroism in compound **[18].** The sample remained unaltered as the polarization of the light was changed by 90° between capturing the two images.

3.2.5 Experimental

3.2.5.1 Synthesis

All reagents, unless described otherwise, were purchased from either Sigma-Aldrich or Fischer Scientific and used as received without further purification. Bulk solvents such as methanol, ethanol, acetone, and dichloromethane were first distilled and stored over drying media (4Å molecular sieves) before their use.

$[Ni_2(camphorate)_2(pyrazine)_{0.5}]_n$, **[14]**, was synthesized *via* a one-pot solvothermal reaction conducted in a 20 mL scintillation vial. In a typical reaction, **pyrazine** (0.1 mmol, 8.0 mg), 2,6-lutidine (0.4 mmol, 46.44 μL), and (1R, 3S)-(+)-1,2,2-trimethyl cyclopentane-1,3-dicarboxylic acid (camphoric acid, Fig. 3.3) (0.2 mmol, 40.05 mg) were combined together with exactly 2 mL of N,N′-dimethylformamide (DMF) and manually agitated until both solids were fully dissolved. To this solution, 1 mL of dimethyl sulfoxide (DMSO) was added and the solution agitated for several seconds. Separately, $Ni(NO_3)_2 \bullet 6H_2O$ (0.2 mmol, 58.2 mg) was dissolved in exactly 1 mL of DMF, and upon dissolution, was added to the camphorate/**pyrazine**/2,6-lutidne/DMSO solution. The vial was sealed with store bought kitchen aluminum foil, capped tightly and placed in a sand bath for transfer to a programmable oven. The heat profile was as follows: the reaction temperature was raised from 30 °C to 115 °C at a rate of 1.5 °C per minute upon which time it was held at that temperature for 24 hours. The temperature was then slowly cooled back down to 30 °C at a rate of 1.0 °C per minute. Upon removal from the oven a large amount of green square-plate crystals suitable for single crystal X-ray diffraction were observed to have formed (67 mg, 50.56% yield).

$[Co_2(camphorate)_2(pyrazine)_{0.5}]_n$, **[15]**, was synthesized *via* a one-pot solvothermal reaction conducted in a 20 mL scintillation reaction vial. In a typical reaction, **pyrazine** (0.1 mmol, 8.0 mg), 2,6-lutidine (0.4 mmol, 46.44 μL), and camphoric acid (0.2 mmol, 40.05 mg) were combined together with exactly 2 mL of N,N′-dimethylformamide (DMF) and manually agitated until both solids were fully dissolved. To this solution, 1 mL of methanol (MeOH) was added and the solution agitated for

several seconds. Separately, $Co(NO_3)_2 \cdot 6H_2O$ (0.2 mmol, 58.2 mg) was dissolved in exactly 1 mL of DMF, and upon dissolution, was added to the camphorate/**pyrazine**/2,6-lutidne/MeOH solution. The vial was sealed with store bought kitchen aluminum foil, capped tightly and placed in a sand bath for transfer to a programmable oven. The heat profile was as follows: the reaction temperature was raised from 30 °C to 115 °C at a rate of 1.5 °C per minute upon which time it was held at that temperature for 24 hours. The temperature was then slowly cooled back down to 30 °C at a rate of 1.0 °C per minute. Upon removal from the oven a large amount of pink square-plate crystals suitable for single crystal X-ray diffraction were observed to have formed (89 mg, 72.3% yield).

$[Zn_2(camphorate)_2(4,4'\text{-dipyridyl})_{0.5}]_n$, **[16]**, was synthesized *via* a one-pot solvothermal reaction conducted in a 20 mL scintillation reaction vial. In a typical reaction, **bipy** (0.1 mmol, 15.62 mg), 2,6-lutidine (0.4 mmol, 46.44 μL), and camphoric acid (0.2 mmol, 40.05 mg) were combined together with exactly 2 mL of N,N′-dimethylformamide (DMF) and manually agitated until both solids were fully dissolved. To this solution, 1 mL of methanol (MeOH) was added and the solution agitated for several seconds. Separately, $Zn(NO_3)_2 \cdot 6H_2O$ (0.2 mmol, 59.5 mg) was dissolved in exactly 1 mL of DMF, and upon dissolution, was added to the camphorate/**bipy**/2,6-lutidne/MeOH solution. The vial was sealed with store bought kitchen aluminum foil, capped tightly and placed in a sand bath for transfer to a programmable oven. The heat profile was as follows: the reaction temperature was raised from 30 °C to 115 °C at a rate of 1.5 °C per minute upon which time it was held at that temperature for 24 hours. The temperature was then slowly cooled back down to 30 °C at a rate of 1.0 °C per minute.

Upon removal from the oven a large amount of colorless square-plate crystals suitable for single crystal X-ray diffraction were observed to have formed (55 mg, 41.7% yield).

$Ni_2(camphorate)_2(4,4'\text{-dipyridyl})_{0.5}]_n$, **[17]**, was synthesized *via* a one-pot solvothermal reaction conducted in a 20 mL scintillation reaction vial. In a typical reaction, **bipy** (0.1 mmol, 15.62 mg), 2,6-lutidine (0.4 mmol, 46.44 μL), and camphoric acid (0.2 mmol, 40.05 mg) were combined together with exactly 2 mL of N,N′-dimethylformamide (DMF) and manually agitated until both solids were fully dissolved. To this solution, 1 mL of ethanol (EtOH) was added and the solution agitated for several seconds. Separately, $Ni(NO_3)_2 \cdot 6H_2O$ (0.201 mmol, 58.45 mg) was dissolved in exactly 1 mL of DMF, and upon dissolution, was added to the camphorate/**bipy**/2,6-lutidne/ EtOH solution. The vial was sealed with store bought kitchen aluminum foil, capped tightly and placed in a sand bath for transfer to a programmable oven. The heat profile was as follows: the reaction temperature was raised from 30 °C to 115 °C at a rate of 1.5 °C per minute upon which time it was held at that temperature for 24 hours. The temperature was then slowly cooled back down to 30 °C at a rate of 1.0 °C per minute. Upon removal from the oven a large amount of green square-plate crystals suitable for single crystal X-ray diffraction were observed to have formed (45 mg, 38.2% yield).

$Co_2(camphorate)_2(4,4'\text{-dipyridyl})_{0.5}]_n$, **[18]**, was synthesized *via* a one-pot solvothermal reaction conducted in a 20 mL scintillation reaction vial. In a typical reaction, **bipy** (0.1 mmol, 15.62 mg), 2,6-lutidine (0.4 mmol, 46.44 μL), and camphoric acid (0.2 mmol, 40.05 mg) were combined together with exactly 2 mL of N,N′-dimethylformamide (DMF) and manually agitated until both solids were fully dissolved.

To this solution, 1 mL of ethanol (EtOH) was added and the solution agitated for several seconds. Separately, $Co(NO_3)_2 \bullet 6H_2O$ (0.199 mmol, 57.91 mg) was dissolved in exactly 1 mL of DMF, and upon dissolution, was added to the camphorate/**bipy**/2,6-lutidne/ EtOH solution. The vial was sealed with store bought kitchen aluminum foil, capped tightly and placed in a sand bath for transfer to a programmable oven. The heat profile was as follows: the reaction temperature was raised from 30 °C to 115 °C at a rate of 1.5 °C per minute upon which time it was held at that temperature for 24 hours. The temperature was then slowly cooled back down to 30 °C at a rate of 1.0 °C per minute. Upon removal from the oven a large amount of what appeared to be purple square-plate crystals suitable for single crystal X-ray diffraction were observed to have formed (63 mg, 51.9% yield).

$Zn_2(camphorate)_2(1,2\text{-Bis}(4\text{-pyridyl})ethane)_{0.5}]_n$, **[19]**, was synthesized *via* a one-pot solvothermal reaction conducted in a 20 mL scintillation reaction vial. In a typical reaction, **bipy ethane** (0.098 mmol, 18.06 mg), 2,6-lutidine (0.4 mmol, 46.44 μL), and camphoric acid (0.2 mmol, 40.05 mg) were combined together with exactly 2 mL of N,N′-dimethylformamide (DMF) and manually agitated until both solids were fully dissolved. To this solution, 1 mL of methanol (MeOH) was added and the solution agitated for several seconds. Separately, $Zn(NO_3)_2 \bullet 6H_2O$ (0.2 mmol, 59.5 mg) was dissolved in exactly 1 mL of DMF, and upon dissolution, was added to the camphorate/ **bipy ethane** /2,6-lutidne/MeOH solution. The vial was sealed with store bought kitchen aluminum foil, capped tightly and placed in a sand bath for transfer to a programmable oven. The heat profile was as follows: the reaction temperature was raised from 30 °C to 115 °C at a rate of 1.5 °C per minute upon which time it was held at that temperature for

24 hours. The temperature was then slowly cooled back down to 30 °C at a rate of 1.0 °C per minute. Upon removal from the oven a large amount of colorless square-plate crystals suitable for single crystal X-ray diffraction were observed to have formed (55 mg, 41.7% yield).

$Ni_2(camphorate)_2(1,2\text{-Bis}(4\text{-pyridyl})ethane)_{0.5}]_n$, **[20]**, was synthesized *via* a one-pot solvothermal reaction conducted in a 20 mL scintillation reaction vial. In a typical reaction, **bipy ethane** (0.1 mmol, 18.42 mg), 2,6-lutidine (0.4 mmol, 46.44 μL), and camphoric acid (0.2 mmol, 40.05 mg) were combined together with exactly 2 mL of N,N′-dimethylformamide (DMF) and manually agitated until both solids were fully dissolved. To this solution, 1 mL of methanol (MeOH) was added and the solution agitated for several seconds. Separately, $Ni(NO_3)_2 \cdot 6H_2O$ (0.201 mmol, 58.45 mg) was dissolved in exactly 1 mL of DMF, and upon dissolution, was added to the camphorate/ **bipy ethane** /2,6-lutidne/MeOH solution. The vial was sealed with store bought kitchen aluminum foil, capped tightly and placed in a sand bath for transfer to a programmable oven. The heat profile was as follows: the reaction temperature was raised from 30 °C to 115 °C at a rate of 1.5 °C per minute upon which time it was held at that temperature for 24 hours. The temperature was then slowly cooled back down to 30 °C at a rate of 1.0 °C per minute. Upon removal from the oven a large amount of green square-plate crystals suitable for single crystal X-ray diffraction were observed to have formed (45 mg, 38.2% yield).

$Co_2(camphorate)_2(1,2\text{-Bis}(4\text{-pyridyl})ethane)_{0.5}]_n$, **[21]**, was synthesized *via* a one-pot solvothermal reaction conducted in a 20 mL scintillation reaction vial. In a typical

reaction, **bipy ethane** (0.1 mmol, 18.40 mg), 2,6-lutidine (0.4 mmol, 46.44 μL), and camphoric acid (0.2 mmol, 40.05 mg) were combined together with exactly 2 mL of N,N′-dimethylformamide (DMF) and manually agitated until both solids were fully dissolved. To this solution, 1 mL of methanol (MeOH) was added and the solution agitated for several seconds. Separately, $Co(NO_3)_2 \cdot 6H_2O$ (0.199 mmol, 57.91 mg) was dissolved in exactly 1 mL of DMF, and upon dissolution, was added to the camphorate/ **bipy ethane** /2,6-lutidne/MeOH solution. The vial was sealed with store bought kitchen aluminum foil, capped tightly and placed in a sand bath for transfer to a programmable oven. The heat profile was as follows: the reaction temperature was raised from 30 °C to 115 °C at a rate of 1.5 °C per minute upon which time it was held at that temperature for 24 hours. The temperature was then slowly cooled back down to 30 °C at a rate of 1.0 °C per minute. Upon removal from the oven a large amount of what appeared to be purple square-plate crystals suitable for single crystal X-ray diffraction were observed to have formed (74 mg, 71% yield).

$[Zn_2(camphorate)_2(1,2\text{-Bis}(4\text{-pyridyl})ethylene)_{0.5}]_n$, **[22]**, was synthesized *via* a one-pot solvothermal reaction conducted in a 20 mL scintillation reaction vial. In a typical reaction, **bipy ethylene** (0.1 mmol, 15.62 mg), 2,6-lutidine (0.4 mmol, 46.44 μL), and camphoric acid (0.2 mmol, 40.05 mg) were combined together with exactly 2 mL of N,N′-dimethylformamide (DMF) and manually agitated until both solids were fully dissolved. To this solution, 1 mL of methanol (MeOH) was added and the solution agitated for several seconds. Separately, $Zn(NO_3)_2 \cdot 6H_2O$ (0.2 mmol, 59.5 mg) was dissolved in exactly 1 mL of DMF, and upon dissolution, was added to the camphorate/

bipy ethylene /2,6-lutidne/MeOH solution. The vial was sealed with store bought kitchen aluminum foil, capped tightly and placed in a sand bath for transfer to a programmable oven. The heat profile was as follows: the reaction temperature was raised from 30 °C to 115 °C at a rate of 1.5 °C per minute upon which time it was held at that temperature for 24 hours. The temperature was then slowly cooled back down to 30 °C at a rate of 1.0 °C per minute. Upon removal from the oven a large amount of colorless square-plate crystals suitable for single crystal X-ray diffraction were observed to have formed (79 mg, 59.3% yield).

$Ni_2(camphorate)_2(1,2\text{-Bis}(4\text{-pyridyl})ethylene)_{0.5}]_n$, **[23]**, was synthesized *via* a one-pot solvothermal reaction conducted in a 20 mL scintillation reaction vial. In a typical reaction, **bipy ethylene** (0.1 mmol, 15.62 mg), 2,6-lutidine (0.4 mmol, 46.44 μL), and camphoric acid (0.2 mmol, 40.05 mg) were combined together with exactly 2 mL of N,N′-dimethylformamide (DMF) and manually agitated until both solids were fully dissolved. To this solution, 1 mL of ethanol (EtOH) was added and the solution agitated for several seconds. Separately, $Ni(NO_3)_2 \cdot 6H_2O$ (0.201 mmol, 58.45 mg) was dissolved in exactly 1 mL of DMF, and upon dissolution, was added to the camphorate/ **bipy ethylene** /2,6-lutidne/ EtOH solution. The vial was sealed with store bought kitchen aluminum foil, capped tightly and placed in a sand bath for transfer to a programmable oven. The heat profile was as follows: the reaction temperature was raised from 30 °C to 115 °C at a rate of 1.5 °C per minute upon which time it was held at that temperature for 24 hours. The temperature was then slowly cooled back down to 30 °C at a rate of 1.0 °C per minute. Upon removal from the oven a large amount of green square-plate crystals

suitable for single crystal X-ray diffraction were observed to have formed (57 mg, 48.2% yield).

Co_2(camphorate)$_2$(1,2-Bis(4-pyridyl)ethylene)$_{0.5}]_n$, **[24]**, was synthesized *via* a one-pot solvothermal reaction conducted in a 20 mL scintillation reaction vial. In a typical reaction, **bipy ethylene** (0.1 mmol, 18.40 mg), 2,6-lutidine (0.4 mmol, 46.44 μL), and camphoric acid (0.2 mmol, 40.05 mg) were combined together with exactly 2 mL of N,N′-dimethylformamide (DMF) and manually agitated until both solids were fully dissolved. To this solution, 1 mL of methanol (MeOH) was added and the solution agitated for several seconds. Separately, $Co(NO_3)_2$•$6H_2O$ (0.199 mmol, 57.91 mg) was dissolved in exactly 1 mL of DMF, and upon dissolution, was added to the camphorate/ **bipy ethylene** /2,6-lutidne/MeOH solution. The vial was sealed with store bought kitchen aluminum foil, capped tightly and placed in a sand bath for transfer to a programmable oven. The heat profile was as follows: the reaction temperature was raised from 30 °C to 115 °C at a rate of 1.5 °C per minute upon which time it was held at that temperature for 24 hours. The temperature was then slowly cooled back down to 30 °C at a rate of 1.0 °C per minute. Upon removal from the oven a large amount of what appeared to be purple square-plate crystals suitable for single crystal X-ray diffraction were observed to have formed (74 mg, 71% yield).

Zn_2(camphorate)$_2$(meso-α,β-Bis(4-pyridyl)glycol)$_{0.5}]_n$, **[25]**, was synthesized *via* a one-pot solvothermal reaction conducted in a 20 mL scintillation reaction vial. In a typical reaction, **bipy glycol** (0.098 mmol, 21.19 mg), 2,6-lutidine (0.4 mmol, 46.44 μL), and camphoric acid (0.2 mmol, 40.05 mg) were combined together with exactly 2 mL of

N,N′-dimethylformamide (DMF) and manually agitated until both solids were fully dissolved. To this solution, 1 mL of methanol (MeOH) was added and the solution agitated for several seconds. Separately, $Zn(NO_3)_2 \cdot 6H_2O$ (0.2 mmol, 59.5 mg) was dissolved in exactly 1 mL of DMF, and upon dissolution, was added to the camphorate/ **bipy glycol** /2,6-lutidne/MeOH solution. The vial was sealed with store bought kitchen aluminum foil, capped tightly and placed in a sand bath for transfer to a programmable oven. The heat profile was as follows: the reaction temperature was raised from 30 °C to 115 °C at a rate of 1.5 °C per minute upon which time it was held at that temperature for 24 hours. The temperature was then slowly cooled back down to 30 °C at a rate of 1.0 °C per minute. Upon removal from the oven a large amount of colorless square-plate crystals suitable for single crystal X-ray diffraction were observed to have formed (34 mg, 20.7% yield).

$Ni_2(camphorate)_2(meso\text{-}\alpha,\beta\text{-}Bis(4\text{-}pyridyl)glycol)_{0.5}]_n$, **[26]**, was synthesized *via* a one-pot solvothermal reaction conducted in a 20 mL scintillation reaction vial. In a typical reaction, **bipy glycol** (0.105 mmol, 22.71 mg), 2,6-lutidine (0.4 mmol, 46.44 μL), and camphoric acid (0.2 mmol, 40.05 mg) were combined together with exactly 2 mL of N,N′-dimethylformamide (DMF) and manually agitated until both solids were fully dissolved. To this solution, 1 mL of ethanol (EtOH) was added and the solution agitated for several seconds. Separately, $Ni(NO_3)_2 \cdot 6H_2O$ (0.201 mmol, 58.45 mg) was dissolved in exactly 1 mL of DMF, and upon dissolution, was added to the camphorate/ **bipy glycol** /2,6-lutidne/ EtOH solution. The vial was sealed with store bought kitchen aluminum foil, capped tightly and placed in a sand bath for transfer to a programmable oven. The heat

profile was as follows: the reaction temperature was raised from 30 °C to 115 °C at a rate of 1.5 °C per minute upon which time it was held at that temperature for 24 hours. The temperature was then slowly cooled back down to 30 °C at a rate of 1.0 °C per minute. Upon removal from the oven a large amount of green square-plate crystals were observed to have formed (63 mg, 40.1 % yield).

$Co_2(camphorate)_2(meso\text{-}\alpha,\beta\text{-}Bis(4\text{-}pyridyl)glycol)_{0.5}]_n$, **[27]**, was synthesized *via* a one-pot solvothermal reaction conducted in a 20 mL scintillation reaction vial. In a typical reaction, **bipy glycol** (0.1 mmol, 21.62 mg), 2,6-lutidine (0.4 mmol, 46.44 μL), and camphoric acid (0.2 mmol, 40.05 mg) were combined together with exactly 2 mL of N,N′-dimethylformamide (DMF) and manually agitated until both solids were fully dissolved. To this solution, 1 mL of methanol (MeOH) was added and the solution agitated for several seconds. Separately, $Co(NO_3)_2 \cdot 6H_2O$ (0.199 mmol, 57.91 mg) was dissolved in exactly 1 mL of DMF, and upon dissolution, was added to the camphorate/ **bipy glycol** /2,6-lutidne/MeOH solution. The vial was sealed with store bought kitchen aluminum foil, capped tightly and placed in a sand bath for transfer to a programmable oven. The heat profile was as follows: the reaction temperature was raised from 30 °C to 115 °C at a rate of 1.5 °C per minute upon which time it was held at that temperature for 24 hours. The temperature was then slowly cooled back down to 30 °C at a rate of 1.0 °C per minute. Upon removal from the oven a large amount of what appeared to be pink square-plate crystals were observed to have formed (103 mg, 77% yield).

$Ni_2(camphorate)_2(BIPA\text{-}Py)_{0.5}]_n$, **[28]**, was synthesized *via* a one-pot solvothermal reaction conducted in a 20 mL scintillation reaction vial. In a typical reaction, **BIPA-PY**

(0.11 mmol, 46.24 mg), 2,6-lutidine (0.4 mmol, 46.44 μL), and camphoric acid (0.2 mmol, 40.05 mg) were combined together with exactly 2 mL of N,N′-dimethylformamide (DMF) and manually agitated until both solids were fully dissolved. To this solution, 1 mL of dimethyl sulfoxide (DMSO) was added and the solution agitated for several seconds. Separately, $Ni(NO_3)_2 \bullet 6H_2O$ (0.201 mmol, 58.45 mg) was dissolved in exactly 1 mL of DMF, and upon dissolution, was added to the camphorate/ **BIPA-PY** /2,6-lutidne/ DMSO solution. The vial was sealed with store bought kitchen aluminum foil, capped tightly and placed in a sand bath for transfer to a programmable oven. The heat profile was as follows: the reaction temperature was raised from 30 °C to 115 °C at a rate of 1.5 °C per minute upon which time it was held at that temperature for 24 hours. The temperature was then slowly cooled back down to 30 °C at a rate of 1.0 °C per minute. Upon removal from the oven a large amount of dirty olive green square-plate crystals suitable were observed to have formed (53 mg, 20.1% yield).

$Co_2(camphorate)_2(BIPA\text{-}Py)_{0.5}]_n$, **[29]**, was synthesized *via* a one-pot solvothermal reaction conducted in a 20 mL scintillation reaction vial. In a typical reaction, **BIPA-PY** (0.099 mmol, 41.62 mg), 2,6-lutidine (0.4 mmol, 46.44 μL), and camphoric acid (0.2 mmol, 40.05 mg) were combined together with exactly 2 mL of N,N′-dimethylformamide (DMF) and manually agitated until both solids were fully dissolved. To this solution, 1 mL of dimethyl sulfoxide (DMSO) was added and the solution agitated for several seconds. Separately, $Co(NO_3)_2 \bullet 6H_2O$ (0.199 mmol, 57.91 mg) was dissolved in exactly 1 mL of DMF, and upon dissolution, was added to the camphorate/ **BIPA-PY** /2,6-lutidne/ DMSO solution. The vial was sealed with store bought kitchen aluminum foil, capped

tightly and placed in a sand bath for transfer to a programmable oven. The heat profile was as follows: the reaction temperature was raised from 30 °C to 115 °C at a rate of 1.5 °C per minute upon which time it was held at that temperature for 24 hours. The temperature was then slowly cooled back down to 30 °C at a rate of 1.0 °C per minute. Upon removal from the oven a large amount of deep purple square-plate crystals suitable for single crystal X-ray diffraction were observed to have formed (110 mg, 63% yield).

3.2.5.2 X-ray Crystallography

Single crystals of compounds **[15[, [16],** and **[29]** suitable for X-ray crystallographic analysis were selected following examination under a microscope. Intensity data were collected on a Bruker-AXS SMART APEX/CCD diffractometer using Cu k\α radiation (λ = 1.54178 Å).[281] The data were corrected for Lorentz and polarization effects and for absorption using the SADABS program (SAINT).[282] The structures were solved using direct methods and refined by full-matrix least-squares on $|F|^2$ (SHELXTL).[283] Additional electron density, located in the void cavity space, assumed to be disordered solvent, was unable to be adequately refined was removed using the SQUEEZE/PLATON program.[284-286] Select crystallographic data is presented in tabular form in Appendix C-14, C-15, and C-16 respectively.

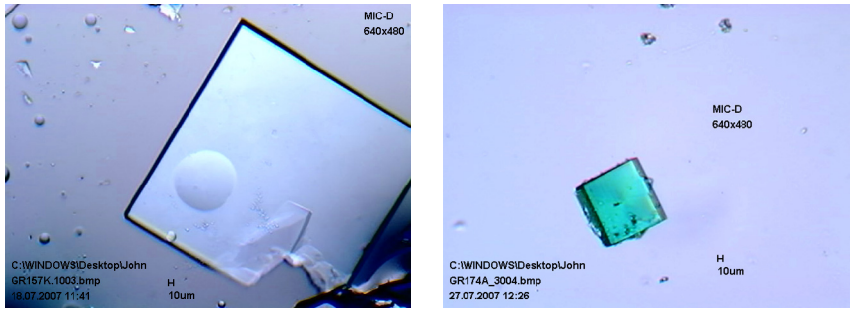

Figure 3.11 Digital photographs of compounds **[16]** (*left*) and **[17]** (*right*).

3.2.5.3 Powder X-ray Diffraction

Powder samples suitable for powder X-ray diffraction, FT-IR spectroscopy, and Thermal Gravimetric Analysis were obtained by removing a large amount of single crystals from the reaction scintillation vial by using a glass Pasteur pipette and depositing these crystal (along with mother liquor) in a small concave agar mortar. Excess solvent was removed *via* pipette, and surface solvent was removed by wicking action with a Kim-Wipe®. Upon wick drying, the crystals were transferred to a small piece of filter paper which was subsequently folded over and they were dried further and slightly crushed with gently pressure. The resulting dry powder (~30 mg) was then immediately applied to a PXRD sample puck prepared with a small amount of vacuum grease to fixate the powder sample, and the PXRD experiment performed without delay.

All pillared camphoric acid compounds were analyzed *via* powder X-ray diffraction. The samples were analyzed on a Bruker AXS D8 Discover X-ray diffractometer, equipped with GADDS™ (General Area Diffraction Detection System) and a Bruker AXS HI-STAR area detector. The X-ray source was Cu (λ= 1.54178 Å) run

on a generator operating at 40 kV and 40 mA. The data was collected within the 2θ range of 3° – 40°, in continuous scan mode using a step-size of 0.02° per step and a rate of 2.5° per minute. (Appendices B-19 – B34)

3.2.5.4 FT-IR Spectroscopy

All compounds **[14] – [29]** were characterized *via* infrared spectroscopy using a Nicolet Avatar 320 Fourier-Transform Infrared Spectrometer (FT-IR). Before each sample was analyzed, a background spectrum was obtained for purposes of zeroing out ambient noise in the form of the laboratory atmosphere. Each sample was measured in the range from 4000 cm^{-1} to 500 cm^{-1} wavenumbers (wavelength of 2500 nm to 20000 nm respectively) and scanned 64 times. Results were recorded in % transmittance and the spectrum analyzed using the EZ OMNIC© (V.5.1b, copyright 1992-199 Nicolet Instruments Corporation) computer software suite. A typical sample was analyzed as a neat, dry solid (~10 mg) obtained *via* either vacuum filtration and air drying or gently drying with laboratory grade filter paper. (Appendices B-19 – B34)

3.2.5.5 Thermal Gravimetric Analysis

Thermal Gravimetric Analysis for compounds **[14] – [29]** was performed on a PerkinElmer STA 6000 Simultaneous Thermal Analyzer. Data acquisition and analysis was performed with the assistance of the Pyris Series suite of software. Roughly 10-20 mg of dry powder was placed in a sample crucible and heated at a rate of 10 °C/min. form a temperature of 30 °C up to 700 °C under N_2 gas flow.

Notably the majority of the pillared camphorate MOMs exhibited exceptional thermal stability. Upon a small amount of weight loss attributed to either loss of mother liquor remnant on the surface of the crystals or small amounts of guest solvent trapped in the cavities being evacuated, typically all of the camphorate compounds showed a nearly flat spectrum indicating no additional weight loss until well past 200 °C

3.3 Conclusion

A series of closely related compounds all based upon the principle of pillaring a MOF-2 like layer constructed from the diacid (1R, 3S)-(+)-1,2,2-trimethyl cyclopentane-1,3-dicarboxylic acid, camphoric acid, into an extended 3-periodic metal-organic material have been described. A large number of reactions were conducted in synthesizing Zn^{2+}, Ni^{2+}, and Co^{2+} versions of the pillared structure for a number of pillars. Single crystal X-ray crystallography of the thin plates which resulted from the solvothermal reactions were often plagued with multiple problems; First many of the thin plate crystals suffered from stacking of multiple plates and resulted in twinning. Additionally, many of the crystal samples appeared to lose solvent upon sitting out on the bench perhaps affecting the crystals diffracting ability. Finally, and probably most fundamentally, the nature of the system provided for much consternation. Even in previously published accounts of related camphoric acid pillared MOFs, the described crystallography was suspect. The existence of the chiral centers within the ligand, and the bow-tie conformation of the individual layers, do not mesh well with the four-fold symmetry preferred by the square paddlewheel SBU. As such the crystallographer found it difficult to correctly assign the appropriate space group and for many of the diffraction collection experiments this lead

to data which was not able to be fully refined. However, generally unit cells obtained matched the expected dimensions and all other physical characterization methods indicated that many of the unsuccessful compounds were isostructural to compounds which were fully refined.

Each of the compounds synthesize in the chapter were also analyzed for their porosity through gas sorption measurements. Only three of the compounds (**[14], [15],** and **[17]**) demonstrated an appreciable extent of gas uptake at low temperatures and low loadings. A fourth sample has been improved through the activation technique of supercritical CO_2 drying, but has still not been completely successful.

Chapter 4

From Metal-Organic Polyhedra to Supermolecular Building Blocks

4.1 Introduction

Until now this dissertation has focused upon structures which repeat periodically in two (2-periodic, Chapter 2) or three (3-periodic, Chapter 3) mutually perpendicular spatial dimensions. For this chapter, the discussion will shift (momentarily) to structures which are not periodic along any one direction, and are therefore referred to by the term discrete or 0-periodic. As we shall see many beautiful structures are attainable when dealing with discrete objects. However, more than simply being aesthetically pleasing, many discrete structures also have intriguing properties not seen in extended structures. This chapter aims to outline several examples of novel discrete metal-organic material nanostructures which adopt polyhedral forms. Additionally, the synthesis, characterization, and some properties of these discrete metal-organic polyhedra are discussed. Finally, a new design strategy for the generation of extended metal-organic materials, whereby nanoscale metal-organic polyhedra are employed as nodes is described.

4.1.1 Discrete Supramolecular Polygons

As a central theme of this dissertation, the inherent complexity of the materials in question is always of key concern. While discrete structures are, by their very nature finite, at first blush they may seem to be the least complex of all the possible architectures observed in metal-organic materials. In the case of molecular and supramolecular polygons this is certainly true. However in the case of *some* polyhedra, it will become evident that this generalization is often unwarranted.

Supramolecular polygons[301-305] are discrete structures, often approaching or well established within the nanoscale, which are typically fabricated in solution and can often be crystallized into a solid state form. They can be generated through either hydrogen bonding or other weak noncovalent interactions, or they might be sustained *via* the coordinate-covalent coordination bond. Early on in the popularization of what might today be called metal-organic materials, many researchers in the field focused upon the synthesis and characterization of discrete supramolecular polygons, often in the form of molecular squares. These squares were typically constructed by utilizing 4,4′-dipyridyl molecules together with square planar transition metal ions (Cd^{2+} and Pd^{2+} were two common examples). Soon other polygons were target as well increasing the library of known compounds and their properties and augmenting synthetic methods at the crystal engineer's disposal. The design principles which were successfully employed for the isolation of these supramolecular polygons laid the foundations for the development of more complicated supramolecular polyhedra which would soon follow.

4.1.2 Polyhedra

Polyhedra are discrete (0-periodic) geometric constructs composed of flat faces and straight line segments. The faces are themselves polygons, formed by a circuit of line segments (edges), and the faces of the polyhedron are parts of larger planes. The polyhedron is generated by the intersection of these planes along the edges so that only two planes meet at an edge; every edge of a particular polygon (face) belongs to exactly one other polygon.[306] If all of the vertices of a polyhedron are identical with respect to symmetry (i.e. if there exists an isometry mapping a vertex into any other vertex) we say that the polyhedron is *uniform* (vertex-transitive). For the purposes of this dissertation we will deal only with uniform polyhedra. A common way of classifying a polyhedron is to describe its *vertex figure*, which is the structure which remains if a single node is lopped off. These vertex figures can often be convoluted, so the use of short hand notation called *vertex configuration* is often used. The vertex configuration is a list of the sequence of polygons located around a vertex, and is written as a series of numbers. In the case of uniform polyhedra, where there is only a single type of vertex, the vertex configuration can completely define and distinguish between different polyhedra. In the situation in which a polyhedron is a single closed surface and when none of the boundary planes which make up the faces penetrate the interior of the polyhedron, we say in that the polyhedron is *convex*. In contrast, a *non-convex* polyhedron (i.e. star polyhedra) will contain faces which intersect with other faces and are inherently more complicated structures. The polyhedra most people are familiar with (and the majority of the type to be discussed in the remainder of this chapter) are classified as convex polyhedra.

4.1.2.1 Platonic Solids

The simplest and most widely recognized of all polyhedra are those five polyhedra which are commonly referred to as the *Platonic Solids*—the tetrahedron (3^3), hexahedron (cube, 4^3), octahedron (3^4), dodecahedron (5^3), and icosahedron (3^5)—which are all constructed from a single type of *regular* polygon meeting at identical vertices and sharing identical edges. By use of the term regular it is implied that the polygon is constructed of equal angles (equiangular) and equal edge lengths (equilateral). Analogously, the *Platonic Solids* (Fig. 4.1) are themselves regular, meaning that in addition to each of its polygonal faces being regular, all of the vertices (vertex-transitive), edges (edge-transitive), and faces (isohedral) are identical respectively.

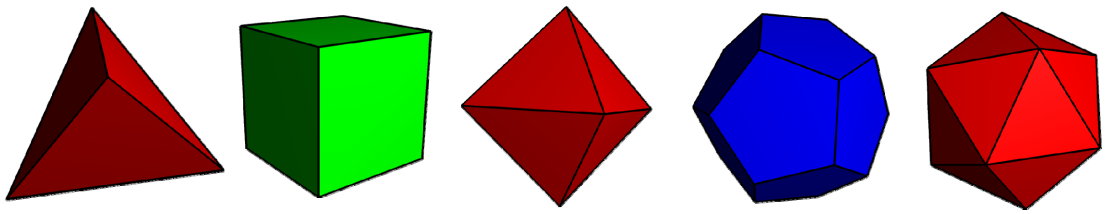

Figure 4.1 The Platonic solids. From left to right: tetrahedron, cube (hexahedron), octahedron, dodecahedron, and icosahedron.[2, 3]

As is obvious from the above figure, the *Platonic Solids* are highly symmetric objects, all of which belong to one of the high symmetry groups; tetrahedral, octahedral, or icosahedral. Though they have been known for millennia going back at least until the time of the Greeks, these objects are still of immense interest to modern day mathematicians and materials scientists. Indeed just this year, researchers have

discovered new dense packings[307] of these and related objects, which have important influences on the sciences of liquid, glassy, and crystalline materials.

4.1.2.2 Archimedean Solids

When the restriction requiring that all polygons meeting at a vertex be of the same type is relaxed, the situation arises where two more types of regular polygon meet at identical vertices and share edges. In this case the polyhedra are semi-regular, and are commonly referred to as being *Archimedean Solids.* There are 13 *Archimedean Solids*: truncated tetrahedron (6.6.3), cuboctahedron (4.3.4.3), truncated octahedron (4.6.6), truncated cube (8.8.3), rhombicuboctahedron (4.4.3.4), truncated cuboctahedron (8.4.6), snub cube (4.3.3.3.3), Icosidodecahedron (5.3.5.3), truncated icosahedron (5.6.6), truncated dodecahedron (10.10.3), rhombicosidodecahedron (5.4.3.4), truncated icosidodecahedron (10.4.6), snub dodecahedron (5.3.3.3.3) (Fig. 4.2). The existence of the *Archimedean Solids* and indeed much more complicated polyhedra is a salient reason for a reluctance to claim that discrete structures, by their very nature of being 0-periodic are less complex than 1-periodic and surely 2-periodic architectures. The very existence of semi-regular polyhedra is much more topologically complex than that of any 1-periodic structure and can be just as complex if not more so than 2-periodic examples. In chapter 2 it was revealed that there were just 8 semi-regular (*Archimedean*) plane tilings, while now we see there are 13 semi-regular polyhedra indicating increased diversity. Additionally, each of the plane tilings is intimately related to a particular polyhedron and can be interpreted as being a projection of the polyhedron onto the plane, making the 2-periodic tilings subjective to that of the 0-periodic polyhedra.

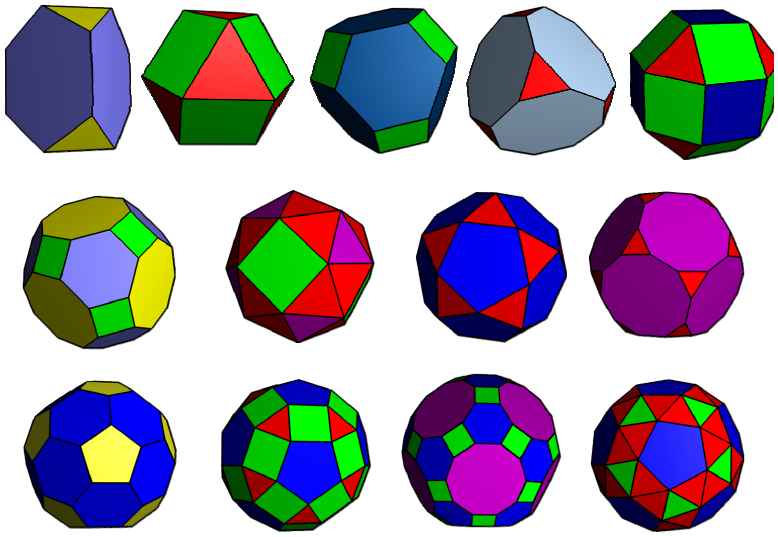

Figure 4.2. The Archimedean Solids. From left to right; ***Top:*** truncated tetrahedron, cuboctahedron, truncated octahedron, truncated cube, and rhombicuboctahedron. ***Middle:*** truncated cuboctahedron, snub cube, icosidodecahedron, and truncated dodecahedron. ***Bottom:*** truncated icosahedron, rhombicosidodecahedron, truncated icosidododecahedron, and snub dodecahedron.[2, 3]

4.1.2.3 Faceted Polyhedra

Another class of polyhedra which will be very pertinent to our discussion of metal-organic polyhedra are the so-called *faceted polyhedra*. These polyhedra result from the linking of regular polygons at identical vertices (making them *uniform polyhedra*), but do not involve the edge-sharing between polygons as was seen in both the *Platonic* and *Archimedean Solids.* By virtue of the polygons meeting at vertices in a manner such that they do not share edges, these non-convex polyhedra inherently contain both closed faces (polygons) and open windows to their hollow interior. There are exactly nine uniform non-convex polyhedra generated *via* the vertex-sharing of regular convex polygons and they can be composed of either a single type of polygon (*regular*) or more

than one type of polygon (*semi-regular*): tetrahemihexahedron (4.4/3.4.3), small icosidhemidodecahedron (10.3/2.10.3), octahemioctahedron (6.3/2.6.3), cubohemioctahedron (6.4/3.6.4), small rhombihexahedron (4.8.4/3.8), small rhombidodecahedron (10.4.10/9.4/3), small dodecahemidodecahedron (10.5/4.10.5), small cubicuboctahedron (8.3/2.8.4), and small dodecaicosidodecahedron (10.3/2.10.5) (Fig. 4.3).

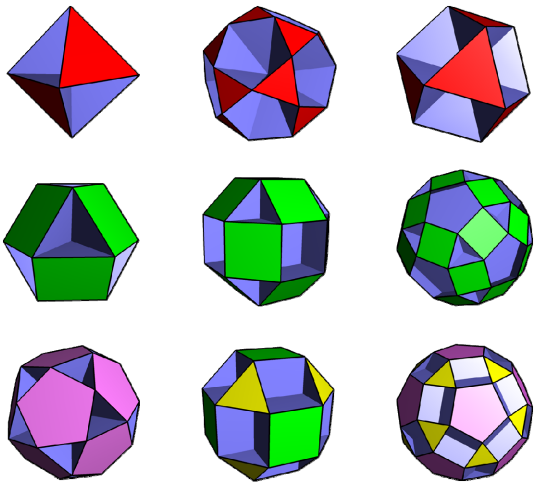

Figure 4.3 Faceted Polyhedra generated *via* vertex linking of regular polygons. From left to right; ***First Row:*** tetrahemihexahedron, small icosidhemidodecahedron, and octahemioctahedron. ***Second Row:*** cubohemioctahedron, small rhombihexahedron, and small rhombidodecahedron. ***Third Row:*** small dodecahemidodecahedron, small cubicuboctahedron, and small dodecicosidodecahedron.[2, 3]

4.1.3 Metal-Organic Polyhedra

Many of the *Platonic* and *Archimedean Solids* are potential target for crystal engineers when designing metal-organic polyhedra[308-311]. MOPs are attractive as they exemplify discrete nanoscale architecturest that will often exhibit unique physical properties in relation to other extended MOMs (i.e. solubility) To date there have been many examples of MOPs which can interpreted as have structures analogous to simple Platonic and more complicated Archimedean solids. Such MOPs as tetrahedra[312-319], cubes[313, 320-322], octahedra[317, 323], cuboctahedron, small rhombihexahedra[324-332], truncated tetrahedra[333], and truncated octahedra[334] have all been synthesized and characterized. Many more examples of more complicated polyhedra have also been investigated.

4.2 Alkoxy Nanoball – Dodecyloxy Cu(II) Nanoball

The first derivative form of 1,3-benzenedicarboxylic (1,3-bdc) acid that was focused upon for the synthesis of a novel functionalized nanoball was that of a dodecyloxy pendant group substituted in the 5-position of the dicarboxylic acid. This ligand, 5-dodecyloxy-1,3-benzenedicarboxylic acid, **L4** (Fig. 4.4), was synthesized in an attempt to discern ways of controlling the supramolecular isomerism[19, 20] observed in the system involving square paddlewheel SBUs and 1,3-bdc. Adopting long alkyl chains in the 5th position of the bdc moiety was expected to preclude the possible synthesis of the so-called square grid or Kagomé lattice 2-periodic layered networks and instead only facilitate the formation of the 0-periodic discrete nanoball isomer. Indeed, the synthesis of a cupric alkyloxy nanoball constructed from **L4** and copper (II) nitrate was achieved,

while extensive attempts to isolate any of the other isomers using this ligand were unsuccessful.

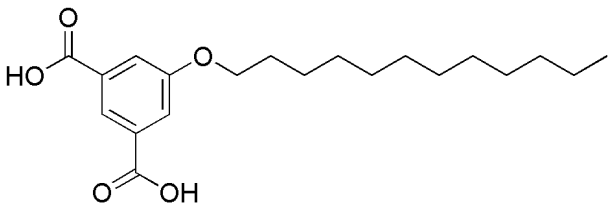

Figure 4.4 5-dodecyloxy-1,3-benzenedicarboxylic acid, **L4.**

4.2.1 Structural Analysis

The reaction of **L4** with copper (II) nitrate under appropriate conditions gives rise to the self-assembly of 0-periodic alkoxy nanoballs of the form Cu_2(5-dodecyloxy-1,3-benzenedicarboxylate)$_2$(MeOH)$_x$(H_2O)$_{2-x}$]$_{12}$, **[30]**, where the nanoball is functionalized with 24 dodecyloxy pendant groups decorating the periphery (Fig. 4.5). These dodecyloxy nanoballs crystallize in the chiral space group $P4_12_12$ with cell parameters of a = b = 38.559(2) Å, c = 54.503(6) Å, $\alpha = \beta = \gamma = 90°$, V = 81,035 (11) Å^3. Before the synthesis of this novel derivative nanoball could be verified and the results published, another research team active in the field reported the synthesis and deposition onto a graphite surface of a nearly identical compound.[335] The synthesis of **[30]** was conducted utilizing a non-coordinating base so that in the case of this nanoball derivative, the 24 axial ligands consist of some combination of methanol or water solvent molecules.

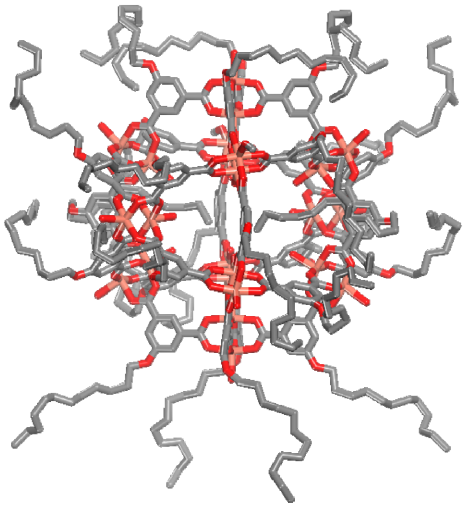

Figure 4.5 Schematic depicting stick view of the dodecyloxy nanoball. In this figure hydrogen atoms have been deleted for clarity (Atom color code: carbon = grey; oxygen = red; copper = salmon).

The addition of dodecyloxy pendant groups to the outer surface of the nanoball greatly augments the overall size of these nanoparticles, while the inner skeleton of the nanoball remains roughly indistinguishable from that of any other example, except for small variations in the inner/outer diameter or slight changes in the angle between SBUs (i.e. some nanoballs are slightly less spherical than others). The largest outer diameter for the *skeleton* of the dodecyloxy nanoball, when not taking into account the alkyl chains, was observed to be 24.744 Å (2.47 nm) as measured from carbon-to-carbon in the 5th position of opposite 1,3-bdc moieties. The shortest inner diameter for the *skeleton* nanoball was observed to be 15.964 Å (~1.6 nm) as measured from inner copper atom to inner copper atom, thus ignoring the presence of any axially bound solvent molecules within the cavity of the nanoball (i.e. as would be expected if fully desolvated of axially ligands). This leads to an inner and outer volume of approximately 2.13 nm^3 and 7.93

nm^3 respectively, well within the ranges estimated for other nanoball derivatives. When the dodecyloxy chains are taken into consideration however, a maximal outer diameter of just over 50 Å (5.0 nm) is observed resulting in an outer volume of nearly 69.5 nm^3. As will be evident momentarily, this volume is simply an idealization of the volume if the dodecyloxy chains are treated as rigid groups protruding from the nanoball and precluding any other objects from closer approach; in fact the nanoballs close pack well within this hypothetical distance.

As might be expected the dodecyloxy pendant groups extending outward from the surface of these nanoballs demonstrate a high degree of flexibility. However, what was not expected was the intriguing way these nanoballs pack in their solid-state crystal structure. While it is understandable that the relatively long alkyl chains of one nanoball should in principle be able to intertwine and co-mingle with the alkyl chains of neighboring nanoballs, especially *via* van der Waal interactions, when several nanoballs are forced into a close approach in the crystalline state, it was somewhat astonishing to observe that these long alkyl chains have the ability to thread through the open windows and into the empty interior of its nearest adjacent neighbors. Additionally, the flexibility of the alkoxy pendant groups is such that the long chains are capable of enduring extreme distortions in their conformation making feasible the observed self-inclusion of these alkyl chains through the open windows of its own nanoball. In fact at least two of the dodecyloxy pendant groups of each nanoball self-include and penetrate into the hollow interior of the nanoball core which they are covalently attached to, entering through two separate open square windows (Fig. 4.6).

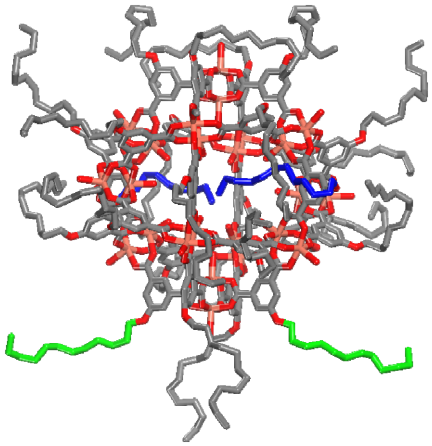

Figure 4.6 Cartoon illustrating the self-inclusion of two dodecyloxy groups (blue chains) into the center of each nanoball. The green colored chains are those that will include into two different adjacent nanoball neighbors. All hydrogen atoms have been deleted for clarity.

In addition to the two self-included chains, the center of each nanoball also plays host to at least two other dodecyloxy chains, one each donated from two different adjacent nanoballs and entering through separate open triangular windows, bringing the total number of included alkyl groups up to four (Fig. 4.7 top). Besides accepting four dodecyloxy chains (two from itself and one each from two nearest neighbors), each nanoball also donates one chain each into two adjacent nanoballs different that those which donated chains to itself (Fig. 4.7 bottom).

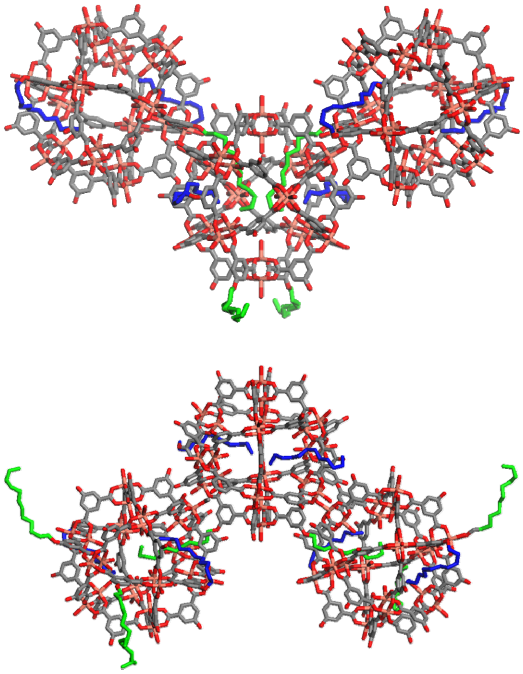

Figure 4.7 Cartoon illustrating the interactions between nearest neighbor nanoballs in compound **[30].** ***Top:*** Two nearest neighbors donate a single dodecyloxy chain (green) each into the hollow interior of the same nanoball. ***Bottom:*** The central nanoball donates two dodecyloxy chains (green) into two nearest neighbors different from those which donate to it.

This generates a motif in which a central nanoball accepts chains from two unique adjacent nanoballs while simultaneously donating separate chains to two unique neighboring nanoballs. Therefore it is entirely reasonable to interpret any one of these nanoballs as being a type of 4-connected supramolecular node since it interacts with four nearest neighbors strictly thorough noncovalent interactions. More precisely this supramolecular node adopts the geometry of a distorted tetrahedron which in turn results in the dodecyloxy nanoballs packing into a distorted supramolecular diamondoid network. Interestingly, this supramolecular diamondoid network packing of dodecyloxy nanoballs was also observed and described in the previous report of the related structure,

albeit in that structure no threading of the alkyl chains into the open windows of the nanoballs was apparent. In the first instance it was observed that these chains, while adopting variable confirmations, either protruded away from its own nanoball core or became entangled with the chain of a neighboring nanoball. As to the reason behind the discrepancy in packing motifs realized in these two solid state structures, we can only presume that it arises due to the nature of the crystallization processes and/or to the effect of axial ligands present. In the previously published example, the powdery precipitate that was collected from the direct mixing of the cupric and **L4** ligand N,N′-dimethylformamide solutions was recrystallized from a hexane/octanol mixture. This solvent system is decidedly more nonpolar than that which was used to obtain the single crystals of **[30]** in which the powder precipitate was dissolved in tetrahydrofuran while neat acetonitrile was layered over this solution and the two solvents were allowed to slowly diffuse into one another. The increased polarity of the crystallizing solvents is perhaps a driving force for the threading of dodecyloxy pendant chains into the hollow interior of the alkoxy nanoballs.

Except for the mechanism of how the individual dodecyloxy nanoballs interact when packing (*via* the threading of alkoxy chains through open windows in my structure versus the lack of penetration in the previously published example), the dimensions of the distorted supramolecular tetrahedron and subsequent diamondoid networks of the two structures are nearly identical. In the case of the distorted supramolecular tetrahedron, the observed angles generated by linking the center of the central dodecyloxy nanoball to the centers of each of its nearest neighbors range from 98.571° in the case of the

$Nanoball_{acceptor}$-$Nanoball_{center}$-$Nanoball_{acceptor}$, 108.506° (x2) and 109.209° (x2) for $Nanoball_{donor}$-$Nanoball_{center}$-$Nanoball_{acceptor}$, and 120.596° for the case of $Nanoball_{donor}$-$Nanoball_{center}$-$Nanoball_{donor}$ (Fig 4.8). The center-to-center distance between the central dodecyloxy nanoball and that of each of its four adjacent nearest neighbors was measured to be 23.755 Å (as opposed to 23.935 Å in the previous structure) and combined with the observed angles between neighbors, generated individual edge lengths (measured centroid-to-centroid) for the distorted supramolecular tetrahedron were measured to be 36.011 Å, 38.559 Å (x2), 38.729 Å (x2), and 41.268 Å (previously observed to be 33.571 Å and 41.568 Å).

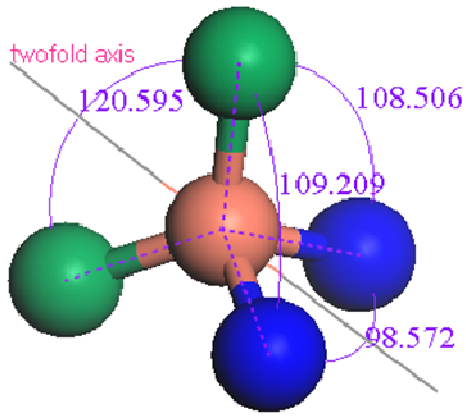

Figure 4.8 Scheme illustrating the distorted supramolecular tetrahedron (with some angles shown) generated by the four nearest neighbors of a central (red sphere) dodecyloxy nanoball. The green spheres represent those nanoballs donating alkyl chains into the central nanoball, while the blue spheres represent those nanoballs accepting chains from the central nanoball.

4.2.2 Properties

With the addition of long alkyl chains in the dodecyloxy derivative of the nanoball, we expect the potential to observe drastically altered properties for these discrete metal-organic materials in comparison with either the parent nanoball structure or those derivatives already characterized. Indeed a significant property of these nanostructures, namely their ability to interact in the solid-state through chain threading as described in the previous section, is in fact quite distinct from that observed for other derivatives of nanoballs. This ability to interact *via* threading is a direct consequence of the both the flexible nature of the dodecyloxy group as well as their unique chemical nature (non-polarity). In addition to how the dodecyloxy nanoballs interact within the solid-state, the presence of these long alkyl chains should have significant influence upon their solution properties, especially in dictating the nature of solvents they might be soluble in.

Briefly, I would also like to take a moment to mention a property of these materials which lead to an intriguing application already described by another research group. The fact that these materials possess openings in the form of open square and triangular windows leading into their hollow interior cavities has already been discussed. As such the potential for encapsulation of functional molecular species for various applications is of great interest. However, in addition to the ability to encapsulate larger guests that might otherwise not be able to depart from within the interior (Ship-in-a-bottle), these hollow spheres with small windows should be able to allow smaller moieties (especially ions) to easily ingress and egress from their center. With this in

mind, Kim and co-workers[336] have demonstrated the ability to imbed cupric dodecyloxy nanoballs into synthetic membrane bilayers thanks in large part to the presence of the long nonpolar alkyl chains. The dodecyloxy nanoballs then bridge the membrane such that select ions can travel through the nanoball to transverse the membrane, thus utilizing the nanoballs as a form of synthetic ion channel.

4.2.2.1 Solubility

Whereas the original nanoball was described to be soluble in common polar organic solvents most notably alcohols (methanol, ethanol, etc.), the dodecyloxy derivative is soluble in a range of solvents decidedly more nonpolar. Qualitative solubility experiments were conducted using the turquoise powdery precipitate formed *via* the direct mixing of $Cu(NO_3)_2$ and **L4** ligand solutions, upon vacuum filtration and air drying of the solid. A small sample of the dry powder (~10-20 mg) was placed into a clean, labeled test tube, and to this ~ 1 mL of neat solvent was added. With the aid of manual as well as mechanical (Maxi-Mix®) agitation, dissolution of the solid was attempted. If upon agitation for several minutes, the solid was still not dissolved (as evidenced by possible color change; noticeable loss of solid), the use of a hot water bath (steaming, yet not boiling ~85-90 °C) was implemented and the test tube allowed to sit for several minutes before reobserving. Through following this protocol it was determined that the dodecyloxy nanoball is readily soluble in chloroform, dichloromethane, toluene, carbon tetrachloride, 1,4-dioxane, tetrahydrofuran, ethyl acetate, benzene, nitrobenzene, and hot N,N′-dimethylformamide. They were determined to be insoluble in dimethyl sulfoxide, methanol, ethanol, acetonitrile, and neat hexane, as

well as instable in neat *D.I.* H_2O (collapse of nanoball structure was taken with the concomitant loss of characteristic blue color and the emergence of a milky white precipitate which is presumably insoluble free ligand).

4.2.3 Experimental

4.2.3.1 Synthesis

All reagents, unless described otherwise, were purchased from either Sigma-Aldrich or Fischer Scientific and used as received without further purification. Bulk solvents such as methanol, ethanol, acetone, and dichloromethane were first distilled and stored over drying media (4Å molecular sieves) before their use.

5-Dodecyloxy-1,3-benzenedicarboxylic acid, **L4** (Fig. 4.4), was synthesized from commercially available dimethyl-5-hydroxy-1,3-benzenedicarboxylate and 1-bromododecane *via* established procedures for the alkylation of phenols.[277, 337] In a typical reaction dimethyl-5-hydroxy-1,3-benzenedicarboxylic acid (5.00 g, 0.0238 mol) and potassium carbonate (K_2CO_3, 9.88 g, 0.0715 mol, 3 equivalents) were weighed out separately and dried on a vacuum pump for approximately three hours. A 3-neck round bottom flask was sealed with rubber septa and the air purged with N_2 for 15 minutes prior to the start of the reaction. Upon drying the diester and K_2CO_3 were dissolved together in approximately 75 mL of dry acetone and added to the 3-neck round bottom flask equipped with two rubber septa and a cold-water condenser situated in a hot oil bath held at 80° C. The solution was allowed to reflux for 30 minutes before 1-bromododecane (17.2 mL, 0.0715 mol; 3 equivalents) was added *via* syringe through a rubber septum.

The reaction was allowed to reflux for approximately 12 hours before monitoring the extent of completion through TLC.

Upon completion the solution was cooled to room temperature, filtered through Celite, and the solvent removed by heating under vacuum (Rotavap) leaving behind a dark yellow oil which solidified upon cooling. This solid was dissolved in ~100 mL dichloromethane (DCM), transferred to a separatory funnel, washed three times with *D. I.* H_2O, and dried over anhydrous Na_2SO_4. The DCM solvent was removed *via* rotavap and the solid recrystallized from hot ethanol. The ester product crystals were collected *via* filtration and dried, upon which they were added to a NaOH solution (20% by volume, 3 equivalents to the ester) and allowed to stir with a magnetic stir bar on a hot plate until fully dissolved. The conversion from ester to carboxylate was monitored *via* TLC and upon completion was worked up with HCl (10 % by volume) added drop-wise until the solution was acidic by pH paper. The precipitate was filtered, washed with *D.I.* H_2O, and allowed to dry at which time 5.015 g (60.1 % yield) of white solid was obtained. The spectroscopic data for **L4** (Appendix A-4, B-4) were consistent with previously reported data for this compound.[338]

^{1}H NMR (250 MHz, DMSO-d_6, δ): 0.9(t, J = 6.3 Hz, 3H, -CH_3), 1.2(m, 18 H, -CH_2-), 1.7(m, 2H, -CH_2-), 4.1(t, J = 6.4 Hz, 2H, -O-CH_2-), 7.6(s, 2H, -ArH), 8.1(s, 1H, -ArH), 13.3(br, 2H, -COOH); mp 166-168 ºC (lit. 163-166 ºC).

Cu(II) dodecyloxy nanoballs **[30],** were synthesized *via* a reflux reaction conducted in a round bottom flask using methanol as the solvent. In a typical reaction, $Cu(NO_3)_2$•2.5 H_2O (699 mg, 3.01 mmol) was dissolved in 10 mL of methanol and subsequently added to a refluxing solution of 5-dodecyloxy-1,3-benzenedicarboxylic acid (**L4**) (1.078 g, 3.076 mmol) dissolved in 50 mL of methanol. To this solution 2,6-lutidine (1.08 mL, 9.27 mmol) was added and the mixture was allowed to continue refluxing for one hour. Upon cooling, the solution and precipitate were separated *via* vacuum filtration and the filtrand was allowed to air dry overnight in the fume hood resulting in 1.027 g of a turquoise-blue microcrystalline powder being collected for an overall yield of 82%.

4.2.3.2 X-ray Crystallography

Crystals suitable for single crystal X-ray diffraction were grown through the process of recrystallization from a mixed solvent system. The turquoise-blue microcrystalline powder was first dissolved in tetrahydrofuran resulting in a concentrated deep blue solution. Acetonitrile was then carefully layered over this nanoball solution using a small volume of pure THF as a blank middle layer. The crystallization vessel was left to sit on the lab bench at room temperature and the solvents allowed to slowly diffuse into one another over the period of a couple weeks resulting in the formation of dark blue prisms of **[30]** (Fig. 4.9).

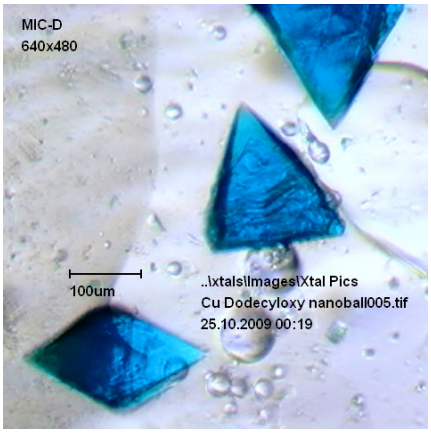

Figure 4.9 Digital photograph depicting single crystals of compound **[30]**.

Single crystals suitable for X-ray crystallographic analysis were selected following examination under a microscope. Intensity data were collected on a Bruker-AXS SMART APEX/CCD diffractometer using Mo k\α radiation (λ = 0.7107 Å).[281] The data were corrected for Lorentz and polarization effects and for absorption using the SADABS program (SAINT).[282] The structures were solved using direct methods and refined by full-matrix least-squares on $|F|^2$ (SHELXTL).[283] Additional electron density, located in the void cavity space, assumed to be disordered solvent, was unable to be adequately refined was removed using the SQUEEZE/PLATON program.[284-286] Select crystallographic data is presented in tabular form in Appendix C-17.

4.2.3.3 Powder X-ray Diffraction

Powder samples of **[30]** suitable for powder X-ray diffraction, FT-IR spectroscopy, and Thermal Gravimetric Analysis were obtained by removing a large amount of single crystals from the reaction scintillation vial by using a glass Pasteur pipette and depositing these crystal (along with mother liquor) in a small concave agar

mortar. Excess solvent was removed *via* pipette, and surface solvent was removed by wicking action with a Kim-Wipe®. Upon wick drying, the crystals were transferred to a small piece of filter paper which was subsequently folded over and they were dried further and slightly crushed with gently pressure. The resulting dry powder (~30 mg) was then immediately applied to a PXRD sample puck prepared with a small amount of vacuum grease to fixate the powder sample, and the PXRD experiment performed without delay.

The Cu(II) dodecyloxy nanoballs, compound **[30],** was characterized for bulk composition purity *via* PXRD. The samples were analyzed on a Bruker AXS D8 Discover X-ray diffractometer, equipped with GADDS™ (General Area Diffraction Detection System) and a Bruker AXS HI-STAR area detector. The X-ray source was Cu (λ= 1.54178 Å) run on a generator operating at 40 kV and 40 mA. The data was collected within the 2θ range of 3° – 40°, in continuous scan mode using a step-size of 0.02° per step and a rate of 2.5° per minute. (Appendix B-35)

4.2.3.4 FT-IR Spectroscopy

All compounds, including synthesized ligands, were characterized *via* infrared spectroscopy using a Nicolet Avatar 320 Fourier-Transform Infrared Spectrometer (FT-IR). Before each sample was analyzed, a background spectrum was obtained for purposes of zeroing out ambient noise in the form of the laboratory atmosphere. Each sample was measured in the range from 4000 cm^{-1} to 500 cm^{-1} wavenumbers (wavelength of 2500 nm to 20000 nm respectively) and scanned 64 times. Results were recorded in %

transmittance and the spectrum analyzed using the EZ OMNIC© (V.5.1b, copyright 1992-199 Nicolet Instruments Corporation) computer software suite. A typical sample was a analyzed as a neat, dry solid (~10 mg) obtained *via* either vacuum filtration and air drying or gently drying with laboratory grade filter paper.

5-dodecyloxy-1,3-benzenedicarboxylic acid, **L4**: IR (dry powder) $\tilde{\upsilon}_{max}$ (cm^{-1}): 3535 m (-OH, free carboxylic acid), 3451 w (-OH, free carboxylic acid), 3122 br (-OH, carboxylic acid Hydrogen bonded), 2922 m sh. (-CH, aliphatic), 2847 m sh. (-CH, aliphatic), 1707 s sh. (C=O, carboxylic acid), 1677 m sh. (C=O, carboxylic acid). (Appendix B-4)

$[Cu_2$(5-dodecyloxy-1,3-benzenedicarboxylate)$_2(MeOH)_x(H_2O)_{2-x}]_{12}$,**[30]**: IR (dry powder) $\tilde{\upsilon}_{max}$ (cm^{-1}): 3402 v br (-OH, alcohol solvent), 2922 m sh. (-CH, aliphatic), 2852 m sh. (-CH, aliphatic), 1635 m sh. (COO^-, carboxylate), 1587 m sh. (C=O, carboxylate), 1378 v sh. (COO^-, carboxylate). The most notable changes between the IR spectrum for the ligand **L4** and compound [**30**] is the disappearance of the OH stretch due to the carboxylic acid that was centered around 3122 cm^{-1} and bleed into the 3000 cm^{-1} region as well as the two sharp peaks at 3535 cm^{-1} and 3451 cm^{-1} which arose from free acids. There are two moderately intense and sharp peaks at 2922.81 cm^{-1} and 2852.29 cm^{-1} which remained from the ligand IR spectrum and are due to the large presence of $–CH_2$ and $–CH_3$ groups. Additionally, we notice drastic shifts in frequency for the C=O stretches which is expected upon coordination of the carboxylate. (Appendix B-35)

4.2.3.5 Thermal Gravimetric Analysis

Thermal gravimetric analysis (Appendix B-35) for Cu(II) dodecyloxy nanoballs, $[Cu_2(5\text{-dodecyloxy-1,3-benzenedicarboxylate})_2(MeOH)_x(H_2O)_{2-x}]_{12}$, **[30]** was conducted on a T.A. Instruments 2950 TGA operating in the High Resolution Dynamic mode. The program was run from 30 °C up to 1000 °C and was performed under a flow of N_2 gas. The resulting data was graphed as a function of weight percent (wt. %) versus change in temperature. Upon acquisition the data was evaluated using T.A. Instruments Thermal Advantage suite of analyzing software.

Initial weight loss of 7.6 % from ~30°C to 50 °C was observed and interpreted to be loss of mother liquor still present on the crystalline sample. A small amount of additional weight loss (5.67 %) was observed over a large temperature range of ~50 °C to 220 °C and thought to be low boiling interstitial guest molecules in the crystal lattice. The first major weight loss results in a moderately sharp weight loss seen form about 220°C until approximately 300 °C which may be do the first loss of coordinated solvent molecules or possibly trapped solvent molecules being removed over a large temperature range. This represents ~18% of the sample and most likely was due to the various types of solvent molecules (MeOH, H_2O, etc.). The largest weight loss of ~35 % was observed to occur in the temperature range of 310 °C unit 380 °C. After 380 °C, the sample decomposed with a final weight loss of 15.5%.

4.3 Aryloxy Nanoballs – Benzyloxy and Naphthyloxy Cu(II) Nanoballs

As already outlined in the introduction (4.1.3) and clearly demonstrated by the previous section of this dissertation describing the dodecyloxy derivative, the nanoball is more than an aesthetically pleasing structure of mundane interest. It represents a platform of many different possible compounds which can be fabricated using an identical synthesis strategy. In principle one can alter the metal ion holding the structure together or functionalize the bridging ligand and thus alter the nature of the outer surface of the nanoball and in turn influence its physical and chemical properties. But what alterations should be made and which properties should be targeted for influence may not always be clear. However, in the case of the nanoball derivatives, a survey of those types of functionalization which already exist may prove fruitful. This exercise led to the realization that no derivative of the nanoballs existed with aryl groups positioned around the periphery of the sphere. Aromatic groups such as phenyls and naphthyls could prove interesting additions to the nanoball for several reasons. They should increase the nanoballs solubility in aromatic hydrocarbon solvents, while also providing external functional groups known to undergo reliable noncovalent interactions (π•••π stacking and CH•••π interactions) in both solution and the solid state. This may make a properly derivatized nanoball amenable to crystal engineering and allow further investigation into how these supermolecules interact with one another through self-assembly. Finally, simple aryl groups such as phenyl and naphthyl rings are good starting points for the incorporation of fluorescent active groups on the exterior of the nanoball as they are relatively facile to synthesis. Their adoption could provide useful insights into the

methodology necessary for the future integration of more interesting fluorescent active groups for many potential applications.

4.3.1 Structural Analysis

As is the case with all nanoballs compound **[31],** [Cu_2(5-benzyloxy-1,3-benzenedicarboxylate)$_2$$(DMF)_x(H_2O)_{2-x}]_{12}$, or the benzyloxy nanoball, is constructed from the vertex sharing of 12 molecular squares linked together *via* 24 bridging ligands. These molecular squares are fashioned from dimetal tetracarboxylate subunits and therefore each nanoball is composed of exactly 24 transition metals. The benzyloxy nanoball was synthesized from copper (II) nitrate and ligand **L1** through self-assembly, so that there are 24 copper ions as well as 24 5-benzyloxy-1,3-benzenedicarboxylates. Each of the benzyloxy groups is located at the 5^{th} position of the dicarboxylate which is oriented outward away from the surface of the nanoball (Fig. 4.10).

This nanoball was synthesized in the presence of the non-coordinating base 2,6-lutidine and as such the axial position of the SBU is occupied with a variable amount of solvent molecules or water. Single-crystal X-ray diffraction was unable to completely refine the identity of all axial ligands where electron density was located, but disordered solvent molecules (DMF) or water is expected. The benzyloxy nanoballs **[31],** self-assemble and crystallize in the tetragonal space group P4/mnc with cell parameters a = b = 27.974 (5) Å, c = 39.321 (5) Å, $\alpha = \beta = \gamma = 90°$, and a cell volume of 30770 (9) $Å^3$ with Z =2.

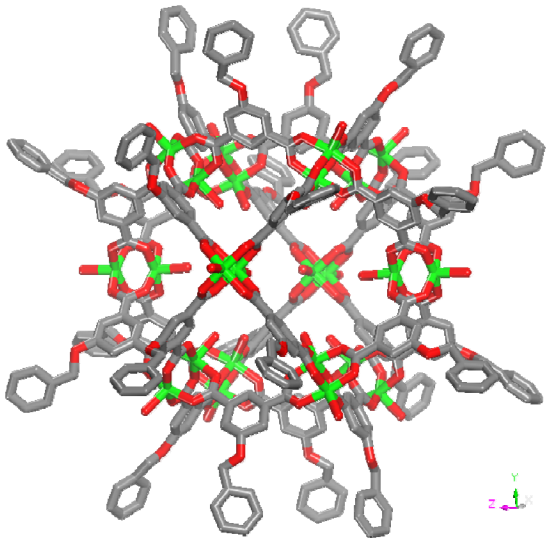

Figure 4.10 Schematic illustrating a stick view of the benzyloxy nanoball, compound **[31]** (grey = carbon, red = oxygen, green = copper; hydrogen atoms have been deleted for clarity).

The inner core of the benzyloxy nanoball, as would be expected when using a 1,3-bdc derivative, is essentially identical to that of most other derivatives including the parent version. The shortest inner diameter, as measured from one inner copper atom to the opposite inner copper atom is 15.833 Å (1.58 nm) meaning the interior volume of this nanoball is approximately 2.08 nm^3. This distance was taken as the inner diameter for two salient reasons; the variable presence of unidentified inner axial ligands makes it difficult to involve these molecules in the calculation, and secondly the labile nature of these axial ligands gives rise to their potential removal from the structure and subsequent increase of the inner core volume. Thus it was decided to measure the volume of the hollow interior while disregarding the presence of these axially bound solvent molecules. The longest outer diameter of the nanoball skeleton as measured from the 5^{th} position

carbons on opposite 1,3-bdc rings was measured to be 24.040 Å (2.4 nm), while the longest measured diameter for this nanoball including the benzyloxy groups was measured to be 36.732 Å (3.67 nm), resulting in outer volumes of ~ 7.24nm^3 and 25.9 nm^3 respectively.

As can be expected from a tetragonal space group, the benzyloxy nanoballs pack in a body-centered cubic (bcc) arrangement (Fig. 4.11) where each nanoball can be viewed as being placed at the center of a cube (though somewhat distorted along the c-axis to make it tetragonal) and having eight nearest neighbors positioned at the corners of said cube. The centroid-to-centroid distance between the central benzyloxy nanoball and its nearest neighbors residing at the corners of the cube was measured to be 27.889 Å (~2.79 nm). As the nanoballs are positioned around the elongated cube which also represents the unit cell, it follows that the centroid-to-centroid distance between two adjacent nanoballs which are both nearest neighbors to the same central nanoball can be only one of two dimensions; either they rest in the same *ab* plane and have a distance of 27.974 Å (length of *a*-axis) or they are adjacent along the *c*-axis in which they are separated by a distance of 39.321 Å (length of *c*-axis). The central benzyloxy nanoball also has six second nearest neighbors oriented at the six faces of the cube and located at the slightly longer distance of 27.974 Å, because if viewed carefully, it becomes obvious that these neighborly nanoballs can act as the corners to some other central nanoball and a simple redefining of the unit cell.

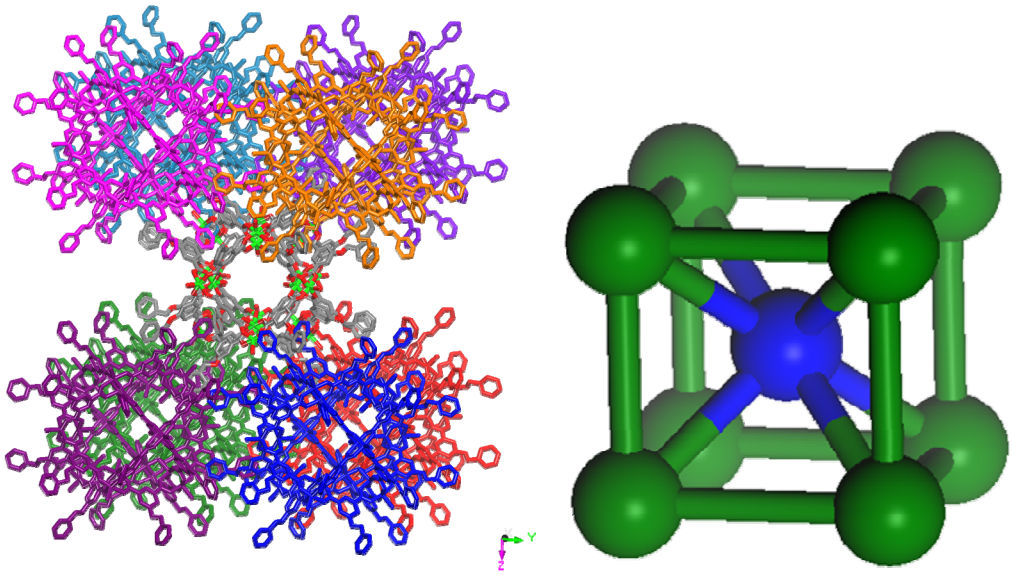

Figure 4.11 Body centered cubic close packing of benzyloxy nanoballs. The figure of the right depicts the eight nearest neighbors (green) of the central (blue) nanoball in question. In this view the *c*-axis is vertical in the page so that the four neighbors above (or below) lie in the *ab*-plane.

The most obvious first impression when the packing of the benzyloxy nanoballs is viewed is that while the relatively long pendant groups surround the sphere do indeed protrude to a significant degree, the nanoballs themselves still manage to pack tightly together in one of the most efficient packing schemes known for spheres (an observation reminiscent of the dodecyloxy nanoballs). This is achieved because while the pendant groups may be long, they are also, relatively speaking, thin. Therefore they have the ability to slip past one another when one nanoball approaches another as is required for the formation of a crystal. In addition to being able to slide beyond pendant chains from other nanoballs and allowing the shells of the nanoballs to approach rather closely, the benzyloxy groups are also able to interact with benzyloxy groups from other nanoballs through weak noncovalent interactions such as π•••π stacking and CH•••π interactions. In

particular, every nanoball interacts with each of its eight nearest neighbors through four benzyloxy side chains with two such chains originating from each nanoball respectively. The phenyl ring at the end of each group threads past another pendant arm which arises from a neighboring nanoball, in an anti-parallel fashion and this phenyl group is located within the proximity of the benzene ring that constitutes the isophthalic portion of the second glancing ligand (Fig. 4.12).

The phenyl group is situated there in such a manner so as there is likely to be favorable noncovalent interactions between the two moieties. The phenyl ring from one ligand is oriented in a face-to-face motif (albeit slightly slipped) with the isophthalic benzene ring of another ligand and the centroid-to-centroid distance for this face-to-face arrangement was observed to be 3.960 Å, within the expected range for a weak π•••π stacking interaction. Additionally, the phenyl ring is positioned in a manner so that it is very likely also interacting with a second ligand's isophthalic acid benzene ring, this time through two edge-to-face CH•••π interactions. The centroid-to-carbon distances for the two rings here are 3.728 Å and 3.797 Å respectively, placing them both well within the distance range normally observed for these types of weak noncovalent interactions.[18, 21, 24, 30, 339, 340] The fact that there may be two different CH•••π interactions with this second ligand is due to the positioning of the phenyl ring from the original pendant arm. The edge of the phenyl ring is nearly centered over the face of the isophthalic benzene ring, so that both of the nearest hydrogen atoms on the phenyl ring may be interacting with the isophthalic group's π-cloud.

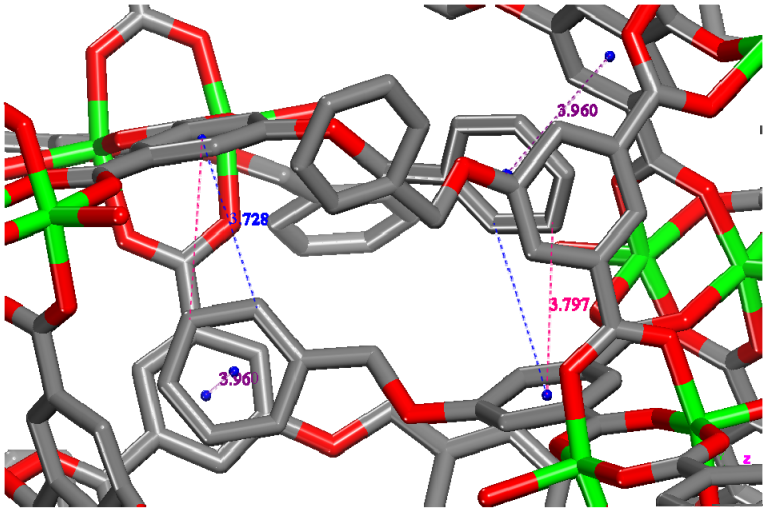

Figure 4.12 Illustration of the close approach of four benzyloxy pendant arms, two each from two separate benzyloxy nanoballs. The face-to-face π•••π stacking is shown in purple, while the two edge-to-face CH•••π interactions are colored blue and pink respectively. Notice there are a total of two π•••π stacking and four CH•••π interactions for a total of 6weak noncovalent interactions between every two nearest neighbors (grey = carbon, red = oxygen, green = copper; hydrogen atoms have been deleted for clarity).

There are two face-to-face π•••π stacking and four edge-to-face CH•••π interactions, for a total of six weak noncovalent interaction between every two nearest neighbors. Since each benzyloxy nanoball has eight nearest neighbors that indicates 48 total interactions.

We have already mentioned that each nanoball, in addition to the eight nearest neighbors, also comes within close contact to six additional second nearest neighbors. Upon close examination it appears that there are interacting pendant arms between these neighbors as well. Each next nearest neighbor supplies two protruding pendant arms each towards these interactions, which are observed to be CH•••π interactions. Since these nearest neighbors are not as close to one another as was the case for the nearest

neighbors, it turns out that the pendant arms are not able to extend completely to the isophthalic benzene rings of the partner ligands. Instead what is observed is that the phenyl ring from one ligand is positioned in the proximity of the CH_2 directly adjacent the oxygen atom attached to the 5th position of the isophthalic benzene ring, while that isophthalic benzene ligand's phenyl group resides adjacent to the –O-CH_2 of the first ligand (Fig. 4.13). The measured centroid-to-carbon distance for these interactions was observed to be 3.8 Å, also within expected distance ranges for these interactions. This makes for two interactions between a pair of ligands with two pairs of ligands for a total of four interactions between any two next nearest neighbors. Since there are six next nearest neighbors, each benzyloxy nanoball is involved with an additional 24 weak noncovalent interactions bringing the total number of interactions for any given nanoball including all of its closest neighbors to 72.

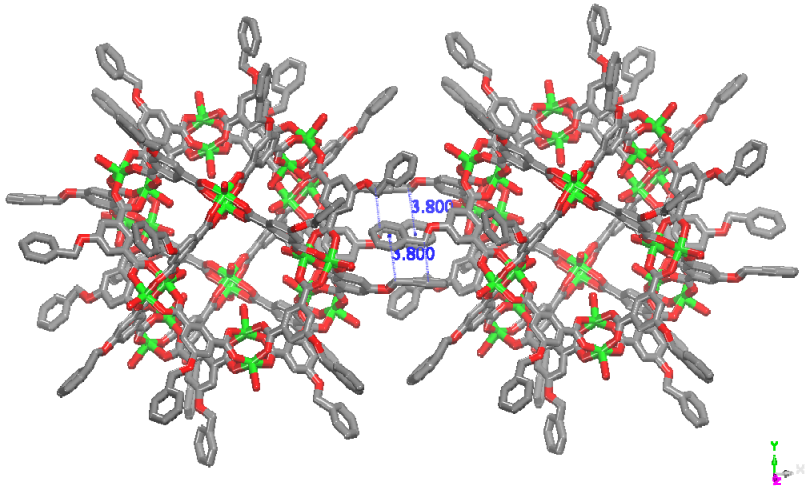

Figure 4.13 Illustration of the four CH•••π interactions (blue) between next nearest neighbors in compound **[31]**. All hydrogen atoms have been deleted for clarity (grey = carbon, red = oxygen, green = copper; hydrogen atoms have been deleted for clarity).

Compound **[32],** $[Cu_2(5\text{-}(2\text{-naphthylmethoxy})\text{-}1,3\text{-benzene-dicarboxylate})_2(py)_{0.66}(DMF)(H_2O)_{0.33}]_{12}$**,** is a discrete functionalized nanoball constructed from the vertex sharing of 12 molecular squares linked together *via* 24 bridging ligands. The Cu(II) naphthylmethoxy nanoball **[32],** or naphthylmethoxy nanoball, is the result of self-assembly of 24 Cu^{2+} ions together with 24 5-(2-naphthylmethoxy)-1,3-bdc ligands (**L2**) in the presence of pyridine, a known coordinating base. It is therefore unsurprising that at least some of the axial ligands on this nanoball are indeed pyridine moieties. Pyridine is not the only axial ligand however, and in fact there are at least four disordered N,N′-dimethylformamide (DMF) together with eight well refined pyridine molecules in the 12 axial positions located around the outside of the nanoball. There were no observed pyridine moieties on any of the axial position located within the hollow interior of the naphthylmethoxy nanoball. Instead there are eight well defined DMF solvent molecules coordinating as ligands to the interior axial position of the SBU. The remaining four axial ligands were not clearly identified by single crystal X-ray diffraction and are believed to be some form of disordered solvent molecules, most likely water. The 24 naphthylmethoxy pendant chains decorating the 5^{th} position of the basal isophthalic acid benzene ring are all situated on the periphery of the nanoball and extend outward away from the nanoball core (Fig. 4.14).

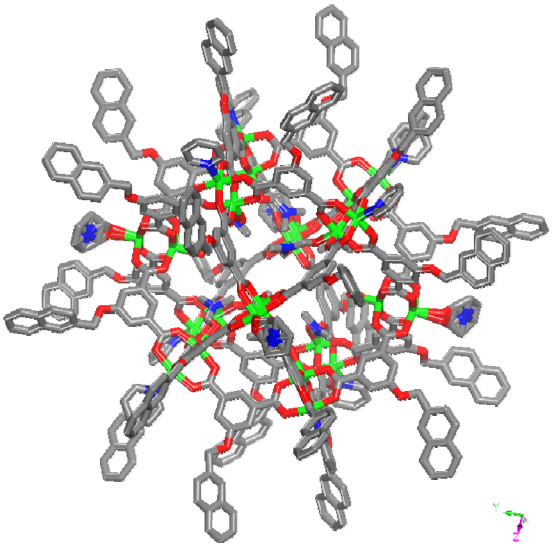

Figure 4.14 Schematic illustrating a stick view of the naphthylmethoxy nanoball, compound **[32]**. All hydrogen atoms have been deleted for clarity (Atom color code: carbon = grey; oxygen = red; copper = green).

Discrete naphthylmethoxy nanoballs **[32]**, crystallize in the tetragonal space group I4/m with unit cell parameters a = b = 27.645 (20) Å, c = 39.9159 (60) Å, α = β = γ = 90°, V = 30524.7 (60) $Å^3$, and Z = 2. The inner core skeleton of the naphthylmethoxy nanoball is essentially identical to that of most other nanoball derivatives including that of the parent version. This is due to the fact that each decorated version of the nanoball is still based upon the base isophthalic acid bridging ligand. The shortest inner diameter, as measured from one inner copper atom to the opposite inner copper atom is 15.859 Å (1.59 nm) meaning the interior volume of this nanoball is approximately 2.10 nm^3. It was decided to measure the volume of the hollow interior while disregarding the presence of axially bound solvent molecules, to better represent the *potential* volume that might be obtained if all labile axial ligands could be removed from this compound. The longest

outer diameter for this nanoball skeleton as measured from the 5th position carbons on opposite 1,3-bdc rings was measured to be 24.546 Å (2.45 nm), while the longest measured diameter including the naphthylmethoxy groups was measured to be 41.097 Å (4.11 nm), resulting in outer volumes of ~ 7.7 nm^3 and 36.34 nm^3 respectively.

In a manner which is analogous to that of the benzyloxy nanoball **[31],** the crystal structure of the naphthylmethoxy nanoball **[32],** reveals a unit cell with a central nanoball surrounded by eight others centered on the corners of the unit cell (Fig.4.15). The centroid-to-centroid distance between the central naphthylmethoxy nanoball and that of one of these corners was measured to be 27.941 Å, slightly longer than what was observed in the case of the benzyloxy nanoball. As the eight nanoballs surrounding the central nanoball are centered on the corners of the unit cell, the centroid-to-centroid distances measured between these nanoballs correspond to the unit cell dimensions of 27.654 Å along the *a*- and *b*-axes, and 39.915 Å along the *c*-axis. In the naphthylmethoxy nanoballs, it was observed that the neighboring nanoballs which reside in the *ab* plane where relatively closer together, while the distance between those nanoballs situated above and below that central nanoball were pushed farther apart in comparison to the benzyloxy nanoballs. This elongation of the unit cell along the *c*-axis with concomitant shrinking along the *a*- and *b*-axes, allows for the central nanoballs of the adjacent unit cells to approach closer than was observed in the benzyloxy structure.

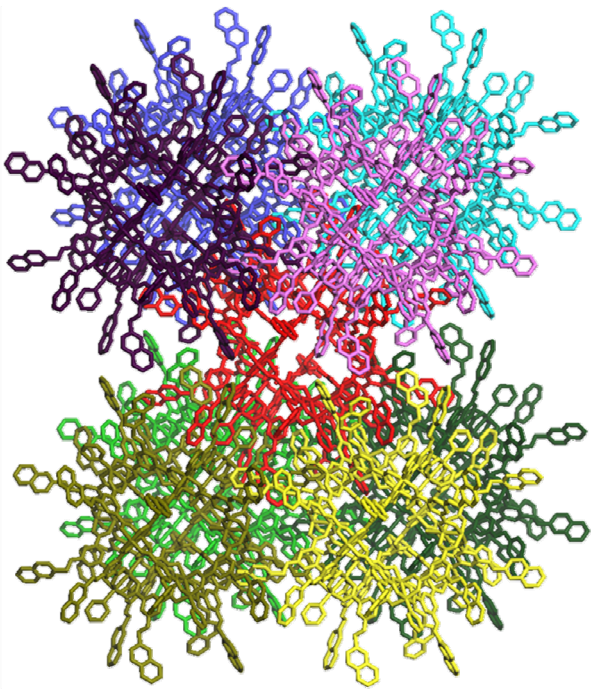

Figure 4.15 The close packing of naphthylmethoxy nanoballs observed in compound **[32].** Notice the eight neighbors centered on the corners of the unit cell mimic a bcc close packing, but in fact these are the next nearest neighbors as the six nanoballs centering the adjacent unit cells are closer to the central (red) nanoball.

In compound **[32]**, we see that the six nanoballs which constituent the centers of the six face-adjacent unit cells, were observed to be at a distance of 27.654 Å (the *a*-, *b*-*axes* lengths of the unit cell), but also point out that this distance was *shorter* than the observed distance from the central nanoball to the corner nanoballs. This means that the nearest neighbors in the naphthylmethoxy nanoball structure are the six nanoballs which are located at the centers of the surrounding unit cells and not the eight nanoballs positioned at the corners of the central nanoball's own unit cell. This is the reverse of the situation observed in the benzyloxy nanoballs, where the nearest neighbors were the eight corners while the six nanoballs centering adjacent cells were the next nearest neighbors.

When analyzing the interactions between the central nanoball and its eight next nearest neighbors positioned at the corners of the unit cell, the same type of weak noncovalent interactions as was seen in the benzyloxy nanoballs are present. The naphthylmethoxy pendant arms from neighboring nanoballs have the same capacity to thread past one another and interact through edge-to-face CH•••π and face-to-face π-π stacking interactions. Each naphthylmethoxy nanoball contributes a single pendant arm for a total of two. The pendant arm arising from one nanoball then interacts *via* a face-to-face π-π stacking interaction with the isophthalic acid benzene ring of the adjacent nanoball. The orientation of the naphthyl groups with respect to each other is rather slipped, which can be common in the observation of π-π stacking. The rings are so slipped however, that the carbon atom at the end of one ring is effectively situated over the center of the π-cloud of the other ring and *vice versa*. The two distances as measured from these carbons to the corresponding centroid of the adjacent ring were measured to be 3.369 Å and 3.474 Å, respectively. The centroid-to-centroid distance for this complex, which is how π-π stacking interactions are typically measured[21, 30], was observed to be 3.743 Å, still well within the norm for this type of weak noncovalent interaction (Fig. 4.16).

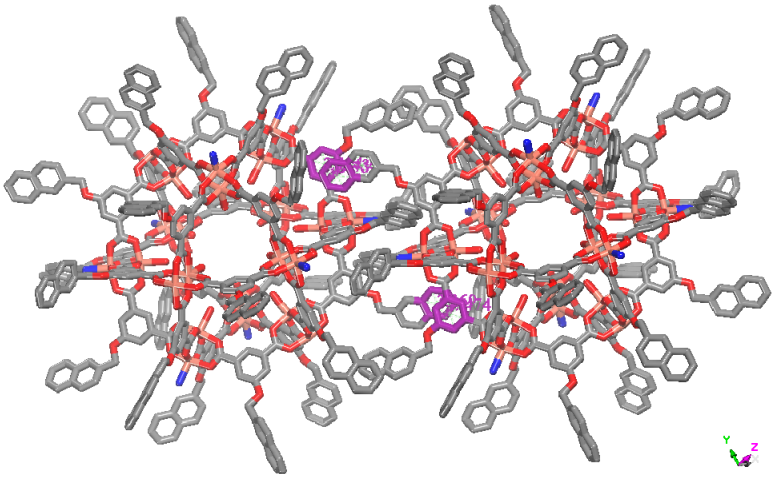

Figure 4.16 Stick representation of face-to-face π-π stacking interactions (purple) observed between next nearest neighbors in the crystal packing of naphthylmethoxy nanoballs **[32].** (grey = carbon, red = oxygen, green = copper; hydrogen atoms have been deleted for clarity).

As each pendant arm of a naphthylmethoxy nanoball is involved in a single face-to-face π-π stacking interaction, and there are two such interactions between every set of next nearest neighbors, each nanoball undergoes 16 face-to-face π-π stacking interactions. In the benzyloxy nanoball, these ligands were situated so that as one ligand approached a nanoball for the stacking interaction, the ligand being approached reciprocated and provided its benzyl group to an interaction with the original nanoball, doubling the number of these interactions observed. In the case of the naphthylmethoxy nanoballs, the ligand which is donated to the next nearest neighbor is not matched by a pendant arm returning to the original nanoball. Instead this ligand's pendant arm meanders in space making no observable close approaches to other naphthyl rings.

Analysis of the interactions between a central nanoball and its six nearest neighbors, which themselves are the center of adjacent unit cells, reveals that the same types of edge-to-face CH•••π and face-to-face π-π stacking interactions as was witnessed in the benzyloxy nanoballs are again present (Fig. 4.17). Here two pendant arms each from two nearest neighboring nanoballs (for a total of four ligands) are involved in a total of four edge-to-face CH•••π interactions. The distance for these interactions, as measured from the centroid of the closest ring in the naphthylmethoxy group to the carbon atom of the corresponding naphthylmethoxy group, was observed to be 3.582 Å. As every nanoball interacts with each of its six nearest neighbors through these four CH•••π interactions, there are a total of 24 interactions with relation to a single nanoball.

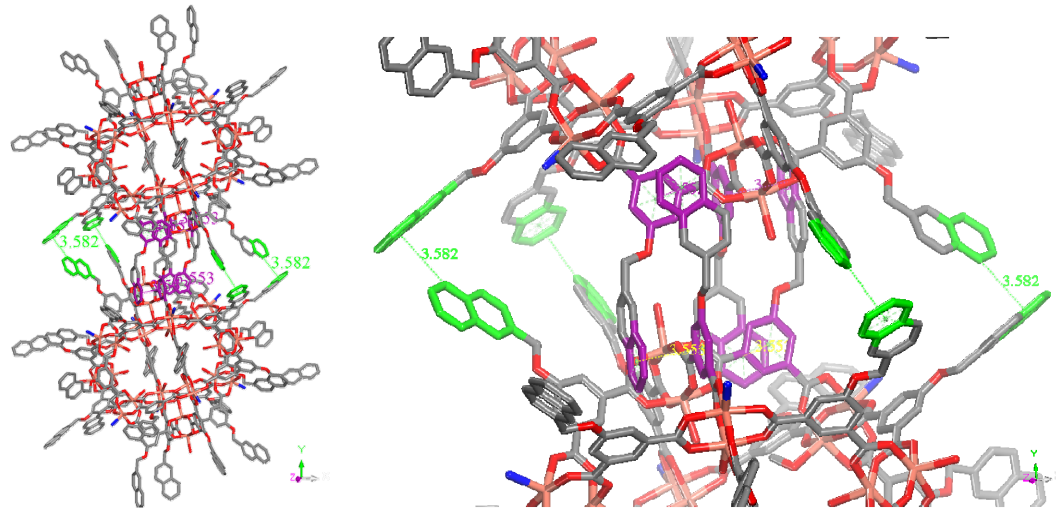

Figure 4.17 Stick representation depicting the two types of weak noncovalent interactions between nearest neighbors in the crystal packing of naphthylmethoxy nanoballs **[32].** ***Left:*** Zoomed out view of the interaction between two adjacent nanoballs illustrates the four CH•••π (green) and four π-π stacking (purple) interactions. ***Right:*** A zoomed in view facilitates observation of the described interactions (grey = carbon, red = oxygen, green = copper; hydrogen atoms have been deleted for clarity).

Interestingly, the interactions of this type are in close proximity to the interactions between neighboring nanoballs so that a concerted quadruple phenyl embrace (QPE) is generated between four nanoballs adjacent in the *ab*-plane (Fig. 4.18). This QPE motif is a well known supramolecular structure, and in the crystal structure of the naphthylmethoxy nanoballs, these QPE are located within the well of another nanoball's metallocalixarene along the *c*-axis. It is within this square metallocalixarene cavity that the rings forming the QPE also π-π stacking with the ligands of the nanoball forming the calyx.

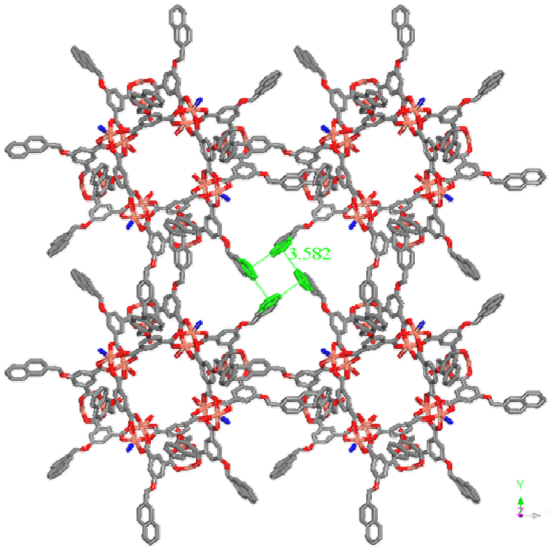

Figure 4.18 Illustration of the quadruple phenyl embrace of concerted edge-to-face CH•••π interactions as seen in the crystal structure of compound **[32].**

Additionally, each naphthylmethoxy nanoball donates two more pendant arms for a total of four ligands, which then interact through face-to-face π-π stacking. This motif is reminiscent of the benzyloxy nanoball structure in that for every pair of pendant arms

there are two stacking interactions, instead of the single interaction seen between next nearest neighbors described above. Since each pair of ligands involves two such interactions and there are two pairs of ligands, there are a total of four edge-to-face CH•••π interactions between every two nearest neighbors and therefore every nanoball is involved with 24 such interactions. Taken collectively this means there are 48 interactions between a nanoball and its six nearest neighbors and an additional 16 interactions between the same nanoball and its eight next nearest neighbors for a total of 64 weak noncovalent interactions associated with every naphthylmethoxy nanoball. While there are a slightly lower total number of interactions observed in the naphthylmethoxy structure as compared with that of the benzyloxy nanoball structure (64 versus 72), it should also be noted that the observed distance for the interactions were shorter comparatively, than in the benzyloxy structure. A shorter distance between groups in noncovalent interactions implies a stronger interaction, something that is also borne out by the observation that while the pendant arm in the naphthylmethoxy nanoball is somewhat larger than its benzyloxy counterpart, the naphthylmethoxy nanoballs make a closer approach to one another than that which was observed in benzyloxy derivative.

4.3.2 Properties

As with all derivatives of the nanoball, both aryloxy versions described in the previous section are constructed *via* the vertex linking of molecular squares (square paddlewheel SBUs) to generate a discrete architecture that contains both open and closed "windows". With a hollow interior that approaches a volume of approximately 1 nm^3, and small pores making this space accessible, the potential to encapsulate small

molecules (especially gases such as CO_2, H_2, etc.) is present. As such, experiments were undertaken in an attempt to analyze these materials porosity. Crystalline samples of each aryloxy nanoball were obtained following the detailed synthesis described in a section to follow below. Once synthesized, the crystalline materials were treated through a number of protocols in an attempt to "activate" them prior to gas sorption measurements. By "activate", we mean to replace otherwise higher boiling solvent molecules and guests present in the crystal structure with relatively low boiling solvent molecules, in an attempt to facilitate the complete removal of all guest and solvent molecules upon vacuum evacuation. The presence of any higher boiling solvent molecules, such as N,N′-dimethylformamide which is present in the reaction solution, may mitigate the materials ability to uptake the sorbent gas being investigated. In a typical activation the reaction solution in the vial containing the crystalline samples of aryloxy nanoballs was removed *via* Pasture pipette and the crystals washed with neat reaction solvent, in this case DMF. The washing process is prescribed to remove any unreacted starting materials such as ligand or metal ions which may still be present in the mother liquor and possibly coat the sample crystals. The crystals were allowed to sit in the fresh DMF for approximately 15 minutes before the process was repeated, the DMF removed and replaced with a fresh aliquot. The sample was washed three times with fresh DMF. After the third washing, the DMF solvent was removed and a second, typically a low boiling solvent was introduced. Again the crystals were allowed to sit immersed in the new solvent, however now the sample was left undisturbed for ~12 hours. After ample time immersed in the exchange solvent, so chosen so that is may diffuse into the material while any other solvent guest

present will subsequently diffuse out of the material into the bulk exchange solvent, the process is repeated. Typically the samples were exchanged at least three times before the sorption experiments commenced. In the case of both aryloxy nanoballs attempts to activate the crystalline material with several exchange solvents was undertaken; chloroform, ethanol, methanol, dichloromethane, carbon tetrachloride, and acetonitrile were all used in trying to activate the samples. Additionally, the two crystalline materials were investigated when prepared by washing with DMF alone and no exchange solvent was employed (as synthesized).

After activation protocols were preformed, the sample was exposed to N_2 gas under reduced pressure in an attempt to measure the capacity of the material to adsorb the gas. The amount of N_2 adsorbed by the materials can potentially be used in several theoretical models for the prediction of that materials' accessible surface area. Unfortunately, in the case of both aryloxy nanoballs the measured five-point N_2 B.E.T. surface area never amounted to more than ~40 m^2/g for any of the outlined activation procedures. Whether a failure to activate the materials properly, or simply the case that these materials, being discrete and capable of small rearrangements on the molecular scale, are generally not porous in nature, could not be determined at this time.

In addition to attempts to measure these materials porosity with respect to gas sorbents, their solubility in common laboratory solvents was also of interest. Other derivatives of the nanoball have been shown to be soluble in several solvents, facilitating the investigation of their solution properties. One derivative nanoball, the hydroxylated version, has been shown to be soluble in pre-polymer monomers, so that upon polymer

formation the nanoballs are incorporated into the polymer material through persistent interactions and can alter the chemical and physical properties when compared with the neat polymer.[341, 342] This could play a role in leading to potential application of made to order nanocomposites. Additionally, the hydroxylated nanoballs have been investigated for their solution photophysical properties through Fluorescence and UV/VIS spectroscopy. The aryloxy nanoballs were targeted in part precisely because the presence of naphthyl and benzyl rings on the ligands should provide for interesting fluorescent markers. Therefore knowledge of which solvents these discrete compounds are soluble in could greatly benefit the development of their properties.

Qualitative solubility experiments were conducted using a powder sample obtained *via* vacuum filtration and air drying of the solid. A small sample of the dry powder (~10-20 mg) was placed into a clean, labeled test tube, and to this ~ 1 mL of neat solvent was added. With the aid of manual as well as mechanical (Maxi-Mix®) agitation, dissolution was attempted. If upon agitation for several minutes, the solid was still undissolved, the use of a hot water bath (steaming, yet not boiling ~85-90 °C) was implemented and the test tube allowed to sit for several minutes before reobserving. Numerous laboratory solvents covering a range of properties such as polar versus nonpolar and protic versus aprotic, were used in these qualitative solubility experiments including such common solvents as methanol, ethanol, chloroform, dichloromethane, acetonitrile, carbon tetrachloride, hexanes, isopropanol, DMF, DMSO, ethyl acetate, benzene, nitrobenzene, *o*-dichlorobenzene, chlorobenzene, acetone, toluene, tetrahydrofuran, 1,4-dioxane, and cyclohexane among others. Neither aryloxy nanoball

was observed to be soluble in any of these solvents even though they are discrete compounds and solubility in at least some solvents was expected. The lack of solubility has impeded the ability to incorporate these nanoballs in polymers as well as the study of their solution photophysics. It is believed that the large number of individually weak albeit concerted noncovalent interactions in the form of face-to-face π-π stacking and CH•••π interactions plays a significant role in the insolubility of the discrete molecular architectures. The aryloxy nanoballs were also exposed to neat *D.I* H_2O were it was determined that they are instable and likely collapse. This was evidenced by the observed disappearance of the characteristic blue color as well as the appearance of white milky precipitate which was presumed to be the insoluble (in water) dicarboxylate ligand.

4.3.3 Experimental

4.3.3.1 Synthesis

All reagents, unless described otherwise, were purchased from either Sigma-Aldrich or Fischer Scientific and used as received without further purification. The synthesis procedures for the two ligands 5-benzyloxy-1,3-benzenedicarboxylic acid (**L1**) and 5-(2-naphthylmethoxy)-1,3-benzenedicarboxylic acid (**L2**) were reported in a previous section (2.2.3.1).

$[Cu_2(5\text{-benzyloxy-1,3-benzenedicarboxylate})_2(DMF)_x(H_2O)_{2-x}]_{12}$ **[31]**, was synthesized from a solvothermal reaction involving $Cu(NO_3)_2 \cdot 2.5H_2O$ (46.9 mg, 0.201 mmol) and **L1** (54.7 mg, 0.201 mmol) together with 2,6-lutidine as a non-coordinating base (72 μL, 0.599 mmol) in a molar ratio of one ligand to one metals to three 2,6-

lutidine molecules. All components, in addition to 3 mL of N, N′-Dimethylformamide and 2 mL of nitrobenzene, were added to a 20 mL scintillation vial which was sealed with aluminum foil and capped tightly. The vial was then placed in a sand bath and heated in a programmable oven. The heat profile was as follows: the reaction temperature was raised from 30 °C to 115 °C at a rate of 1.5 °C per minute upon which time it was held at that temperature for 24 hours. The temperature was then slowly lowered back to 30 °C at a rate of 1 °C per minute. Upon removal from the oven a large amount of prismatic green-blue crystals **[31]** suitable for single crystal X-ray diffraction were observed to have formed (85 mg, 60.1% yield).

[Cu_2(5-(2-naphthylmethoxy)-1,3-benzene-dicarboxylate)$_2$(py)$_{0.66}$(DMF)(H_2O)$_{0.33}$]$_{12}$, **[32]**, was synthesized from a solvothermal reaction involving $Cu(NO_3)_2 \cdot 2.5H_2O$ (46.8 mg, 0.201 mmol) and **L2** (66.1 mg, 0.205 mmol) together with pyridine as a coordinating base (48.5 μL, 0.601 mmol) in a molar ratio of one ligand to one metals to three pyridine molecules. All components, in addition to 3 mL of N, N′-Dimethylformamide and 2 mL of tetrahydrofuran, were added to a 20 mL scintillation vial which was sealed with aluminum foil and capped tightly. The vial was then placed in a sand bath and heated in a programmable oven. The heat profile was as follows: the reaction temperature was raised from 30 °C to 115 °C at a rate of 1.5 °C per minute upon which time it was held at that temperature for 24 hours. The temperature was then slowly lowered back to 30 °C at a rate of 1 °C per minute. Upon removal from the oven a large amount of prismatic green-blue crystals **[32]** suitable for single crystal X-ray diffraction were observed to have formed (67 mg, 73.4% yield).

4.3.3.2 X-ray Crystallography

Single crystals of compound **[31]** suitable for X-ray crystallographic analysis (Fig. 4.19) were selected following examination under a microscope. Intensity data were collected on a Bruker-AXS SMART APEX/CCD diffractometer using Cu k\α radiation (λ = 1.54178 Å).[281] The data were corrected for Lorentz and polarization effects and for absorption using the SADABS program (SAINT).[282] The structures were solved using direct methods and refined by full-matrix least-squares on $|F|^2$ (SHELXTL).[283] Additional electron density, located in the void cavity space, assumed to be disordered solvent, was unable to be adequately refined was removed using the SQUEEZE/PLATON program.[284-286] The phenyl rings of the benzyloxy pendant arm were constrained during refinement. All atoms were refined isotropically except for the Cu atoms which were refines anisotropically. Crystal provided quality diffraction (at frame times utilized) for lower angles only leading to lower resolution (1.2 Å). Select crystallographic data is presented in tabular form in Appendix C-18.

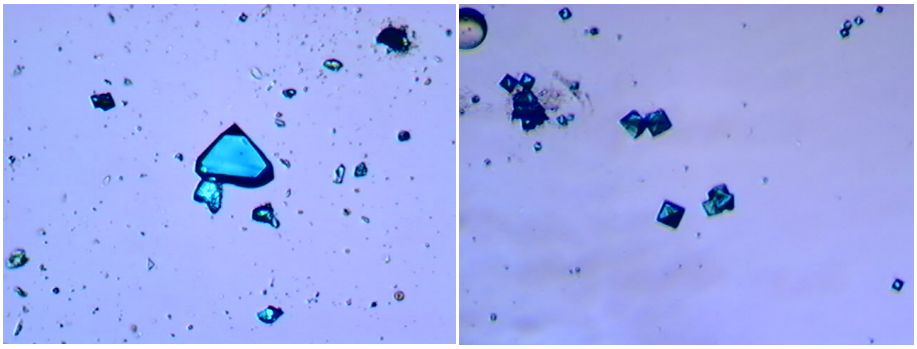

Figure 4.19 Digital photographs depicting single crystals of compound **[31]**.

Single crystals of compound **[32]** (Fig. 4.20) suitable for X-ray crystallographic analysis were selected following examination under a microscope. Intensity data were collected on a Bruker-AXS SMART APEX/CCD diffractometer using Mo k\α radiation (λ = 0.7107 Å).[281] The data were corrected for Lorentz and polarization effects and for absorption using the SADABS program (SAINT).[282] The structures were solved using direct methods and refined by full-matrix least-squares on $|F|^2$ (SHELXTL).[283] Additional electron density, located in the void cavity space, assumed to be disordered solvent, was unable to be adequately refined was removed using the SQUEEZE/PLATON program.[284-286] Select crystallographic data is presented in tabular form in Appendix C-19.

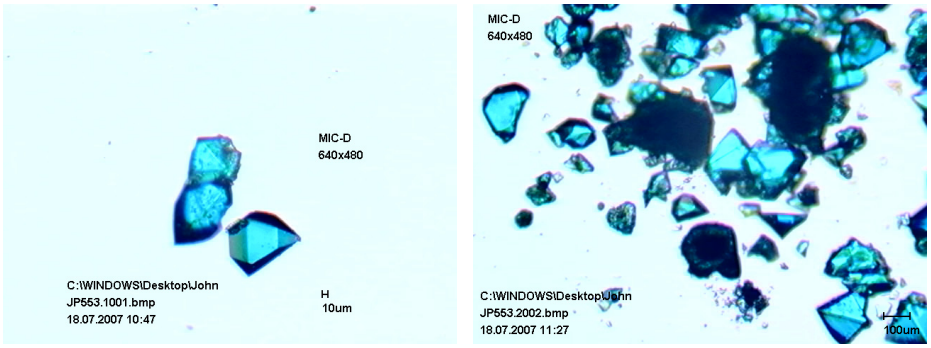

Figure 4.20 Digital photographs depicting single crystals of compound **[32]**.

4.3.3.3 Powder X-ray Diffraction

Powder samples suitable for powder X-ray diffraction, FT-IR spectroscopy, and Thermal Gravimetric Analysis were obtained by removing a large amount of single crystals from the reaction scintillation vial by using a glass Pasteur pipette and depositing these crystal (along with mother liquor) in a small concave agar mortar. Excess solvent

was removed *via* pipette, and surface solvent was removed by wicking action with a Kim-Wipe®. Upon wick drying, the crystals were transferred to a small piece of filter paper which was subsequently folded over and they were dried further and slightly crushed with gently pressure. The resulting dry powder (~30 mg) was then immediately applied to a PXRD sample puck prepared with a small amount of vacuum grease to fixate the powder sample, and the PXRD experiment performed without delay.

A sample of Cu(II) benzyloxy nanoballs, compound **[31],** was characterized for bulk composition purity *via* PXRD. The samples were analyzed on a Bruker AXS D8 Discover X-ray diffractometer, equipped with GADDS™ (General Area Diffraction Detection System) and a Bruker AXS HI-STAR area detector. The X-ray source was Cu (λ= 1.54178 Å) run on a generator operating at 50 kV and 40 mA. The data was collected within the 2θ range of 3° – 40°, in continuous scan mode using a step-size of 0.02° per step and a rate of 2 seconds per step. (Appendix B-36)

A sample of Cu(II) naphthylmethoxy nanoballs, compound **[32],** was characterized for bulk composition purity *via* PXRD. The samples were analyzed on a Bruker AXS D8 Discover X-ray diffractometer, equipped with GADDS™ (General Area Diffraction Detection System) and a Bruker AXS HI-STAR area detector. The X-ray source was Cu (λ= 1.54178 Å) run on a generator operating at 50 kV and 40 mA. The data was collected within the 2θ range of 3° – 40°, in continuous scan mode using a step-size of 0.02° per step and a rate of 2 seconds per step. (Appendix B-37)

4.3.3.4 FT-IR Spectroscopy

All compounds, including synthesized ligands, were characterized *via* infrared spectroscopy using a Nicolet Avatar 320 Fourier-Transform Infrared Spectrometer (FT-IR). Before each sample was analyzed, a background spectrum was obtained for purposes of zeroing out ambient noise in the form of the laboratory atmosphere. Each sample was measured in the range from 4000 cm^{-1} to 500 cm^{-1} wavenumbers (wavelength of 2500 nm to 20000 nm respectively) and scanned 64 times. Results were recorded in % transmittance and the spectrum analyzed using the EZ OMNIC© (V.5.1b, copyright 1992-199 Nicolet Instruments Corporation) computer software suite. A typical sample was a analyzed as a neat, dry solid (~10 mg) obtained *via* either vacuum filtration and air drying or gently drying with laboratory grade filter paper.

$[Cu_2(5\text{-benzyloxy-1,3-benzenedicarboxylate})_2(DMF)_x(H_2O)_{2-x}]_{12}$, **[31]**: IR (dry powder) $\tilde{\upsilon}_{max}$ (cm^{-1}): 1662 med. sh., 1627 m sh. (carboxylate), 1586 m sh. (C=O, carboxylate), 1378 v sh. (COO^-, carboxylate), 1028 vs sh (ether). The most notable changes between the IR spectrum for the ligand **L1** and compound [**31**] is the disappearance of the OH stretch due to the carboxylic acid that was centered around 3122 cm^{-1} and bleed into the 3000 cm^{-1} region as well as the two sharp peaks at 3535 cm^{-1} and 3451 cm^{-1} which arose from free acids. Shifts in frequency for the C=O stretches were observed which is expected upon coordination of the carboxylate. (Appendix B-36)

$[Cu_2(5\text{-}(2\text{-naphthylmethoxy})\text{-}1,3\text{-benzene-dicarboxylate})_2(py)_{0.66}(DMF)(H_2O)_{0.33}]_{12}$, **[32]**: IR (dry powder) $\tilde{\upsilon}_{max}$ (cm^{-1}): 1664 med.

sh., 1629 m sh. (carboxylate), 1586 m sh. (C=O, carboxylate), 1376 v sh. (COO^-, carboxylate), 1038 vs sh (ether). The most notable changes between the IR spectrum for the ligand **L2** and compound [**32**] is the disappearance of the OH stretch due to the carboxylic acid that was centered around 3122 cm^{-1} and bleed into the 3000 cm^{-1} region as well as the two sharp peaks at 3535 cm^{-1} and 3451 cm^{-1} which arose from free acids. Shifts in frequency for the C=O stretches were observed which is expected upon coordination of the carboxylate. (Appendix B-37)

4.3.3.5 Thermal Gravimetric Analysis

Thermal Gravimetric Analysis for $[Cu_2(5\text{-(benzyloxy)-1,3-benzenedicarboxylate})_2(py)_{0.66}(DMF)(H_2O)_{0.33}]_{12}$ compound [**31**] was performed on a PerkinElmer STA 6000 Simultaneous Thermal Analyzer. Data acquisition and analysis was performed with the assistance of the Pyris Series suite of software. Roughly 10-20 mg of dry powder was placed in a sample crucible and heated at a rate of 10 °C/min. form a temperature of 30 °C up to 700 °C.

The results of the TGA experiment (Appendix B-36) was a featureless curve with numerous broad weight losses taking place in extended temperature ranges. This is probably due to the loss of several different "types" of solvent molecules which are guests in the crystal structure, from H_2O and DMF moieties located between nanoballs, those present in the cavities of the nanoballs themselves, and finally those bound to the nanoball as axially coordinated ligands. Additional difficulties in assigning the exact identity of the solvent molecules responsible for weight loss upon leaving the sample

arises from the imprecise nature of the crystal structure. Some unrefined solvent in the form of electron density was observed in the crystal structure, as well as the fact the exact number of each type of solvent ligand coordinated to a particular nanoball is unknown.

Thermal Gravimetric Analysis for $[Cu_2(5\text{-}(2\text{-naphthylmethoxy})\text{-}1,3\text{-benzenedicarboxylate})_2(py)_{0.66}(DMF)(H_2O)_{0.33}]_{12}$, compound [**32**], the Cu(II) naphthylmethoxy nanoball was performed on a PerkinElmer STA 6000 Simultaneous Thermal Analyzer. Data acquisition and analysis was performed with the assistance of the Pyris Series suite of software. Roughly 10-20 mg of dry powder was placed in a porcelain sample crucible and heated at a rate of 10 °C/min. from a temperature of 30 °C up to 700 °C.

The result of the TGA experiment (Appendix B-37) was a featureless curve with numerous broad weight losses taken place of extended temperature ranges. This is probably due to the loss of several different "types" of solvent molecules which are guests in the crystal structure, from H_2O and DMF moieties located between nanoballs, those present in the cavities of the nanoballs themselves, and finally those bound to the nanoball as axially coordinated ligands. Additional difficulties in assigning the exact identity of the solvent molecules responsible for weight loss upon leaving the sample arises from the imprecise nature of the crystal structure. Some unrefined solvent in the form of electron density was observed in the crystal structure, as well as the fact the exact number of each type of solvent ligand coordinated to a particular nanoball is unknown.

4.4 Supermolecular Building Blocks

4.4.1 Introduction

The evolution from the use of single metal ion nodes to the adoption of multiple metal, ligand-bridged clusters or secondary building units (SBUs) as nodes was a watershed moment in the development of metal-organic materials. The importance of the addition of SBUs to the crystal engineer's toolbox is centered on their ability to augment the numbers and types of materials that can be made. Clearly the use of scaled-up nodes that are composed of several metal and bridging atoms (typically oxygen from carboxylates) as opposed to a single metal ion will result in a metal-organic material (MOM) which is itself scaled up by comparison. However, more than simply a method of increasing the dimensions of the resultant material, the use of SBUs as a design principle could help guide the synthetic chemist toward previously elusive network topologies. The real accomplishment of SBUs as a design strategy was its ability to lead the field forward in terms of the types of unprecedented materials which could be made and in illustrating how those materials could be achieved.

The final section of this chapter aims to introduce a new extension to the hierarchy that has come before it. In a manner analogous to the change from metal ions to SBUs, a new design strategy based upon the implementation of metal-organic polyhedra, themselves composed of SBUs (which in turn are themselves constructed from metal ions), as new *supermolecular building blocks* (SBBs)[343-345] to perform as the nodes in the design of extended metal-organic materials. Just as the move from a single metal ion to

an SBU provided new insights into MOMs, so too will the adoption of the SBB design strategy lead to an increase in the amount of materials which can be fabricated as well as a better understanding of how to get there.

4.4.1.1 A Matter of Scale

As was the case for the implementation of SBUs, the first noticeable advantage for the adoption of metal-organic polyhedra as supermolecular building blocks is that they are inherently larger than their SBU counterparts. Similar to the jump in scale from a single metal ion (one atom) to a structure composed of several atoms in a cluster, the SBBs of this design strategy are themselves constructed from several smaller SBUs. This guarantees that the scale of the final material to be fabricated will also be enhanced. If you begin to build with bigger blocks, you insure that your structure will be grandiose. Additionally, the SBB nodes are typically hollow and contain small windows providing small molecules or ions access to their interior. With the incorporation of SBBs into MOMs, even in the presence of interpenetration, the hollow nodes themselves will preclude interpenetration remaining open, and thus cavities with controllable dimensions and functionality can be incorporated into a framework with high fidelity. The inclusion of some SBBs, with their relatively small windows, is also an astute method of controllably incorporating these small pores into a desired framework.

4.4.1.2 Rare and Unprecedented Node Connectivities

In the case of single transition metal ions, the geometry and connectivity of the node depends upon the identity of the metal used. In some instances the metal ion can

adopt only a single, *reliable* coordination geometry, thus limiting what the shape and connectivity of the node will be, or worse still precluding the use of that metal for the fabrication of certain frameworks. With other metals a limited number of different coordination geometries are possible so that precise control over reaction conditions may be warranted for the ability to control which chromophore is generated and therefore which MOM is produced. Even in the case of transition metal ions, which are celebrated for their ability to adopt several different geometries, the total possible number of geometries and coordination connectivities are limited to a handful (i.e. square planar, octahedral, tetrahedral etc.). Nodes with higher coordination numbers or unique geometries are therefore unattainable.

With the use of SBBs it is possible to design nodes which have coordination numbers unheard of with either single metal ions or SBUs. As specifically designed metal-organic polyhedra, SBBs represent nodes that can easily have coordination numbers that are higher than those possible for SBUs alone. If the vertices of the polyhedron are taken to be the points of extension, much as the carboxylates of most SBUs were, then the number of vertices for a polyhedron *may* also represent the connectivity of that SBB node. In this case nodes with very high connectivity should, in principle, be possible as there are many examples of metal-organic polyhedra which have 8, 12, 20, 24, or even more vertices. Additionally, it may be possible to adopt certain SBBs not for the incidence of extra coordination sites, but rather due to the controlled geometry of the existing coordination sites. As a quick example, both an octahedron (common in octahedral transition metals and SBUs alike) and a trigonal prism have six

vertices which can be used as points of extension making them six-connected to a chemist. However the geometry of how the vertices are positioned around the central point of the object are clearly very different. As such the incorporation of one of these nodes in perspective to the other will lead to different topologies. In fact the existence of different topologies within the same connectivity class arises not only from the different possible orientations of some building block with that connectivity, but also from the existence of more than one type of geometry for that connectivity. This is why square planar and tetrahedral nodes, while both 4-connected, often lead to very different topologies. If a particular framework topology required a unique geometrical shape, the use of SBBs may facilitate formation of a structure which adopts the necessary geometry.

4.4.1.3 Out of Increased Complexity, Increased Control

While at first glance the metal-organic polyhedra, imbued with their large number of vertices and unique geometries, appear to be more complex building units than that of the typical SBU (and they are), this does not necessarily indicate that the incorporation of these SBBs into extended frameworks will also be more difficult. In fact thanks to the highly symmetric nature of most MOPs, their incorporation into MOMs may actually help limit the possible outcomes of the construction process. That is to say certain high coordination number, highly symmetric SBBs may only have a few highly selective framework topologies which it can make (default structures). Once a framework topology has been identified as being particularly predisposed toward formation with the use of a particular SBB, that SBB can be designed in such a way so as to incorporate features of the MOP the SBB is based on into the new extended MOMs. That is to say that control

over pore sizes (windows of the MOP), the presence of functional groups inside the hollow interior of the SBB, and other aspects intrinsic to the metal-organic polyhedra can controllably be instilled into the MOM, a feat that can sometimes be difficult with the use building blocks lower in the hierarchy.

4.4.1.4 Inherent Structural Diversity

Finally, as was the case at each level of complexity in the building blocks used to construct metal-organic materials, the use of SBBs will also provide an increased level of structural diversity. Just as the same metal-organic polyhedron can often be made from different metal ions and different (functionalized) ligands, so too can the SBB. Identification of a particularly attractive network, sustained by SBBs should be just as amenable to variation in the metals and ligands used as other MOMs. Moreover, SBBs will be able to generate known common topologies (i.e. diamondoid, *bcu*, *pcu*, etc.) albeit with dimensions, and structural characteristics not possible with single metal ions and SBUs. This leads to a much greater diversity in the amount of materials which will be possible to synthesis and in what we can do with them.

4.4.2 Structural Analysis

The nanoball[346-353] (*small rhombihexahedron*) as a platform of diverse nanostructures, represents one of the most widely studied[131, 336, 341, 354-357] metal-organic polyhedra. Its facile synthesis achieved *via* modular self-assembly together with its nearly spherical geometry, make the nanoball a particularly attractive target for the investigation of metal-organic polyhedra properties. The presence of 12 square paddlewheel SBUs

with their outer axial positions available for coordination, along with 24 1,3-benzenedicarboxylate moieties with their 5th positions amenable toward pre-synthesis of covalent extensions, all of which are pointing outward from the surface and situated

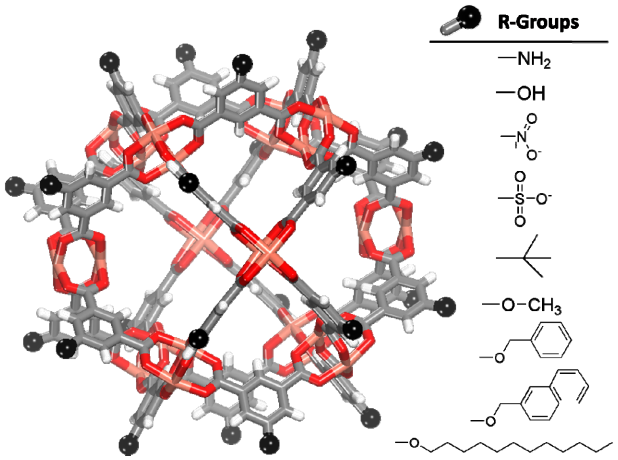

Figure 4.21 Schematic of a *small rhombihexahedron* depicting the peripheral nature of the functional groups (black balls) when the 1,3-BDC moiety is derivatized in the 5th-position. Atoms are color coded as follows: carbon (grey), oxygen (red), hydrogen (white), nitrogen (blue), sulfur (yellow), transition metal (salmon).

around the periphery of the nanoball (Fig. 4.21), also makes them attractive candidates for use a supermolecular building block (SBB) nodes in extended frameworks.

Indeed the nanoball has already been incorporated into extended MOMs in the form of 1-periodic chains and 3-periodic *bcu*-like networks, although serendipitously, through coordination bonds.[349] At first glance, the use of the nanoball's 24 vertices, which is the 5th position of the 1,3-benzendicarboxylate moiety, as the points of extension for new MOMs seems daunting. It is hard to see the possibility of a periodic network

being constructed from a node with so many points. In fact only recently did a research team that works on the enumeration of networks that are feasible for the synthesis of MOMs, publish an account of a (3,24) net (*rht*) constructed from rhombicuboctahedra (which shares the edge skeleton and thus the arrangement of vertices with the nanoball).[358] What may be key however, is the idea that you need not use the nanoballs as *solely* 24 connected nodes; it is also feasible to use multiple connections between the same two nodes to generate a network. In this case the number of extensions will be reduced by the number of cross-links between two nodes (granting that all the nodes share the same number of cross-links). Therefore if each node is doubly connected to its nearest neighbors, the nanoball would be reduced to being a twelve-connected node; if triply connected, then the node would be expected to be 8-connected. To envision how this might be possible, one need only look at the symmetries of the nanoball itself (Fig. 4.22). Careful observation of the nanoball reveals that it has three-fold rotational symmetry axes passing through each of the eight triangular windows (for a total of four axes). As was just mentioned, if the node were to be triply connected to other nodes we would expect it to be eight connected. Thus the symmetry of the nanoball itself dictates how this connectivity might occur; if the three cross-links were symmetrically oriented around the triangular windows, of which there are precisely eight, both the conditions of the cross-linking and connectivity would be satisfied with the additional benefit that these cross-links would automatically be situated in the most symmetrical manner possible.

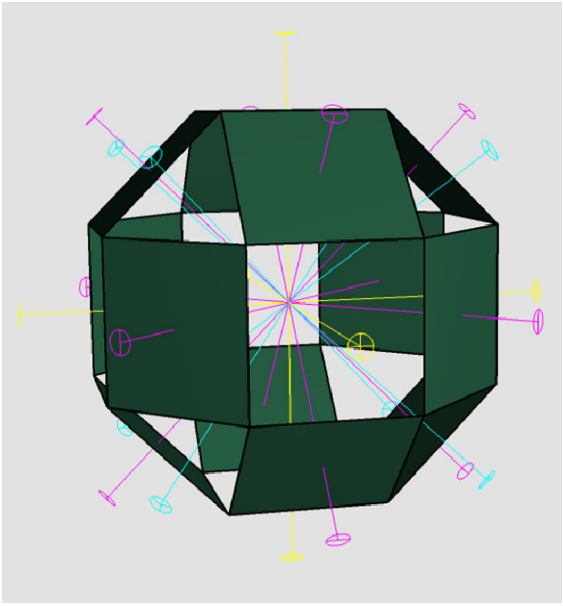

Figure 4.22 Cartoon illustrating the various rotational symmetry elements of the small rhombihexahedron (O_h). Purple = 2-fold, Light Blue = 3-fold, yellow = 4-fold.

In a similar vein the symmetry elements of the nanoball also dictate how the MOP will behave as two distinct 6-connected nodes (Fig 4.23). The existence of the three four-fold rotational axes passing through the six open square windows indicates that four-fold cross-linking centered on these windows, should be symmetrically favored. Another 6-connected node is possible, which at first may be difficult to see, but if one of the two-fold rotation axes passing through two opposite closed faces (SBUs), in conjunction with the appropriate four open square windows, are used as the points of cross-linking, then a node with clearly different symmetry than the first example of a 6-connected node would exist. The two different 6-connected nodes, while very similar (they result from a simple reorientation of the nanoball), would ultimately crystallize in different space groups due to the symmetry involved.

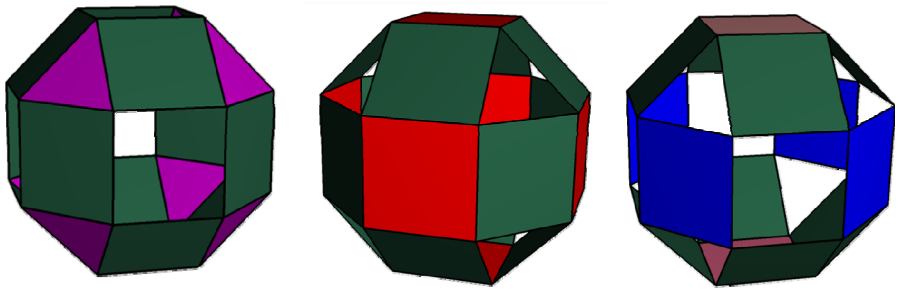

Figure 4.23 Three possible connectivities for the small rhombihexahedron SBB. ***Left:*** Triple cross-linking centered on the eight triangular windows (purple, one not shown) will result in an 8-connected *bcu*-like network. ***Center:*** Quadruple cross-linking through the six open square windows (red) results a six-connected SBB with O_h symmetry. ***Right:*** Quadruple cross-linking through four closed faces (SBUs, blue) and two open square windows (plum) will result in a different 6-connected SBB with local D_{4h} symmetry. While both six-connected nodes should generate a *pcu-i*-like network, the symmetry and space groups of the networks will be different.

In an attempt to implement this new-found design strategy for the cross-linking of *small rhombihexahedra*, a tetracarboxylic acid composed of two 1,3-benzenedicarboxylic acid moieties tethered together *via* a dimethoxy-benzene group was synthesized (Fig. 4.24). The two 1,3-bdc moieties were bridged at their respective 5th positions, so that upon generation of the nanoball on at the diacid would facilitate concomitant cross-linking to another nanoball.

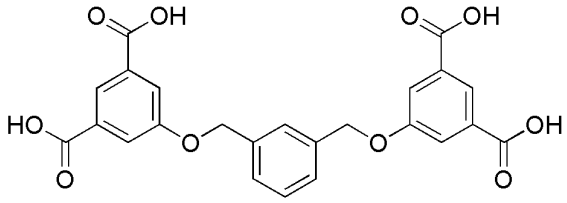

Figure 4.24 1,3-bis(5-methoxy-1,3-benzenedicarboxylic acid)benzene, **L5**

Reactions carried out using Cu^{2+} and **L5**, resulted in the formation of quadruply cross-linked nanoballs, compound **[33]** which exists as a 2-fold interpenetrated *pcu-i* like network. Here *pcu-i* is the RCSR term for an augmented *pcu* network where the vertex is a rhombicuboctahedron (nanoball), and is face sharing with cubes. The compound crystallized in the tetragonal spacegroup I422, with a = b = 28.885(4) Å, c = 28.305(6) Å, V = 23616(7) $Å^3$ with Z = 2. The nanoball nodes cross-link *via* the dimethoxy benzene tethers to 6 adjacent nanoballs positioned around the central nanoball in manner so as to generate D_{4h} symmetry. The cross-linking occurs through four square faces (the SBUs) along the *ab*-plane (Fig. 4.25). The presence of SBUs along these axes, prevents any type of channel running through the nanoball and aligned with these axes. The four bridging ligands generate a pseudo-cylinder cavity, as they are bowed outward from the cross-linking axis rather than straight. This was made possible by the flexible nature of the ligand **L5**. In fact the flexible nature of the ligand may also contribute to the tetragonal spacegroup of the crystal structure, as the conformations of the ligands are different along the *a*-axis (and *b*-axis) and that of the *c*-axis. Along both the *a*- and *b*-axes the ligands adopt a *syn*-conformation while along the *c*-axis they adopt an *anti*-conformation (Fig. 4.25). The dimensions of the cylinders (formed by bridging ligands) directed along the *ab*-plane was measured to be 7.24 Å long (as measure Cu to Cu form the two capping SBU faces) with a diameter of 10.54 Å (as measure centroid-to-centroid of the bridging benzene moieties).

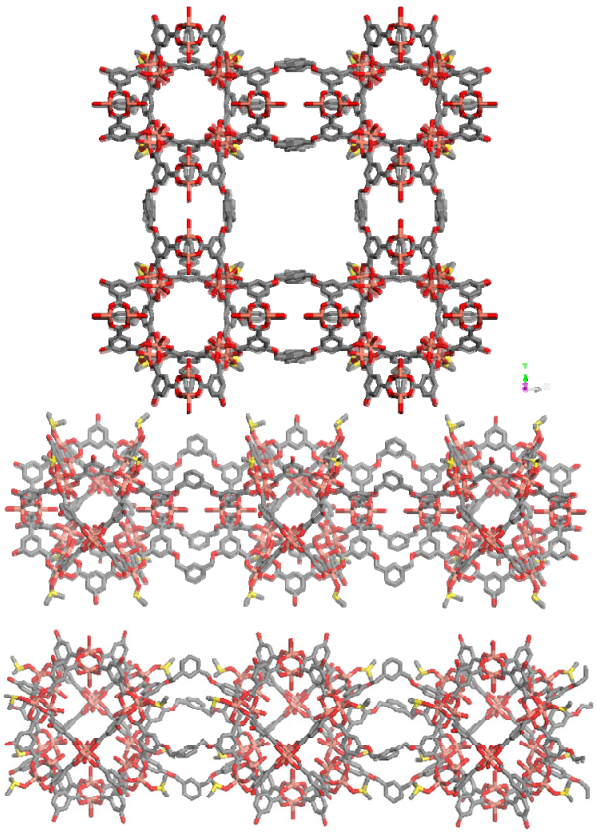

Figure 4.25 Stick representation illustrating the cross-linking observed in the Cu linked-nanoballs, compound **[33].** ***Top:*** A view of the *ab*-plane depicts the large square cavities formed by quadruple cross-linking of nanoballs. As this structure involves 2-fold interpenetration, this large cavity is filled with a nanoball node from the second framework (not shown). ***Middle:*** cross-linking as observed along the *a*- and *b*-axes. Note here the *syn*-conformation adopted by the bridging portion of the ligand and how the SBUs which are present in the cylinder along both the *a*- and *b*-axes are perfectly collimated. ***Bottom:*** cross-linking as observed along the *c*-axis. Note here the *anti*-conformation adopted by the bridging portion of the ligand and the lack of SBUs, allowing for a persistent channel directed along the *c*-axis. (grey = carbon, red = oxygen, salmon = copper, yellow = sulfur; hydrogen atoms have been deleted for clarity).

The axial sites of the SBUs in these cavities contain unrefined solvent molecules as ligands, probably MeOH or water, filing up the majority of this void. Along the *c*-axis, the cylinder is formed by the *anti*-conformation ligands and was observed to have a length of 5.86 Å and a diameter of 17.88 Å. In this cylinder the length is diminished as

the ligands bow out more pronouncedly. Along this axis, there is no SBU capping the cylinder, as the ligands are centered on an open square window. Thus along this *c*-axis there is a continuous cylinder.

Within the *ab*-plane, the nanoball SBB nodes cross-link to form a cavity with impressive dimensions. As measured from opposing benzene moieties of the bridging ligands (centroid-to-centroid), the cavity was observed to be ~ 18.3 Å or 1.8 nm in length. This square cavity has a diagonal length of ~ 2.5 nm. Measured along the *c*-axis, the cavity is 13.56 Å tall, making for a rectangular cavity with dimensions ~ 1.8 x 1.8 x 1.4 nm. However, this large void is precisely where a nanoball SBB node from the second interpenetrating framework resides.

Topologically, the structure generates an augmented *pcu-i* like network which can be decomposed into four symmetrically unique nodes. Further analysis of the structure revealed the coordination sequence recorded in Table 4.1. Review of O'Keeffe's indispensable text[170], also indicates that this structure is very closely related to an infinite polyhedron formed from rhombicuboctahedra and cubes, and given by the notation 3.4^4. This infinite polyhedron seem to be more closely related to the potential octahedral node isomer, however, as the cubes are all positioned in what would essentially be the six open square windows. Yet another way of interpreting this structure is that it is a zeolite-like metal-organic framework. Zeolites are an important and expansive class of inorganic compounds which are microporous aluminosilicates. They are useful for a wide array of industrial applications, most notably in detergents and water softeners (ion exchange). Zeolites are generically 3-periodic structures that can be conceptually seen as different

types of cages joining together to generate the architecture. This analogy is apt as the cross-linked nanoball structure can also be viewed as being the result of several types of cages face-sharing. In the case of the cross-linked nanoballs, the nanoball SBB node is one type of cage which is then connected to other SBB nanoball nodes through a separate cage, this time in the form of a rectangular box (Fig. 4.26). The four ligands responsible for the quadruple cross-linking between nanoballs form the edges of this rectangular box. A third cage is represented by the void space which is generated when a single nanoballs SBB node is connected to its six neighbors to generate a framework. Since the nanoball SBB in this structure is six-connected, it can loosely be interpreted to be similar in structure to the ubiquities sodalite cage found in zeolites, making the cross-linked nanoball structure closely related to Zeolite A (**LTA**) which is constructed from sodalite cages bridged by face-sharing with cubes in an octahedral arrangement.

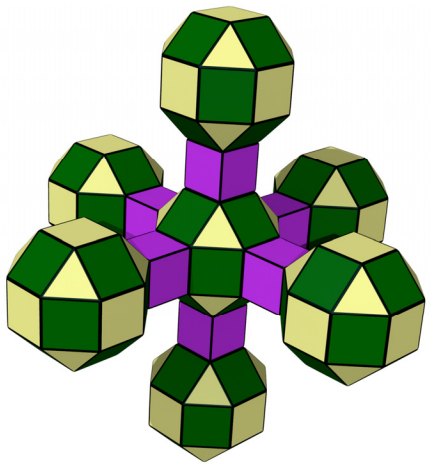

Figure 4.26 Cage sharing view of the cross-linked nanoballs structure. Here the purple cubes are the cages generated by the bridging ligands.

Table 4.1 Coordination sequences and TD_{10} for the four unique nodes found in compound **[33].**

k	1	2	3	4	5	6	7	8	9	10	TD_{10}
Node 1	4	9	20	37	64	88	124	161	214	236	957
Node 2	4	10	24	36	60	86	120	168	208	244	960
Node 3	4	9	20	40	68	92	116	184	216	232	981
Node 4	4	11	22	40	60	91	126	164	210	264	992

Reactions carried out using Zn^{2+} and **L5**, also resulted in the formation of quadruple cross-linked nanoballs which are 2-fold interpenetrated. The compound crystallized in the tetragonal spacegroup I4/m, with a = b = 30.144(7) Å, c = 27.944(11) Å, V = 25391(13) $Å^3$ with Z = 2. The structures of **[33]** and **[34]** are nearly identical, except for small variations in the conformations of their ligands and relative dimensions of some of the cavities. The Zn version of the linked nanoballs has the same coordination sequence and TD_{10} values that were observed for the Cu analogue. Additionally, the connectivity and orientation of the respective nanoball SBBs is identical; the cross-linking observed in the *ab*-plane occurs *via* the 4 square faces due to the SBU, while the cross-linking witnessed along the *c*-axis centers on two square open windows. The dimensions of the cylindrical SBB connectors are also roughly similar; along the *a*- and *b*- axes, the cylinder measures 14.76 Å (carbon-to-carbon of opposing carbon atoms on the bridging benzene ring) by 8.033 Å as measured from Zn-to-Zn. One very obvious difference between the Zn analogue and that of the copper version is the presence of pyridine ligands bound in the axial position of some of the SBUs. Inside of the nanoball

SBBs there are eight DMF and four pyridine axial ligands with all of the pyridine molecules being positioned either along the *a*- or *b*-axis. The presence of pyridine molecules within the cylindrical cavities situated along the *ab*-plane (Fig. 4.27), causes the linear orientation of SBUs as seen in compound **[33],** to be somewhat distorted and greatly reduces any possible free volume there, albeit removal of the pyridine molecules may be feasible. The pyridine molecules seem to be involved in weak CH•••π interactions (3.461 Å measure centroid to centroid) due to a slipped face stacking arrangement.

Along the *c*-axis the dimensions of the bridging cylinder were observed to be 16.092 Å x 11.63 Å, when measured from oxygen atoms bridging metal ions in the SBUs. Here the ligands are severely disordered over at least two positions; however the persistent channel along the *c*-axis is reminiscent of that observed in the Cu analogue. The dimensions of the large rectangular cavity are similar as well; 17.019 Å long with a diameter of ~ 27 Å. The length of this box along the *c*-axis is somewhat shorter at 12.782 Å.

4.4.3 Properties

One of the more intriguing facets of these linked nanoball structures, is the fact that in addition to the immense size of the cavities generated, the small pores inherent to the nanoball SBB node persist as well. The design strategy of SBBs has allowed for the controlled incorporation of nanoscale cavities with predetermined pores shapes and sizes into an extended periodic structure that simultaneously generates vast cavities. This could

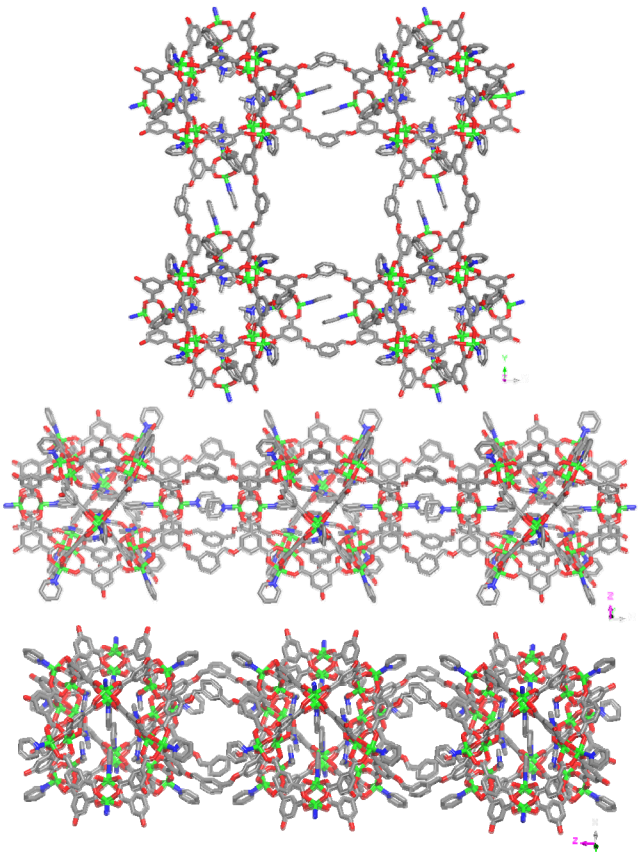

Figure 4.27 Stick representation illustrating the cross-linking observed in the Zn linked nanoballs, compound **[34].** ***Top:*** A view of the *ab*-plane depicts the large square cavities. This structure also involves 2-fold interpenetration occluding the large cavity with a nanoball node from the second framework (not shown). ***Middle:*** cross-linking as observed along the *a*- and *b*-axes. Note here the presence of the SBUs which have axially coordinated pyridine molecules inside the cylinders. ***Bottom:*** cross-linking as observed along the *c*-axis. Note here the lack of SBUs allowing for a persistent channel directed along the *c*-axis. (grey = carbon, red = oxygen, blue = nitrogen, salmon = copper, yellow = sulfur; hydrogen atoms have been deleted for clarity).

potentially be very valuable to the goal of effectively adsorbing and storing molecular hydrogen. A current belief by many experts working towards the use of metal-organic materials for the storage of H_2, is that large surface areas (i.e. big, accessible cavities free of occlusions) should be beneficial to storing large amounts of hydrogen (i.e. high %

volume) especially at high pressures, whereas the inclusion of small pore sizes will be beneficial to increasing the strength of the interaction between the framework and H_2 (i.e. higher Q_{st}, isosteric heats of adsorption).[187-190] Therefore, attempts to incorporate both large surface areas and small pore sizes into a MOM are seen as particularly salient. Indeed that is exactly what can be achieved through the use of the SBB design strategy, and thus explains a sudden explosion in the number of research groups publishing materials based upon this strategy.

As for compounds **[33]** and **[34]**, both exhibit 2-fold interpenetration which effectively occupies the entire ~ 1.8 x 1.8 x 1.4 nm cavity. The fact that the SBB nodes themselves are immune to interpenetration assists in the formation of persistent channels directed along the *c*-axis only. Therefore the ability of these materials to adsorb small guest molecules in the form of gases (N_2, H_2) was of particular interest. As such experiments were conducted in an attempt to activate the crystalline materials *via* solvent guest exchange with low boiling solvents. Upon solvent guest exchange, the samples were exposed to nitrogen gas at 77 K and low pressures and the volumetric uptake recorded. Using this data 5 point B.E.T. surface areas were calculated to estimate the materials' potential accessible surface area. Unfortunately, neither material ever demonstrated a B.E.T. surface area greater than ~ 50 m^2/g making their porosity questionable. Whether the lack of porosity was due to the presence of solvent or guest molecules inside the nanoball SBBs which could not be evacuated and thus occluded the potential free volume, or if it's a factor of the material not surviving the evacuation process and either partially or totally collapsing, could not be determined. Powder X-ray

diffraction patterns obtained after sorption analysis seem to indicate that the material had not completely collapsed. However, this is not conclusive, as the PXRD was not conducted under identical conditions to the sorption experiment (low temperature and pressure) and does not speak to the possibility of surface damage to the microcrystals in which the entrance to extended channels are effectively sealed off while overall the channels persist. In this case the PXRD may not be indicative of a material's channels being unattainable.

As a point of interest, another research group, following our strategy and adopting a ligand nearly identical to **L5** was able to synthesis a related structure (*pcu*-like from quadruply linked nanoballs) albeit without the observed interpenetration. This is because the ligand was slightly shorter in length, reducing the dimensions of the cavity and precluding the presence of a second interpenetrating nanoball network. Consequently, this material has shown one of the highest Q_{st} values for any know metal-organic material, thus validating the design strategy.[359]

4.4.4 Experimental

4.4.4.1 Synthesis

All reagents, unless described otherwise, were purchased from either Sigma-Aldrich or Fischer Scientific and used as received without further purification. Bulk solvents such as methanol, ethanol, acetone, and dichloromethane were first distilled and stored over drying media (4Å molecular sieves) before their use.

1,3-Bis(5-methoxy-1,3-benzenedicarboxylic acid)benzene, **L5** (Fig. 4.24) was synthesized from commercially available dimethyl-5-hydroxy-1,3-benzenedicarboxylate and α,α′-Dibromo-*m*-xylene *via* established procedures.[360] In a typical reaction the dimethyl-5-hydroxy-1,3-benzenedicarboxylate (3.185 g, 0.0152 mol, 2 equivalents with respect to xylene) and K_2CO_3 (5.97 g, 0.0432 mmol, 3 equivalents to ester) were weighed out separately and dried on a vacuum pump for three hours prior to use. After drying, the two solids were placed in a 3-neck round bottom flask which was purged of air using N_2 for ~15 minutes prior to the start of the reaction. Upon the addition of the two solids ~100 mL of dry acetone was added and the mixture stirred utilizing a stir bar and hot plate. The round bottom flask was placed in a hot oil bath which was held at a temperature of 80 °C. Separately, the dibromoxlyene (2.00 g, 0.0076 mmol) was dissolved in 20 mL of dry acetone, and then added to the refluxing mixture. The solution was allowed to reflux for ~24 hours and the reaction was monitored *via* TLC. Upon completion of the reaction, the solution was allowed to cool to room temperature and then filtered through Celite. The solvent was then removed with heat under vacuum, to leave behind a dark yellow oil which solidified upon cooling in the refrigerator (10 °C). The solid that remained was then dissolved in ~100 mL dichloromethane, washed three times with *D.I.* H_2O, and dried over anhydrous Na_2SO_4. Once more the solvent (DCM) was removed with heat under a vacuum, the resulting oil solidified, and the solid was finally recrystallized from hot ethanol. Upon recrystallization very fine colorless needles where collected *via* vacuum filtration and allowed to air dry in the hood.

The crystalline ester product was then dissolved in a methanol/ H_2O solution of NaOH (20% by volume, 6 equivalents to the ester). Upon full dissolution the solution was allowed to stir for ~12 more hours, after which the completion of the saponification was verified *via* TLC. The final product was obtained by precipitating the carboxylic acid out of solution by the dropwise addition of HCl solution (10% by volume) until a pH < 2 for the solution was obtained as determined by pH paper. The resultant white solid was washed several times with *D.I.* H_2O, vacuum filtered and then dried in a vacuum oven at 60 °C. 1,3-bis(5-methoxy-1,3-benzenedicarboxylic acid)benzene (**L5**) was collected (2.15g, 85.8%) as a pure white powdery solid with spectroscopic data that was consistent to those previously reported (Appendix A-5, B-5).[360]

^{1}H NMR (250 MHz, DMSO-d_6, δ): 5.3(s, 4H, , -O-CH_2-), 7.5(d, J = 0.9 Hz, 3 H, -ArH), 7.6(s, 1H, -ArH), 7.8(d, J = 1.39 Hz, 4H, -ArH), 8.1(t, J = 1.38 Hz, 2H, -ArH), 13.4(br, 4H, -COOH); mp 279-281 °C (lit 230-246 °C).

In a typical reaction $[Cu_{24}(\mathbf{L5})_{12}(H_2O)_{16}(DMF)_8]_n$ [**33**], was synthesized from a solvothermal reaction involving $Cu(NO_3)_2{\cdot}2.5H_2O$ (47.2 mg, 0.203 mmol) and **L5** (47.1 mg, 0.101 mmol) together with pyridine as a coordinating base (48 μL, 0.599 mmol) in a molar ratio of one ligand to two metals to six pyridine molecules. All components, in addition to 2 mL of N, N′-Dimethylformamide and 1 mL of *o*-dichlorobenzene, were added to a 20 mL scintillation vial which was sealed with aluminum foil and capped tightly. The vial was then placed in a sand bath and heated in a programmable oven. The heat profile was as follows: the reaction temperature was raised from 30 °C to 105 °C at a rate of 1.5 °C per minute upon which time it was held at that temperature for 24 hours.

The temperature was then slowly lowered back to 30 °C at a rate of 1.0 °C per minute. At this time the solution was a noticeable deep green color, but contained no precipitate or crystals. The reaction vial was then subjected to an additional round of heating, raised at rate of 1.5 °C per minute to a holding temperature of 115 °C. After 24 hours, the temperature was cooled again at a rate of 1.0 °C per minute, and the vials again contained a deep green solution was no visible precipitate. The vials were left undisturbed on the lab bench, still capped, and after approximately three months, large prismatic green-blue crystals of compound **[33]** suitable for single crystal X-ray diffraction were observed to have formed (65 mg, 20.65% yield).

In a typical reaction $[Zn_{24}(\mathbf{L5})_{12}(H_2O)_{16}(DMF)_8]_n$ [**34**], was synthesized from a solvothermal reaction involving $Zn(NO_3)_2{\cdot}6H_2O$ (60 mg, 0.202 mmol) and **L5** (46.78 mg, 0.100 mmol) together with pyridine as a coordinating base (48.52 μL, 0.601 mmol) in a molar ratio of one ligand to two metals to six pyridine molecules. All components, in addition to 3 mL of N, N′-Dimethylformamide and 1 mL of anisole, were added to a 20 mL scintillation vial which was sealed with aluminum foil and capped tightly. The vial was then placed in a sand bath and heated in a programmable oven. The heat profile was as follows: the reaction temperature was raised from 30 °C to 115 °C at a rate of 1.5 °C per minute upon which time it was held at that temperature for 24 hours. The temperature was then slowly lowered back to 30 °C at a rate of 1.0 °C per minute. Upon cooling to room temperature, the reaction vials were removed from the oven and it was observed that large colorless cube shaped crystals **[34]** suitable for single crystal X-ray diffraction had formed (78 mg, 43% yield)

4.4.4.2 X-ray Crystallography

Single crystals of compound **[33]** (Fig. 4.28) suitable for X-ray crystallographic analysis were selected following examination under a microscope. Intensity data were collected on a Bruker-AXS SMART APEX/CCD diffractometer using $Mo_{k\backslash\alpha}$ radiation (λ = 0.7107 Å).[281] The data were corrected for Lorentz and polarization effects and for absorption using the SADABS program (SAINT).[282] The structures were solved using direct methods and refined by full-matrix least-squares on $|F|^2$ (SHELXTL).[283] Additional electron density, located in the void cavity space, assumed to be disordered solvent, was unable to be adequately refined was removed using the SQUEEZE/PLATON program.[284-286] Select crystallographic data is presented in tabular form in Appendix C-20.

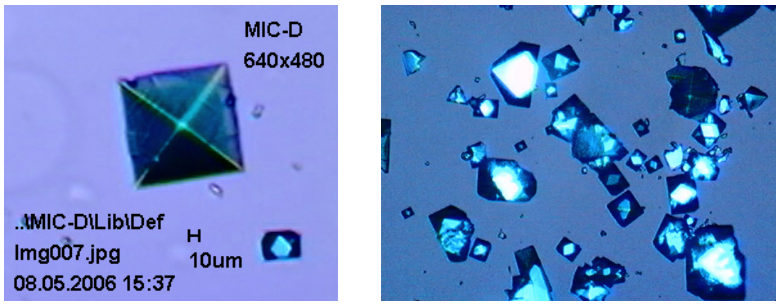

Figure 4.28 Digital photographs depicting single crystals of compound **[33]**.

Single crystals of compound **[34]** (Fig. 4.29) suitable for X-ray crystallographic analysis were selected following examination under a microscope. Intensity data were collected on a Bruker-AXS SMART APEX/CCD diffractometer using Mo k\α radiation (λ = 0.7107 Å).[281] The data were corrected for Lorentz and polarization effects and for

absorption using the SADABS program (SAINT).[282] The structures were solved using direct methods and refined by full-matrix least-squares on $|F|^2$ (SHELXTL).[283] Additional electron density, located in the void cavity space, assumed to be disordered solvent, was unable to be adequately refined was removed using the SQUEEZE/PLATON program.[284-286] Select crystallographic data is presented in tabular form in Appendix C-21.

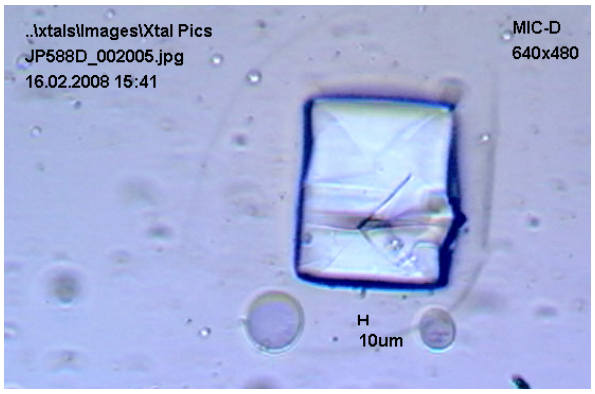

Figure 4.29 Digital photograph depicting a single crystal of compound **[34]**.

4.4.4.3 Powder X-ray Diffraction

Powder samples suitable for powder X-ray diffraction (PXRD), FT-IR spectroscopy, and Thermal Gravimetric Analysis (TGA) were obtained by removing a large amount of single crystals from the reaction scintillation vial by using a glass Pasteur pipette and depositing these crystal (along with mother liquor) in a small concave agar mortar. Excess solvent was removed *via* pipette, and surface solvent was removed by wicking action with a Kim-Wipe®. Upon wick drying, the crystals were transferred to a small piece of filter paper which was subsequently folded over and they were dried

further and slightly crushed with gently pressure. The resulting dry powder (~30 mg) was then immediately applied to a PXRD sample puck prepared with a small amount of vacuum grease to fixate the powder sample, and the PXRD experiment performed without delay.

The Cu(II) version of the linked nanoballs, compound **[33],** was characterized for bulk composition purity *via* PXRD. The samples were analyzed on a Bruker AXS D8 Discover X-ray diffractometer, equipped with GADDS™ (General Area Diffraction Detection System) and a Bruker AXS HI-STAR area detector. The X-ray source was Cu (λ= 1.54178 Å) run on a generator operating at 50 kV and 40 mA. The data was collected within the 2θ range of 3° – 40 °, in continuous scan mode using a step-size of 0.05° per step and a rate of 0.5 seconds per step. (Appendix B-38)

The Zn(II) analogue of the linked nanoballs, compound **[34],** was also characterized for its bulk composition purity *via* PXRD. The samples of **[34]** were analyzed on a Bruker AXS D8 Discover X-ray diffractometer, equipped with GADDS™ (General Area Diffraction Detection System) and a Bruker AXS HI-STAR area detector. The X-ray source was Cu (λ= 1.54178 Å) run on a generator operating at 50 kV and 40 mA. The data was collected in continuous scan mode by sweeping through 2θ angles of 3° – 40 ° and using a step-size of 0.05° and rate of 0.5 seconds per step respectively. (Appendix B-39)

4.4.4.4 FT-IR Spectroscopy

All compounds, including synthesized ligands, were characterized *via* infrared spectroscopy using a Nicolet Avatar 320 Fourier-Transform Infrared Spectrometer (FT-IR). Before each sample was analyzed, a background spectrum was obtained for purposes of zeroing out ambient noise in the form of the laboratory atmosphere. Each sample was measured in the range from 4000 cm^{-1} to 500 cm^{-1} wavenumbers (wavelength of 2500 nm to 20000 nm respectively) and scanned 64 times. Results were recorded in % transmittance and the spectrum analyzed using the EZ OMNIC© (V.5.1b, copyright 1992-199 Nicolet Instruments Corporation) computer software suite. A typical sample was a analyzed as a neat, dry solid (~10 mg) obtained *via* either vacuum filtration and air drying or gently drying with laboratory grade filter paper.

The FT-IR spectrum (Appendix B-5) for 1,3-bis(5-methoxy-1,3-benzenedicarboxylic acid)benzene **L5,** illustrates the same broad featureless hump originating around 3300 cm^{-1} and bleeding into ~3000 cm^{-1} which is typical of carboxylic acids involved in hydrogen bonding, which would be expected in solid state samples such how the ligand was analyzed. The FT-IR spectrum for this ligand indicated the presence of the two ether groups by a moderately intense band appearing at 1044.65 cm^{-1} (expected 1040 cm^{-1}).[287, 288] The presence of the carboxylic acid groups was also confirmed by the strong sharp single band located at 1697.51 cm^{-1}, exactly where an aromatic carboxylic acid should be found.

$[Cu_{24}(\mathbf{L5})_{12}(H_2O)_{16}(N,N'\text{-Dimethylformamide})_8]_n$, **[33]:** IR (dry powder) $\tilde{\upsilon}_{max}$ (cm^{-1}): 3400 v br (-OH, alcohol solvent), 2922 very small, sh. (-CH, aliphatic), 2852 very small, sh. (-CH, aliphatic), 1637 m sh. (COO^-, carboxylate), 1588 m sh. (C=O, carboxylate), 1379 v sh. (COO^-, carboxylate). The most notable changes between the IR spectrum for the ligand **L5** and compound [**33**] is the disappearance of the broad OH stretch due to the carboxylic acid that was centered around 3122 cm^{-1} and bleed into the 3000 cm^{-1} region. There are two very small, but sharp peaks at 2923 cm^{-1} and 2853 cm^{-1} which remained from the ligand IR spectrum and are due to the large presence of $–CH_2$ and $–CH_3$ groups. There is a strong sharp peak at 1014 cm^{-1} which is probably due to the presence of the ether group in the tetracarboxylic acid ligand. Additionally, we notice drastic shifts in frequency for the C=O stretches which is expected upon coordination of the carboxylate. (Appendix B-38)

$[Zn_{24}(\mathbf{L5})_{12}(H_2O)_{16}(N,N'\text{-Dimethylformamide})_8]_n$, **[34]:** IR (dry powder) $\tilde{\upsilon}_{max}$ (cm^{-1}): 2922 very small (-CH, aliphatic), 2852 very small (-CH, aliphatic), 1641 m sh. (COO^-, carboxylate), 1589 m sh. (C=O, carboxylate), 1379 v sh. (COO^-, carboxylate), 1053 m sh. (Ar-O-CH_2-, ether). The most notable changes between the IR spectrum for the ligand **L5** and compound [**34**] is the disappearance of the OH stretch due to the carboxylic acid that was centered around 3122 cm^{-1} and bleed into the 3000 cm^{-1} region as well as the two sharp peaks at 3535 cm^{-1} and 3451 cm^{-1} which arose from free acids. There are two very weak, but sharp peaks at 2922.81 cm^{-1} and 2852.29 cm^{-1} which remained from the ligand IR spectrum and are due to the presence of $–CH_2$ groups.

Additionally, we notice drastic shifts in frequency for the C=O stretches which is expected upon coordination of the carboxylate. (Appendix B-39)

4.4.4.5 Thermal Gravimetric Analysis

Thermal gravimetric analysis for Cu(II) cross-linked nanoballs, $[Cu_{24}(\mathbf{L5})_{12}(H_2O)_{16}(N,N'\text{-Dimethylformamide})_8]_n$, [**33**], was conducted on a T.A. Instruments 2950 TGA operating under the High Resolution Dynamic mode. The heating program was run from 30 °C up to 1000 °C and was performed under a flow of N_2 gas. The resulting data was graphed as a function of weight percent (wt. %) versus change in temperature. Upon acquisition the data was evaluated using T.A. Instruments Thermal Advantage suite of analyzing software.

Initial weight loss of 3.26 % at 42.34 °C was observed and interpreted to be loss of mother liquor still present on the crystalline sample. A small amount of further weight loss (1.43 %, 65 °C) was observed and thought to be low boiling guest molecules in the crystal lattice. The first major weight loss results in a broad, rolling weight loss which may be do the loss of several different types of molecules at roughly the same temperatures over a broad range. This represents 24% of the sample and most likely was due to the various types of coordinated solvent molecules (DMSO, H_2O, etc.) being removed over a large temperature range. (Appendix B-38)

Thermal Gravimetric Analysis for $[Zn_{24}(\mathbf{L5})_{12}(H_2O)_{16}(N,N'\text{-Dimethylformamide})_8]_n$ compound [**34**], the Zn(II) analogue of cross-linked nanoballs was performed on a PerkinElmer STA 6000 Simultaneous Thermal Analyzer. Data

acquisition and analysis was performed with the assistance of the Pyris Series suite of software. Roughly 10-20 mg of dry powder was placed in a sample crucible and heated at a rate of 10 °C/min. form a temperature of 30 °C up to 700 °C.

An immediate broad weight loss of ~ 3.7% for 30 °C until ~100 °C was taken to be the loss of mother liquor solvent still on the surface of the crystal and small amounts of interstitial solvent molecules from within the crystal structure. Over the temperature range of 100 °C to 180 °C, a weight loss of ~12.3 % was observed and is believed to be form solvent molecules trapped within the cavities of the framework, as well as some weaker bound solvent molecules (outside axially bound solvent molecules). At higher temperatures (~180 °C until 240 °C, ~240 °C until 370 °C) weight losses of ~10 % and ~7.5% were observed respectively and should be due to the loss of more tightly held solvent molecules, either trapped in the confines of the nanoballs or perhaps axially coordinated on the interior of the nanoballs or within the small interconnecting cages. After 370 °C, the sample decomposed. (Appendix B-39)

4.5 Conclusion

In summary, this chapter has attempted to emphasize the increased complexity of discrete metal-organic nanostructures based upon polyhedra, when compared to that of simple discrete polygons, 1-periodic architectures, and even most 2-periodic structures as 2-periodic tilings are often based upon some polyhedral form. The reason for this increased complexity is the nature of how the regular polygons which make up the polyhedra can come together to generate the overall superstructure. While generally not

as complicated as 3-periodic structures, they are still rather important structures to investigate. First and foremost they represent intriguingly beautiful structures that are fascinating on a purely aesthetic level. Second, being discrete nanoscale structures, they often have unique chemical and physical properties that can be exploited for the purpose of designing functional materials for specific applications. Finally, these nanoscale metal-organic polyhedra are essential to the investigation of MOMs in general due to the fact that many (if not all) of the more interesting 3-periodic structures can be interpreted as being constructed from polyhedral cages related to metal-organic polyhedra.

Three novel examples of nanoball derivatives— the 5-dodecyloxy, the 5-benzyloxy, and the 5-naphthylmethoxy— have been synthesized and structurally characterized. From this it is demonstrated how these materials are not only complex in the way that they are generated through modular self-assembly, but also in the fact there is often a potential for interesting packing of these nanospheres upon crystallization, a uniquely supramolecular phenomenon. For example the distorted diamondoid packing and concomitant threading of dodecyloxy chains into the interior of the dodecyloxy derivative of the nanoball, was a somewhat unexpected although completely reasonably result of the noncovalent forces at work (supramolecular chemistry) as these materials crystallize from solution.

Additionally, the close packing of the aryloxy derivatives of the nanoball, in a manner much more predictable than was the case for the dodecyloxy form, resulted in a plethora of simultaneous weak noncovalent forces in the form of CH•••π and π-π stacking interactions that effectively alter the observed properties for these materials. As discrete

architectures with the 24 aryloxy groups positioned around the periphery of the sphere, these nanoballs were expected to exhibit increased solubility in common aromatic organic solvents. Alas, as a result of the abundance of concerted weak noncovalent interactions, and the nature of the packing in general, these structures were, somewhat unpredictably, not soluble in any common laboratory solvent. This is a strong illustration of the effect supramolecular chemistry can have of the properties of molecular structures.

Finally, a new design strategy for the design and synthesis of extended metal-organic materials based upon the implementation of supermolecular building blocks (SBBs) was introduced. This concept is an extension of the use of SBUs in general, and is predicated upon the isolation of existing metal-organic polyhedra and then judiciously modifying these MOPs in a manner so as to facilitate their cross-linking into extended structures. The adoption of the SBB design strategy is practical for a number of reasons. The use of MOPs as nodes in extended MOMs will indubitably result in MOMs with enhanced scale. Additionally, SBBs can often be designed in such a way as to adopt unique geometries or coordination numbers not possible with single metal ions or SBUs. Perhaps most importantly, SBBs may provide crystal engineers with increased control of the design and synthesis of novel extended metal-organic materials.

.

Chapter 5

Conclusions and Future Directions

5.1 Summary and Conclusions

In this dissertation I have attempted to survey the field of metal-organic materials through a sampling of my own research. Classifications of what constitutes a metal-organic material were made. A brief history of the subject has been outlined, focusing upon the various design aspects which have been implemented throughout the years. Particular attention has been afforded to distinguishing between the several levels of complexity associated with various MOMs. In attempting to delineate this natural hierarchy of complexity, I have introduced several platforms of MOMs often related by their building components, but vastly different in their structural composition. Specifically, this dissertation has dealt with:

i.) Two different platforms of 2-periodic networks, the 4.8^2 *fes*-like structures which exhibit interdigitation between layers, and Kagomé lattice structures which can be layered controllably and are capable of demonstrating intriguing supramolecular interactions in the solid state.

ii.) The design strategy of pillaring has been exploited to fabricate 3-periodic materials with controllable dimensions and pore sizes. Additionally the concept of

pillaring has been expanded upon to include appropriately designed ligands capable of interconnecting layers though ligand-to-ligand or axial-to-ligand methods.

iii.) Novel examples of 0-periodic nanoscale structures in the form of aryloxy and alkyloxy derivatives of nanoballs were described along with some unique supramolecular chemistry associated with them. The ability of supramolecular chemistry to impact the observable properties of discrete structures was briefly explored.

iv.) Finally, the concept of supermolecular building blocks (SBBs) as a new design strategy for the fabrication of extended metal-organic materials was introduced through two 3-periodic structures self-assembled *via* covalently cross-linking apt nanoballs. The benefits and implications of this new design strategy were also briefly expounded upon.

To briefly summarize, the research presented within the confines of this dissertation deals with the design, synthesis, and characterization of several platforms of metal-organic materials (MOMs). These metal-organic materials represent a bourgeoning class of hybrid materials which are constructed *via* the coordinate covalent bond between metal ions and organic molecules with the capacity to behave as ligands; typically appropriate exo-functional N-donor or O-donor functional groups suffice. These hybrid materials are currently receiving an ever-expanding level of interest, largely due to their myriad of interesting physical and chemical properties and potential useful applications. However, neither the mere existence of intriguing properties nor any potential toward future applications can fully explain the affection a large (and growing) population of

crystal engineers have for these materials. I believe this to be a byproduct of the nature of these materials themselves; whereas many materials have in the past been looked upon with some interest and curiosity regarding their properties, for a large part it was done as spectator. A material was *observed* to have properties, and then those properties were classified, categorized, and catalogued away. To be sure, chemists and materials scientists have probably always made observations about classes of materials and then attempted to generalize. And just as likely these same chemist often desired to be able to extend those generalizations in a manner such that they could harness control over the materials' properties. In short the dream has been the same. What is new is our ability to go about reaching those goals.

Metal-organic materials, being particularly amenable to the principles of crystal engineering, represent a class of materials which not only beg for the active participation of the synthetic chemist in their *design*, they require it. It is wholly unsatisfactory to simply go about randomly making new materials and then hoping for a diamond in the rough in terms of their abilities.

5.2 Future Directions

The future of metal-organic materials is definitely bright. The amount of time and effort that goes into the study of MOMs is increasing (rapidly) every year. This is evidenced by the exponential growth in both the number of papers and the number of citations given to those papers. Hopefully this expansion can be sustained; and I believe it can. But for that to happen, I believe that the field must branch out so to speak. To be

sure there is already a great breadth of applications and uses of MOMs being investigated by the field. This merely needs to be continued, and supplemented, for the field to remain healthy and vibrant. Gone are the days when a new material can be fabricated and the potential properties or applications of it simply be speculated upon with no further action. And the days of making a material and merely recording its properties will soon come to an end as well. As a scientific field we have successfully demonstrated that metal-organic materials can have a truly lasting impact on our technological society. We have outlined numerous possibilities. It is now becoming time that we follow up on these possibilities, and so the next generation of metal-organic chemists will surely need to expound upon these ideas.

While some in the field may make reference to separate "generations" of MOMs based upon either a material's ability to accomplish some specific goal (i.e. porosity), or conversely upon the nature and the strength of the coordination bond involved in sustaining the framework, I find these demarcations to be somewhat arbitrary and overtly subjective. For what other purpose, than an attempt to segregate materials into classes of "proposed" usefulness—*these* materials are promising and worthy of adulation, while *those* materials lack any real function— can defining a material's level of sophistication be based on such narrow definitions of accomplishment? These artificial classifications are mistaken, I believe, for another reason. Generally, such defining of objects into groups is done in order to be beneficial in understanding these objects in some way. How does saying this material sorbs proficient amounts of gas or that material is made from

the *strongest* coordination bonds help other researchers in the field move forward? Where is the benefit?

Better, I would say, would be the classification of metal-organic materials on the natural hierarchy that occurs in the types of structural building units which are employed in their design and synthesis. At the very least this method has the benefit of following a loose, but nonetheless roughly linear timeline of when these materials were created; and the use of the word "generations" surely has connotations of order with respect to time. Additionally, using structural building units as a way of classifying MOMs is neutral to their properties and functions. It does not imply a material must meet some narrow criteria to be considered a significant advancement. A material made from single metal ion nodes may be just as promising (for some application anyway) as a material made from SBUs or SBBs.

I see good things in store for the field of metal-organic materials, especially if collectively as a group we can take an honest look forward at what these materials could potentially be of use for, and try to get away from constantly redefining what it is that we are working with.

References

1. Feynman, R. P. *Plenty of Room at the Bottom*. http://www.its.caltech.edu/~feynman/plenty.html (September 29, 2009).
2. Webb, R. *Symmetry: Culture and Science* **2000,** *11*(1-4), 231-268.
3. Webb, R. *Stella4D*, v4.4; Melbourne, Australia, **2008**. http://www.software3d.com/stella.html.
4. Thoreau, H. D., Journal Volume VIII. In *The Writings of Henry David Thoreau*, Torrey, B., Ed. Houghton Mifflin and Company: Boston, 1906; Vol. 14, pp 87-88.
5. Libbrecht, K. G. *SnowCrystals.com*. http://www.its.caltech.edu/~atomic/snowcrystals/ (August 15, 2009).
6. Bentley, W. A.; Humphreys, W. J., *Snow Crystals*. Dover Publicationhs, Inc.: New York, **1962**.
7. Kepler, J., A New Year's Gift or On the Six-Cornered Snowflake. In *The Six-Cornered Snowflake*, Whyte, L. L., Ed. Clarendon Press: Oxford, 1966.
8. Bloss, F. D., *Crystallography and Crystal Chemistry: an introduction*. Holt, Rinehart and Winston, Inc.: New York, **1971**.
9. Burke, J. G., *Origins of the Science of Crystals*. University of California Press: Berkeley, California, **1966**.

10. Bragg, L., *The Crystalline State*. Cornell University Press: Ithaca, New York, **1965**; Vol. 1.

11. Drexler, K. E., *Nanosystems: Molecular Machinery, Manufacturing, and Computation*. John Wiley & Sons, Inc.: New York, **1992**.

12. Lehn, J.-M., *Supramolecular Chemistry: Concepts and Perspectives*. VCH: Weinheim, **1995**.

13. Steed, J. W.; Turner, D. R.; Wallace, K. J., *Core Concepts in Supramolecular Chemistry and Nanochemistry*. John Wiley & Sons, Ltd.: Chichester, West Sussex, England, **2007**.

14. Steed, J. W.; Atwood, J. L., *Supramolecular Chemistry*. John Wiley & Sons, Ltd.: Chichester, West Sussex, England, **2000**.

15. Schneider, H.-J.; Yatsimirsky, A. K., *Principles and Methods in Supramolecular Chemistry*. John Wiley & Sons, Ltd.: Chichester, West Sussex, England, **2000**.

16. Ehrlich, P., *Studies on Immunity*. Wiley: New York, **1906**.

17. Fischer, E. *Ber. Deutsch Chem. Ges.* **1894,** *27*, 2985.

18. Pauling, L., *The Nature of The Chemical Bond*. 3rd ed.; Cornell University Press: Ithaca, New York, **1960**.

19. Moulton, B.; Zaworotko, M. J. *Chem. Rev.* **2001,** *101*(6), 1629-1658.

20. Hennigar, T. L.; MacQuarrie, D. C.; Losier, P.; Rogers, R. D.; Zaworotko, M. J. *Angew. Chem., Int. Ed.* **1997,** *36*(9), 972-973.

21. Desiraju, G. R., *Crystal Engineering: The Design of Organic Solids*. Elsevier: Amsterdam, **1989**.

22. Schmidt, G. M. J. *Pure Appl. Chem.* **1971,** *27*, 647-678.

23. Seddon, K. R.; Zaworotko, M. J., *Crystal Engineering: The Design and Application of Functional Solids*. NATO ASI Series C: Mathematical and Physical Sciences, *vol. 539*, Kluwer Academic Publishers: Dordrecht, **1999**.

24. Desiraju, G. R. *Journal of Molecular Structure* **2003,** *656*(1-3), 5-15.

25. Pepinsky, R. *Phys. Rev.* **1955,** *100*, 971.

26. Desiraju, G. R. *Angew.Chem., Int. Ed.* **2007,** *46*(44), 8342-8356.

27. Desiraju, G. R. *Chem. Commun.* **2005,** (24), 2995-3001.

28. Desiraju, G. R. *J. Molec. Struct.* **2003,** *656*(1-3), 5-15.

29. Desiraju, G. R. *Acc. Chem. Res.* **2002,** *35*(7), 565-573.

30. Desiraju, G. R.; Steiner, T., *The Weak Hydrogen Bond In Structural Chemistry and Biology*. Oxford University Press: Oxford, **1999**.

31. Nangia, A.; Desiraju, G. R. *Design of Organic Solids* **1998,** *198*, 57-95.

32. Braga, D.; Grepioni, F.; Desiraju, G. R. *Chem. Rev.* **1998,** *98*(4), 1375-1405.

33. Desiraju, G. R. *Chem. Commun.* **1997,** (16), 1475-1482.

34. Thalladi, V. R.; Goud, B. S.; Hoy, V. J.; Allen, F. H.; Howard, J. A. K.; Desiraju, G. R. *Chem. Commun.* **1996,** (3), 401-402.

35. Desiraju, G. R. *Angew.Chem., Int. Ed.* **1995,** *34*(21), 2311-2327.

36. Desiraju, G. R. *Acc. Chem. Res.* **1991,** *24*(10), 290-296.

37. Desiraju, G. R. *J. Chem. Soc., Chem. Commun.* **1990,** (6), 454-455.

38. Desiraju, G. R.; Parthasarathy, R. *J. Am. Chem. Soc.* **1989,** *111*(23), 8725-8726.

39. Sarma, J.; Desiraju, G. R. *Acc. Chem. Res.* **1986,** *19*(7), 222-228.

40. Theocharis, C. R.; Desiraju, G. R.; Jones, W. *J. Am. Chem. Soc.* **1984,** *106*(12), 3606-3609.

41. Sarma, J.; Desiraju, G. R. *J. Chem. Soc., Chem. Commun.* **1984,** (3), 145-147.

42. Desiraju, G. R.; Sarma, J. *J. Chem. Soc., Chem. Commun.* **1983,** (1), 45-46.

43. Etter, M. C.; Reutzel, S. M. *J. Am. Chem. Soc.* **1991,** *113*(7), 2586-2598.

44. Etter, M. C. *J. Phys. Chem.* **1991,** *95*(12), 4601-4610.

45. Etter, M. C.; Urbanczyklipkowska, Z.; Ziaebrahimi, M.; Panunto, T. W. *J. Am. Chem. Soc.* **1990,** *112*(23), 8415-8426.

46. Etter, M. C.; Macdonald, J. C.; Bernstein, J. *Acta Crystallogr.* **1990,** *B46*(2), 256-262.

47. Etter, M. C.; Adsmond, D. A. *J. Chem. Soc., Chem. Commun.* **1990,** (8), 589-591.

48. Etter, M. C. *Acc. Chem. Res.* **1990,** *23*(4), 120-126.

49. Bernstein, J.; Etter, M. C.; Macdonald, J. C. *J. Chem. Soc., Perkin Trans. 2* **1990,** (5), 695-698.

50. Etter, M. C.; Baures, P. W. *J. Am. Chem. Soc.* **1988,** *110*(2), 639-640.

51. Panunto, T. W.; Urbanczyklipkowska, Z.; Johnson, R.; Etter, M. C. *J. Am. Chem. Soc.* **1987,** *109*(25), 7786-7797.

52. Etter, M. C.; Urbanczyklipkowska, Z.; Jahn, D. A.; Frye, J. S. *J. Am. Chem. Soc.* **1986,** *108*(19), 5871-5876.

53. *Inorganic Crystal Structure Database*. http://icsd.fiz-karlsruhe.de/icsd/ (September 19, 2009).

54. Chen, B. L.; Ockwig, N. W.; Fronczek, F. R.; Contreras, D. S.; Yaghi, O. M. *Inorg. Chem.* **2005,** *44*(2), 181-183.

55. *Nucleic Acid Database*. http://ndbserver.rutgers.edu/ (September 19, 2009).

56. *International Centre for Diffraction Data*. http://www.icdd.com/ (September 19, 2009).

57. Allen, F. H. *Acta Crystallogr.* **2002,** *B58*, 380-388.

58. *Cambridge Structural Database*. http://www.ccdc.cam.ac.uk/products/csd/ (September, 10 2009).

59. Hall, S. R.; Allen, F. H.; Brown, I. D. *Acta Crystallogr.* **1991,** *A47*(6), 655-685.

60. *International Union for Crystallography*. http://www.iucr.org/ (September 11, 2009).

61. Hall, S. R.; Allen, F. H.; Brown, I. D. *Acta Crystallogr.* **1991,** *A47*(6), 637-639.

62. Dunitz, J. D.; Gavezzotti, A. *Chem. Soc. Rev.* **2009,** *38*(9), 2622-2633.

63. Robson, R. *Dalton Trans.* **2008,** (38), 5113-5131.

64. Dunitz, J. D.; Gavezzotti, A. *Cryst. Growth Des.* **2005,** *5*(6), 2180-2189.

65. Gavezzotti, A. *CrystCngComm* **2003,** *5*, 439-446.

66. Motherwell, W. D. S.; Ammon, H. L.; Dunitz, J. D.; Dzyabchenko, A.; Erk, P.; Gavezzotti, A.; Hofmann, D. W. M.; Leusen, F. J. J.; Lommerse, J. P. M.; Mooij, W. T. M.; Price, S. L.; Scheraga, H.; Schweizer, B.; Schmidt, M. U.; van Eijck, B. P.; Verwer, P.; Williams, D. E. *Acta Crystallogr.* **2002,** *B58*, 647-661.

67. Lommerse, J. P. M.; Motherwell, W. D. S.; Ammon, H. L.; Dunitz, J. D.; Gavezzotti, A.; Hofmann, D. W. M.; Leusen, F. J. J.; Mooij, W. T. M.; Price, S.

L.; Schweizer, B.; Schmidt, M. U.; van Eijck, B. P.; Verwer, P.; Williams, D. E. *Acta Crystallogr.* **2000,** *B56*, 697-714.

68. Gavezzotti, A.; Filippini, G. *J. Am. Chem. Soc.* **1996,** *118*(30), 7153-7157.

69. Gavezzotti, A. *J. Am. Chem. Soc.* **1991,** *113*(12), 4622-4629.

70. Desiraju, G. R.; Gavezzotti, A. *Acta Crystallogr.* **1989,** *B45*, 473-482.

71. Bryant, J. A., JR., *The Tragedy of Romeo and Juliet*. The Signet Classic Shakespeare Signet Classic: New York, **1990**; pp 75.

72. Rayner, J. H.; Powell, H. M. *J. Chem. Soc.* **1952**, 319-328.

73. Baur, R.; Schwarzenbach, G. *Helv. Chim. Acta.* **1960,** *43*(3), 842-847.

74. Krishnamurty, K. V.; Harris, G. M. *Chem. Rev.* **1961,** *61*(3), 213-246.

75. Griffin, W. P. *Q. Rev. Chem. Soc.* **1962,** *16*(2), 188-207.

76. Billard, R. D.; Wilkinson, G. *J. Chem. Soc.* **1963**, 3193-3200.

77. Biondi, C.; Bonamico, M.; Torelli, L.; Vaciago, A. *Chem. Commun.* **1965,** (10), 191-192.

78. Tomic, E. A. *J. Appl. Polym. Sci.* **1965,** *9*(11), 3745-3752.

79. Walton, R. A. *Q. Rev. Chem. Soc.* **1965,** *19*(2), 126-143.

80. Krishnamurty, K. V.; Harris, G. M. L.; Sastri, V. S. *Chem. Rev.* **1970,** *70*(2), 171-197.

81. Iwamoto, T.; Kiyoki, M.; Ohtsu, Y.; Takeshigekato, Y. *Bull. Chem. Soc. Jpn.* **1978,** *51*(2), 488-491.

82. Nishikiori, S. I.; Iwamoto, T.; Yoshino, Y. *Bull. Chem. Soc. Jpn.* **1980,** *53*(8), 2236-2240.

83. Underhill, A. E.; Watkins, D. M. *Q. Rev. Chem. Soc.* **1980,** *9*(4), 429-448.

84. Iwamoto, T.; Nakano, T.; Morita, M.; Miyoshi, T.; Miyamoto, T.; Sasaki, Y. *Inorg. Chim. Acta* **1986,** *2*, 313-316.

85. Kitazawa, T.; Nishikiori, S.; Kuroda, R.; Iwamoto, T. *Chem. Lett.* **1988,** *17*(10), 1729-1732.

86. Hoskins, B. F.; Robson, R. *J. Am. Chem. Soc.* **1989,** *111*(15), 5962-5964.

87. Abrahams, B. F.; Hoskins, B. F.; Robson, R. *J. Chem. Soc., Chem. Commun.* **1990,** (1), 60-61.

88. Gable, R. W.; Hoskins, B. F.; Robson, R. *J. Chem. Soc., Chem. Commun.* **1990,** (10), 762-763.

89. Gable, R. W.; Hoskins, B. F.; Robson, R. *J. Chem. Soc., Chem. Commun.* **1990,** (23), 1677-1678.

90. Hoskins, B. F.; Robson, R. *J. Am. Chem. Soc.* **1990,** *112*(4), 1546-1554.

91. Abrahams, B. F.; Hoskins, B. F.; Liu, J. P.; Robson, R. *J. Am. Chem. Soc.* **1991,** *113*(8), 3045-3051.

92. Abrahams, B. F.; Hoskins, B. F.; Robson, R. *J. Am. Chem. Soc.* **1991,** *113*(9), 3606-3607.

93. Batten, S. R.; Hoskins, B. F.; Robson, R. *J. Chem. Soc., Chem.Commun.* **1991,** (6), 445-447.

94. Abrahams, B. F.; Hardie, M. J.; Hoskins, B. F.; Robson, R.; Williams, G. A. *J. Am. Chem. Soc.* **1992,** *114*(26), 10641-10643.

95. Abrahams, B. F.; Hardie, M. J.; Hoskins, B. F.; Robson, R.; Sutherland, E. E. *J. Chem. Soc., Chem. Commun.* **1994,** (9), 1049-1050.

96. Hoskins, B. F.; Robson, R.; Scarlett, N. V. Y. *J. Chem. Soc., Chem. Commun.* **1994,** (18), 2025-2026.

97. Batten, S. R.; Hoskins, B. F.; Robson, R. *J. Am. Chem. Soc.* **1995,** *117*(19), 5385-5386.

98. Robinson, F.; Zaworotko, M. J. *J. Chem. Soc., Chem.Commun.* **1995,** (23), 2413-2414.

99. Fujita, M.; Kwon, Y. J.; Miyazawa, M.; Ogura, K. *J. Chem. Soc., Chem. Commun.* **1994,** (17), 1977-1978.

100. Fujita, M.; Kwon, Y. J.; Washizu, S.; Ogura, K. *J. Am. Chem. Soc.* **1994,** *116*(3), 1151-1152.

101. Fujita, M.; Sasaki, O.; Watanabe, K. Y.; Ogura, K.; Yamaguchi, K. *New J. Chem.* **1998,** *22*(2), 189-191.

102. Biradha, K.; Fujita, M. *J. Chem. Soc., Dalton Trans.* **2000,** (21), 3805-3810.

103. Biradha, K.; Hongo, Y.; Fujita, M. *Angew. Chem., Int. Ed.* **2000,** *39*(21), 3843-3845.

104. Umemoto, K.; Tsukui, H.; Kusukawa, T.; Biradha, K.; Fujita, M. *Angew. Chem., Int. Ed.* **2001,** *40*(14), 2620-2622.

105. Kitagawa, S.; Matsuyama, S.; Munakata, M.; Emori, T. *J. Chem. Soc., Dalton Trans.* **1991,** (11), 2869-2874.

106. Kitagawa, S.; Munakata, M.; Tanimura, T. *Inorg. Chem.* **1992,** *31*(9), 1714-1717.

107. Kitagawa, S.; Kawata, S.; Nozaka, Y.; Munakata, M. *J. Chem. Soc., Dalton Trans.* **1993,** (9), 1399-1404.

108. Kawata, S.; Kitagawa, S.; Kondo, M.; Furuchi, I.; Munakata, M. *Angew. Chem., Int. Ed.* **1994,** *33*(17), 1759-1761.

109. Kondo, M.; Yoshitomi, T.; Seki, K.; Matsuzaka, H.; Kitagawa, S. *Angew. Chem.,. Int. Ed.* **1997,** *36*(16), 1725-1727.

110. Kondo, M.; Okubo, T.; Asami, A.; Noro, S.; Yoshitomi, T.; Kitagawa, S.; Ishii, T.; Matsuzaka, H.; Seki, K. *Angew. Chem., Int. Ed.* **1999,** *38*(1-2), 140-143.

111. Kondo, M.; Shimamura, M.; Noro, S.; Yoshitomi, T.; Minakoshi, S.; Kitagawa, S. *Chem. Lett.* **1999,** (4), 285-286.

112. Noro, S.; Kondo, M.; Ishii, T.; Kitagawa, S.; Matsuzaka, H. *J. Chem. Soc., Dalton Trans.* **1999,** (10), 1569-1574.

113. Noro, S.; Kondo, M.; Kitagawa, S.; Ishii, T.; Matsuzaka, H. *Chem. Lett.* **1999,** (8), 727-728.

114. Macgillivray, L. R.; Subramanian, S.; Zaworotko, M. J. *J. Chem. Soc., Chem. Commun.* **1994,** (11), 1325-1326.

115. Zaworotko, M. J. *Chem. Soc. Rev.* **1994,** *23*(4), 283-288.

116. Carlucci, L.; Ciani, G.; Proserpio, D. M.; Sironi, A. *Angew. Chem., Int. Ed.* **1995,** *34*(17), 1895-1898.

117. Carlucci, L.; Ciani, G.; Proserpio, D. M.; Sironi, A. *J. Am. Chem. Soc.* **1995,** *117*(16), 4562-4569.

118. Carlucci, L.; Ciani, G.; Proserpio, D. M.; Sironi, A. *Inorg. Chem.* **1995,** *34*(22), 5698-5700.

119. Carlucci, L.; Ciani, G.; Proserpio, D. M.; Sironi, A. *J. Am. Chem. Soc.* **1995,** *117*(51), 12861-12862.

120. Subramanian, S.; Zaworotko, M. J. *Angew. Chem., Int. Ed.* **1995,** *34*(19), 2127-2129.

121. Blake, A. J.; Champness, N. R.; Chung, S. S. M.; Li, W. S.; Schroder, M. *Chem. Commun.* **1997,** (17), 1675-1676.

122. Blake, A. J.; Champness, N. R.; Chung, S. S. M.; Li, W. S.; Schroder, M. *Chem. Commun.* **1997,** (11), 1005-1006.

123. Blake, A. J.; Champness, N. R.; Khlobystov, A.; Lemenovskii, D. A.; Li, W. S.; Schroder, M. *Chem. Commun.* **1997,** (21), 2027-2028.

124. Carlucci, L.; Ciani, G.; Proserpio, D. M.; Sironi, A. *Inorg. Chem.* **1997,** *36*(9), 1736-1737.

125. Carlucci, L.; Ciani, G.; vonGudenberg, D. W.; Proserpio, D. M.; Sironi, A. *Chem. Commun.* **1997,** (6), 631-632.

126. Moulton, B.; Zaworotko, M. J. *Curr. Opin. Solid State Mater. Sci.* **2002,** *6*(2), 117-123.

127. Spokoyny, A. M.; Kim, D.; Sumrein, A.; Mirkin, C. A. *Chem. Soc. Rev.* **2009,** *38*(5), 1218-1227.

128. O'Keeffe, M. *Chem. Soc. Rev.* **2009,** *38*(5), 1215-1217.

129. Long, J. R.; Yaghi, O. M. *Chem. Soc. Rev.* **2009,** *38*(5), 1213-1214.

130. Volkringer, C.; Meddouri, M.; Loiseau, T.; Guillou, N.; Marrot, J.; Ferey, G.; Haouas, M.; Taulelle, F.; Audebrand, N.; Latroche, M. *Inorg. Chem.* **2008,** *47*(24), 11892-11901.

131. Larsen, R. W.; McManus, G. J.; Perry, J. J.; Rivera-Otero, E.; Zaworotko, M. J. *Inorg. Chem.* **2007,** *46*(15), 5904-5910.

132. Robin, A. Y.; Fromm, K. M. *Coord. Chem. Rev.* **2006,** *250*(15-16), 2127-2157.

133. Cheetham, A. K.; Rao, C. N. R.; Feller, R. K. *Chem. Commun.* **2006,** (46), 4780-4795.

134. Biradha, K.; Sarkar, M.; Rajput, L. *Chem. Commun.* **2006,** (40), 4169-4179.

135. Shimizu, G. K. H. *J. Solid State Chem.* **2005,** *178*(8), 2519-2526.

136. Rosseinsky, M. J. *Micropor. Mesopor. Mater.* **2004,** *73*(1-2), 15-30.

137. James, S. L. *Chem. Soc. Rev.* **2003,** *32*(5), 276-288.

138. Rosi, N. L.; Eddaoudi, M.; Kim, J.; O'Keeffe, M.; Yaghi, O. M. *CrystEngComm* **2002,** *4*(68), 401-404.

139. Batten, S. R. *Curr. Opin. Solid State Mater. Sci.* **2001,** *5*(2-3), 107-114.

140. Zaworotko, M. J. *Nature Chemistry* **2009,** *1*(4), 267-268.

141. *ISI Web of Science*. http://apps.isiknowledge.com/UA_GeneralSearch_input.do?product=UA&search_mode=GeneralSearch&SID=1BBcKA83icpCFEAbkKA&preferencesSaved= (August 2009).

142. Wells, A. F. *Acta Crystallogr.* **1954,** *7*(8-9), 535-544.

143. Wells, A. F. *Acta Crystallogr.* **1954,** *7*(8-9), 545-554.

144. Wells, A. F. *Acta Crystallogr.* **1954,** *7*(12), 842-848.

145. Wells, A. F. *Acta Crystallogr.* **1954,** *7*(12), 849-853.

146. Wells, A. F. *Acta Crystallogr.* **1955,** *8*(1), 32-36.

147. Wells, A. F. *Acta Crystallogr.* **1956,** *9*(1), 23-28.

148. Wells, A. F.; Sharpe, R. R. *Acta Crystallogr.* **1963,** *16*(9), 857-871.

149. Wells, A. F., *Three-Dimensional Nets and Polyhedra*. John Wiley & Sons: New York, **1977**.

150. Tranchemontagne, D. J.; Mendoza-Cortes, J. L.; O'Keeffe, M.; Yaghi, O. M. *Chem. Soc. Rev.* **2009,** *38*(5), 1257-1283.

151. Kim, J.; Chen, B. L.; Reineke, T. M.; Li, H. L.; Eddaoudi, M.; Moler, D. B.; O'Keeffe, M.; Yaghi, O. M. *J. Am. Chem. Soc.* **2001,** *123*(34), 8239-8247.

152. Eddaoudi, M.; Moler, D. B.; Li, H. L.; Chen, B. L.; Reineke, T. M.; O'Keeffe, M.; Yaghi, O. M. *Acc. Chem. Res.* **2001,** *34*(4), 319-330.

153. Li, H.; Eddaoudi, M.; O'Keeffe, M.; Yaghi, O. M. *Nature* **1999,** *402*(6759), 276-279.

154. Baerlocher, C.; McCusker, L. B. *Database of Zeolite Structures*. http://www.iza-structure.org/databases/ (August 12, 2009).

155. Knight, C. T. G. *Zeolites* **1990,** *10*(2), 140-144.

156. Meier, W. M.; Olson, D. H.; Baerlocher, C., *Atlas of Zeolite Strucutre Types*. 5th ed.; Elsevier Science B.V.: Amsterdam, The Netherlands, **2001**.

157. Al-Rasbi, N. K.; Tidmarsh, I. S.; Argent, S. P.; Adams, H.; Harding, L. P.; Ward, M. D. *J. Am. Chem. Soc.* **2008,** *130*(35), 11641-11649.

158. Yoshizawa, M.; Nagao, M.; Umemoto, K.; Biradha, K.; Fujita, M.; Sakamoto, S.; Yamaguchi, K. *Chem. Commun.* **2003,** (15), 1808-1809.

159. Chand, D. K.; Fujita, M.; Biradha, K.; Sakamoto, S.; Yamaguchi, K. *Dalton Trans.* **2003,** (13), 2750-2756.

160. Chand, D. K.; Biradha, K.; Fujita, M.; Sakamoto, S.; Yamaguchi, K. *Chem. Commun.* **2002,** (21), 2486-2487.

161. Yamanoi, Y.; Sakamoto, Y.; Kusukawa, T.; Fujita, M.; Sakamoto, S.; Yamaguchi, K. *J. Am. Chem. Soc.* **2001,** *123*(5), 980-981.

162. Fujita, M.; Umemoto, K.; Yoshizawa, M.; Fujita, N.; Kusukawa, T.; Biradha, K. *Chem. Commun.* **2001,** (6), 509-518.

163. Umemoto, K.; Yamaguchi, K.; Fujita, M. *J. Am. Chem. Soc.* **2000,** *122*(29), 7150-7151.

164. Fujita, M., Molecular Paneling through metal-directed self-assembly. In *Molecular Self-Assembly: Organic Versus Inorganic Approaches*, Fujita, M., Ed. Springer: Berlin, 2000; Vol. 96, pp 177-201.

165. Blatov, V. A. *Acta Crystallogr.* **2007,** *A63*(4), 329-343.

166. Delgado-Friedrichs, O.; O'Keeffe, M.; Yaghi, O. M. *Acta Crystallogr.* **2006,** *A62*(5), 350-355.

167. Blatov, V. A.; Proserpio, D. M. *Acta Crystallogr.* **2009,** *A65*(3), 202-212.

168. Delgado-Friedrichs, O.; O'Keeffe, M. *J. Solid State Chem.* **2005,** *178*(8), 2480-2485.

169. Delgado-Friedrichs, O.; O'Keeffe, M.; Yaghi, O. M. *Phys. Chem. Chem. Phys.* **2007,** *9*(9), 1035-1043.

170. O'Keeffe, M.; Hyde, B. G., *Crystal Structures: I. Patterns and Symmetry*. Mineralogical Society of America: Washington, D.C., **1996**.

171. Grunbaum, B.; Shephard, G. C., *Tilings and Patterns*. W. H. Freeman and Company: New York, **1987**.

172. Blatov, V. A.; Delgado-Friedrichs, O.; O'Keeffe, M.; Proserpio, D. M. *Acta Crystallogr.* **2007,** *A63*(5), 418-425.

173. Frondel, C.; Marvin, U. B. *Nature* **1967,** *214*(5088), 587-589.

174. O'Keeffe, M.; Peskov, M. A.; Ramsden, S. J.; Yaghi, O. M. *Acc. Chem. Res.* **2008,** *41*(12), 1782-1789.

175. *Reticular Chemistry Structure Resource*. http://rcsr.anu.edu.au/ (September 2, 2009).

176. Delgado-Friedrichs, O. *The Gavrog Project*. http://gavrog.sourceforge.net/ (August 10, 2009).

177. Barton, T. J.; Bull, L. M.; Klemperer, W. G.; Loy, D. A.; McEnaney, B.; Misono, M.; Monson, P. A.; Pez, G.; Scherer, G. W.; Vartuli, J. C.; Yaghi, O. M. *Chem. Mater.* **1999,** *11*(10), 2633-2656.

178. Rouquerol, F.; Rouquerol, J.; Sing, K., *Adsorption by Powders and Porous Solids*. Academic Press: London, **1999**.

179. Eddaoudi, M.; Li, H. L.; Yaghi, O. M. *J. Am. Chem. Soc.* **2000,** *122*(7), 1391-1397.

180. Eddaoudi, M.; Kim, J.; Rosi, N.; Vodak, D.; Wachter, J.; O'Keeffe, M.; Yaghi, O. M. *Science* **2002,** *295*(5554), 469-472.

181. Rowsell, J. L. C.; Yaghi, O. M. *Micropor. Mesopor. Mater.* **2004,** *73*(1-2), 3-14.

182. Fletcher, A. J.; Thomas, K. M.; Rosseinsky, M. J. *J. Solid State Chem.* **2005,** *178*(8), 2491-2510.

183. Collins, D. J.; Zhou, H.-C. *J. Mater. Chem.* **2007,** *17*(30), 3154-3160.

184. Maji, T. K.; Kitagawa, S. *Pure Appl. Chem.* **2007,** *79*(12), 2155-2177.

185. Furukawa, H.; Yaghi, O. M. *J. Am. Chem. Soc.* **2009,** *131*(25), 8875-8883.

186. Duren, T.; Bae, Y. S.; Snurr, R. Q. *Chem. Soc. Rev.* **2009,** *38*(5), 1237-1247.

187. Thomas, K. M. *Dalton Trans.* **2009,** (9), 1487-1505.

188. Murray, L. J.; Dinca, M.; Long, J. R. *Chem. Soc. Rev.* **2009,** *38*(5), 1294-1314.

189. Han, S. S.; Mendoza-Cortes, J. L.; Goddard, W. A. *Chem. Soc. Rev.* **2009,** *38*(5), 1460-1476.

190. Zhao, D.; Yuan, D. Q.; Zhou, H. C. *Energy Environ. Sci.* **2008,** *1*(2), 222-235.

191. Ferey, G. *Chem. Soc. Rev.* **2008,** *37*(1), 191-214.

192. Dinca, M.; Long, J. R. *Angew. Chem., Int. Ed.* **2008,** *47*(36), 6766-6779.

193. Lin, X.; Jia, J. H.; Hubberstey, P.; Schroder, M.; Champness, N. R. *CrystEngComm* **2007,** *9*(6), 438-448.

194. Collins, D. J.; Zhou, H. C. *J. Mater. Chem.* **2007,** *17*(30), 3154-3160.

195. Dinca, M.; Yu, A. F.; Long, J. R. *J. Am. Chem. Soc.* **2006,** *128*(27), 8904-8913.

196. Rowsell, J. L. C.; Yaghi, O. M. *Angew. Chem., Int. Ed.* **2005,** *44*(30), 4670-4679.

197. Fletcher, A. J.; Thomas, K. M.; Rosseinsky, M. J. *J. Solid State Chem.* **2005,** *178*(8), 2491-2510.

198. Yaghi, O. M.; O'Keeffe, M.; Ockwig, N. W.; Chae, H. K.; Eddaoudi, M.; Kim, J. *Nature* **2003,** *423*(6941), 705-714.

199. *U.S. Department of Energy: Multi-Year Research, Development and Demonstration Plan: Planned Program Activities for 2005-2015*. http://www1.eere.energy.gov/hydrogenandfuelcells/mypp/ (August, 2009).

200. Kurmoo, M. *Chem. Soc. Rev.* **2009,** *38*(5), 1353-1379.

201. Pardo, E.; Ruiz-Garcia, R.; Cano, J.; Ottenwaelder, X.; Lescouezec, R.; Journaux, Y.; Lloret, F.; Julve, M. *Dalton Trans.* **2008,** (21), 2780-2805.

202. Miller, J. S. *Dalton Trans.* **2006,** (23), 2742-2749.

203. Real, J. A.; Gaspar, A. B.; Munoz, M. C. *Dalton Trans.* **2005,** (12), 2062-2079.

204. Murray, K. S.; Kepert, C. J., Cooperativity in spin crossover systems: Memory, magnetism and microporosity. In *Spin Crossover in Transition Metal Compounds I*, Springer-Verlag: Berlin, 2004; Vol. 233, pp 195-228.

205. Maspoch, D.; Ruiz-Molina, D.; Veciana, J. *J. Mater. Chem.* **2004,** *14*(18), 2713-2723.

206. Maspoch, D.; Ruiz-Molina, D.; Wurst, K.; Domingo, N.; Cavallini, M.; Biscarini, F.; Tejada, J.; Rovira, C.; Veciana, J. *Nature Mater.* **2003,** *2*(3), 190-195.

207. Ferey, G. *Nature Mater.* **2003,** *2*(3), 136-137.

208. Batten, S. R.; Murray, K. S. *Coord. Chem. Rev.* **2003,** *246*(1-2), 103-130.

209. Batten, S. R.; Jensen, P.; Moubaraki, B.; Murray, K. S.; Robson, R. *Chem. Commun.* **1998,** (3), 439-440.

210. Shultz, A. M.; Farha, O. K.; Hupp, J. T.; Nguyen, S. T. *J. Am. Chem. Soc.* **2009,** *131*(12), 4204-4205.

211. Marat, K. *SpinWorks*, v3.1; University of Manitoba: Winnipeg, Manitoba, Canada, **2009**.

212. Lee, J.; Farha, O. K.; Roberts, J.; Scheidt, K. A.; Nguyen, S. T.; Hupp, J. T. *Chem. Soc. Rev.* **2009,** *38*(5), 1450-1459.

213. Hong, D. Y.; Hwang, Y. K.; Serre, C.; Ferey, G.; Chang, J. S. *Adv. Funct. Mater.* **2009,** *19*(10), 1537-1552.

214. Maspoch, D.; Ruiz-Molina, D.; Veciana, J. *Chem. Soc. Rev.* **2007,** *36*(5), 770-818.

215. Hasegawa, S.; Horike, S.; Matsuda, R.; Furukawa, S.; Mochizuki, K.; Kinoshita, Y.; Kitagawa, S. *J. Am. Chem. Soc.* **2007,** *129*(9), 2607-2614.

216. Dybtsev, D. N.; Nuzhdin, A. L.; Chun, H.; Bryliakov, K. P.; Talsi, E. P.; Fedin, V. P.; Kim, K. *Angew. Chem., Int. Ed.* **2006,** *45*(6), 916-920.

217. Cho, S. H.; Ma, B. Q.; Nguyen, S. T.; Hupp, J. T.; Albrecht-Schmitt, T. E. *Chem. Commun.* **2006,** (24), 2563-2565.

218. Wu, C. D.; Hu, A.; Zhang, L.; Lin, W. B. *J. Am. Chem. Soc.* **2005,** *127*(25), 8940-8941.

219. Forster, P. M.; Cheetham, A. K. *Top. Catalysis* **2003,** *24*(1-4), 79-86.

220. Evans, O. R.; Manke, D. R.; Lin, W. B. *Chem. Mater.* **2002,** *14*(9), 3866-3874.

221. Seo, J. S.; Whang, D.; Lee, H.; Jun, S. I.; Oh, J.; Jeon, Y. J.; Kim, K. *Nature* **2000,** *404*(6781), 982-986.

222. Alkordi, M. H.; Liu, Y.; Larsen, R. W.; Eubank, J. F.; Eddaoudi, M. *J. Am. Chem. Soc.* **2008,** *130*(38), 12639-12641.

223. Ingleson, M. J.; Barrio, J. P.; Basca, J.; Dickinson, C.; Park, H.; Rosseinsky, M. J. *Chem. Commun.* **2008,** (11), 1287-1289.

224. Allendorf, M. D.; Bauer, C. A.; Bhakta, R. K.; Houk, R. J. T. *Chem. Soc. Rev.* **2009,** *38*(5), 1330-1352.

225. McManus, G. J.; Perry, J. J.; Perry, M.; Wagner, B. D.; Zaworotko, M. J. *J. Am. Chem. Soc.* **2007,** *129*(29), 9094-9101.

226. Chen, B. L.; Yang, Y.; Zapata, F.; Lin, G. N.; Qian, G. D.; Lobkovsky, E. B. *Adv. Mater.* **2007,** *19*(13), 1693-1696.

227. Cahill, C. L.; de Lill, D. T.; Frisch, M. *CrystEngComm* **2007,** *9*(1), 15-26.

228. Hill, R. J.; Long, D. L.; Hubberstey, P.; Schroder, M.; Champness, N. R. *J. Solid State Chem.* **2005,** *178*(8), 2414-2419.

229. Bose, D.; Rahaman, S. H.; Mostafa, G.; Walsh, R. D. B.; Zaworotko, M. J.; Ghosh, B. K. *Polyhedron* **2004,** *23*(4), 545-552.

230. Bose, D.; Banerjee, J.; Rahaman, S. H.; Mostafa, G.; Fun, H. K.; Walsh, R. D. B.; Zaworotko, M. J.; Ghosh, B. K. *Polyhedron* **2004,** *23*(12), 2045-2053.

231. Wagner, B. D.; McManus, G. J.; Moulton, B.; Zaworotko, M. J. *Chem. Commun.* **2002,** (18), 2176-2177.

232. Reineke, T. M.; Eddaoudi, M.; Fehr, M.; Kelley, D.; Yaghi, O. M. *J. Am. Chem. Soc.* **1999,** *121*(8), 1651-1657.

233. Birks, J. B., *Photophysics of Aromatic Molecules*. Wiley-Interscience: London, **1970**.

234. Li, J. R.; Kuppler, R. J.; Zhou, H. C. *Chem. Soc. Rev.* **2009,** *38*(5), 1477-1504.

235. Ferey, G.; Serre, C. *Chem. Soc. Rev.* **2009,** *38*(5), 1380-1399.

236. Allendorf, M. D.; Houk, R. J. T.; Andruszkiewicz, L.; Talin, A. A.; Pikarsky, J.; Choudhury, A.; Gall, K. A.; Hesketh, P. J. *J. Am. Chem. Soc.* **2008,** *130*(44), 14404-14405.

237. Yaghi, O. M.; Davis, C. E.; Li, G. M.; Li, H. L. *J. Am. Chem. Soc.* **1997,** *119*(12), 2861-2868.

238. Czaja, A. U.; Trukhan, N.; Muller, U. *Chem. Soc. Rev.* **2009,** *38*(5), 1284-1293.

239. Liu, Y.; Li, G.; Li, X.; Cui, Y. *Angew. Chem., Int. Ed.* **2007,** *46*(33), 6301-6304.

240. Maury, O.; Le Bozec, H. *Acc. Chem. Res.* **2005,** *38*(9), 691-704.

241. Evans, O. R.; Lin, W. B. *Acc. Chem. Res.* **2002,** *35*(7), 511-522.

242. Lacroix, P. G. *Eur. J. Inorg. Chem.* **2001,** (2), 339-348.

243. Zhang, H.; Wang, X. M.; Zhang, K. C.; Teo, B. K. *Coord. Chem. Rev.* **1999,** *183*(1), 157-195.

244. Struve, W. S., *Fundamentals of Molecular Spectroscopy*. John Wiley & Sons: New York, **1989**.

245. Steinfeld, J. I., *Molecules and Radiation: An Introduction to Modern Molecular Spectroscopy*. 2nd ed.; The MIT Press: Cambridge, Massachusetts, **1985**.

246. Maji, T. K.; Kitagawa, S. *Pure Appl. Chem.* **2007,** *79*(12), 2155-2177.

247. Mueller, U.; Schubert, M.; Teich, F.; Puetter, H.; Schierle-Arndt, K.; Pastre, J. *J. Mater. Chem.* **2006,** *16*(7), 626-636.

248. Kitagawa, S.; Kitaura, R.; Noro, S. *Angew. Chem., Int. Ed.* **2004,** *43*(18), 2334-2375.

249. Janiak, C. *Dalton Trans.* **2003,** (14), 2781-2804.

250. Uemura, T.; Yanai, N.; Kitagawa, S. *Chem. Soc. Rev.* **2009,** *38*(5), 1228-1236.

251. Yoshizawa, M.; Kusukawa, T.; Fujita, M.; Sakamoto, S.; Yamaguchi, K. *J. Am. Chem. Soc.* **2001,** *123*(43), 10454-10459.

252. Zou, X. Q.; Zhu, G. S.; Hewitt, I. J.; Sun, F. X.; Qiu, S. L. *Dalton Trans.* **2009,** (16), 3009-3013.

253. Zacher, D.; Shekhah, O.; Woll, C.; Fischer, R. A. *Chem. Soc. Rev.* **2009,** *38*(5), 1418-1429.

254. Yoo, Y.; Lai, Z. P.; Jeong, H. K. *Micropor. Mesopor. Mater.* **2009,** *123*(1-3), 100-106.

255. Horcajada, P.; Serre, C.; Grosso, D.; Boissiere, C.; Perruchas, S.; Sanchez, C.; Ferey, G. *Adv. Mater.* **2009,** *21*(19), 1931-1935.

256. Allendorf, M. D.; Houk, R. J. T.; Andruszkiewicz, L.; Talin, A. A.; Pikarsky, J.; Choudhury, A.; Gall, K. A.; Hesketh, P. J. *J. Am. Chem. Soc.* **2008,** *130*(44), 14404-+.

257. Hermes, S.; Zacher, D.; Baunemann, A.; Woll, C.; Fischer, R. A. *Chem. Mater.* **2007,** *19*(9), 2168-2173.

258. Mahata, P.; Raghunathan, R.; Banerjee, D.; Sen, D.; Ramasesha, S.; Bhat, S. V.; Natarajan, S. *Chem. Asian J.* **2009,** *4*(6), 936-947.

259. Nytko, E. A.; Helton, J. S.; Muller, P.; Nocera, D. G. *J. Am. Chem. Soc.* **2008,** *130*(10), 2922-2923.

260. Mahata, P.; Sen, D.; Natarajan, S. *Chem. Commun.* **2008,** (11), 1278-1280.

261. Horike, S.; Hasegawa, S.; Tanaka, D.; Higuchi, M.; Kitagawa, S. *Chem. Commun.* **2008,** (37), 4436-4438.

262. Chun, H.; Moon, J. *Inorg. Chem.* **2007,** *46*(11), 4371-4373.

263. Liu, Y. L.; Kravtsov, V. C.; Beauchamp, D. A.; Eubank, J. F.; Eddaoudi, M. *J. Am. Chem. Soc.* **2005,** *127*(20), 7266-7267.

264. Rao, C. N. R.; Sampathkumaran, E. V.; Nagarajan, R.; Paul, G.; Behera, J. N.; Choudhury, A. *Chem. Mater.* **2004,** *16*(8), 1441-1446.

265. Perry, J. J.; McManus, G. J.; Zaworotko, M. J. *Chem. Commun.* **2004,** (22), 2534-2535.

266. Murugesu, M.; Clerac, R.; Anson, C. E.; Powell, A. K. *J. Phys. Chem. Solids* **2004,** *65*(4), 667-676.

267. Behera, J. N.; Paul, G.; Choudhury, A.; Rao, C. N. R. *Chem. Commun.* **2004,** (4), 456-457.

268. Barthelet, K.; Marrot, J.; Ferey, G.; Riou, D. *Chem. Commun.* **2004,** (5), 520-521.

269. Srikanth, H.; Hajndl, R.; Moulton, B.; Zaworotko, M. J. *J. Appl.Phys.* **2003,** *93*(10), 7089-7091.

270. Shin, D. M.; Lee, I. S.; Chung, Y. K.; Lah, M. S. *Inorg. Chem.* **2003,** *42*(18), 5459-5461.

271. Rusanov, E. B.; Ponomarova, V. V.; Komarchuk, V. V.; Stoeckli-Evans, H.; Fernandez-Ibanez, E.; Stoeckli, F.; Sieler, J.; Domasevitch, K. V. *Angew. Chem., Int. Ed.* **2003,** *42*(22), 2499-2501.

272. Moulton, B.; Lu, J. J.; Hajndl, R.; Hariharan, S.; Zaworotko, M. J. *Angew. Chem., Int. Ed.* **2002,** *41*(15), 2821-2824.

273. Eddaoudi, M.; Kim, J.; Vodak, D.; Sudik, A.; Wachter, J.; O'Keeffe, M.; Yaghi, O. M. *Proceedings of the National Academy of Sciences of the United States of America* **2002,** *99*(8), 4900-4904.

274. Diederich, F.; Schurmann, G.; Chao, I. *J. Org. Chem.* **1988,** *53*(12), 2744-2757.

275. Schwende, C. F.; Sunday, B. R.; Shavel, J.; Giles, R. E. *J. Med. Chem.* **1974,** *17*(10), 1112-1115.

276. Coco, S.; Cordovilla, C.; Donnio, B.; Espinet, P.; Garcia-Casas, M. J.; Guillon, D. *Chem.-Eur. J.* **2008,** *14*(12), 3544-3552.

277. Valiyaveettil, S.; Enkelmann, V.; Mullen, K. *J. Chem. Soc., Chem. Commun.* **1994,** (18), 2097-2098.

278. Valiyaveettil, S.; Gans, C.; Klapper, M.; Gereke, R.; Mullen, K. *Polym. Bull.* **1995,** *34*(1), 13-19.

279. Valiyaveettil, S.; Mullen, K. *New J. Chem.* **1998,** *22*(2), 89-95.

280. Kimura, K.; Yamashita, Y.; Sakaguchi, Y.; Takase, S. *Alkoxysulfonic acid-group-containing polyarylene ether, composition containing the same, ion-conductive*

film, adhesive, composite, and fuel cell, and manufacture thereof. **JP 2003272695 A**, September 26, 2003.

281. *SMART*, v5.05; Siemens Analytical X-ray Instruments Inc.: Madison, WI, USA, **1995**.

282. *SAINT*, v6.28a; Bruker AXS Inc.: Madison, WI, USA, **1995**.

283. Sheldrick, G. M. *Acta Crystallogr.* **2008,** *A64*, 112-122.

284. Spek, A. L. *J. Appl. Crystallogr.* **2003,** *36*(1), 7-13.

285. Spek, A. L. *PLATON, A Multipurpose Crystallographic Tool*, v1.15; Utrecht University: Utrecht, The Netherlands, **2008**.

286. van der Sluis, P.; Spek, A. L. *Acta Crystallogr.* **1990,** *A46*(3), 194-201.

287. Pretsch, E.; Buhlmann, P.; Affolter, C., *Structure Determination of Organic Compounds*. Springer: Berlin, **2000**.

288. Silverstein, R. M.; Webster, F. X., *Spectrometric Identification of Organic Compounds*. 6th ed.; John Wiley & Sons, Inc.: New York, **1998**.

289. Zhang, J.; Bu, X. H. *Chem. Commun.* **2009,** (2), 206-208.

290. Zhang, R. F.; Wang, Q. F.; Yang, M. Q.; Wang, Y. R.; Ma, C. L. *Polyhedron* **2008,** *27*(14), 3123-3131.

291. Zhang, J.; Chew, E.; Chen, S.; Pham, J. T. H.; Bu, X. *Inorg. Chem.* **2008,** *47*(9), 3495-3497.

292. Macrae, C. F.; Bruno, I. J.; Chisholm, J. A.; Edgington, P. R.; McCabe, P.; Pidcock, E.; Rodriguez-Monge, L.; Taylor, R.; van de Streek, J.; Wood, P. A. *J. Appl. Crystallogr.* **2008,** *41*(2), 466-470.

293. Chen, S. M.; Zhang, J.; Bu, X. H. *Inorg. Chem.* **2008,** *47*(13), 5567-5569.

294. Zhang, J.; Yao, Y. G.; Bu, X. H. *Chem. Mater.* **2007,** *19*(21), 5083-5089.

295. Rood, J. A.; Boggess, W. C.; Noll, B. C.; Henderson, K. W. *J. Am. Chem. Soc.* **2007,** *129*(44), 13675-13682.

296. Dybtsev, D. N.; Yutkin, M. P.; Peresypkina, E. V.; Virovets, A. V.; Serre, C.; Ferey, G.; Fedin, V. P. *Inorg. Chem.* **2007,** *46*(17), 6843-6845.

297. Zeng, M. H.; Wang, B.; Wang, X. Y.; Zhang, W. X.; Chen, X. M.; Gao, S. *Inorg. Chem.* **2006,** *45*(18), 7069-7076.

298. Thuery, P. *Eur. J. Inorg. Chem.* **2006,** (18), 3646-3651.

299. Mulfort, K. L.; Hupp, J. T. *Inorg. Chem.* **2008,** *47*(18), 7936-7938.

300. Brunauer, S.; Deming, L. S.; Deming, W. E.; Teller, E. *J. Am. Chem. Soc.* **1940,** *62*, 1723-1732.

301. Byrnes, M. J.; Chisholm, M. H.; Patmore, N. J. *Inorg. Chem.* **2005,** *44*(25), 9347-9352.

302. Olenyuk, B.; Whiteford, J. A.; Stang, P. J. *J. Am. Chem. Soc.* **1996,** *118*(35), 8221-8230.

303. Stang, P. J.; Cao, D. H. *J. Am. Chem. Soc.* **1994,** *116*(11), 4981-4982.

304. Stang, P. J.; Cao, D. H.; Saito, S.; Arif, A. M. *J. Am. Chem. Soc.* **1995,** *117*(23), 6273-6283.

305. Stang, P. J.; Olenyuk, B. *Angew. Chem., Int. Ed.* **1996,** *35*(7), 732-736.

306. Coxeter, H. S. M., *Regular Polytopes*. MacMillan: New York, **1963**.

307. Torquato, S.; Jiao, Y. *Nature* **2009,** *460*(7257), 876-879.

308. Dalgarno, S. J.; Power, N. P.; Atwood, J. L. *Coord. Chem. Rev.* **2008,** *252*(8-9), 825-841.

309. Hamilton, T. D.; MacGillivray, L. R. *Cryst. Growth Des.* **2004,** *4*(3), 419-430.

310. Prakash, M. J.; Lah, M. S. *Chem. Commun.* **2009,** (23), 3326-3341.

311. Tranchemontagne, D. J. L.; Ni, Z.; O'Keeffe, M.; Yaghi, O. M. *Angew. Chem., Int.Ed.* **2008,** *47*(28), 5136-5147.

312. Wang, Y.; Okamura, T. A.; Sun, W. Y.; Ueyama, N. *Crystal Growth & Design* **2008,** *8*(3), 802-804.

313. Zhu, H. F.; Fan, J.; Okamura, T.; Zhang, Z. H.; Liu, G. X.; Yu, K. B.; Sun, W. Y.; Ueyama, N. *Inorganic Chemistry* **2006,** *45*(10), 3941-3948.

314. Umemoto, K.; Yamaguchi, K.; Fujita, M. *Journal of the American Chemical Society* **2000,** *122*(29), 7150-7151.

315. Oppel, I. M.; Focker, K. *Angewandte Chemie-International Edition* **2008,** *47*(2), 402-405.

316. Umemoto, K.; Yamaguchi, K.; Fujita, M. *J. Am. Chem. Soc.* **2000,** *122*(29), 7150-7151.

317. Chand, D. K.; Biradha, K.; Kawano, M.; Sakamoto, S.; Yamaguchi, K.; Fujita, M. *Chemistry-an Asian Journal* **2006,** *1*(1-2), 82-90.

318. Sudik, A. C.; Millward, A. R.; Ockwig, N. W.; Cote, A. P.; Kim, J.; Yaghi, O. M. *J. Am. Chem. Soc.* **2005,** *127*(19), 7110-7118.

319. Yoshizawa, M.; Nagao, M.; Umemoto, K.; Biradha, K.; Fujita, M.; Sakamoto, S.; Yamaguchi, K. *Chem. Commun.* **2003,** (15), 1808-1809.

320. Roche, S.; Haslam, C.; Adams, H.; Heath, S. L.; Thomas, J. A. *Chemical Communications* **1998,** (16), 1681-1682.

321. Sava, D. F.; Kravtsov, V. C.; Eckert, J.; Eubank, J. F.; Nouar, F.; Eddaoudi, M. *Journal of the American Chemical Society* **2009,** *131*(30), 10394-+.

322. MacGillivray, L. R.; Atwood, J. L. *Nature* **1997,** *389*(6650), 469-472.

323. Liu, Y. L.; Kravtsov, V. C.; Beauchamp, D. A.; Eubank, J. F.; Eddaoudi, M. *Journal of the American Chemical Society* **2005,** *127*(20), 7266-7267.

324. Furukawa, H.; Kim, J.; Ockwig, N. W.; O'Keeffe, M.; Yaghi, O. M. *Journal of the American Chemical Society* **2008,** *130*(35), 11650-11661.

325. Ke, Y. X.; Collins, D. J.; Zhou, H. C. *Inorganic Chemistry* **2005,** *44*(12), 4154-4156.

326. Tominaga, M.; Suzuki, K.; Murase, T.; Fujita, M. *Journal of the American Chemical Society* **2005,** *127*(34), 11950-11951.

327. Moulton, B.; Lu, J. J.; Mondal, A.; Zaworotko, M. J. *Chemical Communications* **2001,** (9), 863-864.

328. Abourahma, H.; Coleman, A. W.; Moulton, B.; Rather, B.; Shahgaldian, P.; Zaworotko, M. J. *Chemical Communications* **2001,** (22), 2380-2381.

329. Mohomed, K.; Abourahma, H.; Zaworotko, M. J.; Harmon, J. P. *Chemical Communications* **2005,** (26), 3277-3279.

330. Larsen, R. W.; McManus, G. J.; Perry, J. J.; Rivera-Otero, E.; Zaworotko, M. J. *Inorganic Chemistry* **2007,** *46*(15), 5904-5910.

331. Furukawa, H.; Kim, J.; Plass, K. E.; Yaghi, O. M. *Journal of the American Chemical Society* **2006,** *128*(26), 8398-8399.

332. Jung, M.; Kim, H.; Baek, K.; Kim, K. *Angewandte Chemie-International Edition* **2008,** *47*(31), 5755-5757.

333. Schweiger, M.; Yamamoto, T.; Stang, P. J.; Blaser, D.; Boese, R. *Journal of Organic Chemistry* **2005,** *70*(12), 4861-4864.

334. Ni, Z.; Yassar, A.; Antoun, T.; Yaghi, O. M. *J. Am. Chem. Soc.* **2005,** *127*(37), 12752-12753.

335. Furukawa, H.; Kim, J.; Plass, K. E.; Yaghi, O. M. *Journal of the American Chemical Society* **2006,** *128*(26), 8398-8399.

336. Jung, M.; Kim, H.; Baek, K.; Kim, K. *Angew. Chem., Int. Ed.* **2008,** *47*(31), 5755-5757.

337. vanGenderen, M. H. P.; Pfaadt, M.; Moller, C.; Valiyaveettil, S.; Spiess, H. W. *J. Am. Chem. Soc.* **1996,** *118*(15), 3661-3665.

338. Venkataramanan, B.; Ning, Z.; Vittal, J. J.; Valiyaveettil, S. *CrystEngComm* **2005,** *7*, 108-112.

339. Nishio, M.; Hirota, M.; Umezawa, Y., *The CH/π Interaction: Evidence, Nature, and Consequences*. Wiley-VCH: New York, **1998**.

340. Desiraju, G. R. *Accounts of Chemical Research* **2002,** *35*(7), 565-573.

341. Mohomed, K.; Abourahma, H.; Zaworotko, M. J.; Harmon, J. P. *Chem. Commun.* **2005,** (26), 3277-3279.

342. Mohomed, K.; Abourahma, H.; Zaworotko, M. J.; Harmon, J. P. *Chem.Commun.* **2005,** (26), 3277-3279.

343. Perry, J. J.; Perman, J. A.; Zaworotko, M. J. *Chem. Soc. Rev.* **2009,** *38*(5), 1400-1417.

344. Nouar, F.; Eubank, J. F.; Bousquet, T.; Wojtas, L.; Zaworotko, M. J.; Eddaoudi, M. *J. Am. Chem. Soc.* **2008,** *130*(6), 1833-1835.

345. Cairns, A. J.; Perman, J. A.; Wojtas, L.; Kravtsov, V. C.; Alkordi, M. H.; Eddaoudi, M.; Zaworotko, M. J. *J. Am. Chem. Soc.* **2008,** *130*(5), 1560-1561.

346. Abourahma, H.; Coleman, A. W.; Moulton, B.; Rather, B.; Shahgaldian, P.; Zaworotko, M. J. *Chemical Communications* **2001,** (22), 2380-2381.

347. Eddaoudi, M.; Kim, J.; Wachter, J. B.; Chae, H. K.; O'Keeffe, M.; Yaghi, O. M. *J. Am. Chem. Soc.* **2001,** *123*(18), 4368-4369.

348. Moulton, B.; Lu, J. J.; Mondal, A.; Zaworotko, M. J. *Chem.Commun.* **2001,** (9), 863-864.

349. McManus, G. J.; Wang, Z. Q.; Zaworotko, M. J. *Cryst. Growth Des.* **2004,** *4*(1), 11-13.

350. Ke, Y. X.; Collins, D. J.; Zhou, H. C. *Inorg. Chem.* **2005,** *44*(12), 4154-4156.

351. Furukawa, H.; Kim, J.; Plass, K. E.; Yaghi, O. M. *J. Am. Chem. Soc.* **2006,** *128*(26), 8398-8399.

352. Ghosh, S.; Mukherjee, P. S. *J. Org. Chem.* **2006,** *71*(22), 8412-8416.

353. Furukawa, H.; Kim, J.; Ockwig, N. W.; O'Keeffe, M.; Yaghi, O. M. *J. Am. Chem. Soc.* **2008,** *130*(35), 11650-11661.

354. Tonigold, M.; Hitzbleck, J.; Bahnmuller, S.; Langstein, G.; Volkmer, D. *Dalton Trans.* **2009,** (8), 1363-1371.

355. Duriska, M. B.; Neville, S. M.; Moubaraki, B.; Cashion, J. A.; Halder, G. J.; Chapman, K. W.; Balde, C.; Letard, J. F.; Murray, K. S.; Kepert, C. J.; Batten, S. R. *Angew. Chem., Int. Ed.* **2009,** *48*(14), 2549-2552.

356. Larsen, R. W. *J. Am. Chem. Soc.* **2008,** *130*(34), 11246-11247.

357. Mohomed, K.; Gerasimov, T. G.; Abourahma, H.; Zaworotko, M. J.; Harmon, J. P. *Mat. Sci. Eng., A* **2005,** *409*(1-2), 227-233.

358. Delgado-Friedrichs, O.; O'Keeffe, M. *Acta Crystallogr.* **2007,** *A63*(4), 344-347.

359. Wang, X. S.; Ma, S. Q.; Forster, P. M.; Yuan, D. Q.; Eckert, J.; Lopez, J. J.; Murphy, B. J.; Parise, J. B.; Zhou, H. C. *Angew. Chem., Int. Ed.* **2008,** *47*(38), 7263-7266.

360. Zafar, A.; Yang, J.; Geib, S. J.; Hamilton, A. D. *Tetrahedron Lett.* **1996,** *37*(14), 2327-2330.

Appendices

Appendix A. ^{1}H NMR spectra for synthesized ligands.

Appendix A-1. ^{1}H NMR spectrum for L1: 5-benzyloxy-1,3-bdc

^{1}H NMR spectrum of 5-benzyloxy-1,3-benzenedicarboxylic acid (**L1**) dissolved in Acetone-d_6. The spectrum was obtained on a Bruker DPX-250 MHz spectrometer. The FID data was processed and displayed using SpinWorks 3.1.

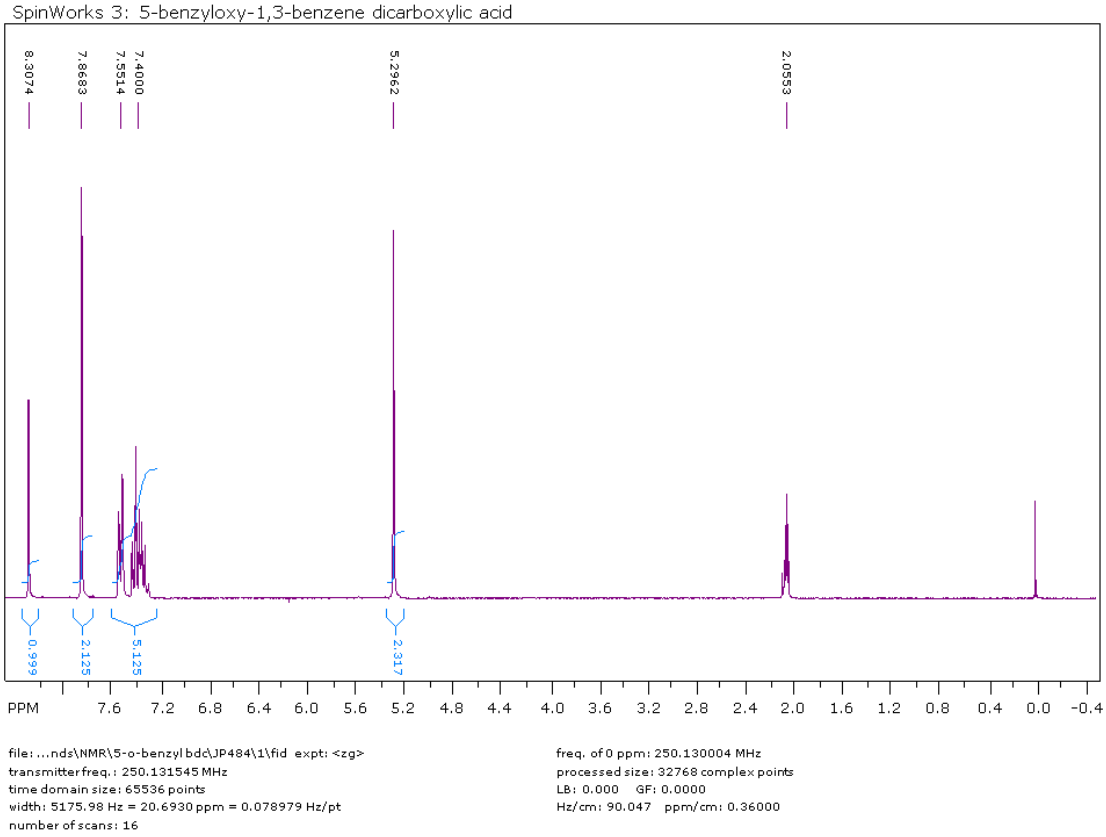

^{1}H NMR (250 MHz, Acetone-d_6, δ): 5.3(s, 2H, -O-CH_2-), 7.4(m, 3 H, -ArH), 7.6(d, J = 7.4 Hz, 2H, -ArH), 7.9(d, J = 1.44 Hz, 2H, -ArH), 8.3(t, J = 1.4 Hz, 1H, -ArH), 11.2(br, 2H, -COOH). The carboxylic acid peak was so broad it is not shown in this spectrum, but was found upon increasing the vertical scale.

Appendix A-2. ^{1}H NMR spectrum for L2: 5-naphthyloxy-1,3-bdc

^{1}H NMR spectrum of 5-naphthyloxy-1,3-benzenedicarboxylic acid (**L2**) dissolved in DMSO-d_6. The spectrum was obtained on a Bruker DPX-250 MHz spectrometer. The FID data was processed and displayed using SpinWorks 3.1.

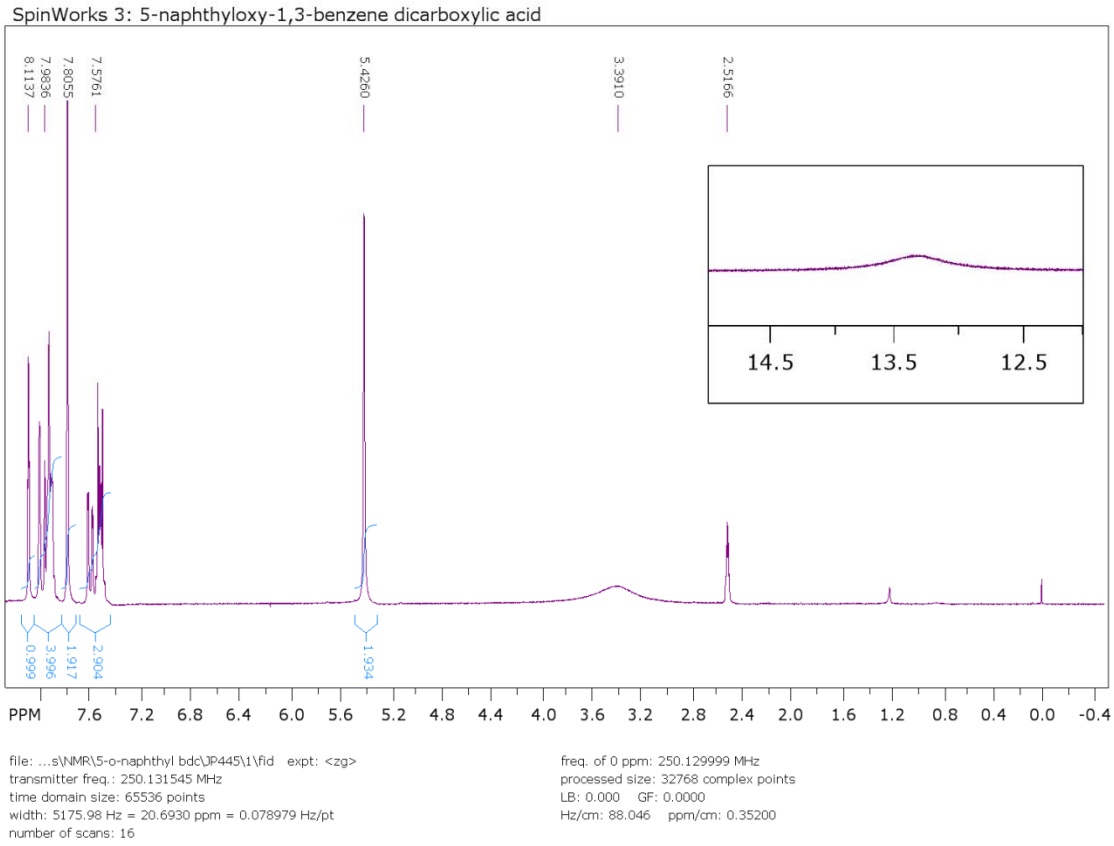

^{1}H NMR (250 MHz, DMSO-d_6, δ): 5.4(s, 2H, -O-CH_2-), 7.6(m, 4 H, -ArH), 7.8(d, 2H, -ArH), 7.98(m, 3H, -ArH), 8.0(s, 1H, -ArH), 8.1(t, J = 1.3 Hz, 1H, -ArH), 13.3(br, 2H, -COOH, inset).

Appendix A-3. ^{1}H NMR spectrum for L3: 5-hexyloxy-1,3-bdc

^{1}H NMR spectrum of 5-hexyloxy-1,3-benzenedicarboxylic acid (**L3**) dissolved in DMSO-d_6. The spectrum was obtained on a Bruker DPX-250 MHz spectrometer. The FID data was processed and displayed using SpinWorks 3.1.

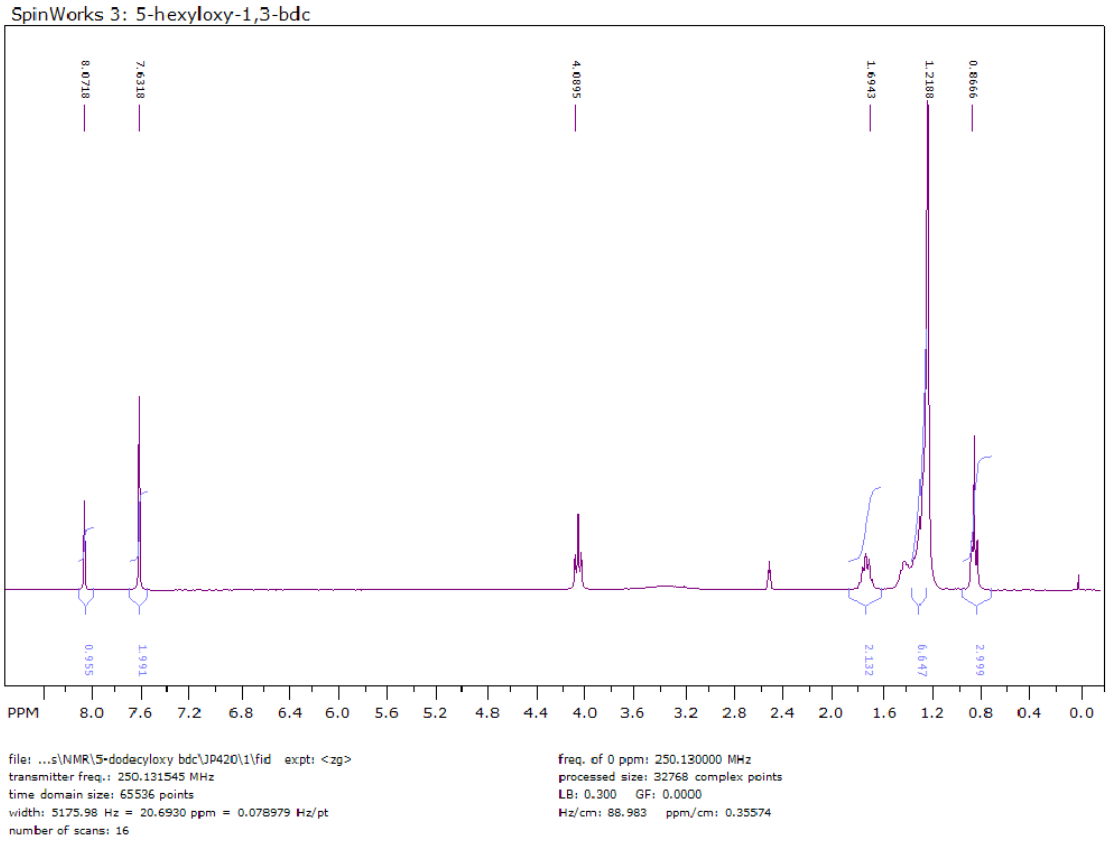

^{1}H NMR (250 MHz, DMSO-d_6, δ): 0.9(t, J = 6.3 Hz, 3H, -CH_3), 1.2(m, 6 H, -CH_2-), 1.7(m, 2H, -CH_2-), 4.1(t, J = 6.4 Hz, 2H, -O-CH_2-), 7.6(s, 2H, -ArH), 8.1(t, J = 1.4 Hz, 1H, -ArH), 13.3(br, 2H, -COOH). The carboxylic acid peak was so broad that it is not shown on this spectrum, however it was found by increasing the vertical scale quite a bit.

Appendix A-4. ^{1}H NMR spectrum for L4: 5-dodecyloxy-1,3-bdc

^{1}H NMR spectrum of 5-dodecyloxy-1,3-benzenedicarboxylic acid (**L4**) dissolved in DMSO-d_6. The spectrum was obtained on a Bruker DPX-250 MHz spectrometer. The FID data was processed and displayed using SpinWorks 3.1.

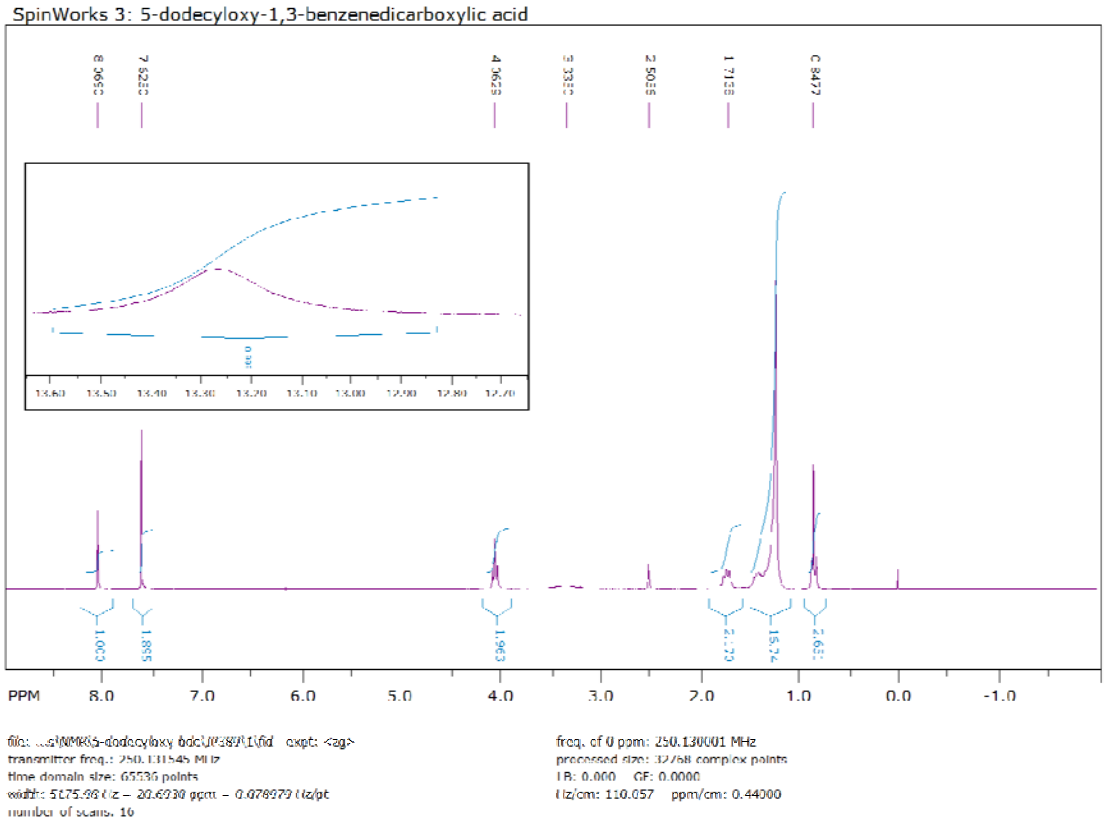

^{1}H NMR (250 MHz, DMSO-d_6, δ): 0.9(t, J = 6.3 Hz, 3H, -CH_3), 1.2(m, 18 H, -CH_2-), 1.7(m, 2H, -CH_2-), 4.1(t, J = 6.4 Hz, 2H, -O-CH_2-), 7.6(s, 2H, -ArH), 8.1(t, J = 1.4 Hz, 1H, -ArH), 13.3(br, 2H, -COOH, inset).

Appendix A-5. ^{1}H NMR spectrum for L5: 1,3-bis(5-methoxy-1,3-bdc)benzene

^{1}H NMR spectrum of 1,3-bis(5-methoxy-1,3-benzenedicarboxylic acid)benzene (**L5**) dissolved in DMSO-d_6. The spectrum was obtained on a Bruker DPX-250 MHz spectrometer. The FID data was processed and displayed using SpinWorks 3.1.

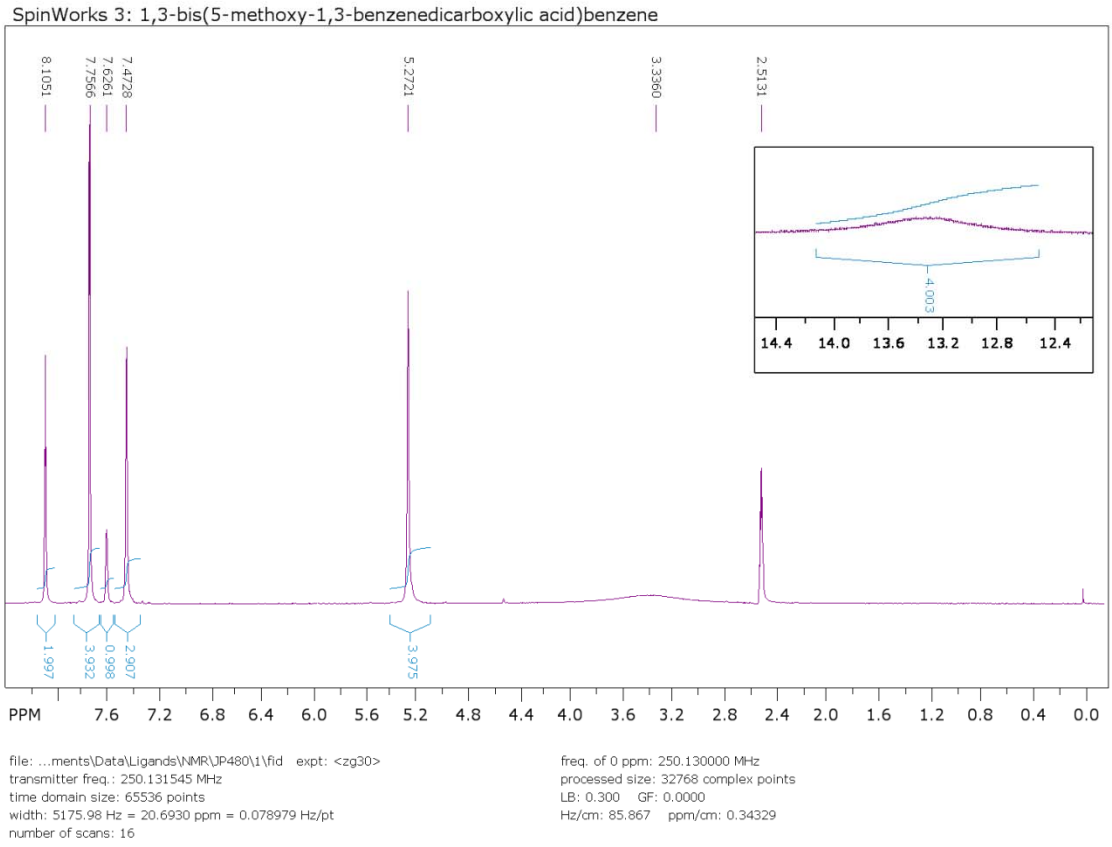

^{1}H NMR (250 MHz, DMSO-d_6, δ): 5.3(s, 4H, , -O-CH_2-), 7.5(d, J = 0.9 Hz, 3 H, -ArH), 7.6(s, 1H, -ArH), 7.8(d, J = 1.39 Hz, 4H, -ArH), 8.1(t, J = 1.38 Hz, 2H, -ArH), 13.4(br, 4H, -COOH, inset).

Appendix B. FT-IR spectra for synthesized ligands; FT-IR spectra, PXRD patterns, and Thermal Gravimetric Analysis for synthesized compounds.

Appendix B-1. FT-IR spectrum for L1: 5-benzyloxy-1,3-bdc

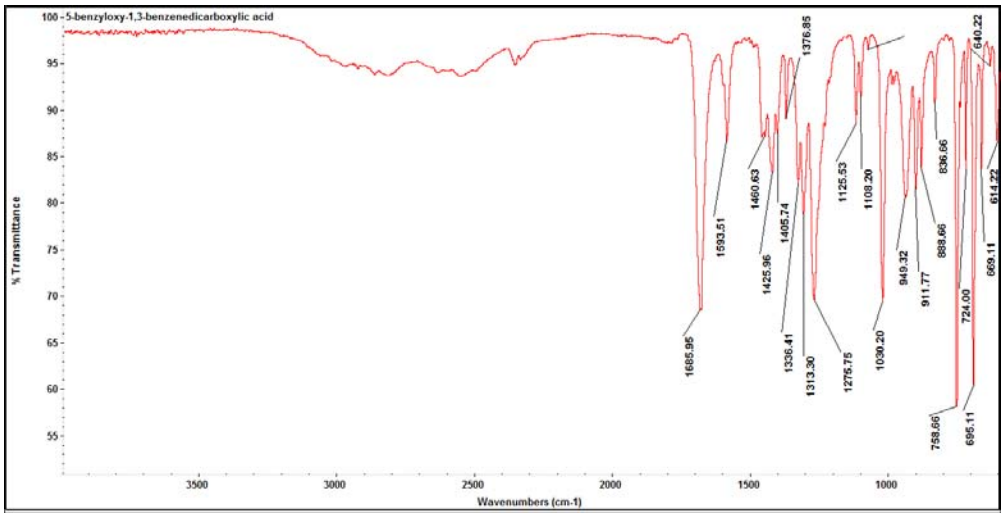

Appendix B-2. FT-IR spectrum for L2: 5-naphthyloxy-1,3-bdc

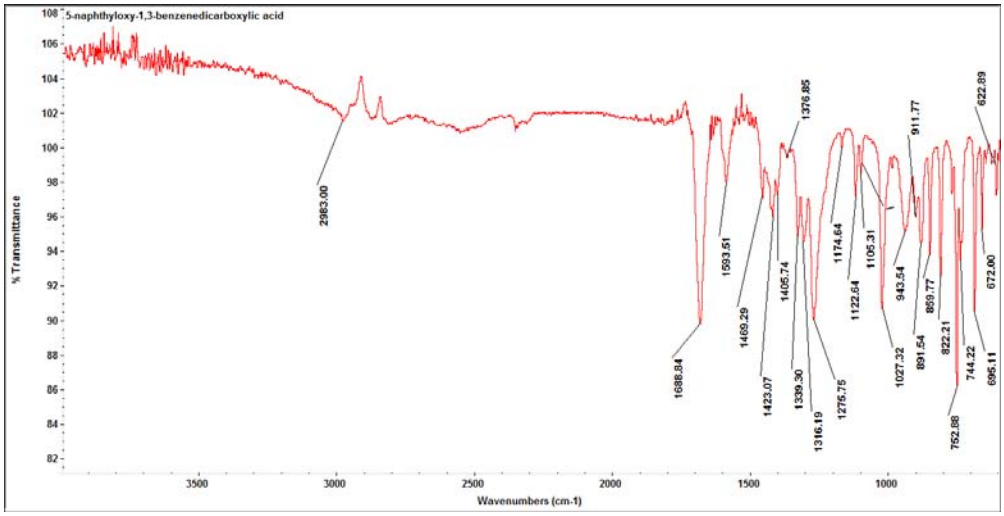

Appendix B-3. FT-IR spectrum for L3: 5-hexyloxy-1,3-bdc

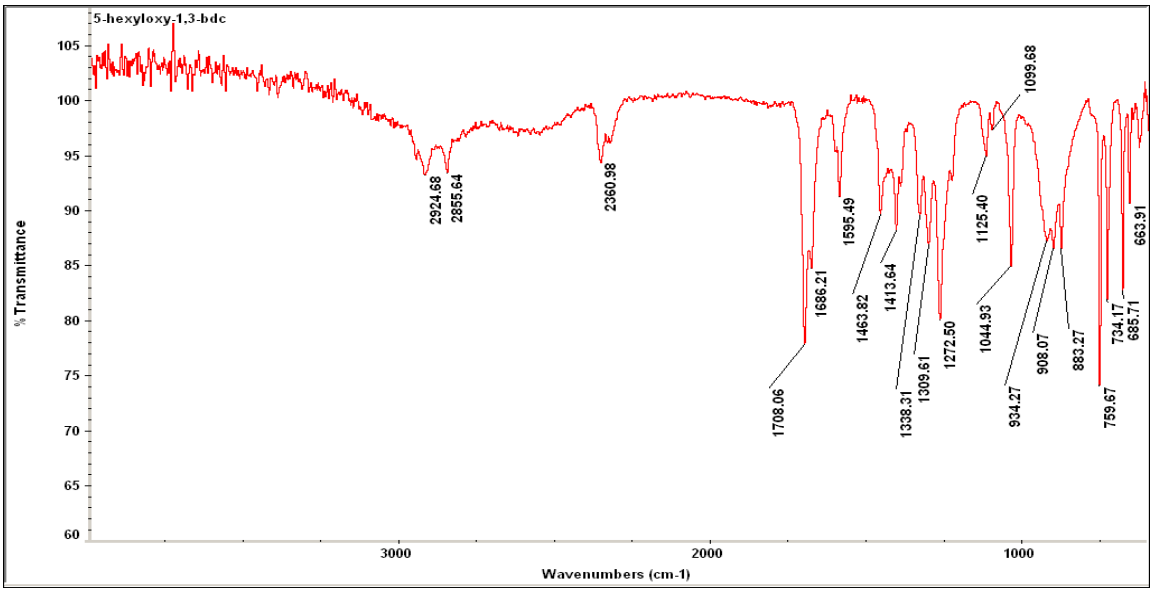

Appendix B-4. FT-IR spectrum for L4: 5-dodecyloxy-1,3-bdc

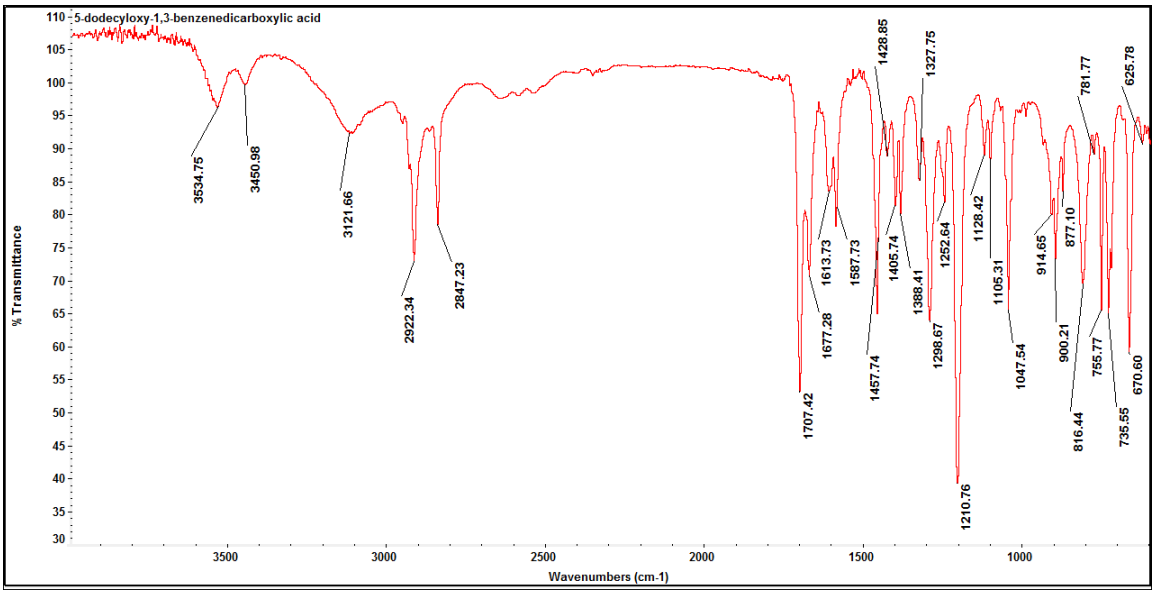

Appendix B-5. FT-IR spectrum for L5: 1,3-bis(5-methoxy-1,3-bdc)benzene

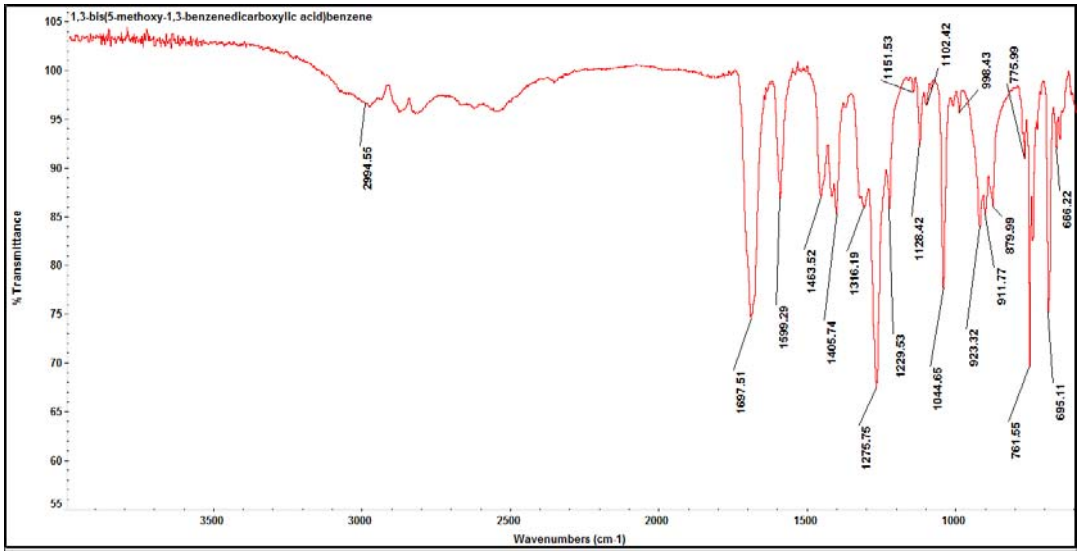

Appendix B-6. Experimental data for compound [1].

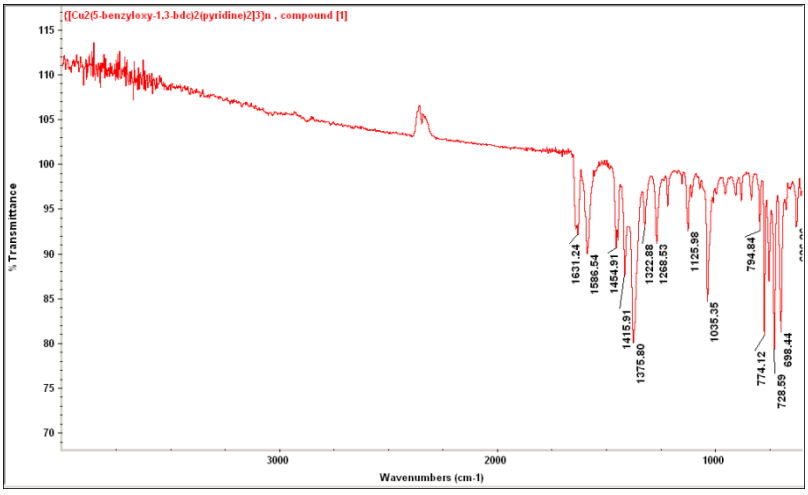

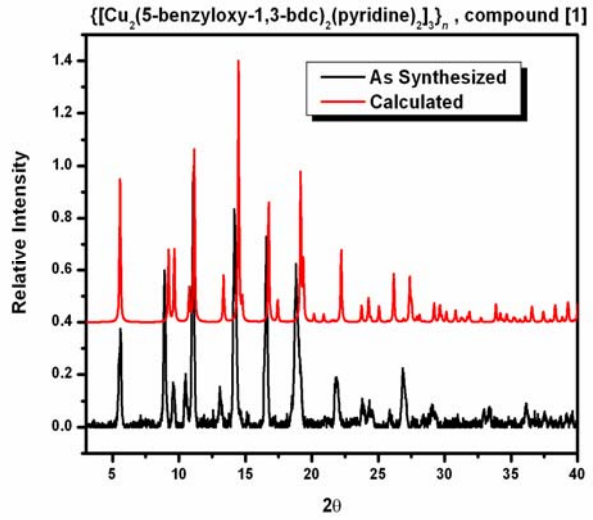

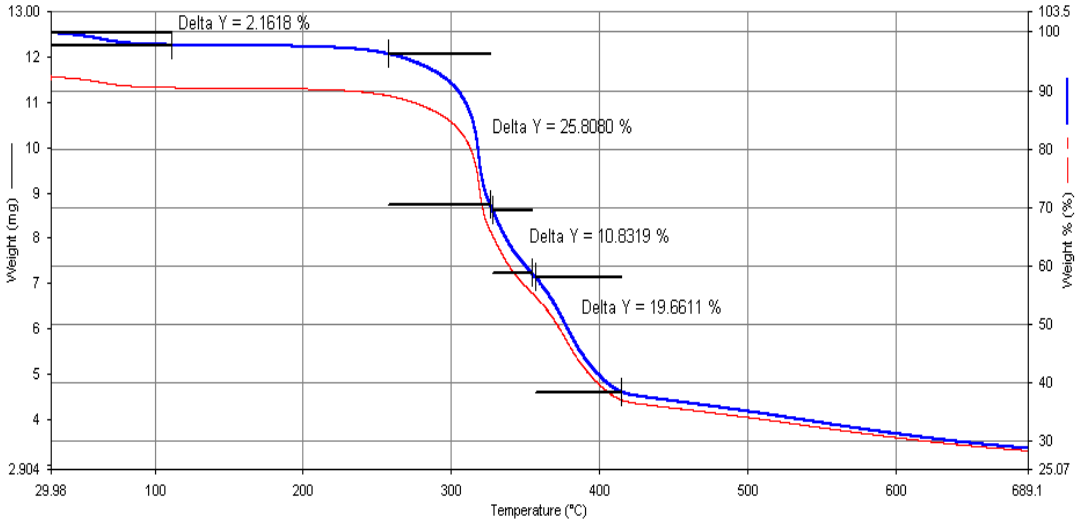

Appendix B-7. Experimental data for compound [2].

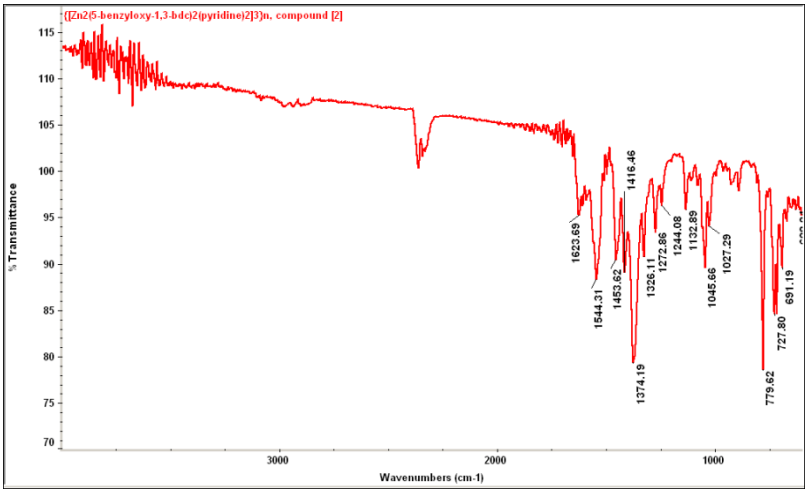

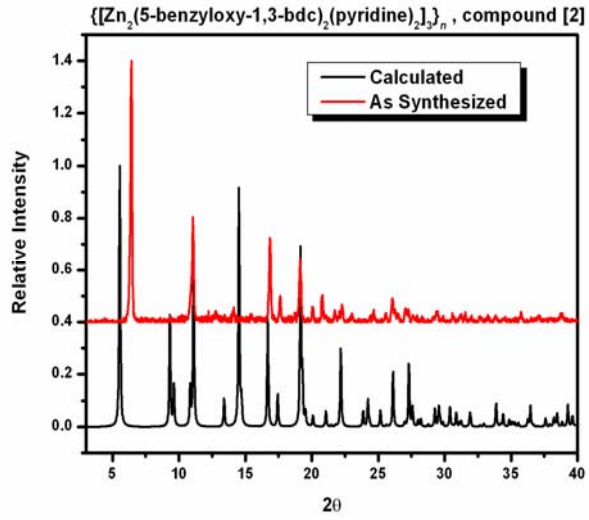

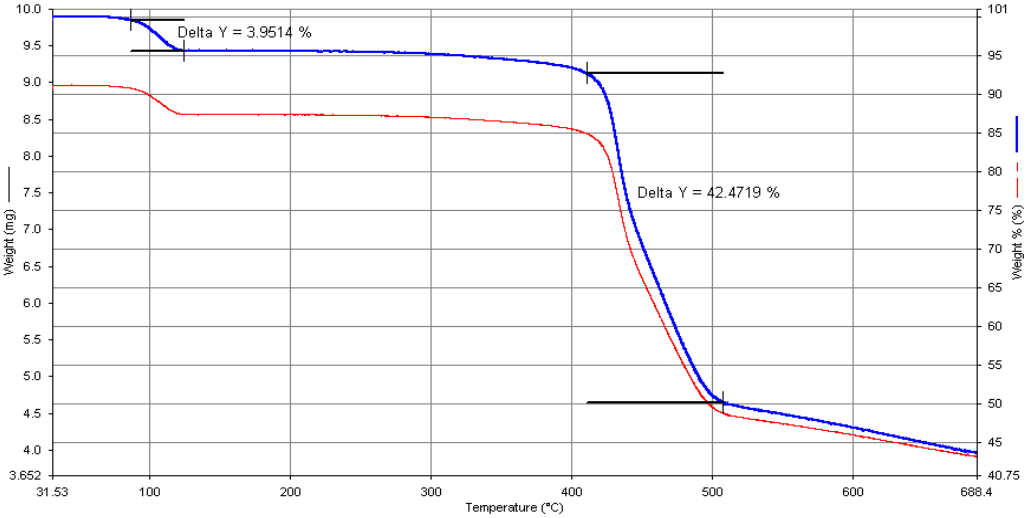

Appendix B-8. Experimental data for compound [3].

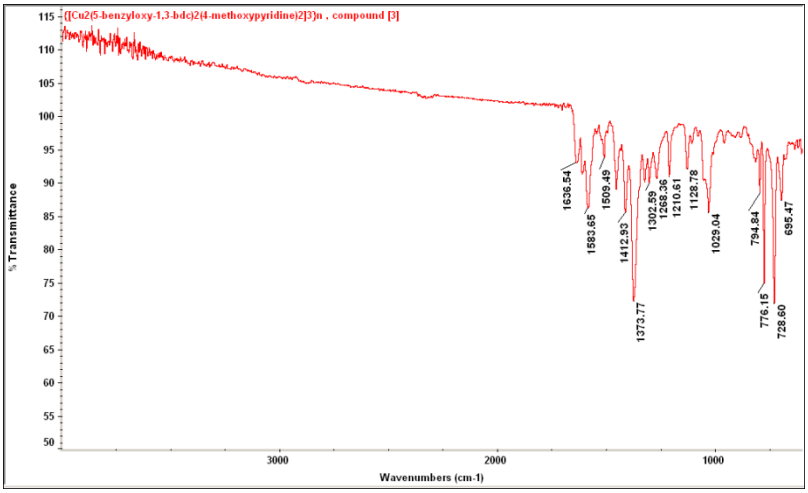

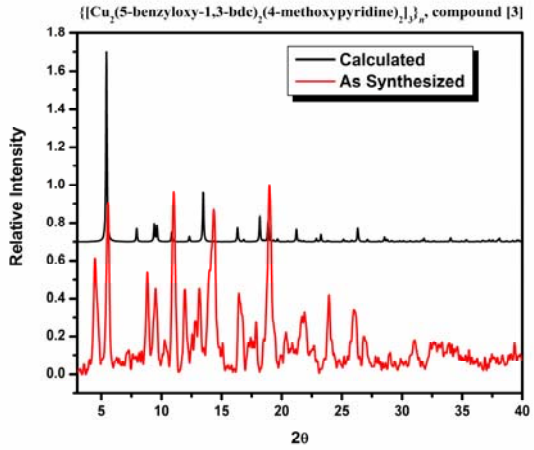

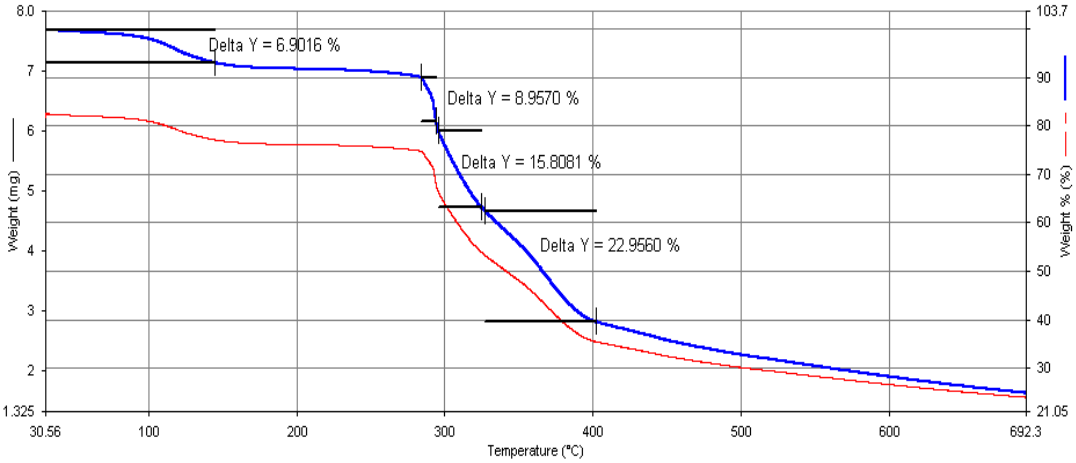

Appendix B-9. Experimental data for compound [4].

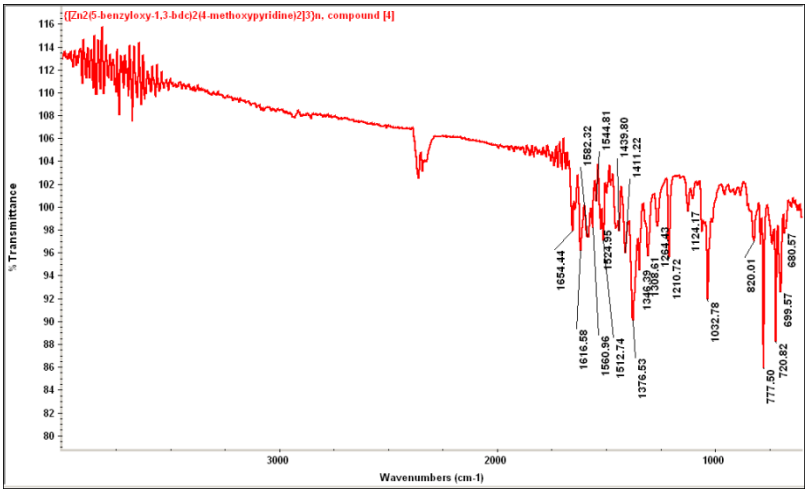

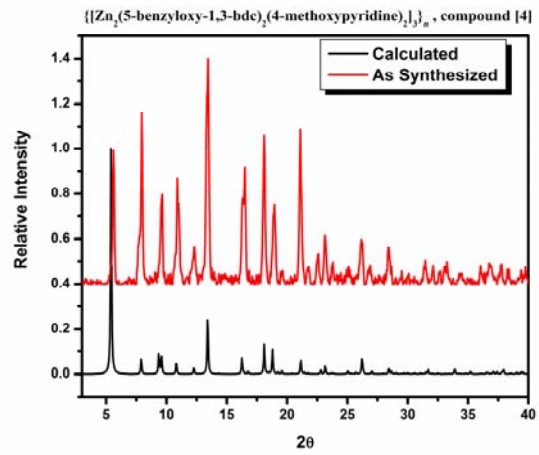

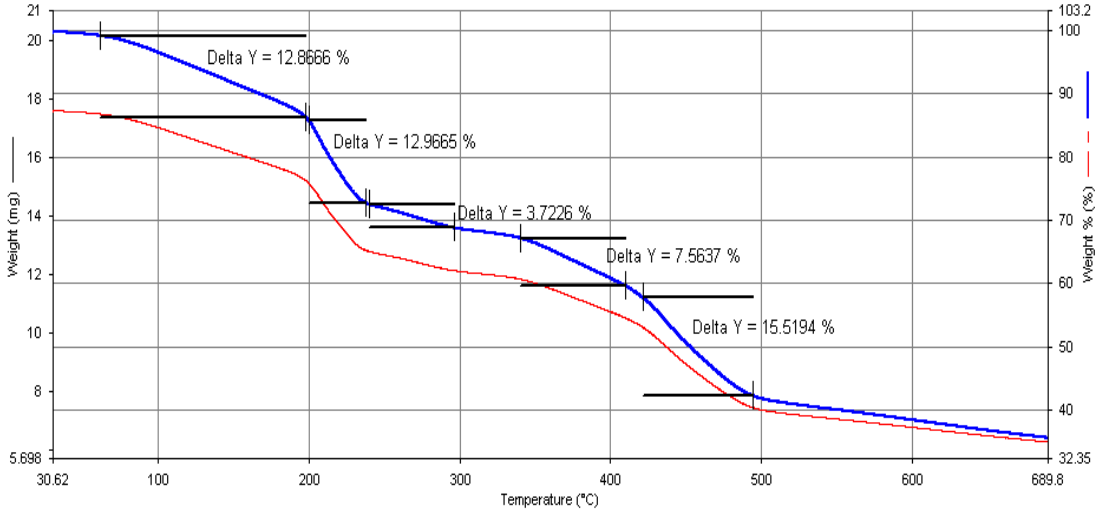

Appendix B-10. Experimental data for compound [5].

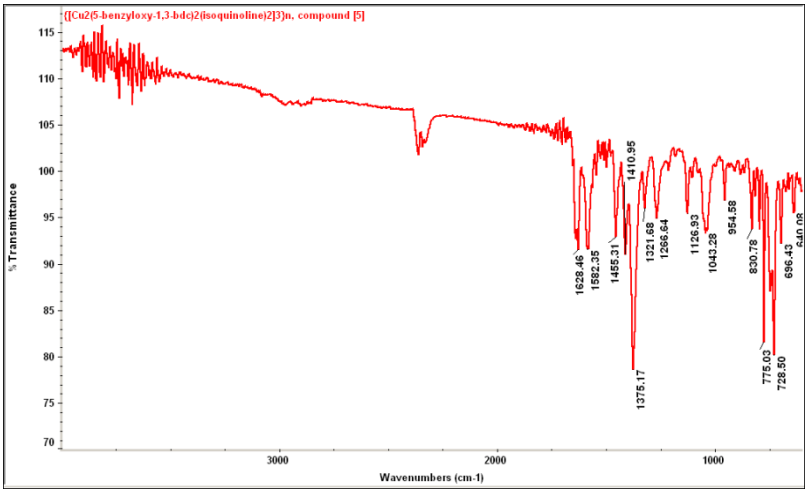

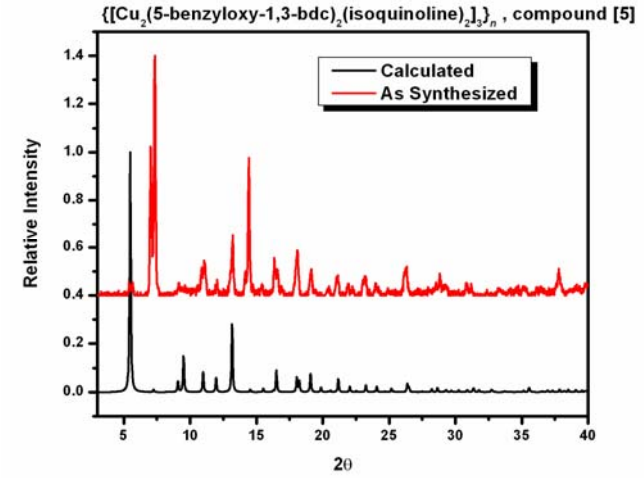

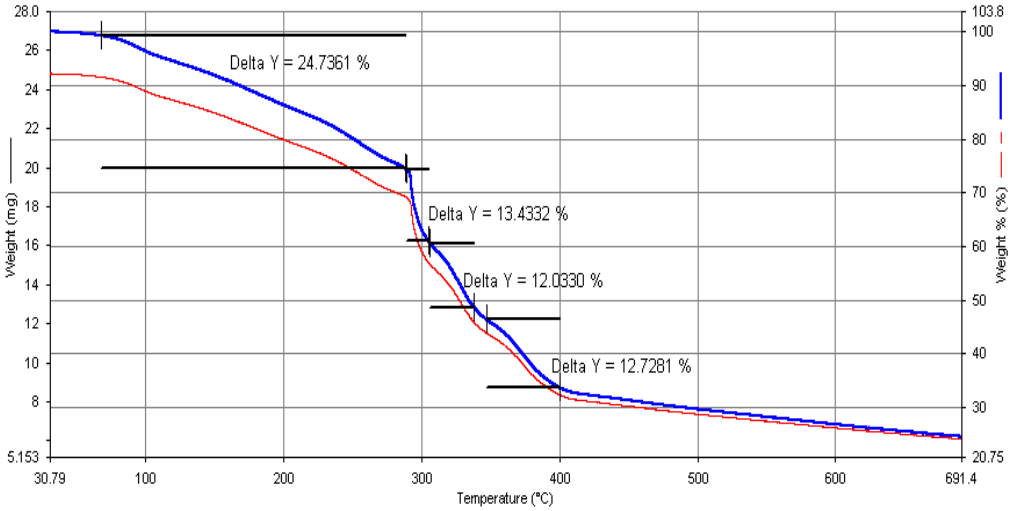

Appendix B-11. Experimental data for compound [6].

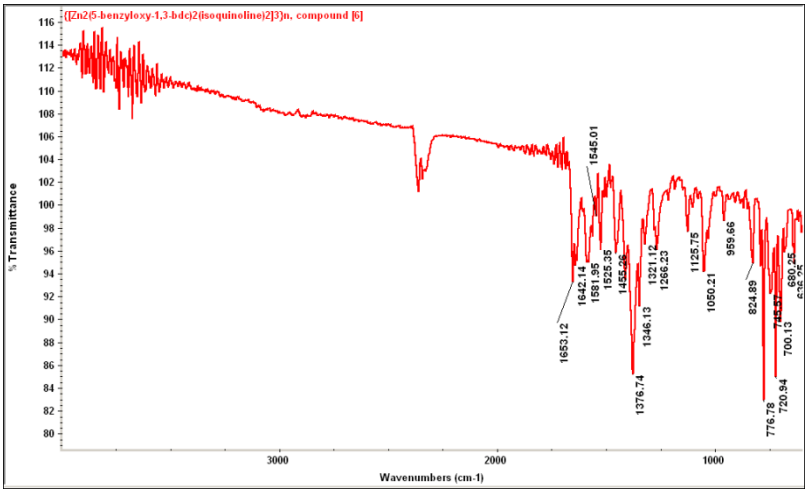

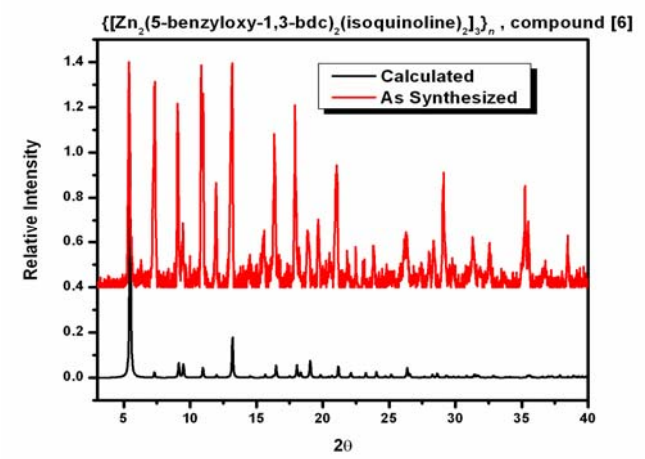

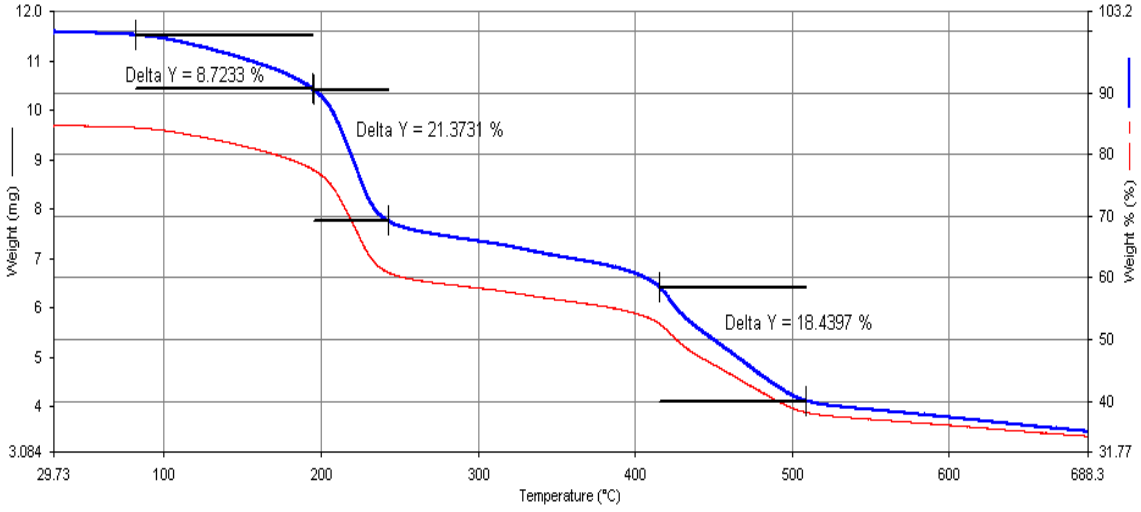

Appendix B-12. Experimental data for compound [7].

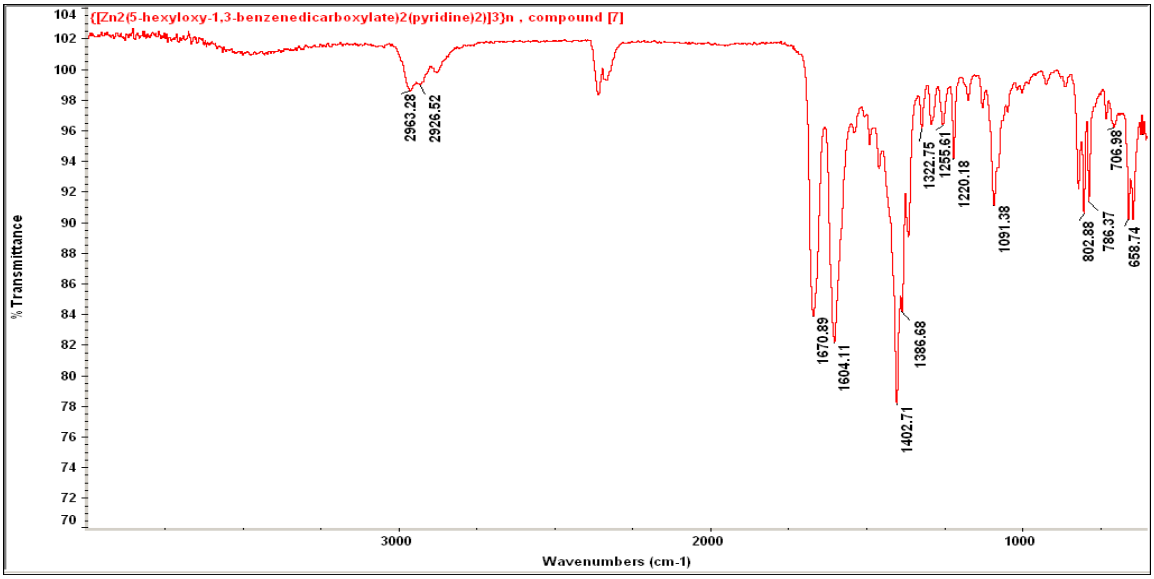

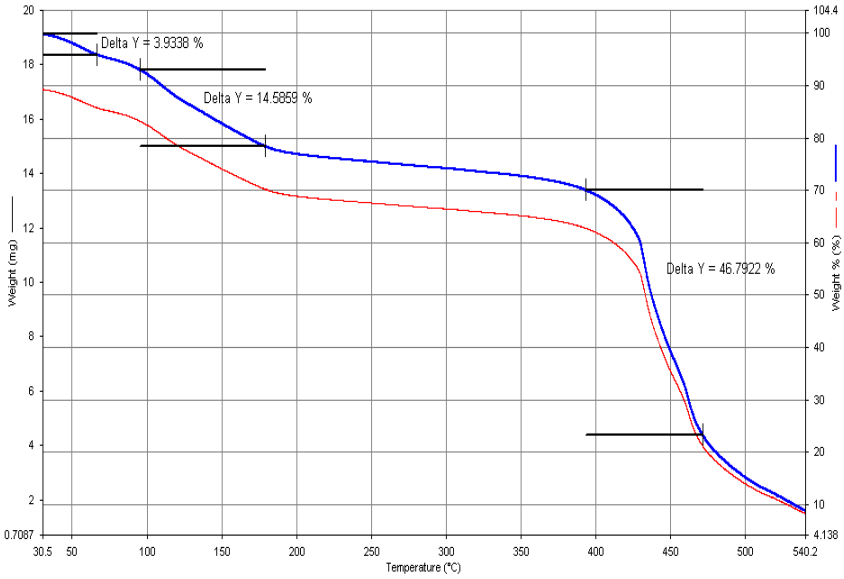

Appendix B-13. Experimental data for compound [8].

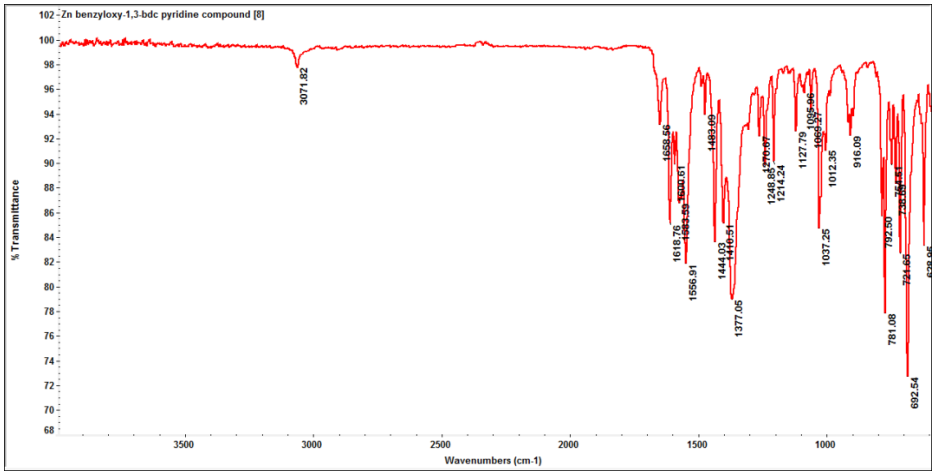

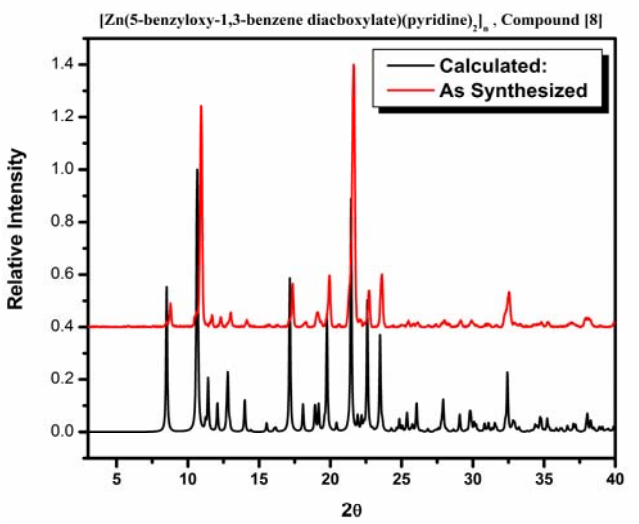

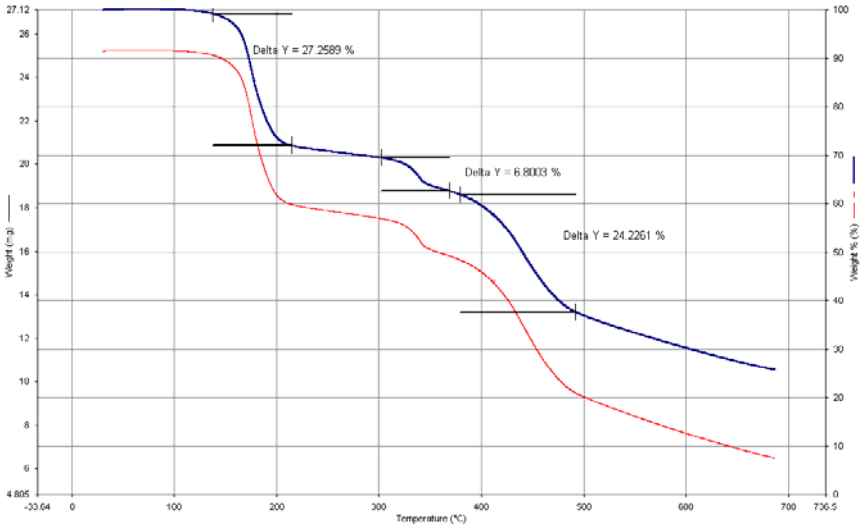

Appendix B-14. Experimental data for compound [9].

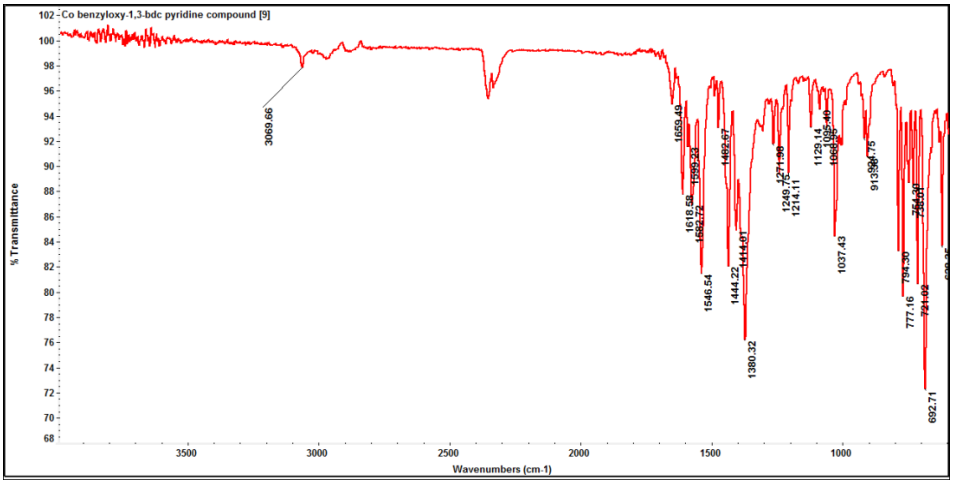

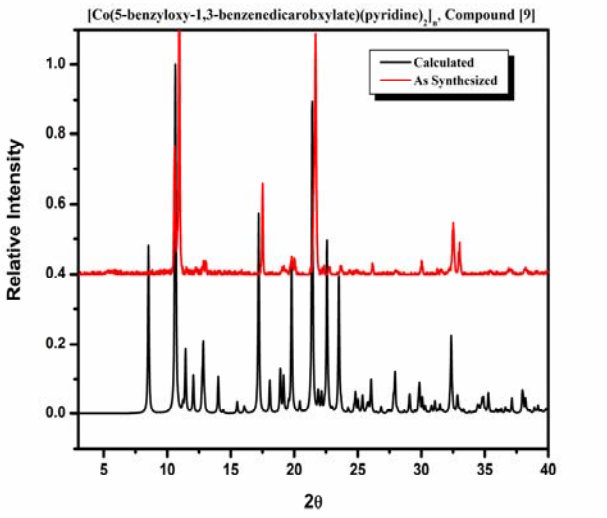

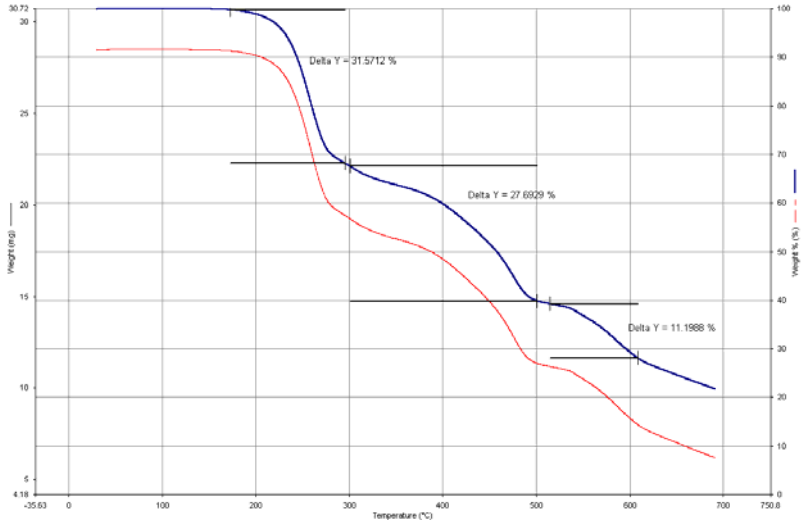

Appendix B-15. Experimental data for compound [10].

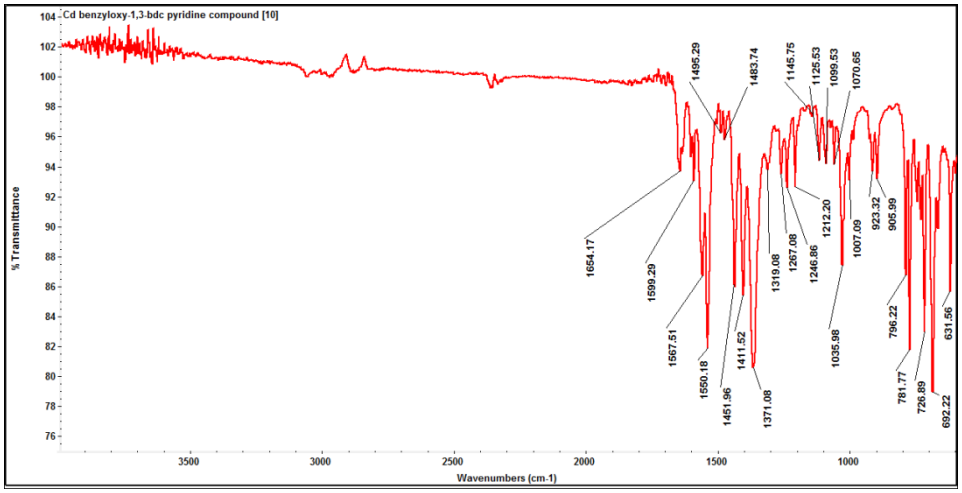

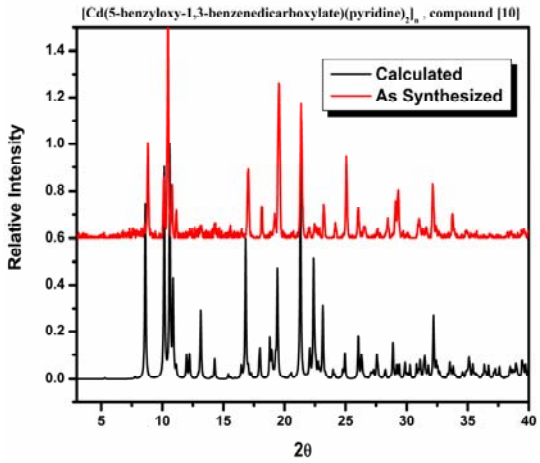

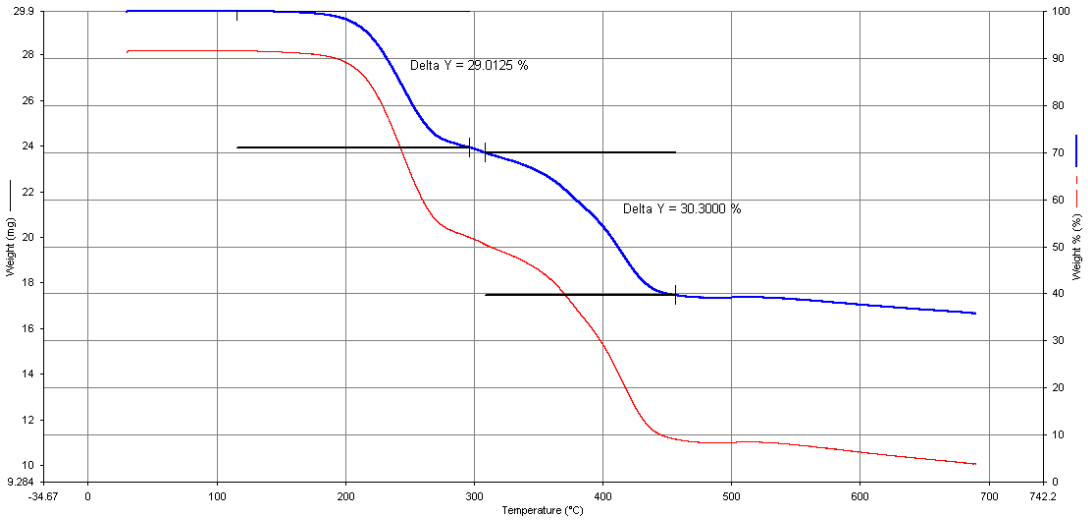

Appendix B-16. Experimental data for compound [11].

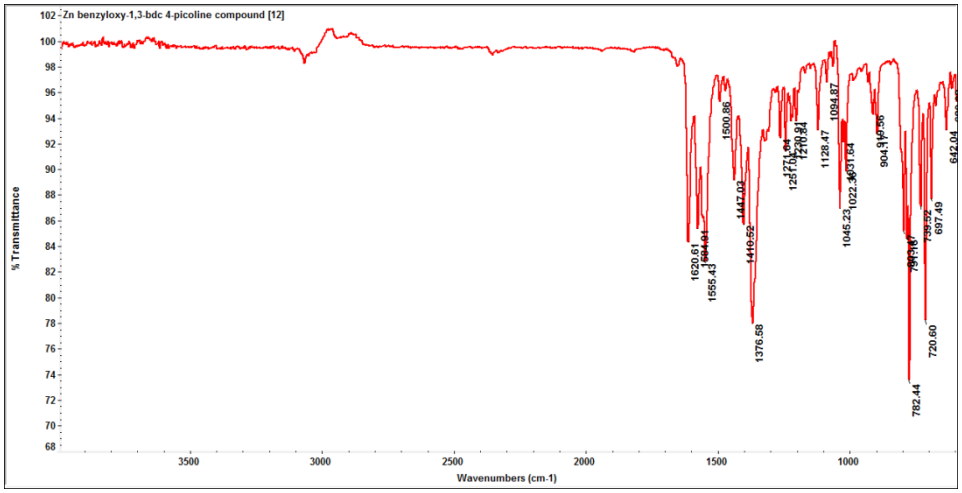

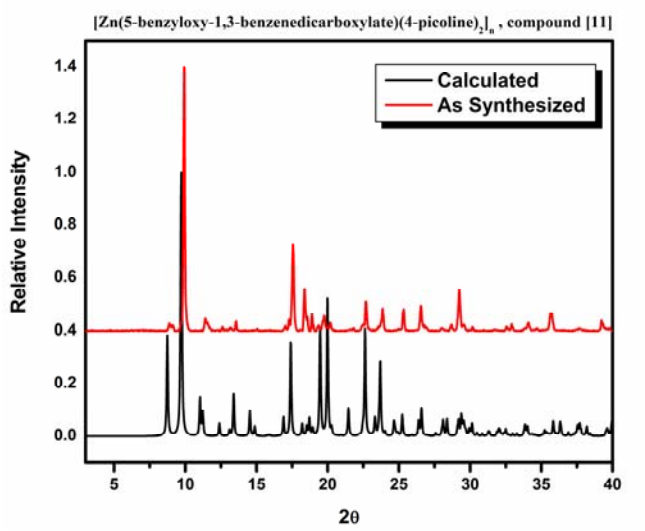

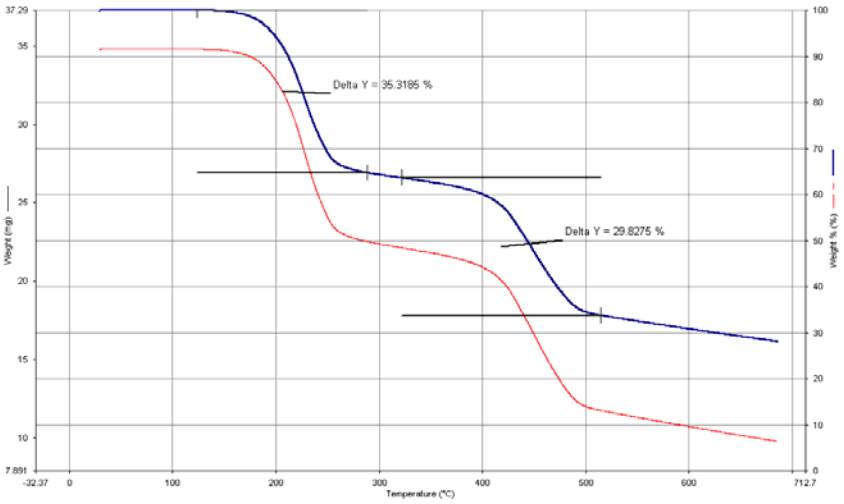

Appendix B-17. Experimental data for compound [12].

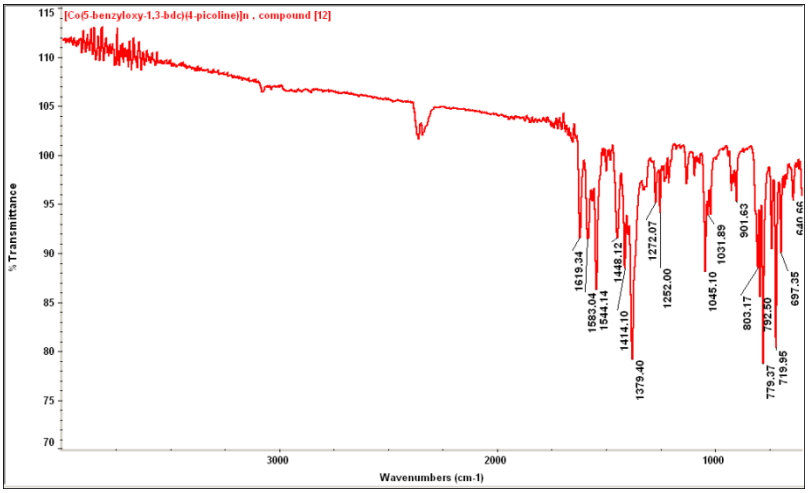

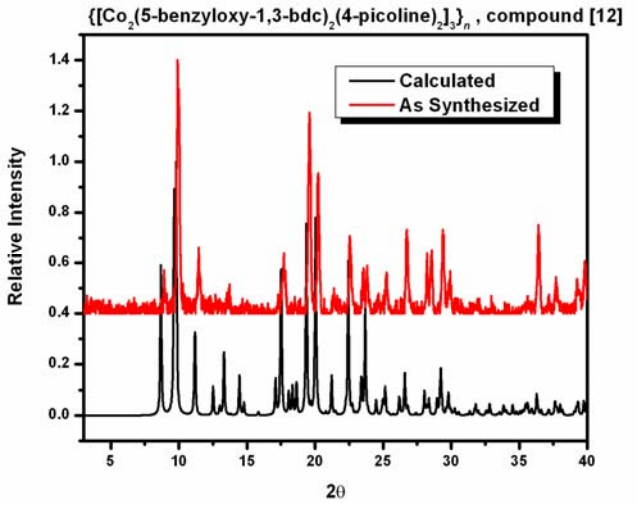

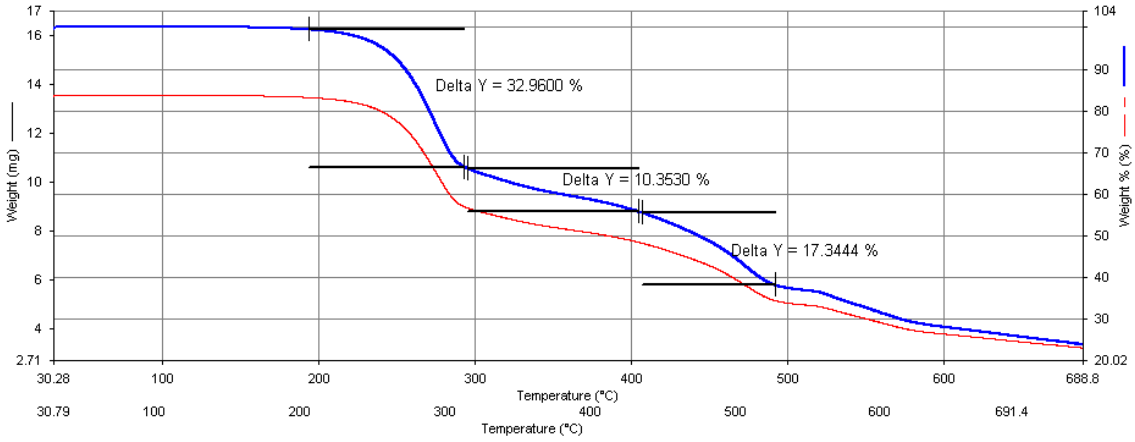

Appendix B-18. Experimental data for compound [13].

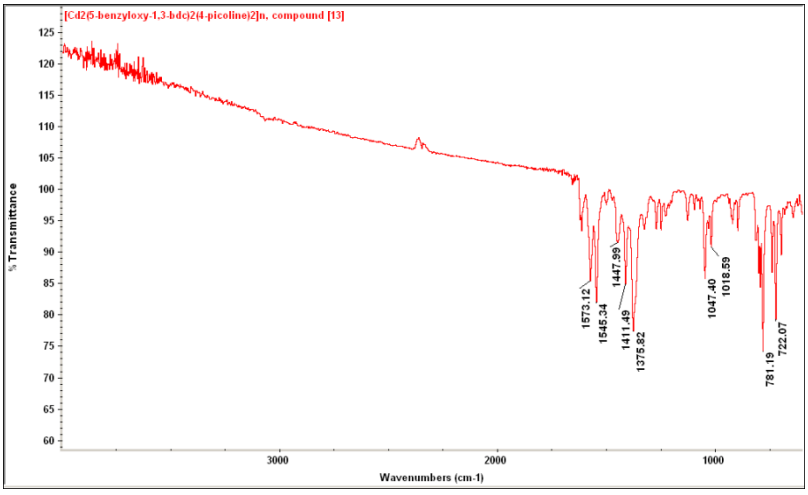

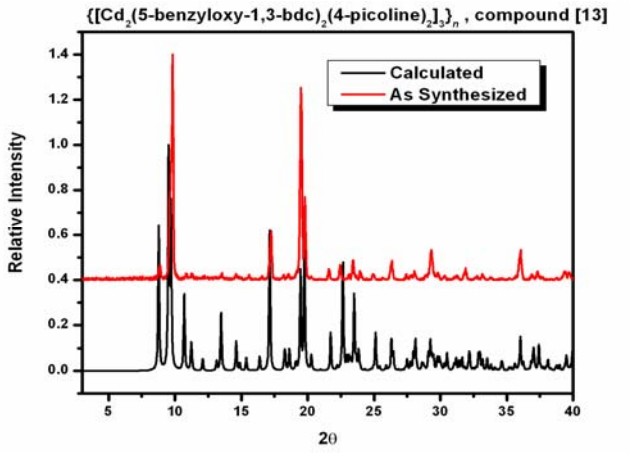

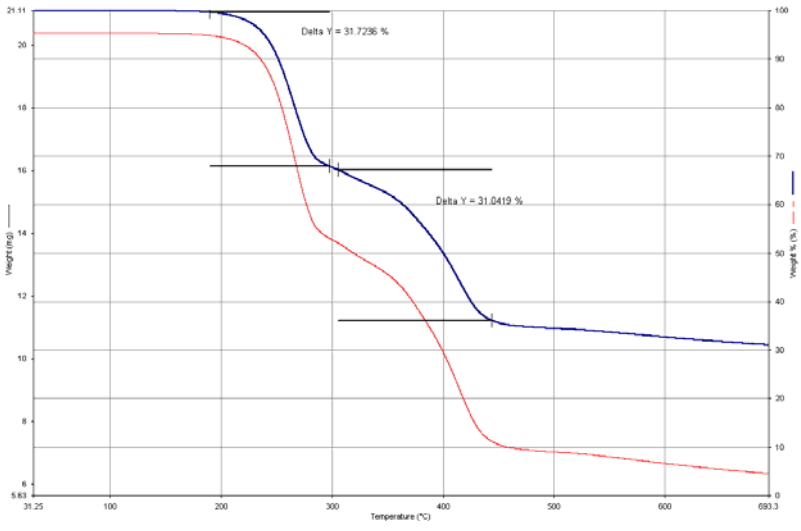

Appendix B-19. Experimental data for compound [14].

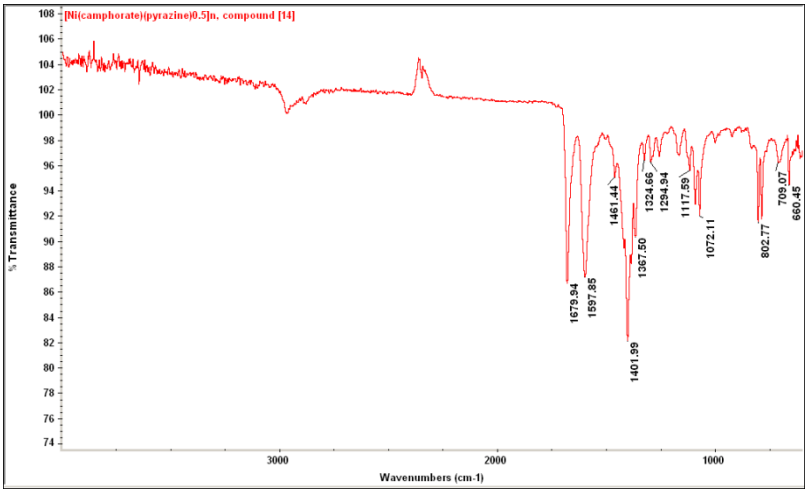

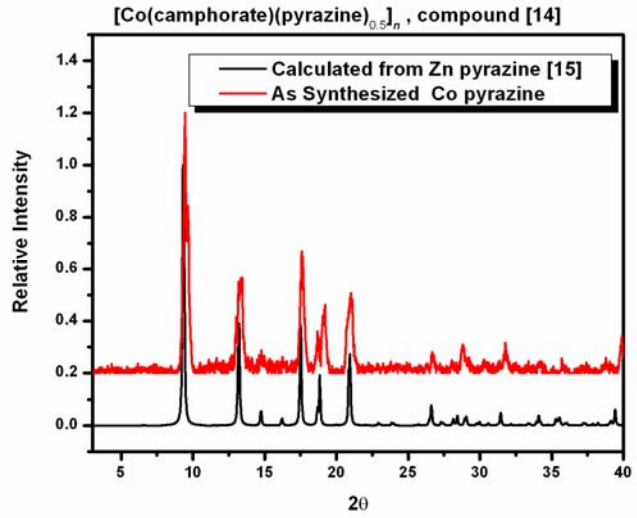

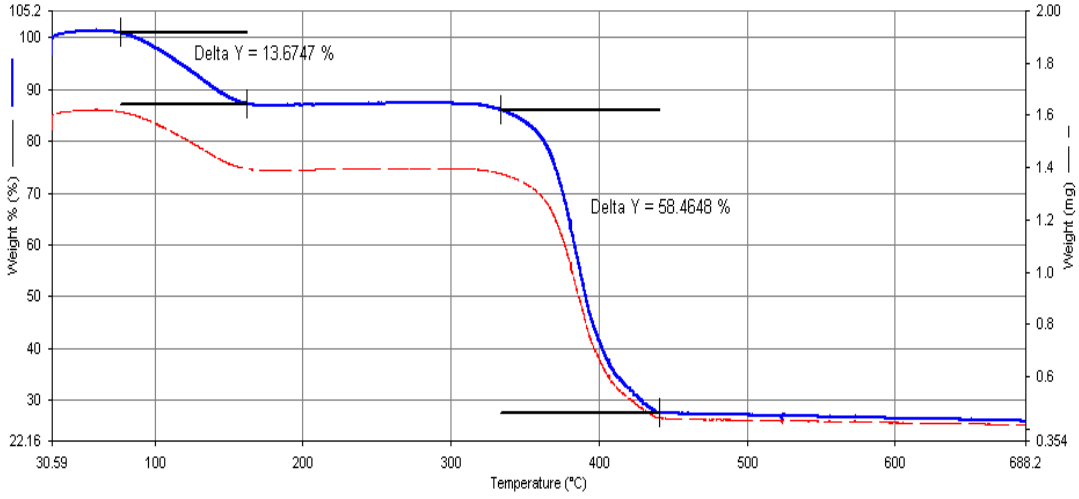

Appendix B-20. Experimental data for compound [15].

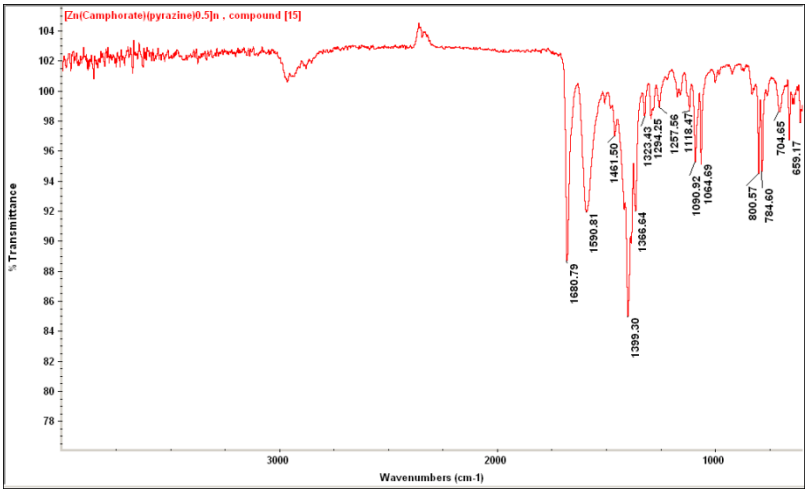

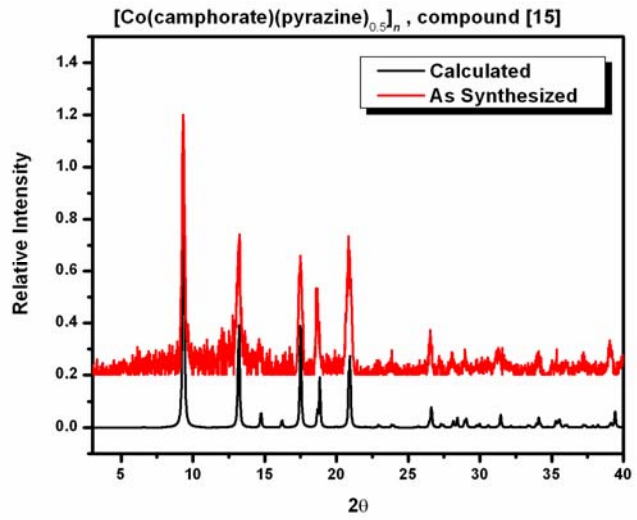

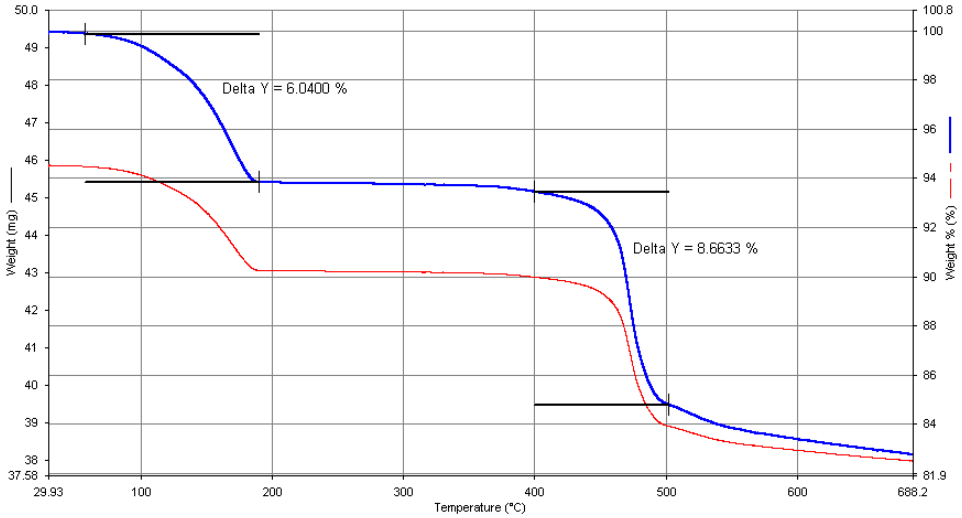

Appendix B-21. Experimental data for compound [16].

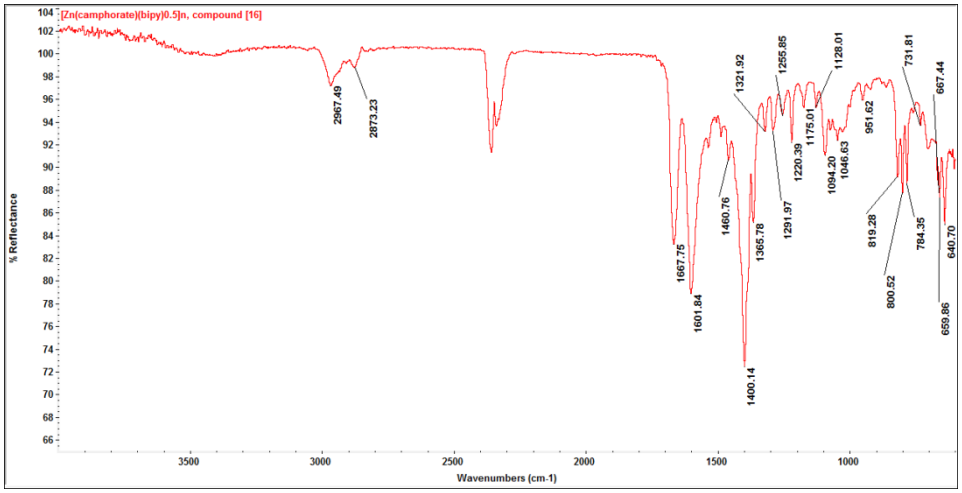

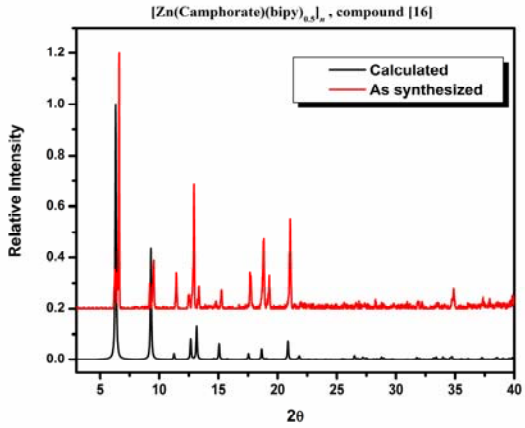

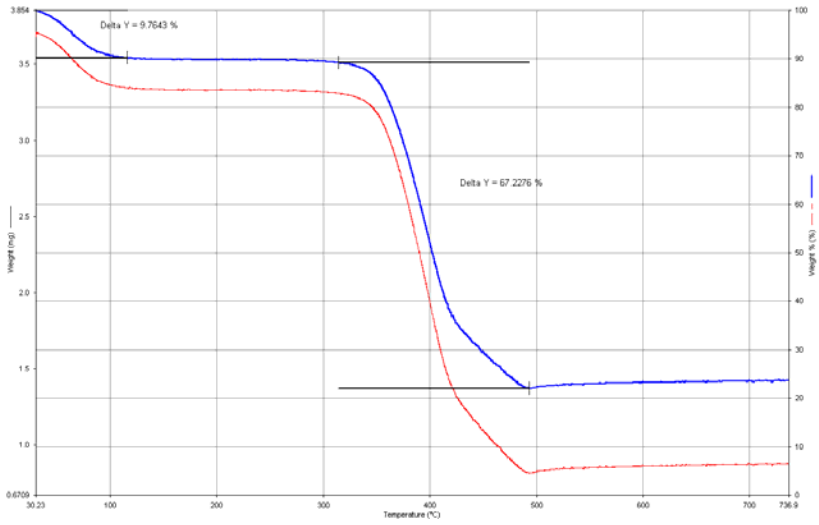

Appendix B-22. Experimental data for compound [17].

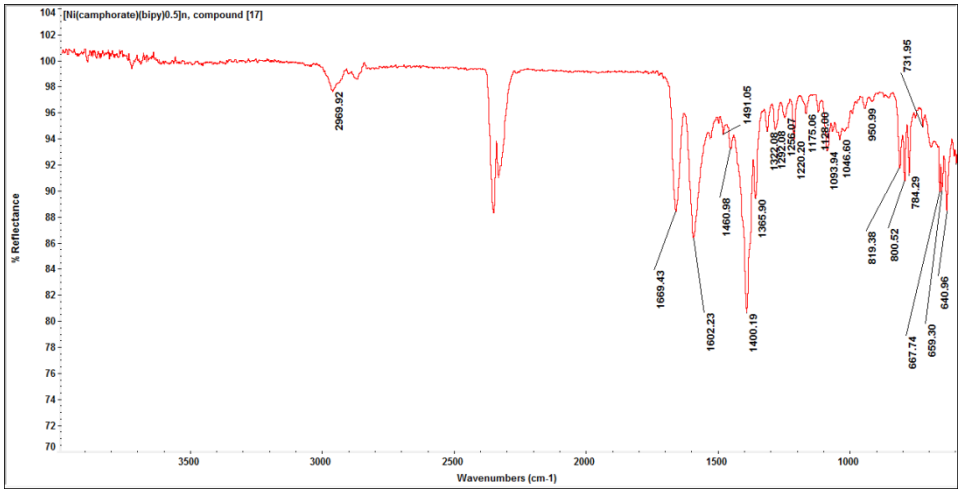

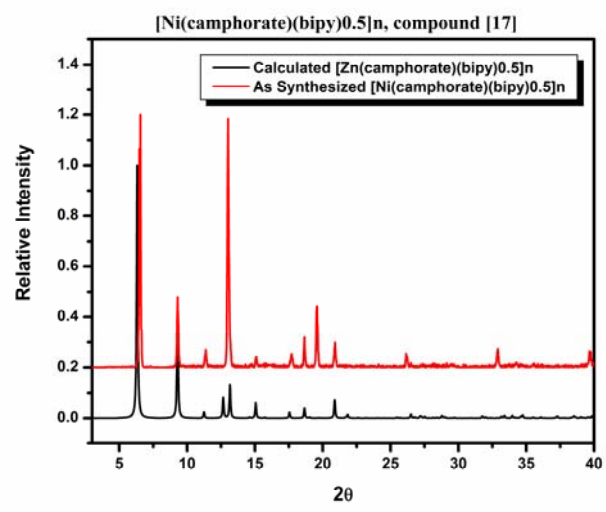

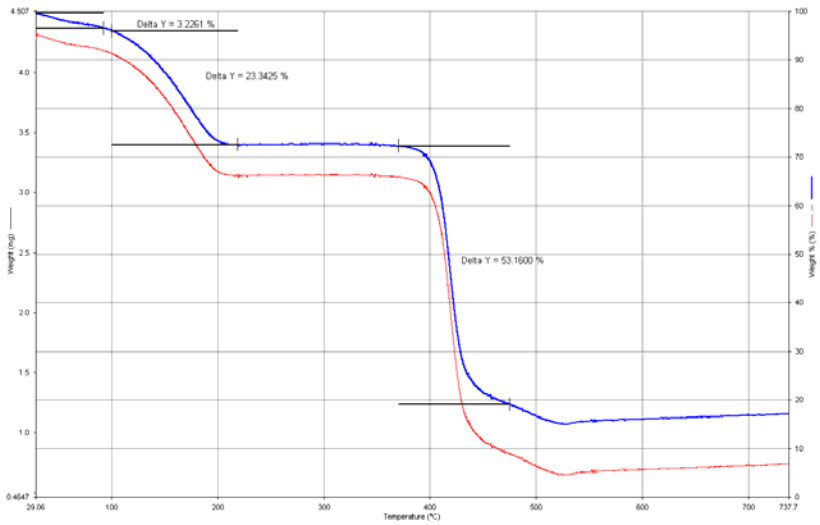

Appendix B-23. Experimental data for compound [18].

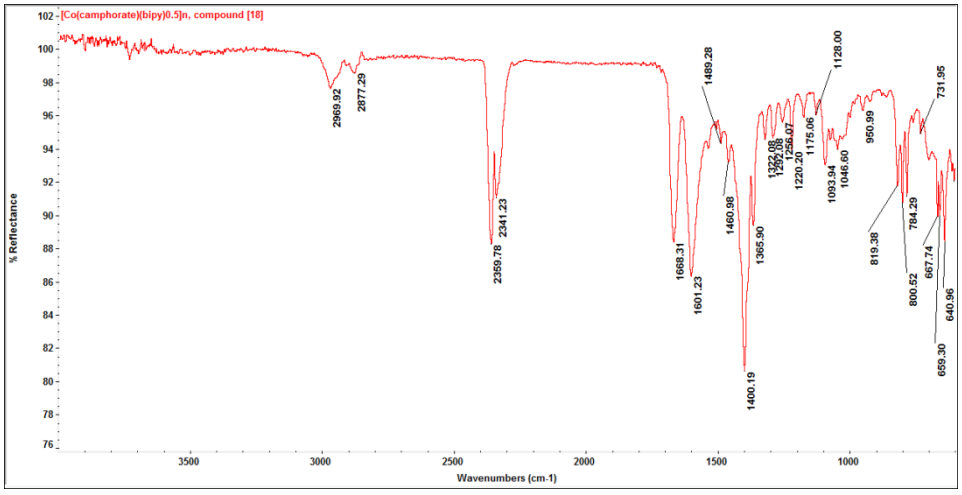

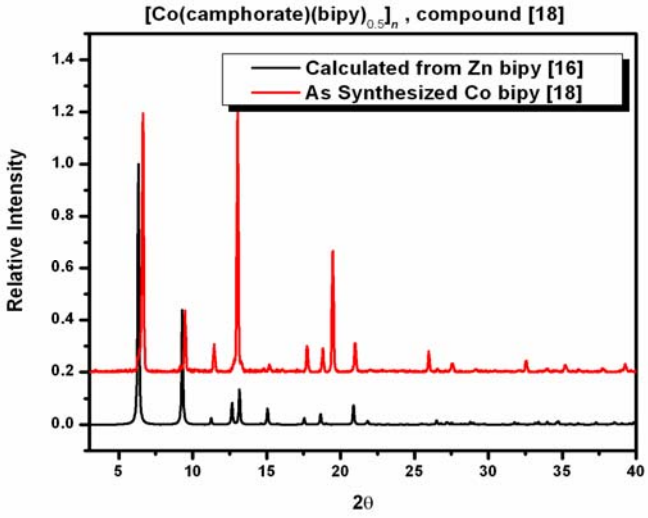

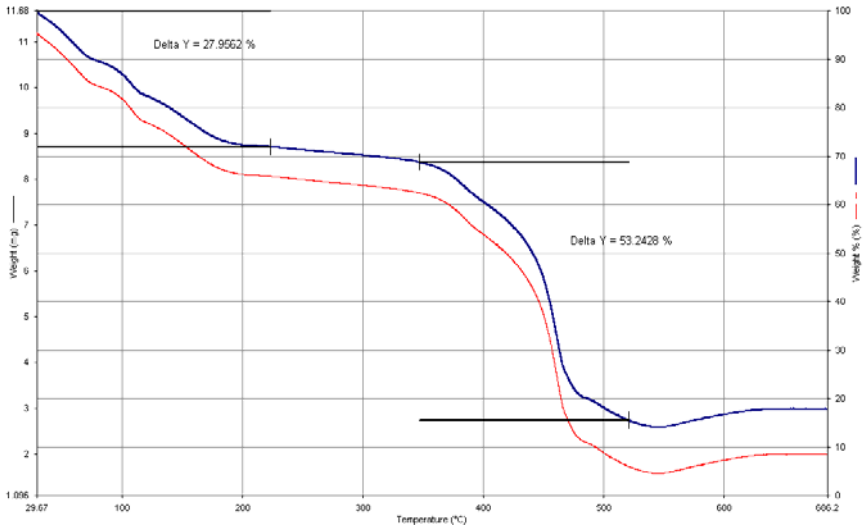

Appendix B-24. Experimental data for compound [19].

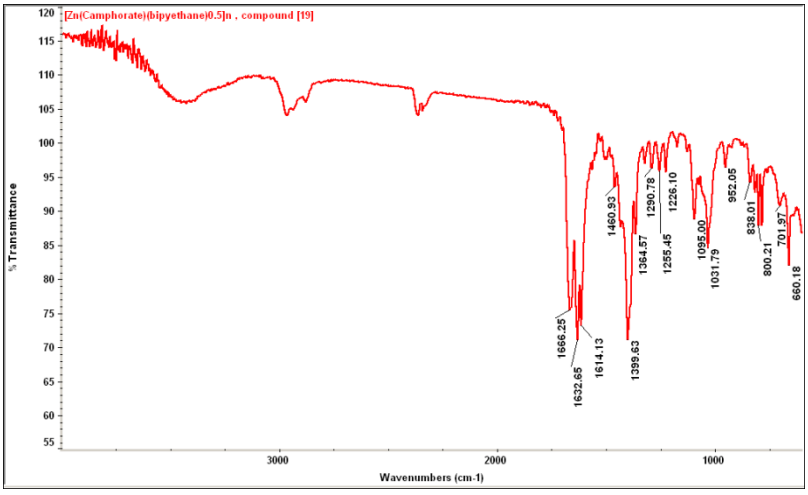

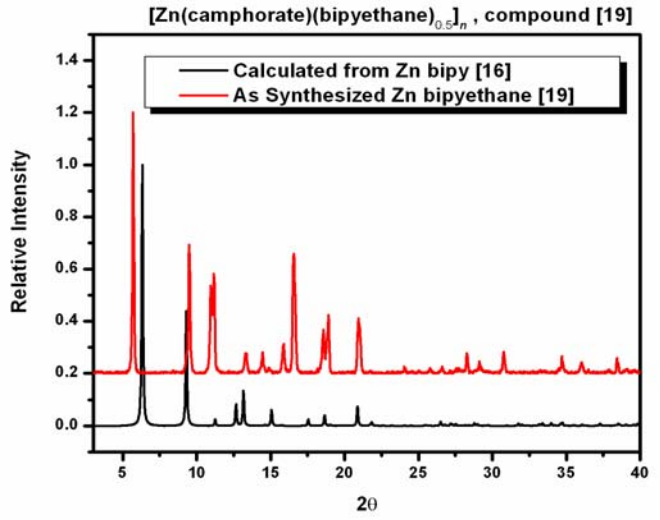

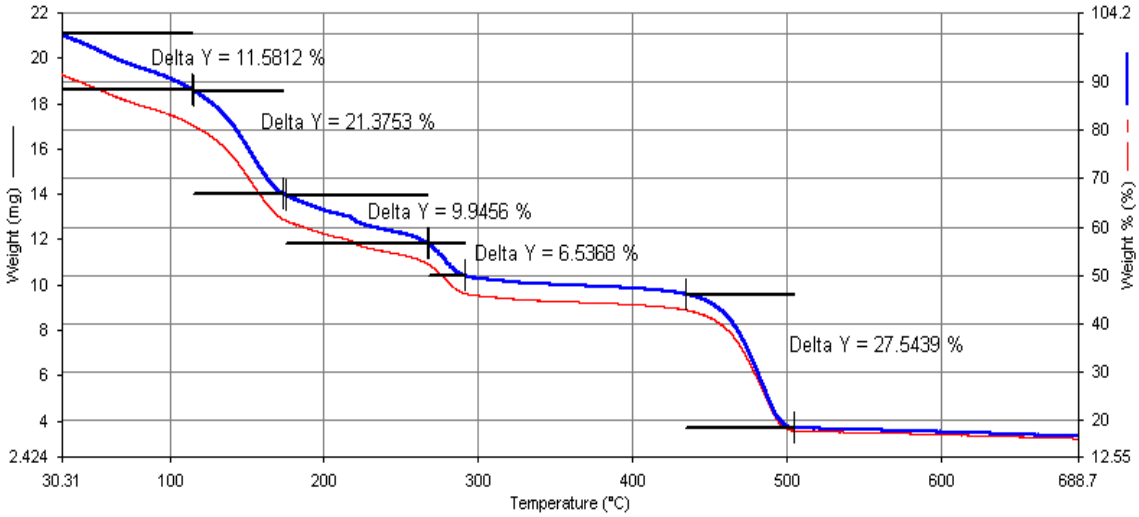

Appendix B-25. Experimental data for compound [20].

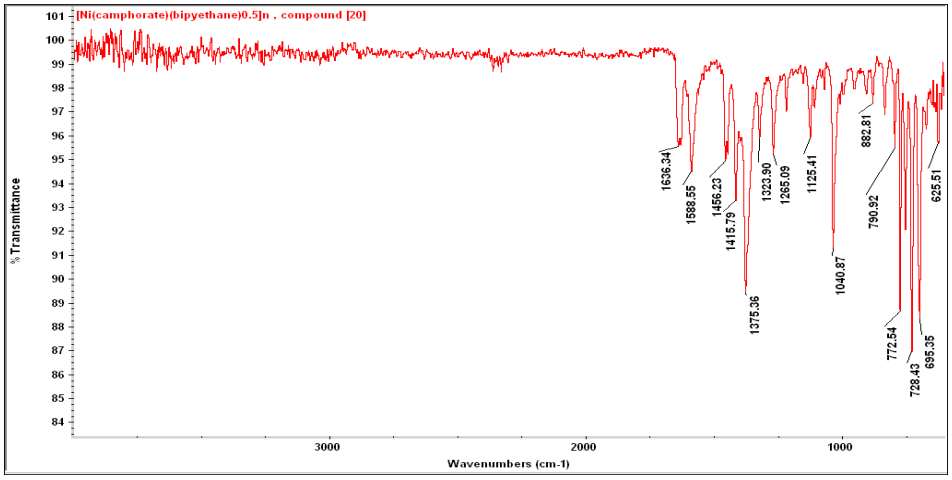

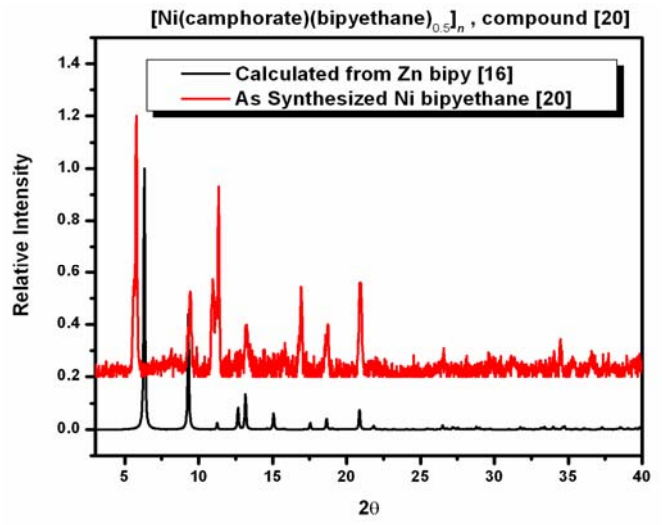

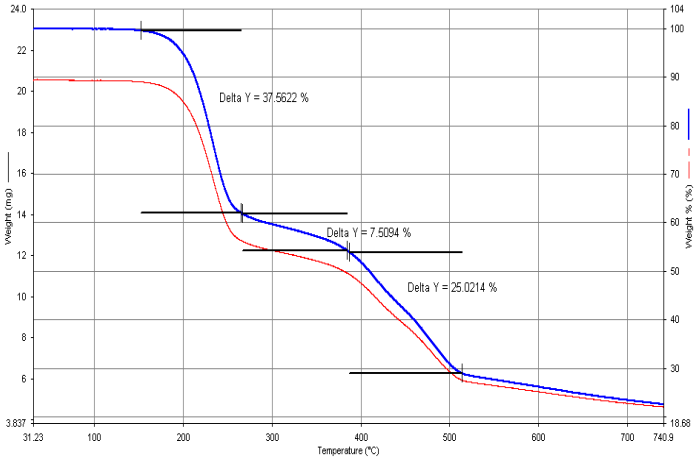

Appendix B-26. Experimental data for compound [21].

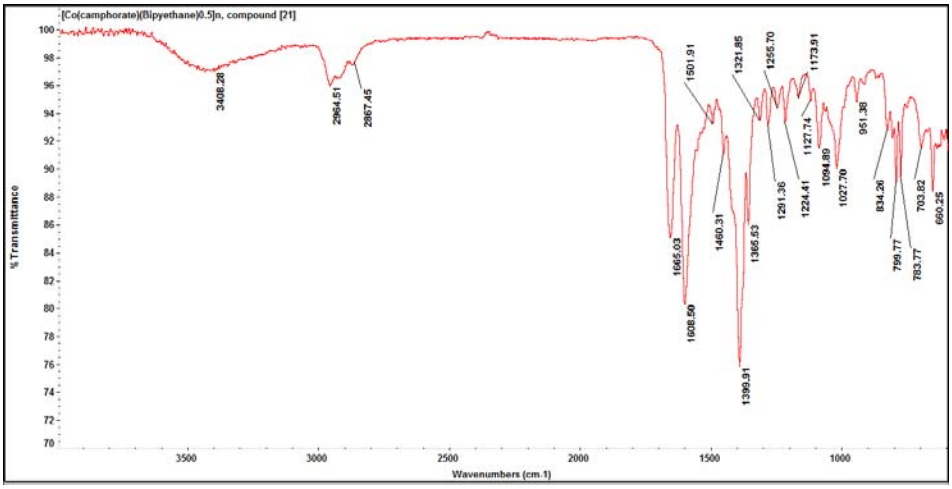

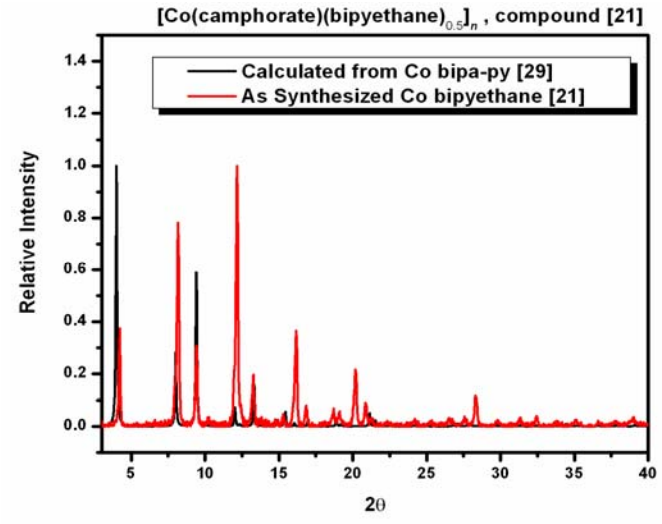

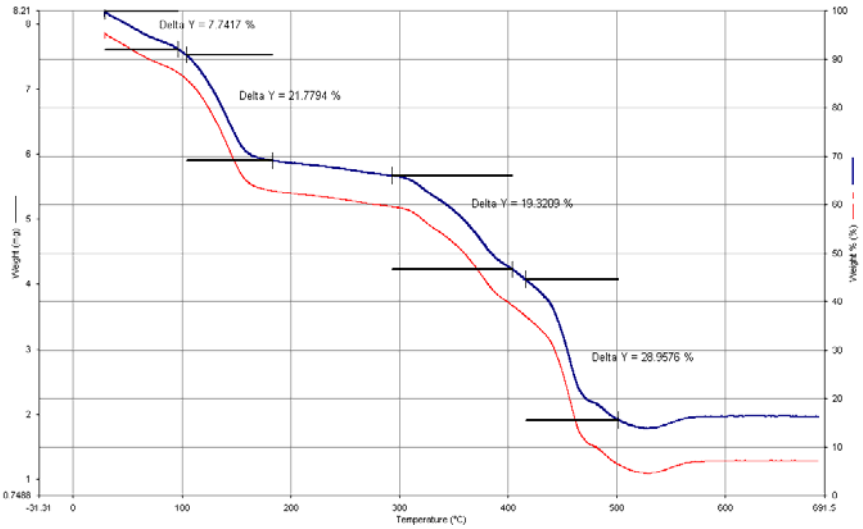

Appendix B-27. Experimental data for compound [22].

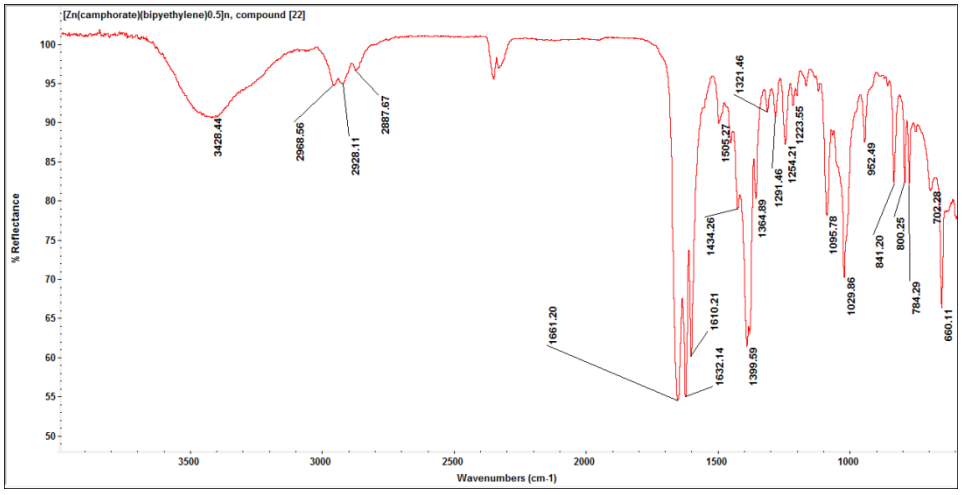

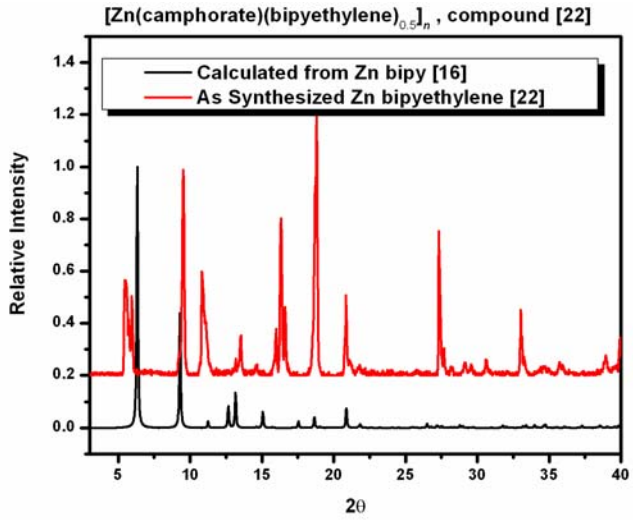

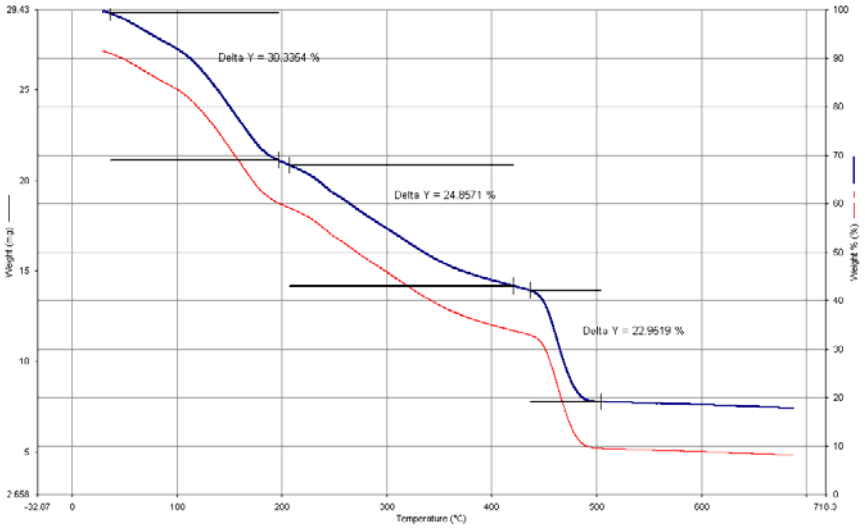

Appendix B-28. Experimental data for compound [23].

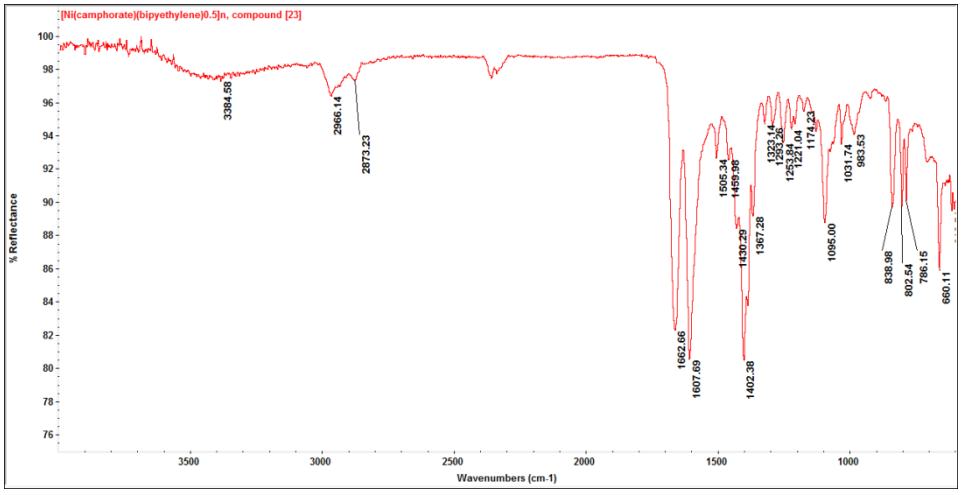

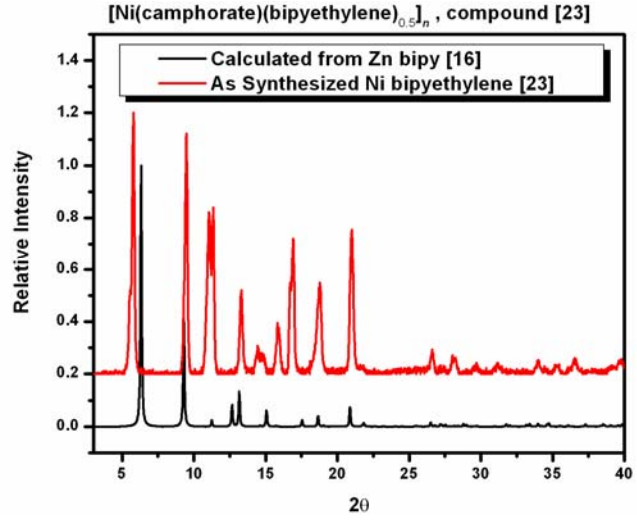

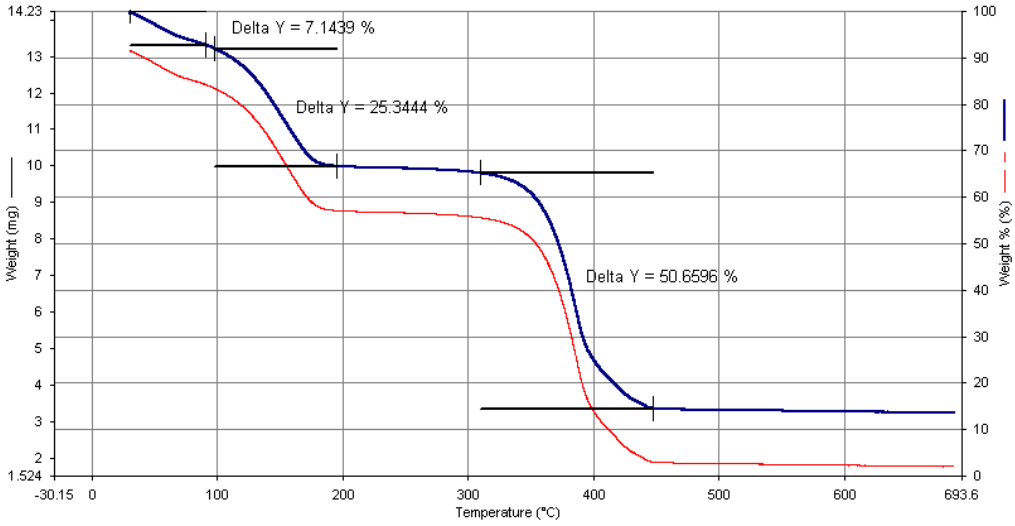

Appendix B-29. Experimental data for compound [24].

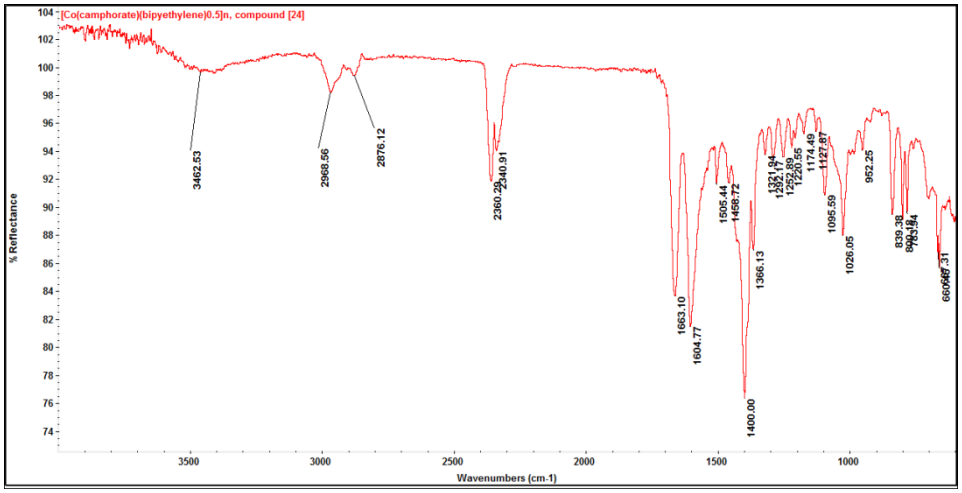

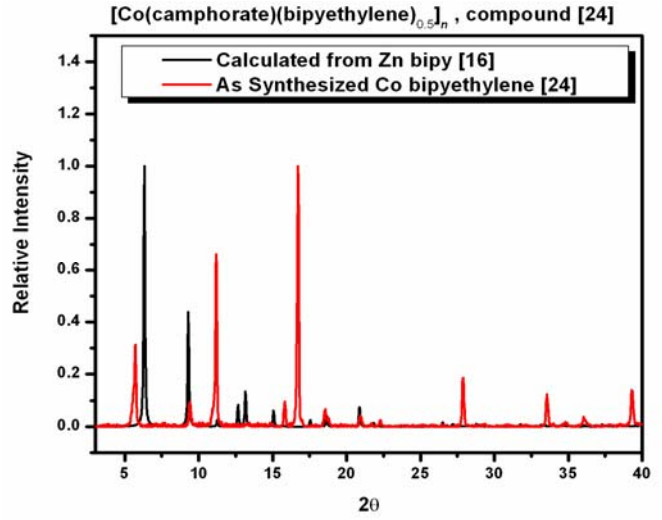

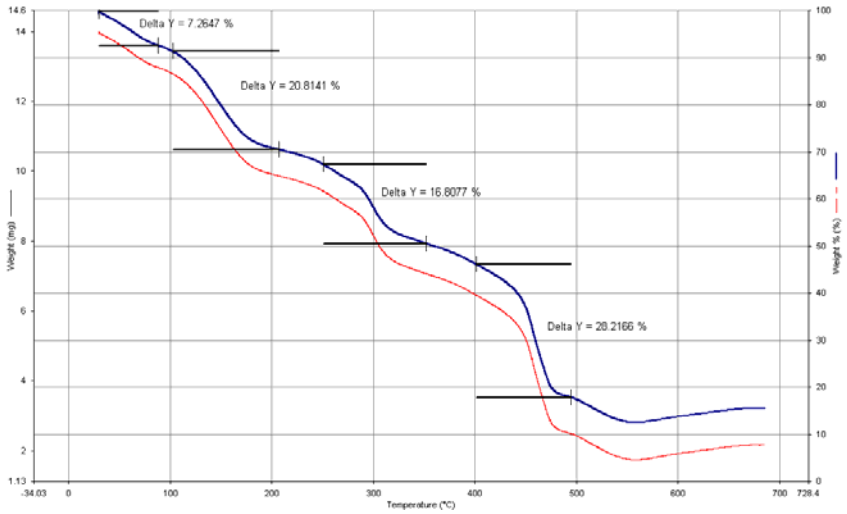

Appendix B-30. Experimental data for compound [25].

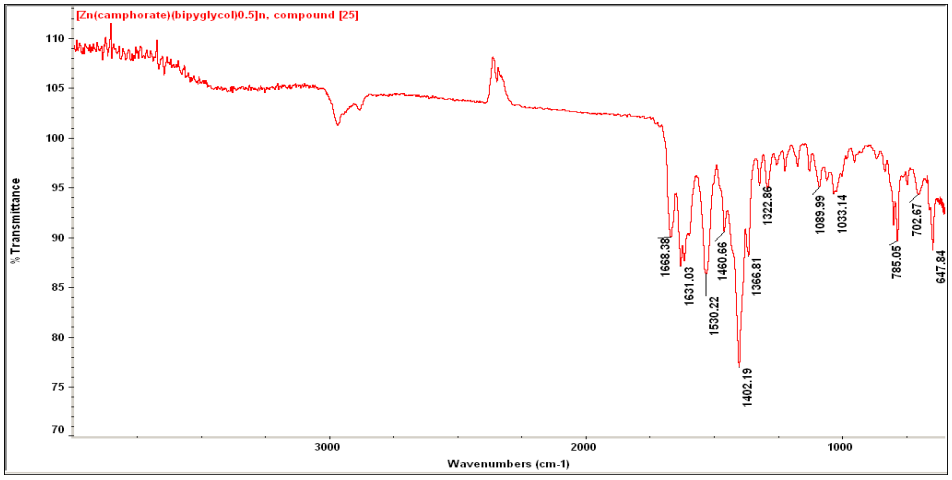

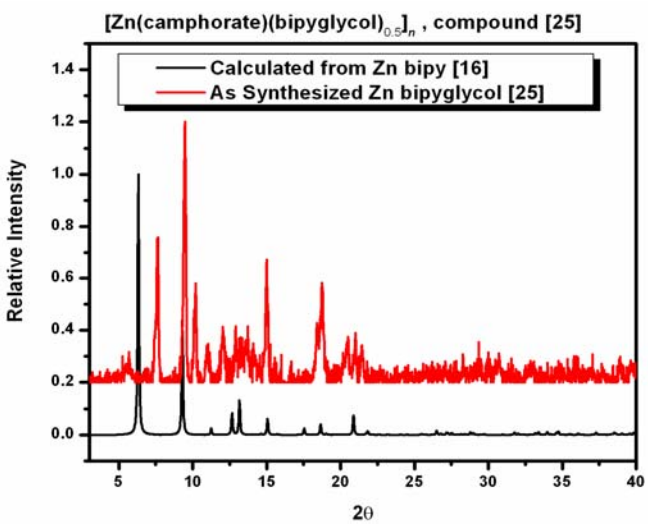

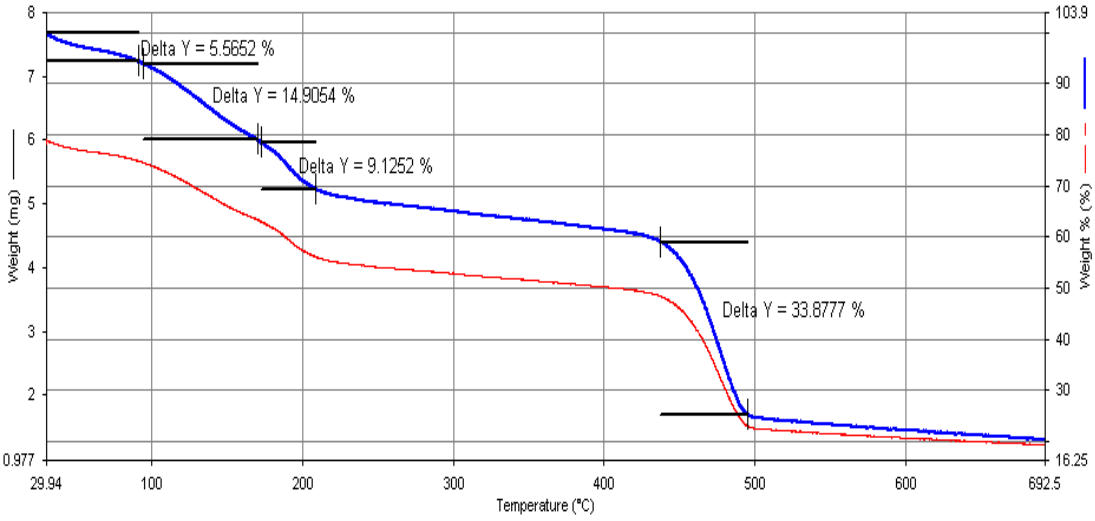

Appendix B-31. Experimental data for compound [26].

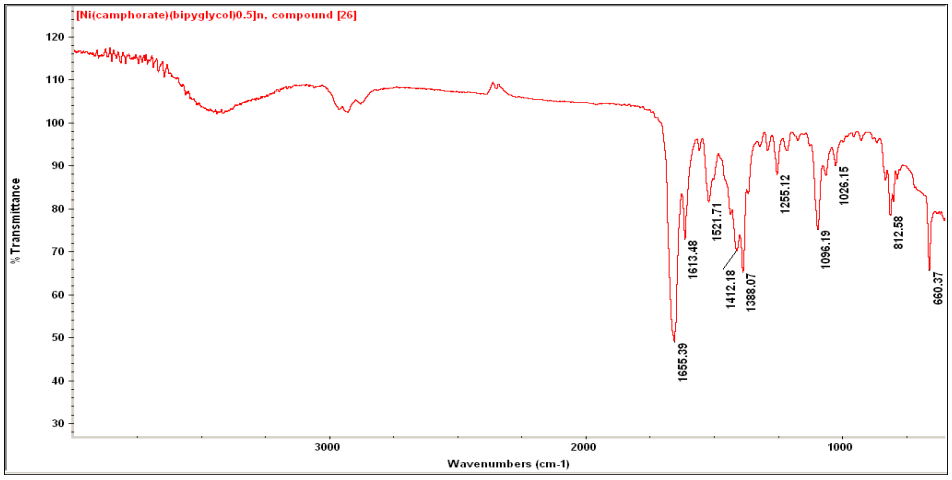

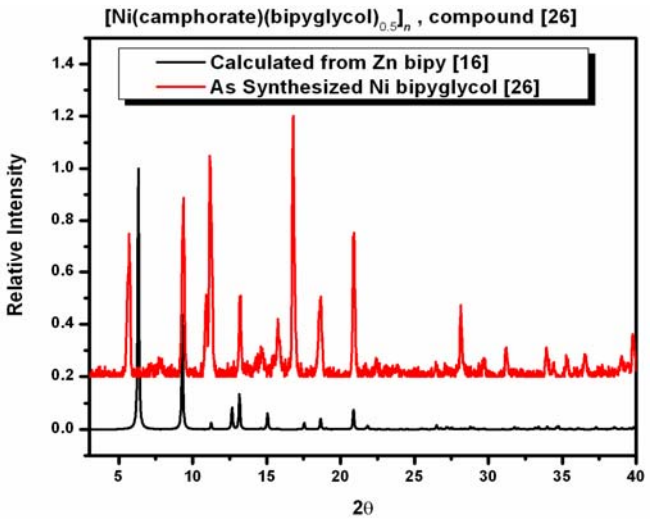

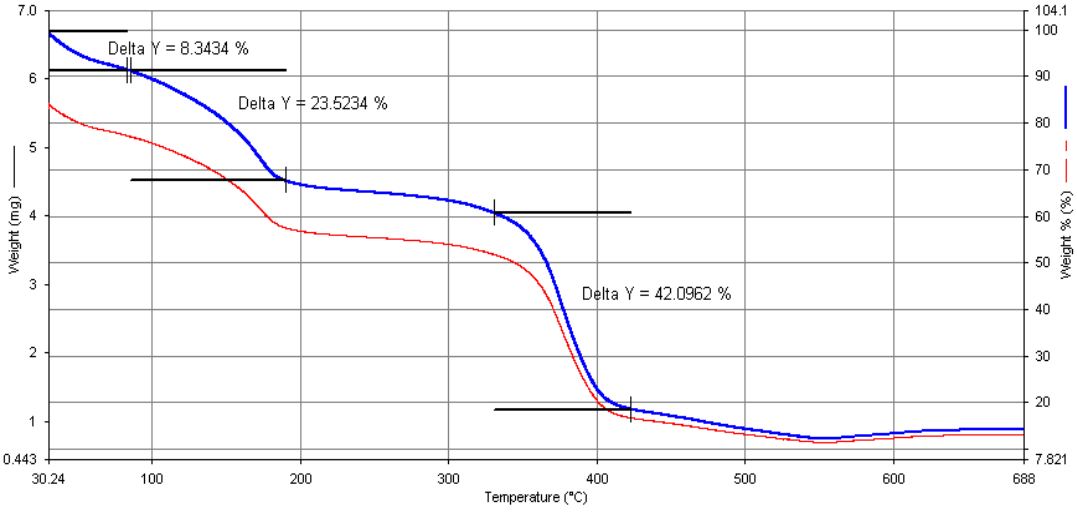

Appendix B-32. Experimental data for compound [27].

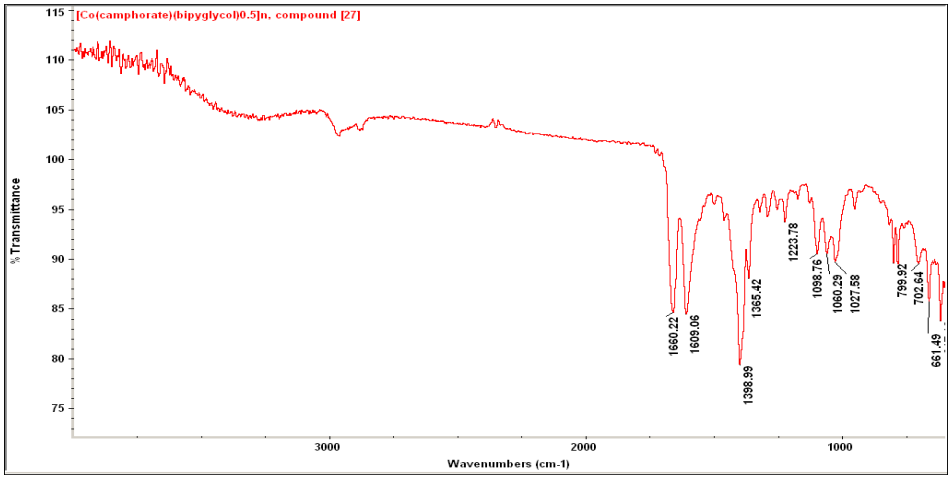

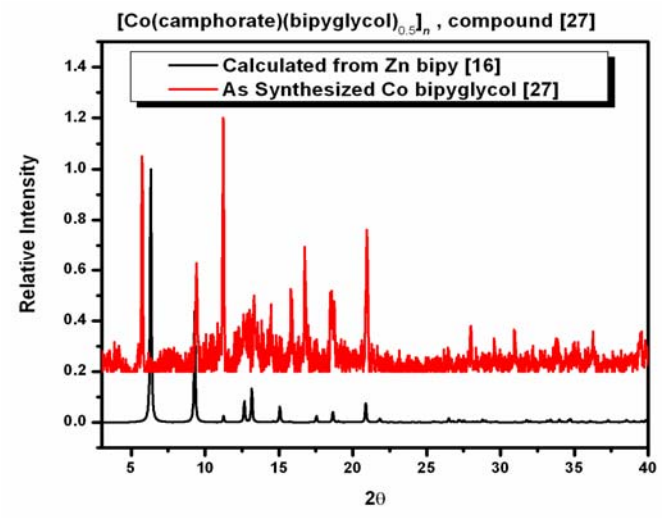

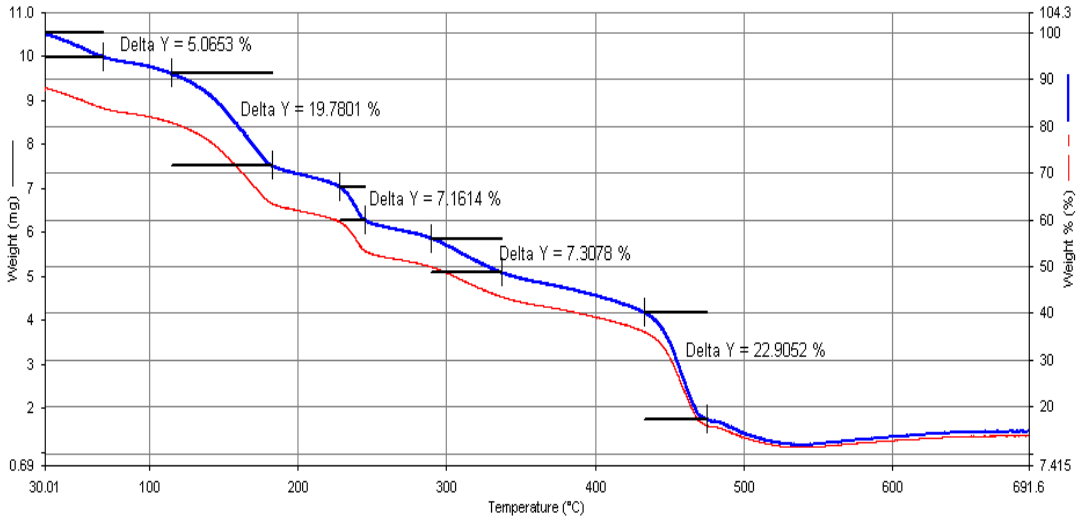

Appendix B-33. Experimental data for compound [28].

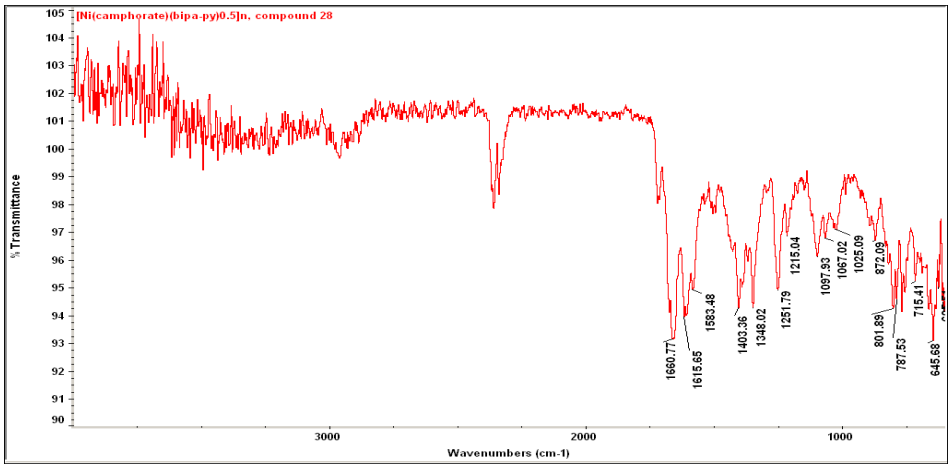

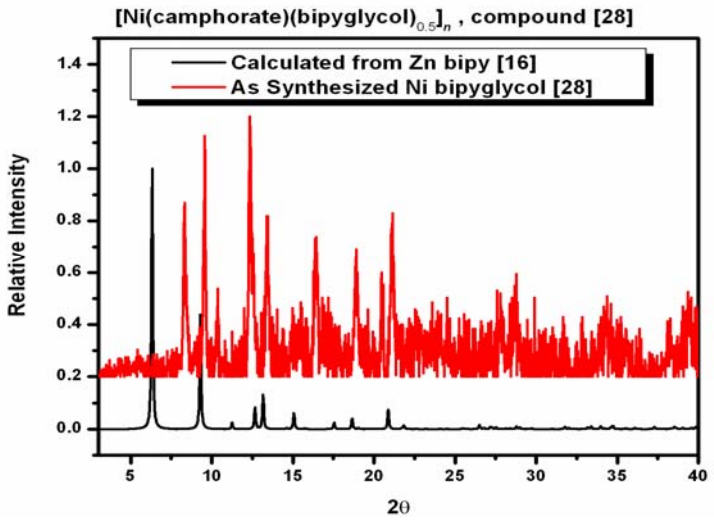

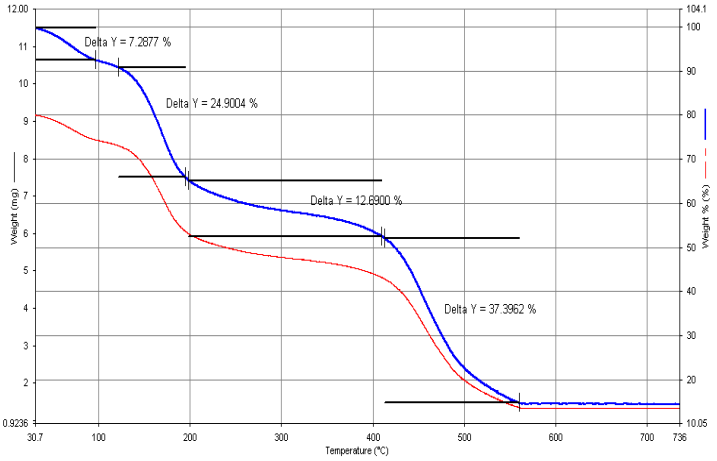

Appendix B-34. Experimental data for compound [29].

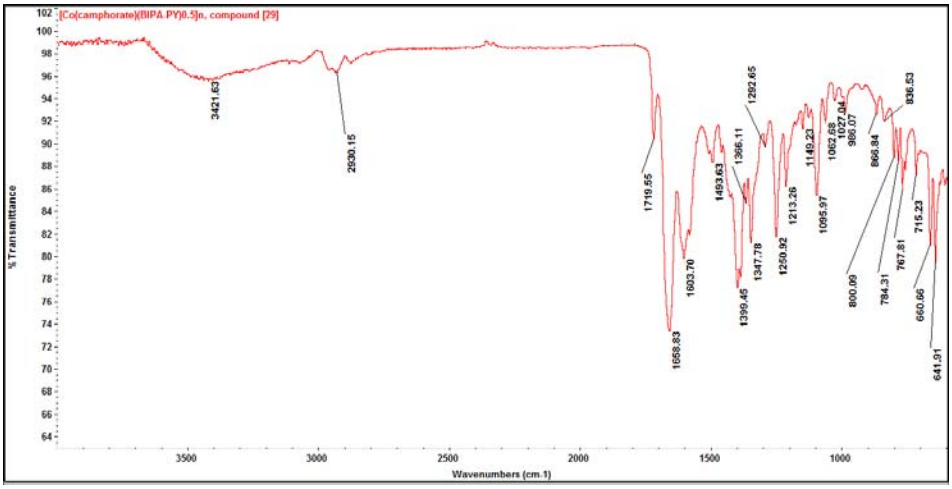

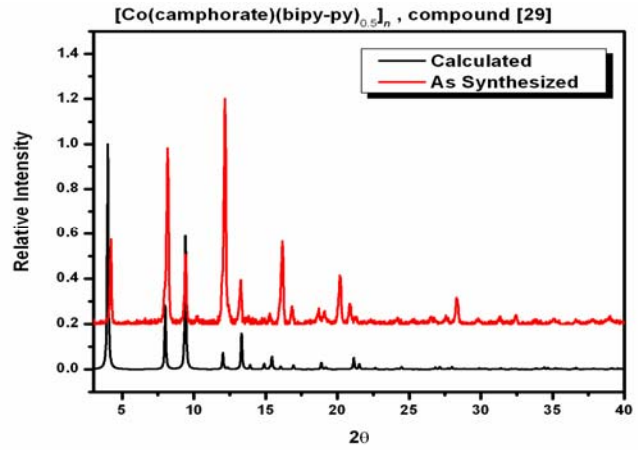

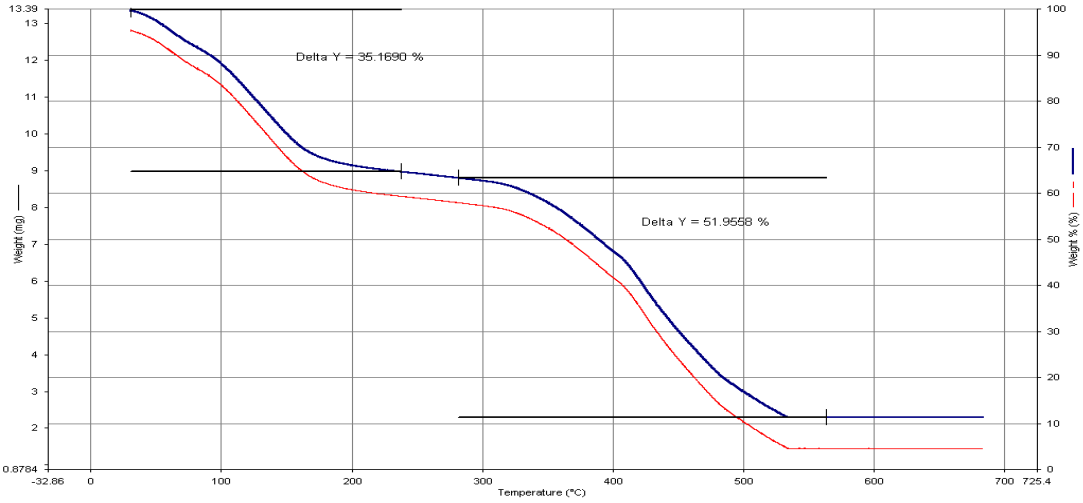

Appendix B-35. Experimental data for compound [30].

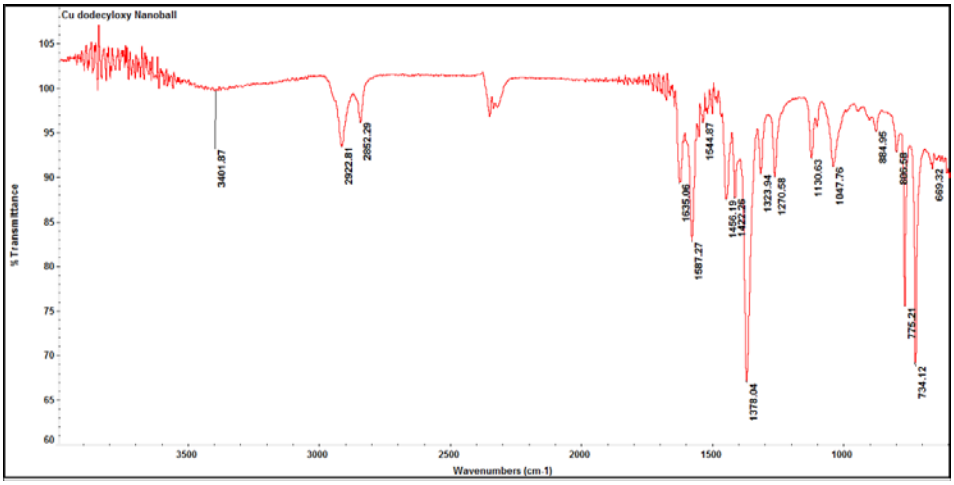

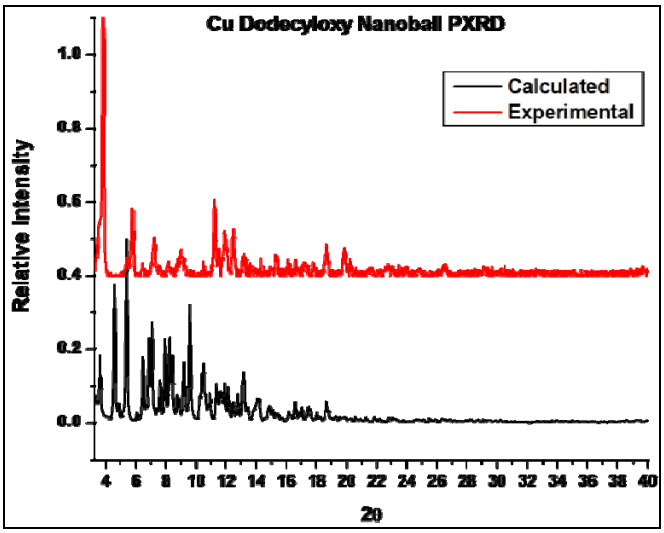

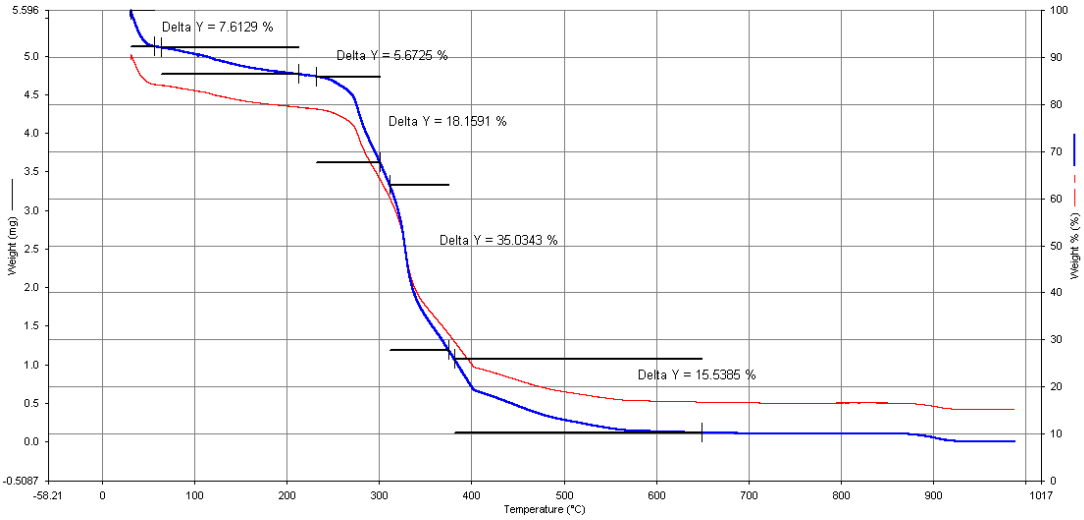

Appendix B-36. Experimental data for compound [31].

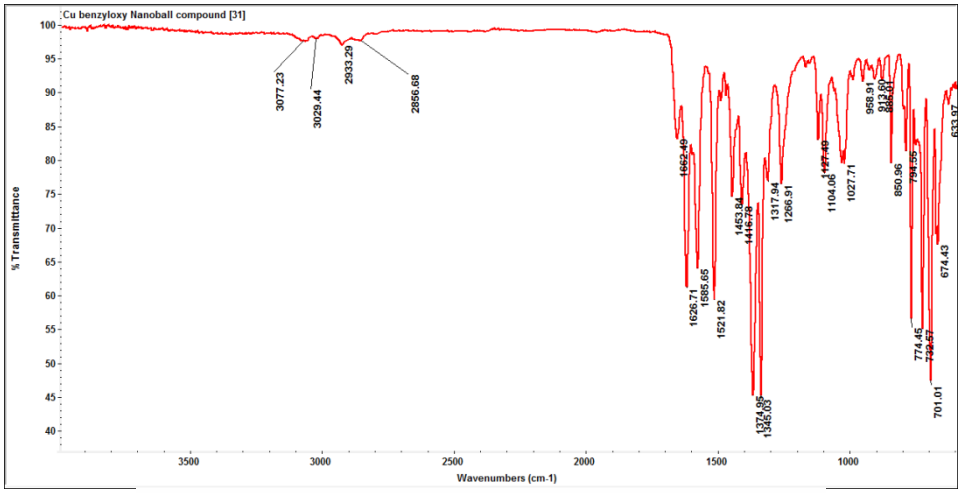

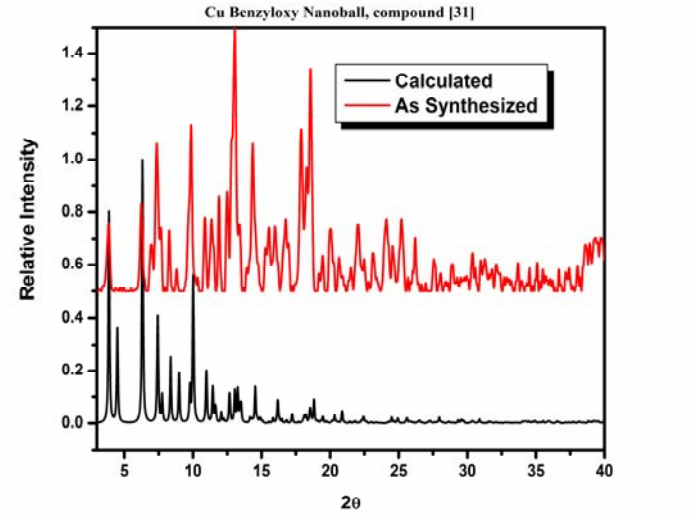

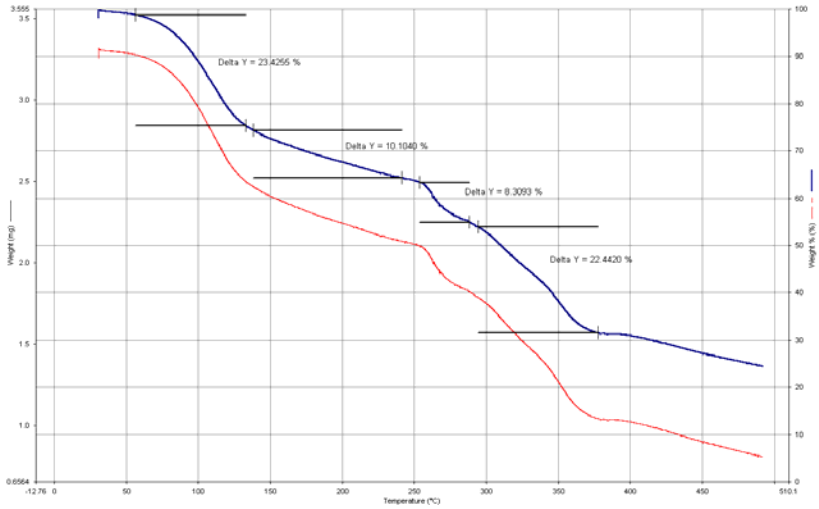

Appendix B-37. Experimental data for compound [32].

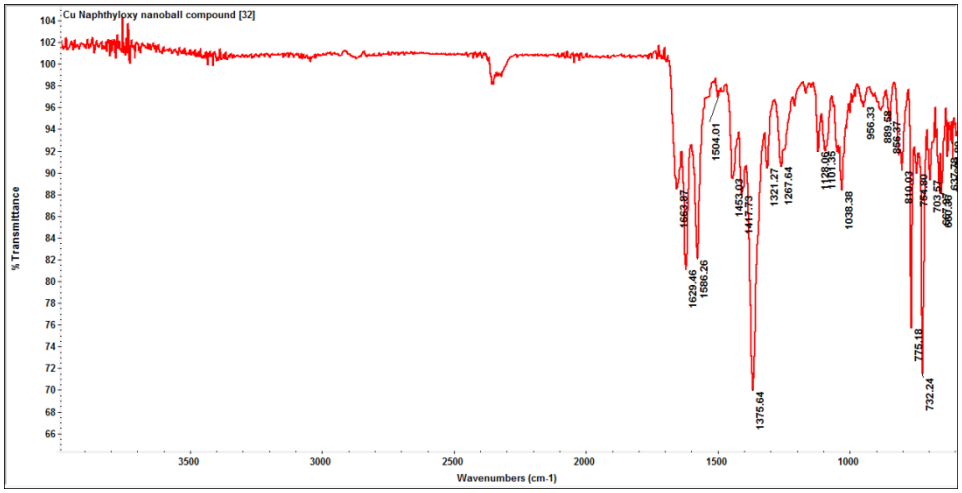

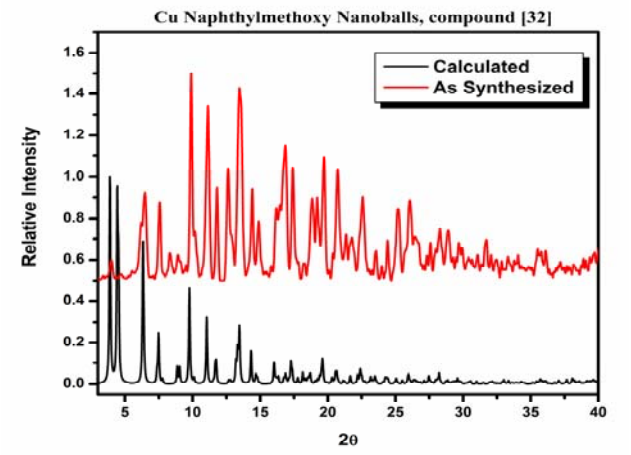

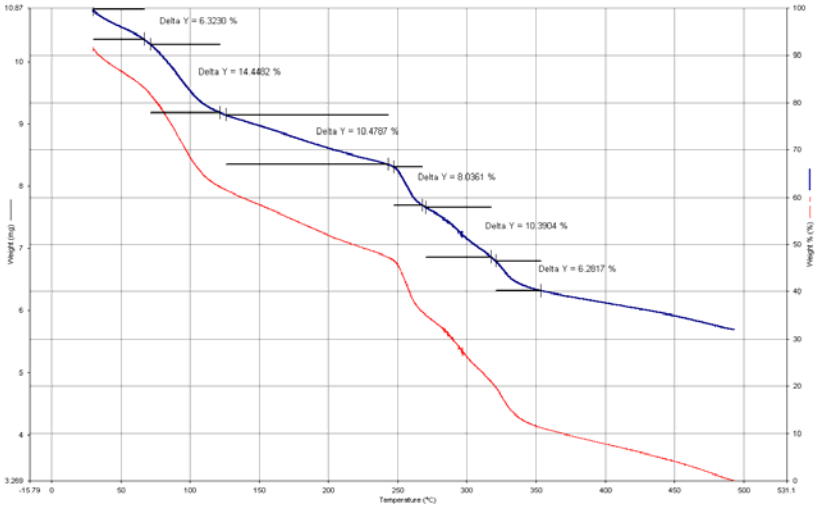

Appendix B-38. Experimental data for compound [33].

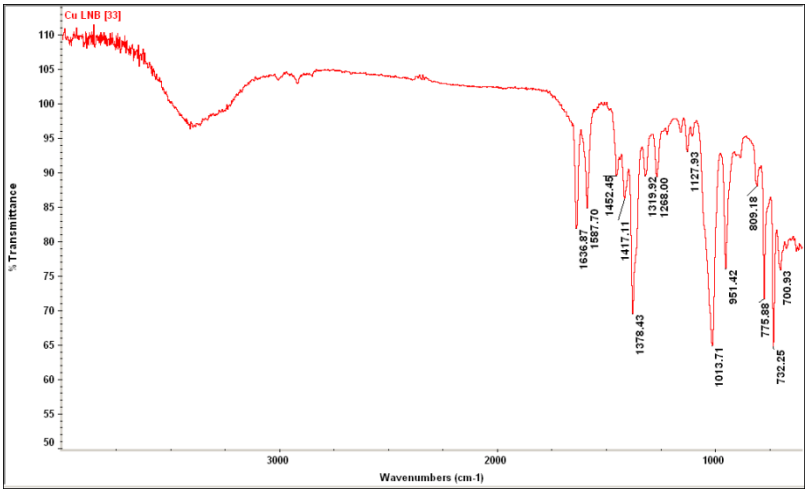

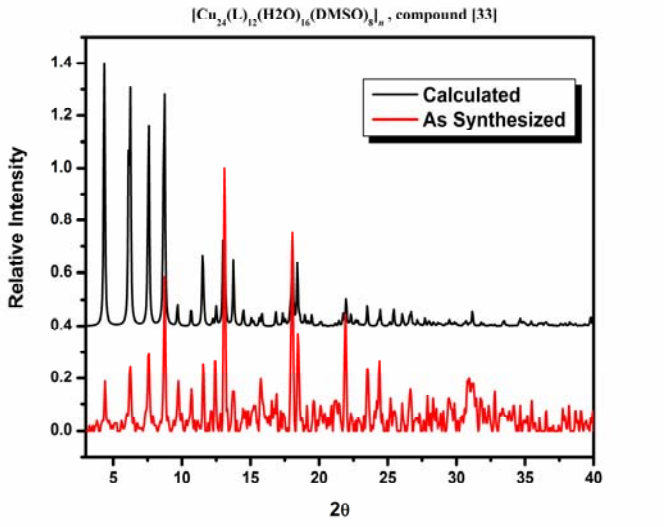

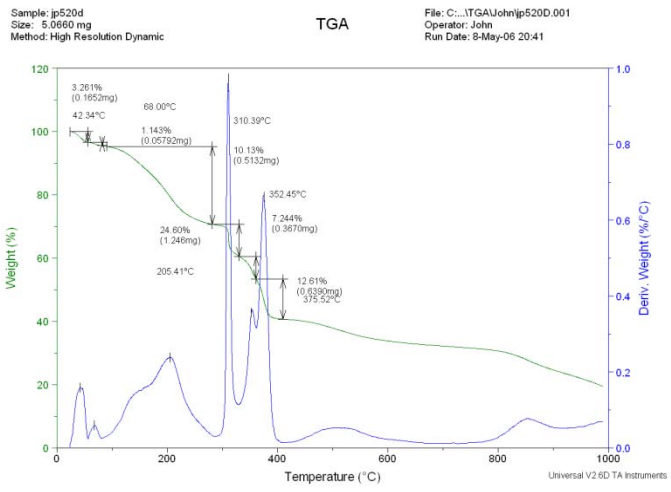

Appendix B-39. Experimental data for compound [34].

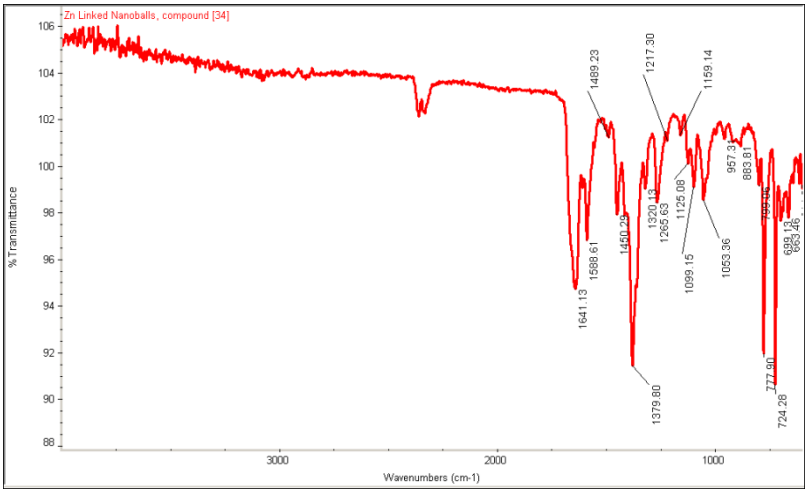

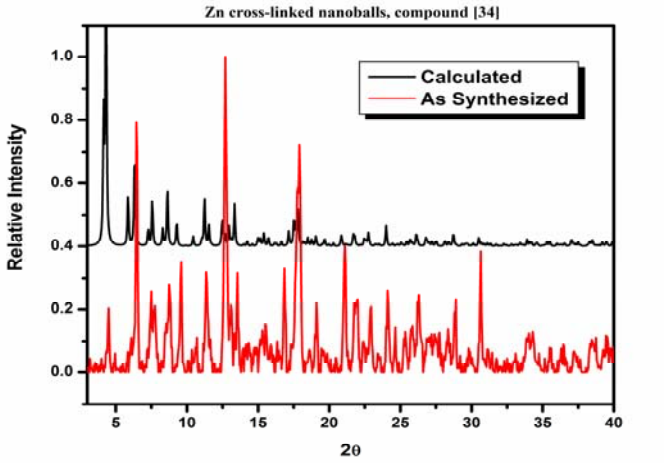

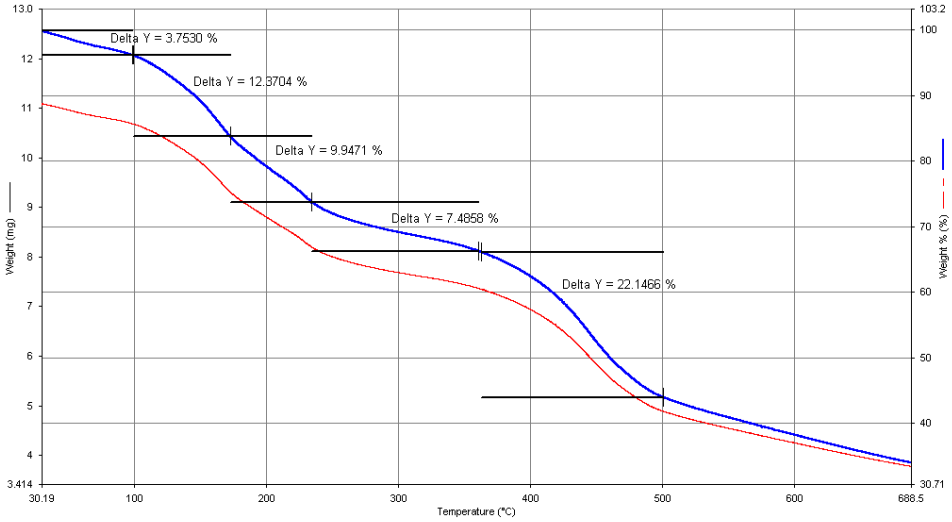

Appendix C. Crystal data and structure refinement for select compounds.

Appendix C-1. Crystal data and structure refinement for compound [1].

Empirical formula	C40 H30 Cu2 N2 O10	
Formula weight	825.74	
Temperature	100(2) K	
Wavelength	0.71073 Å	
Crystal system	Trigonal	
Space group	P-3	
Unit cell dimensions	a = 18.4013(8) Å	α = 90°.
	b = 18.4013(8) Å	β = 90°.
	c = 9.6305(9) Å	γ = 120°.
Volume	2824.1(3) $Å^3$	
Z	3	
Density (calculated)	1.457 Mg/m^3	
Absorption coefficient	1.190 mm^{-1}	
F(000)	1266	
Crystal size	0.20 x 0.15 x 0.05 mm^3	
Theta range for data collection	1.28 to 28.30°	
Index ranges	-23<=h<=22, -24<=k<=23, -12<=l<=8	
Reflections collected	18160	
Independent reflections	4496 [R(int) = 0.0411]	
Completeness to theta = 28.30°	95.6 %	
Absorption correction	multi-scan	
Max. and min. transmission	1.00000 and 0.783850	
Refinement method	Full-matrix least-squares on F^2	
Data / restraints / parameters	4496 / 0 / 256	
Goodness-of-fit on F^2	1.136	
Final R indices [I>2sigma(I)]	R1 = 0.0421, wR2 = 0.0970	
R indices (all data)	R1 = 0.0546, wR2 = 0.1094	

Appendix C-2. Crystal data and structure refinement for compound [2].

Empirical formula	$C_{42}H_{30}N_2O_{12}Zn_2$	
Formula weight	885.42	
Temperature	100(2) K	
Wavelength	0.71073 Å	
Crystal system	Trigonal	
Space group	P-3	
Unit cell dimensions	a = 18.476(3) Å	α = 90°.
	b = 18.476(3) Å	β = 90°.
	c = 9.528(3) Å	γ = 120°.
Volume	2817.0(10) $Å^3$	
Z	3	
Density (calculated)	1.566 Mg/m^3	
Absorption coefficient	1.347 mm^{-1}	
F(000)	1356	
Crystal size	0.15 x 0.08 x 0.0 mm^3	
Theta range for data collection	1.27 to 25.03°	
Index ranges	-10<=h<=21, -21<=k<=10, -11<=l<=11	
Reflections collected	8186	
Independent reflections	3282 [R(int) = 0.2151]	
Completeness to theta = 25.03°	98.2 %	
Absorption correction	multi-scan	
Max. and min. transmission	1.0000 and 0.252832	
Refinement method	Full-matrix least-squares on F^2	
Data / restraints / parameters	3282 / 0 / 256	
Goodness-of-fit on F^2	1.028	
Final R indices [I>2sigma(I)]	R1 = 0.1335, wR2 = 0.3249	
R indices (all data)	R1 = 0.1958, wR2 = 0.3701	

Appendix C-3. Crystal data and structure refinement for compound [3].

Empirical formula	C42 H6 N2 O12 Cu2	
Formula weight	860.57	
Temperature	100(2) K	
Wavelength	0.71073 Å	
Crystal system	Trigonal	
Space group	P-3	
Unit cell dimensions	a = 18.8401(14) Å	α = 90°.
	b = 18.8401(14) Å	β = 90°.
	c = 11.2040 (18) Å	γ = 120°.
Volume	3405.7(3) $Å^3$	
Z	3	
Density (calculated)	1.437 Mg/m^3	
Absorption coefficient	1.088 mm^{-1}	
F(000)	1285	
Crystal size	0.20 x 0.15 x 0.05 mm^3	
Theta range for data collection	1.24 to 25.30°	
Index ranges	-22<=h<=22, -19<=k<=22, -13<=l<=11	
Reflections collected	18364	
Independent reflections	3967 [R(int) = 0.0541]	
Completeness to theta = 26.30°	97.6 %	
Absorption correction	multi-scan	
Max. and min. transmission	1.00000 and 0.753650	
Refinement method	Full-matrix least-squares on F^2	
Data / restraints / parameters	3068 / 0 / 315	
Goodness-of-fit on F^2	1.536	
Final R indices [I>2sigma(I)]	R1 = 0.1321, wR2 = 0.2670	
R indices (all data)	R1 = 0.1546, wR2 = 0.2894	

Appendix C-4. Crystal data and structure refinement for compound [4].

Empirical formula	C42 H6 N2 O12 Zn2	
Formula weight	861.23	
Temperature	100(2) K	
Wavelength	0.71073 Å	
Crystal system	Trigonal	
Space group	P-3	
Unit cell dimensions	a = 18.8852(16) Å	α = 90°.
	b = 18.8852(16) Å	β = 90°.
	c = 11.1751(11) Å	γ = 120°.
Volume	3451.6(5) $Å^3$	
Z	3	
Density (calculated)	1.243 Mg/m^3	
Absorption coefficient	1.098 mm^{-1}	
F(000)	1284	
Crystal size	0.20 x 0.15 x 0.10 mm^3	
Theta range for data collection	1.82 to 25.11°	
Index ranges	-22<=h<=22, -22<=k<=22, -11<=l<=13	
Reflections collected	18331	
Independent reflections	4090 [R(int) = 0.0333]	
Completeness to theta = 25.11°	99.5 %	
Absorption correction	multi-scan	
Max. and min. transmission	1.0000 and 0.645304	
Refinement method	Full-matrix least-squares on F^2	
Data / restraints / parameters	4090 / 0 / 359	
Goodness-of-fit on F^2	1.176	
Final R indices [I>2sigma(I)]	R1 = 0.0813, wR2 = 0.2385	
R indices (all data)	R1 = 0.0892, wR2 = 0.2449	

Appendix C-5. Crystal data and structure refinement for compound [5].

Empirical formula	C48 H34 Cu2 N2 O10	
Formula weight	925.85	
Temperature	100(2) K	
Wavelength	1.54178 Å	
Crystal system	Trigonal	
Space group	P-3	
Unit cell dimensions	a = 18.6078(6) Å	α = 90°.
	b = 18.6078(6) Å	β = 90°.
	c = 12.2129(5) Å	γ = 120°.
Volume	3662.2(2) $Å^3$	
Z	3	
Density (calculated)	1.259 Mg/m^3	
Absorption coefficient	1.529 mm^{-1}	
F(000)	1422	
Crystal size	0.50 x 0.30 x 0.20 mm^3	
Theta range for data collection	2.74 to 67.82°	
Index ranges	-19<=h<=20, -22<=k<=16, -14<=l<=13	
Reflections collected	14420	
Independent reflections	4235 [R(int) = 0.0801]	
Completeness to theta = 67.82°	95.3 %	
Absorption correction	multi-scan	
Max. and min. transmission	0.7496 and 0.5153	
Refinement method	Full-matrix least-squares on F^2	
Data / restraints / parameters	4235 / 0 / 281	
Goodness-of-fit on F^2	0.933	
Final R indices [I>2sigma(I)]	R1 = 0.0791, wR2 = 0.2004	
R indices (all data)	R1 = 0.1126, wR2 = 0.2193	

Appendix C-6. Crystal data and structure refinement for compound [6].

Empirical formula	C58 H34 N2 O12 Zn2	
Formula weight	1081.61	
Temperature	100(2) K	
Wavelength	0.71073 Å	
Crystal system	Trigonal	
Space group	P-3	
Unit cell dimensions	a = 18.7097(12) Å	α = 90°.
	b = 18.7097(12) Å	β = 90°.
	c = 12.1704(11) Å	γ = 120°.
Volume	3689.5(5) $Å^3$	
Z	3	
Density (calculated)	1.460 Mg/m^3	
Absorption coefficient	1.044 mm^{-1}	
F(000)	1656	
Crystal size	0.20 x 0.18 x 0.09 mm^3	
Theta range for data collection	1.67 to 25.07°	
Index ranges	-22<=h<=19, -19<=k<=22, -14<=l<=13	
Reflections collected	19812	
Independent reflections	4394 [R(int) = 0.0577]	
Completeness to theta = 25.07°	99.9 %	
Absorption correction	multi-scan	
Max. and min. transmission	1.00000 and 0.783850	
Refinement method	Full-matrix least-squares on F^2	
Data / restraints / parameters	4394 / 0 / 328	
Goodness-of-fit on F^2	1.533	
Final R indices [I>2sigma(I)]	R1 = 0.1015, wR2 = 0.3217	
R indices (all data)	R1 = 0.1105, wR2 = 0.3370	

Appendix C-7. Crystal data and structure refinement for compound [7].

Empirical formula	C43.33 H43.33 Cl N2 O10.67 Zn2	
Formula weight	928.99	
Temperature	100(2) K	
Wavelength	0.71073 Å	
Crystal system	Trigonal	
Space group	P-3	
Unit cell dimensions	a = 18.9529(6) Å	$\alpha = 90°$.
	b = 18.9529(6) Å	$\beta = 90°$.
	c = 10.7825(7) Å	$\gamma = 120°$.
Volume	3354.3(3) $Å^3$	
Z	3	
Density (calculated)	1.380 Mg/m^3	
Absorption coefficient	1.190 mm^{-1}	
F(000)	1439	
Crystal size	0.2 x 0.15 x 0.10 mm^3	
Theta range for data collection	1.89 to 28.28°	
Index ranges	-25<=h<=24, -21<=k<=24, -11<=l<=14	
Reflections collected	21567	
Independent reflections	5329 [R(int) = 0.0434]	
Completeness to theta = 28.28°	95.8 %	
Absorption correction	Semi-empirical	
Max. and min. transmission	0.6427 and 0.5500	
Refinement method	Full-matrix least-squares on F^2	
Data / restraints / parameters	5329 / 14 / 270	
Goodness-of-fit on F^2	1.067	
Final R indices [I>2sigma(I)]	R1 = 0.0502, wR2 = 0.1374	
R indices (all data)	R1 = 0.0668, wR2 = 0.1449	

Appendix C-8. Crystal data and structure refinement for compound [8].

Empirical formula	C25 H20 N2 O5 Zn	
Formula weight	493.80	
Temperature	100(2) K	
Wavelength	1.54178 Å	
Crystal system	Monoclinic	
Space group	P2(1)/n	
Unit cell dimensions	a = 9.8421(5) Å	α = 90°.
	b = 15.7560(7) Å	β = 94.132(3)°.
	c = 13.8865(7) Å	γ = 90°.
Volume	2147.81(18) $Å^3$	
Z	4	
Density (calculated)	1.527 Mg/m^3	
Absorption coefficient	1.940 mm^{-1}	
F(000)	1016	
Crystal size	0.35 x 0.30 x 0.25 mm^3	
Theta range for data collection	4.25 to 67.55°	
Index ranges	-11<=h<=11, -18<=k<=18, -16<=l<=16	
Reflections collected	15321	
Independent reflections	3467 [R(int) = 0.0459]	
Completeness to theta = 67.55°	89.5 %	
Absorption correction	Semi-empirical from equivalents	
Max. and min. transmission	0.6427 and 0.5500	
Refinement method	Full-matrix least-squares on F^2	
Data / restraints / parameters	3467 / 0 / 298	
Goodness-of-fit on F^2	1.087	
Final R indices [I>2sigma(I)]	R1 = 0.0619, wR2 = 0.1461	
R indices (all data)	R1 = 0.0721, wR2 = 0.1512	

Appendix C-9. Crystal data and structure refinement for compound [9].

Empirical formula	C25 H20 Co N2 O5	
Formula weight	487.36	
Temperature	100(2) K	
Wavelength	1.54178 Å	
Crystal system	Monoclinic	
Space group	P2(1)/n	
Unit cell dimensions	a = 9.8526(3) Å	α = 90°.
	b = 15.7543(5) Å	β = 94.272(2)°.
	c = 13.8302(4) Å	γ = 90°.
Volume	2140.77(11) $Å^3$	
Z	4	
Density (calculated)	1.512 Mg/m^3	
Absorption coefficient	6.638 mm^{-1}	
F(000)	1004	
Crystal size	0.20 x 0.20 x 0.05 mm^3	
Theta range for data collection	4.26 to 60.00°	
Index ranges	-11<=h<=10, -15<=k<=17, -15<=l<=15	
Reflections collected	10322	
Independent reflections	3143 [R(int) = 0.0813]	
Completeness to theta = 60.00°	98.9 %	
Absorption correction	Semi-empirical from equivalents	
Max. and min. transmission	0.7325 and 0.3503	
Refinement method	Full-matrix least-squares on F^2	
Data / restraints / parameters	3143 / 0 / 299	
Goodness-of-fit on F^2	1.030	
Final R indices [I>2sigma(I)]	R1 = 0.0489, wR2 = 0.1103	
R indices (all data)	R1 = 0.0634, wR2 = 0.1179	

Appendix C-10. Crystal data and structure refinement for compound [10].

Empirical formula	C25 H20 Cd N2 O5	
Formula weight	540.83	
Temperature	100(2) K	
Wavelength	1.54178 Å	
Crystal system	Monoclinic	
Space group	P2(1)/c	
Unit cell dimensions	a = 17.2395(5) Å	α = 90°.
	b = 15.8856(4) Å	β = 104.6200(10)°.
	c = 16.8097(4) Å	γ = 90°.
Volume	4454.4(2) $Å^3$	
Z	8	
Density (calculated)	1.613 Mg/m^3	
Absorption coefficient	8.194 mm^{-1}	
F(000)	2176	
Crystal size	0.30 x 0.20 x 0.10 mm^3	
Theta range for data collection	3.84 to 68.04°	
Index ranges	-19<=h<=20, -19<=k<=18, -19<=l<=20	
Reflections collected	37840	
Independent reflections	7911 [R(int) = 0.0479]	
Completeness to theta = 68.04°	97.3 %	
Absorption correction	Semi-empirical from equivalents	
Max. and min. transmission	0.4946 and 0.1052	
Refinement method	Full-matrix least-squares on F^2	
Data / restraints / parameters	7911 / 0 / 584	
Goodness-of-fit on F^2	1.027	
Final R indices [I>2sigma(I)]	R1 = 0.0518, wR2 = 0.1230	
R indices (all data)	R1 = 0.0591, wR2 = 0.1281	

Appendix C-11. Crystal data and structure refinement for compound [11].

Empirical formula	C27 H24 N2 O5 Zn	
Formula weight	521.85	
Temperature	100(2) K	
Wavelength	0.71073 Å	
Crystal system	Monoclinic	
Space group	P2(1)/n	
Unit cell dimensions	a = 11.2273(13) Å	α = 90°.
	b = 15.7208(18) Å	β = 97.471(2)°.
	c = 13.3310(15) Å	γ = 90°.
Volume	2333.0(5) $Å^3$	
Z	4	
Density (calculated)	1.486 Mg/m^3	
Absorption coefficient	1.095 mm^{-1}	
F(000)	1080	
Crystal size	0.15 x 0.10 x 0.07 mm^3	
Theta range for data collection	2.01 to 25.04°	
Index ranges	-13<=h<=13, -9<=k<=18, -15<=l<=15	
Reflections collected	12037	
Independent reflections	4114 [R(int) = 0.0380]	
Completeness to theta = 25.04°	99.7 %	
Absorption correction	None	
Max. and min. transmission	1.0000 and 0.735425	
Refinement method	Full-matrix least-squares on F^2	
Data / restraints / parameters	4114 / 0 / 316	
Goodness-of-fit on F^2	0.925	
Final R indices [I>2sigma(I)]	R1 = 0.0317, wR2 = 0.0805	
R indices (all data)	R1 = 0.0361, wR2 = 0.0836	

Appendix C-12. Crystal data and structure refinement for compound [12].

Empirical formula	C27 H24 Co N2 O5	
Formula weight	515.41	
Temperature	298(2) K	
Wavelength	0.71073 Å	
Crystal system	Monoclinic	
Space group	P2(1)/n	
Unit cell dimensions	a = 11.1436(19) Å	α = 90°.
	b = 15.910(3) Å	β = 98.614(3)°.
	c = 13.503(2) Å	γ = 90°.
Volume	2367.1(7) $Å^3$	
Z	4	
Density (calculated)	1.446 Mg/m^3	
Absorption coefficient	0.767 mm^{-1}	
F(000)	1068	
Crystal size	0.10 x 0.10 x 0.04 mm^3	
Theta range for data collection	1.99 to 25.12°	
Index ranges	-13<=h<=13, -18<=k<=11, -15<=l<=16	
Reflections collected	12091	
Independent reflections	4184 [R(int) = 0.0819]	
Completeness to theta = 25.12°	99.3 %	
Absorption correction	None	
Refinement method	Full-matrix least-squares on F^2	
Data / restraints / parameters	4184 / 0 / 317	
Goodness-of-fit on F^2	0.941	
Final R indices [I>2sigma(I)]	R1 = 0.0570, wR2 = 0.1107	
R indices (all data)	R1 = 0.1115, wR2 = 0.1279	

Appendix C-13. Crystal data and structure refinement for compound [13].

Empirical formula	C27 H24 Cd1 N2 O5	
Formula weight	568.88	
Temperature	100(2) K	
Wavelength	1.54178 Å	
Crystal system	Monoclinic	
Space group	P2(1)/n	
Unit cell dimensions	a = 11.5852(2) Å	α = 90°.
	b = 15.6988(3) Å	β = 95.6450(10)°.
	c = 13.2064(2) Å	γ = 90°.
Volume	2390.25(7) $Å^3$	
Z	4	
Density (calculated)	1.581 Mg/m^3	
Absorption coefficient	7.666 mm^{-1}	
F(000)	1152	
Crystal size	0.24 x 0.20 x 0.18 mm^3	
Theta range for data collection	4.39 to 67.78°	
Index ranges	-13<=h<=13, -18<=k<=18, -15<=l<=15	
Reflections collected	18300	
Independent reflections	4143 [R(int) = 0.0463]	
Completeness to theta = 67.78°	95.7 %	
Absorption correction	Semi-empirical from equivalents	
Max. and min. transmission	0.3391 and 0.2606	
Refinement method	Full-matrix least-squares on F^2	
Data / restraints / parameters	4143 / 0 / 318	
Goodness-of-fit on F^2	1.054	
Final R indices [I>2sigma(I)]	R1 = 0.0357, wR2 = 0.1197	
R indices (all data)	R1 = 0.0368, wR2 = 0.1211	

Appendix C-14. Crystal data and structure refinement for compound [15].

Empirical formula	C30 H46 Co2 N4 O10	
Formula weight	740.57	
Temperature	293(2) K	
Wavelength	1.54178 Å	
Crystal system	Monoclinic	
Space group	P2	
Unit cell dimensions	a = 13.4027(15) Å	α = 90°.
	b = 9.4194(11) Å	β = 90.040 (6)°.
	c = 13.4730(15) Å	γ = 90°.
Volume	1700.9(3) $Å^3$	
Z	2	
Density (calculated)	1.446 Mg/m^3	
Absorption coefficient	8.144mm^{-1}	
F(000)	776	
Crystal size	0.10 x 0.10 x 0.10 mm^3	
Theta range for data collection	3.28 to 58.90 °	
Index ranges	-14<=h<=14, -9<=k<=10, -14<=l<=14	
Reflections collected	7189	
Independent reflections	3928 [R(int) = 0.0500]	
Completeness to theta = 58.90°	92.2 %	
Absorption correction	Semi-empirical from equivalents	
Max. and min. transmission	0.4964 and 0.4964	
Refinement method	Full-matrix least-squares on F^2	
Data / restraints / parameters	3928 / 1 / 197	
Goodness-of-fit on F^2	1.078	
Final R indices [I>2sigma(I)]	R1 = 0.0954, wR2 = 0.2568	
R indices (all data)	R1 = 0.1362, wR2 = 0.2833	

Appendix C-15. Crystal data and structure refinement for compound [16].

Empirical formula	C30 H36 N2 O8 Zn2	
Formula weight	683.35	
Temperature	100(2) K	
Wavelength	0.71073Å	
Crystal system	Orthorhombic	
Space group	I222	
Unit cell dimensions	a = 13.444(4) Å	α = 90°.
	b = 13.444(4) Å	β = 90°.
	c = 27.943(8) Å	γ = 90°.
Volume	5050(2) $Å^3$	
Z	4	
Density (calculated)	0.899 Mg/m^3	
Absorption coefficient	0.981 mm^{-1}	
F(000)	1416	
Crystal size	0.10 x 0.10 x 0.10 mm^3	
Theta range for data collection	1.68 to 25.0°	
Index ranges	-13<=h<=16, -16<=k<=15, -33<=l<=24	
Reflections collected	7189	
Independent reflections	4445 [R(int) = 0.0325]	
Completeness to theta = 25.02°	99.9 %	
Absorption correction	Semi-empirical from equivalents	
Max. and min. transmission	0.4964 and 0.4964	
Refinement method	Full-matrix least-squares on F^2	
Data / restraints / parameters	4445 / 4 / 195	
Goodness-of-fit on F^2	1.115	
Final R indices [I>2sigma(I)]	R1 = 0.0623, wR2 = 0.1980	
R indices (all data)	R1 = 0.0790, wR2 = 0.2157	

Appendix C-16. Crystal data and structure refinement for compound [29].

Empirical formula	C44 H40 Co2 N4 O12	
Formula weight	934.66	
Temperature	293(2) K	
Wavelength	0.71073Å	
Crystal system	Monoclinic	
Space group	P 2	
Unit cell dimensions	a = 13.291(5) Å	α = 90°.
	b = 13.291(5) Å	β = 90.01(10)°.
	c = 22.084(6) Å	γ = 90°.
Volume	3901(2) $Å^3$	
Z	2	
Density (calculated)	0.796 Mg/m^3	
Absorption coefficient	0.462 mm^{-1}	
F(000)	964	
Crystal size	0.1 x 0.1 x 0.1 mm^3	
Theta range for data collection	0.92 to 23.25°	
Index ranges	14<=h<=13, -11<=k<=14, -24<=l<=24	
Reflections collected	16925	
Independent reflections	11205 [R(int) = 0.0331]	
Completeness to theta = 23.25°	99.8 %	
Absorption correction	Semi-empirical from equivalents	
Max. and min. transmission	0.4946 and 0.1052	
Refinement method	Full-matrix least-squares on F^2	
Data / restraints / parameters	11205 / 3 / 88	
Goodness-of-fit on F^2	1.045	
Final R indices [I>2sigma(I)]	R1 = 0.1062, wR2 = 0.2998	
R indices (all data)	R1 = 0.1183, wR2 = 0.3125	

Appendix C-17. Crystal data and structure refinement for compound [30].

Empirical formula	C446.50 H579.50 Cu24 O144	
Formula weight	9775.56	
Temperature	296(2) K	
Wavelength	0.71073 Å	
Crystal system	Tetragonal	
Space group	P4(1)2(1)2	
Unit cell dimensions	a = 38.559(2) Å	α = 90°.
	b = 38.559(2) Å	β = 90°.
	c = 54.503(6) Å	γ = 90°.
Volume	81035(11) $Å^3$	
Z	4	
Density (calculated)	0.801 Mg/m^3	
Absorption coefficient	0.664 mm^{-1}	
F(000)	20426	
Crystal size	0.2 x 0.15 x 0.1 mm^3	
Theta range for data collection	0.91 to 16.00°	
Index ranges	-29<=h<=29, -29<=k<=29, -42<=l<=20	
Reflections collected	115996	
Independent reflections	19801 [R(int) = 0.3397]	
Completeness to theta = 16.00°	99.9 %	
Absorption correction	Semi-empirical from equivalents	
Max. and min. transmission	1.00 and 0.89	
Refinement method	Full-matrix least-squares on F^2	
Data / restraints / parameters	19801 / 449 / 775	
Goodness-of-fit on F^2	1.317	
Final R indices [I>2sigma(I)]	R1 = 0.1873, wR2 = 0.4067	
R indices (all data)	R1 = 0.2226, wR2 = 0.4386	

Appendix C-18. Crystal data and structure refinement for compound [31].

Empirical formula	C720 H432 Cu48 O288	
Formula weight	16740.58	
Temperature	100(2) K	
Wavelength	1.54178 Å	
Crystal system	Tetragonal	
Space group	P4/mnc	
Unit cell dimensions	a = 27.974(5) Å	α = 90.000(5) °.
	b = 27.974(5) Å	β = 90.000(5) °.
	c = 39.321(5) Å	γ = 90.000(5) °.
Volume	30770(9) $Å^3$	
Z	2	
Density (calculated)	0.903 Mg/m^3	
Absorption coefficient	1.349 mm^{-1}	
F(000)	8448	
Crystal size	0.10 x 0.10 x 0.10 mm^3	
Theta range for data collection	1.94 to 39.96 °	
Index ranges	-15<=h<=22, -22<=k<=22, -32<=l<=31	
Reflections collected	41589	
Independent reflections	4548 [R(int) = 0.1175]	
Completeness to theta = 39.96 °	95.0 %	
Absorption correction	Semi-empirical from equivalents	
Max. and min. transmission	0.8769 and 0.8769	
Refinement method	Full-matrix least-squares on F^2	
Data / restraints / parameters	4548 / 7 / 232	
Goodness-of-fit on F^2	1.113	
Final R indices [I>2sigma(I)]	R1 = 0.1097, wR2 = 0.2959	
R indices (all data)	R1 = 0.1504, wR2 = 0.3217	

Appendix C-19. Crystal data and structure refinement for compound [32].

Empirical formula	$C_{1248}H_{200}Cu_{48}N_{40}O_{352}$	
Formula weight	24433.28	
Temperature	100(2) K	
Wavelength	0.71073 Å	
Crystal system	Tetragonal	
Space group	I4/m	
Unit cell dimensions	a = 27.654(20) Å	α= 90 °.
	b = 27.654(20) Å	β= 90°.
	c = 39.9159(60) Å	γ = 90 °.
Volume	30524.7(60) $Å^3$	
Z	2	
Density (calculated)	0.984 Mg/m^3	
Absorption coefficient	1.178 mm^{-1}	
F(000)	9845	
Crystal size	0.10 x 0.10 x 0.10 mm^3	
Theta range for data collection	1.90 to 24.45 °	
Index ranges	-15<=h<=22, -22<=k<=22, -32<=l<=31	
Reflections collected	12235	
Independent reflections	6342 [R(int) = 0.2237]	
Completeness to theta = 24.45 °	93.0 %	
Absorption correction	Semi-empirical from equivalents	
Max. and min. transmission	0.8769 and 0.8769	
Refinement method	Full-matrix least-squares on F^2	
Data / restraints / parameters	6342 / 17 / 751	
Goodness-of-fit on F^2	2.13	
Final R indices [I>2sigma(I)]	R1 = 0.1794, wR2 = 0.2959	
R indices (all data)	R1 = 0.2617, wR2 = 0.3217	

Appendix C-20. Crystal data and structure refinement for compound [33].

Empirical formula	C304 H216 Cu24 O144 S8	
Formula weight	7954.21	
Temperature	100(2) K	
Wavelength	0.71073 Å	
Crystal system	Tetragonal	
Space group	I422	
Unit cell dimensions	a = 28.885(4) Å	α = 90°.
	b = 28.885(4) Å	β = 90°.
	c = 28.305(6) Å	γ = 90°.
Volume	23616(7) $Å^3$	
Z	2	
Density (calculated)	1.119 Mg/m^3	
Absorption coefficient	1.159 mm^{-1}	
F(000)	8032	
Crystal size	0.1 x 0.08 x 0.07 mm^3	
Theta range for data collection	2.23 to 23.50°	
Index ranges	-32<=h<=21, -32<=k<=31, -31<=l<=28	
Reflections collected	52801	
Independent reflections	8752 [R(int) = 0.3244]	
Completeness to theta = 23.50°	99.7 %	
Absorption correction	Semi-empirical	
Refinement method	Full-matrix least-squares on F^2	
Data / restraints / parameters	8752 / 635 / 520	
Goodness-of-fit on F^2	1.000	
Final R indices [I>2sigma(I)]	R1 = 0.1032, wR2 = 0.2570	
R indices (all data)	R1 = 0.2820, wR2 = 0.2874	

Appendix C-21. Crystal data and structure refinement for compound [34].

Empirical formula	4441 H376 N32 O152 Zn24	
Formula weight	10126.48	
Temperature	293(2) K	
Wavelength	0.71073 Å	
Crystal system	Tetragonal	
Space group	I4/m	
Unit cell dimensions	a = 30.144(7) Å	α = 90°.
	b = 30.144(7) Å	β = 90°.
	c = 27.944(11) Å	γ = 90°.
Volume	25391(13) $Å^3$	
Z	2	
Density (calculated)	1.325 Mg/m^3	
Absorption coefficient	1.193 mm^{-1}	
F(000)	10366	
Crystal size	0.1 x 0.1 x 0.1 mm^3	
Theta range for data collection	1.68 to 20.82 °	
Index ranges	-30<=h<=29, -29<=k<=14, -17<=l<=27	
Reflections collected	19407	
Independent reflections	6832 [R(int) = 0.1146]	
Completeness to theta = 20.82°	99.7 %	
Absorption correction	semi-empirical	
Refinement method	Full-matrix least-squares on F^2	
Data / restraints / parameters	6832 / 530 / 717	
Goodness-of-fit on F^2	1.047	
Final R indices [I>2sigma(I)]	R1 = 0.1006, wR2 = 0.2329	
R indices (all data)	R1 = 0.1464, wR2 = 0.2555	

About the Author

John Jackson Perry IV was born in Tampa, Florida U.S.A., in 1980. He was salutatorian of his graduating class from the Academy of Health Professions located on the campuses of Tampa Bay Technical High School in 1999. He received two B.A. degrees in chemistry and mathematics (graduating from the Honors College) from the University of South Florida in 2003. In August of 2003, he was admitted into the Ph.D. program in the Department of Chemistry at USF, upon which time he joined the research group of Dr. Michael J. Zaworotko. He is a member of the American Chemical Society, the American Association for the Advancement of Science, and the Mathematical Association of America. In addition to co-authoring six scientific papers in peer-reviewed journals, he has presented his research at numerous local, state, regional, national, and international scientific conferences. He has received several awards and recognitions for his research and in 2005 he was awarded the George Bursa award, given annually to an exceptional graduate student in the Department of Chemistry at USF. In 2008 he was selected to be one of approximately 30 graduate student / post-doctoral fellows to attend the International Center for Materials Research summer school workshop on *Periodic Materials and Crystal Chemistry* where he was afforded the opportunity to interact with some of the current luminaries as well as with future leaders in the field.